



National Library
of Canada

Bibliothèque nationale
du Canada

Canadian Theses Service · Services des thèses canadiennes

Ottawa, Canada
K1A 0N4

CANADIAN THESES

NOTICE

The quality of this microfiche is heavily dependent upon the quality of the original thesis submitted for microfilming. Every effort has been made to ensure the highest quality of reproduction possible.

If pages are missing, contact the university which granted the degree.

Some pages may have indistinct print especially if the original pages were typed with a poor typewriter ribbon or if the university sent us an inferior photocopy.

Previously copyrighted materials (journal articles, published tests, etc.) are not filmed.

Reproduction in full or in part of this film is governed by the Canadian Copyright Act, R.S.C. 1970, c. C-30. Please read the authorization forms which accompany this thesis.

**THIS DISSERTATION
HAS BEEN MICROFILMED
EXACTLY AS RECEIVED**

THÈSES CANADIENNES

AVIS

La qualité de cette microfiche dépend grandement de la qualité de la thèse soumise au microfilmage. Nous avons tout fait pour assurer une qualité supérieure de reproduction.

S'il manque des pages, veuillez communiquer avec l'université qui a conféré le grade.

La qualité d'impression de certaines pages peut laisser à désirer, surtout si les pages originales ont été dactylographiées à l'aide d'un ruban usé ou si l'université nous a fait parvenir une photocopie de qualité inférieure.

Les documents qui font déjà l'objet d'un droit d'auteur (articles de revue, examens publiés, etc.) ne sont pas microfilmés.

La reproduction, même partielle, de ce microfilm est soumise à la Loi canadienne sur le droit d'auteur, SRC 1970, c. C-30. Veuillez prendre connaissance des formules d'autorisation qui accompagnent cette thèse.

**LA THÈSE A ÉTÉ
MICROFILMÉE TELLE QUE
NOUS L'AVONS REÇUE**

Canada

 National Library
of Canada

Bibliothèque nationale
du Canada

Canadian Theses Division

Division des thèses canadiennes

Ottawa, Canada
K1A 0N4

PERMISSION TO MICROFILM — AUTORISATION DE MICROFILMER

• Please print or type — Ecrire en lettres moulees ou dactylographier

Full Name of Author — Nom complet de l'auteur

Robert Gordon McPherson

Date of Birth — Date de naissance

Dec 6, 1952

Country of Birth — Lieu de naissance

Canada

Permanent Address — Residence fixe

P.O. Box 1624

Marinville, Alta

TOGIPCO

Title of Thesis — Titre de la these

High Frequency Electric Heating
of the Athabasca Oilsands

University — Université

University of Alberta

Degree for which thesis was presented — Grade pour lequel cette these fut presentee

PhD in Electrical Engineering

Year this degree conferred — Année d'obtention de ce grade

1985

Name of Supervisor — Nom du directeur de these

Chate/Vermeulen

Permission is hereby granted to the NATIONAL LIBRARY OF CANADA to microfilm this thesis and to lend or sell copies of the film.

The author reserves other publication rights, and neither the thesis nor extensive extracts from it may be printed or otherwise reproduced without the author's written permission.

L'autorisation est, par la presente, accordée à la BIBLIOTHEQUE NATIONALE DU CANADA de microfilmer cette these et de prêter ou de vendre des exemplaires du film.

L'auteur se réserve les autres droits de publication; ni la these ni de longs extraits de celle-ci ne doivent être imprimés ou autrement reproduits sans l'autorisation écrite de l'auteur.

Date

12 Sept 1985

Signature

R. G. McPherson

THE UNIVERSITY OF ALBERTA

High Frequency Electric Heating of the Athabasca Oilsands

by



Robert G. McPherson

A THESIS

SUBMITTED TO THE FACULTY OF GRADUATE STUDIES AND RESEARCH
IN PARTIAL FULFILMENT OF THE REQUIREMENTS FOR THE DEGREE
OF Doctor of Philosophy

Electrical Engineering

EDMONTON, ALBERTA

FALL, 1985

THE UNIVERSITY OF ALBERTA

RELEASE FORM

NAME OF AUTHOR

Robert G. McPherson

TITLE OF THESIS High Frequency Electric Heating of the
Athabasca Oilsands

DEGREE FOR WHICH THESIS WAS PRESENTED Doctor of Philosophy

YEAR THIS DEGREE GRANTED FALL, 1985

Permission is hereby granted to THE UNIVERSITY OF
ALBERTA LIBRARY to reproduce single copies of this
thesis and to lend or sell such copies for private,
scholarly or scientific research purposes only.

The author reserves other publication rights, and
neither the thesis nor extensive extracts from it may
be printed or otherwise reproduced without the author's
written permission.

(SIGNED) *R. G. McPherson*.....

PERMANENT ADDRESS:

..... *P.O. Box 1624*
..... *Morinville, Alta.*
.....

DATED *Sept 12, 1985*

THE UNIVERSITY OF ALBERTA
FACULTY OF GRADUATE STUDIES AND RESEARCH

The undersigned certify that they have read, and recommend to the Faculty of Graduate Studies and Research, for acceptance, a thesis entitled High Frequency Electric Heating of the Athabasca Oilsands submitted by Robert G. McPherson in partial fulfilment of the requirements for the degree of Doctor of Philosophy.

..... F.E. Vermulst

..... J. Chute

Supervisor

..... H. Arnold

..... Peter R. Smy

..... C. G. Englefield

..... D. Rantledge

..... D. G. Hughes

..... J. B. Warren

External Examiner

Date..... 5 Sept 85

Abstract

An investigation is made of the concept of inundating an oil sand formation with electromagnetic energy to generate a hot zone of low viscosity bitumen which is suitable for in-situ recovery. A number of operating concepts and electrode configurations are examined analytically and experimentally to establish possible heating profiles and bitumen production rates.

All of the electrode configurations that are considered employ the concept of establishing a guided high frequency electromagnetic wave which heats the formation by travelling through it. The advantages and limitations of this heating approach are compared to alternate methods of heating the oil sand formation.

Acknowledgements

I would like to thank my supervisors Dr. F.E. Vermeulen and Dr. F.S. Chute for their considerable assistance in all areas of this study.

I would also like to express my appreciation to Mr. J. Fearn whose many talents were essential to the successful construction and execution of the experimental studies.

The execution of this study was made possible by funding provided by the Alberta Oil Sands Technology and Research Authority and the National Sciences and Engineering Research Council.

Table of Contents

Chapter	Page
1. Background and Problem Identification	1
1.1 General Background	1
1.2 Electromagnetic Heating	3
1.2.1 Heating Mechanisms	3
1.2.2 Low Frequency Methods	6
1.2.3 High Frequency Methods	7
1.3 Guided Versus Unguided Electromagnetic Waves	14
1.4 Research Objectives	14
2. A Conceptual Discussion of Possible Electrode Configurations and Modes of Heating	18
2.1 Total Evaporation Boring	18
2.2 Partial Evaporation Boring	22
2.3 Finite Length Dielectric Coated Line	25
2.4 Series Resonated Line	28
2.5 Variable Coupling Electrodes	35
2.6 Production Controlled Heating	38
3. Experimental Case Studies	42
3.1 Total Evaporation Boring: Demonstration of Concept in Athabasca Oilsand	42
3.2 Partial Evaporation Boring: Demonstration of Concept in Athabasca Oilsand	50
3.3 Partial Evaporation Boring: Scaled Electrothermal Models	62
3.4 Dielectric Coated Transmission Line: Scaled Electrothermal Models	73
3.4.1 Applied Coating	73
3.4.2 Self Generated Uniform Coating	80

3.5	Series Resonated Transmission Line:	
	Experimental Results	89
3.5.1	General	89
3.5.2	Wavelength Expansion: Demonstration of Effect	90
3.5.3	Skin Depth Expansion: Demonstration of Effect	98
3.5.4	Conclusions	105
3.6	Variable Coupling Electrodes: Experimental Results	107
3.7	Production Controlled Heating: Experimental Demonstration of Effect	115
3.7.1	General	115
3.7.2	Experimental Setup	118
3.7.3	Experimental Runs	123
4.	Fields of a Lossy Parallel Plate Line	137
4.1	Introduction	137
4.2	Electromagnetic Field Solution	141
4.2.1	Terminology	141
4.2.2	Solution	143
4.3	Field Lines	146
4.4	Validity of Distributed Impedance Representation	149
4.5	Discussion of Field Lines Generated	154
5.	Approximate Numerical Model of a Coated and/or Compensated Transmission Line	159
5.1	General	159
5.2	Model Formulation	160
5.2.1	Line Segment Parameters	161
5.2.2	Energy Deposition Along the Line	166

5.2.3 Model Limitations	171
6. Production Controlled Heating: A First Order Numerical Model	175
6.1 General	175
6.2 Methodology Descriptions	177
6.2.1 Geometry	177
6.2.2 Energy and Flow Balances	179
6.2.3 Distribution of Electromagnetic Wave Energy	179
6.2.4 Thermal Conduction Energy Flows	183
6.2.5 Flow Calculations	187
6.3 Model Runs	192
6.3.1 Material Properties Used	192
6.3.2 Base Case	193
6.3.3 Frequency Variation	197
6.3.4 Power Variation	199
6.3.5 Permeability Variation	202
7. Scaling Criteria for Electrothermal Models	206
7.1 Relations	207
7.2 Scaling Criteria for Dielectric Coated Lines ...	212
7.3 Sample of Scaling Calculations	214
Conclusion	215
Bibliography	222
Appendix A: Transmission Line Theory	226
Appendix B: Microscopic Structure of Oil Sand	230
Appendix C: Economic Considerations	231

List of Tables

Table	page
3.1.1	Full scale field quantities corresponding to the model values in the scale model heating demonstration of the partial evaporation boring concept.....66
3.2:	Material properties used in numerical simulation of production controlled heating experiment.134
6.1	Formation properties used for the base case run of the production controlled heating numerical simulator.....193

List of Figures

Figure	page
1.1: Energy deposition of an electromagnetic wave in a lossy oil sand formation.....	10
1.2: Electrical properties of Athabasca oil sand. Type A is low grade oil sand (high moisture, low bitumen). Type B is high grade oil sand (low moisture, high bitumen). a). Conductivity σ , relative dielectric ϵ , and loss tangent $\sigma/\omega\epsilon$ for oil sand as a function of frequency and at a temperature of 24°C. b) Wavelength λ and skin depth Δ for oilsand as a function of frequency at 24°C.....	12
2.1: A sketch showing one possible means of placing electrodes in the oil sand formation. The electrodes are placed in horizontal bore holes drilled into the formation payzone from mined cross shafts.....	20
2.2: Effects of series compensating capacitance on wave attenuation rate, showing ideally zero attenuation when the line is resonated.....	31
2.3: Effects of series compensating capacitance on wavelength, showing ideally infinite wavelength when the line is resonated.....	32
2.4: An electrode form in which high energy coupling to the formation occurs only over a selected section of the electrode length.....	36
2.5: Representation of an oil sand body as production controlled heating is occurring, showing the generation of a depleted zone as production takes place.....	39
3.1: Experimental demonstration of total evaporation boring concept. a) Apparatus interconnection showing excitation and instrumentation connected to the test cell. b) Construction details of the test cell packed with oil sand. The oil sand is heated by passing a guided electromagnetic wave through it.....	44

- 3.2: Total evaporation boring demonstration. Plot of midpoint temperatures obtained along the length of the waveguide, at various points in time as the heating run progresses.....45
- 3.3: Thermal conduction heating comparison to electromagnetic heating. Oil sand is packed in the same waveguide test cell as used for total evaporation boring experiment. Plots are of midpoint temperatures obtained along the length of the waveguide. The input heater was held at a constant 100°C.....47
- 3.4: Thermal conduction heating comparison to electromagnetic heating. Oil sand is packed in the same waveguide test cell as used for total evaporation boring experiment. Plots are of midpoint temperatures obtained along the length of the waveguide. The input heater was supplied with a constant 220W.....49
- 3.5: Experimental demonstration of partial evaporation boring concept.
 a) Apparatus interconnection showing excitation and instrumentation connected to the test cell.
 b) Construction details of the test cell packed with oil sand. The oil sand is heated by passing a guided electromagnetic wave through it.....51
- 3.6: Skin depth versus frequency of the oil sand used in the partial evaporation boring demonstration....52
- 3.7: Conductivity versus frequency of the oil sand used in the partial evaporation boring demonstration.....53
- 3.8: Conduction to displacement current ratio versus frequency, of the oil sand used in the partial evaporation boring demonstration.54
- 3.9: Temperature measurement locations in the partial evaporation boring demonstration.....56
- 3.10: Partial evaporation boring demonstration. Plot of midpoint temperatures obtained along the length of the transmission line, at various points in time, as the heating run progresses.....57
- 3.11: Partial evaporation boring demonstration. Plot of near electrode temperatures obtained along the length of the transmission line, at various points in time, as the heating run progresses.....58

- 3.12: Thermal conduction heating comparison to electromagnetic heating. Oil sand is packed in the same transmission line test cell as used for partial evaporation boring experiment. Plots are of midpoint temperatures obtained along the length of the line. The input heater was supplied with a constant 200W. Note that the plate temperature given is the temperature at zero cm.61
- 3.13: Scaled electrothermal model of field heating situation.
 a) End view of electrode array in the field with planes of symmetry shown.
 b) Half element of the field array.
 Represents the geometry selected for the scale model.....63
- 3.14: Measured temperatures in the scale model. Temperatures obtained during a partial evaporation heating run. Temperature variation into the formation, measured at a central point 2cm (2.05 m) above the ground plane (above the midplane). Bracketed quantities are the full scale field values corresponding to the model values.68
- 3.15: Measured temperatures in the scale model. Temperatures obtained during a partial evaporation heating run. Temperature variation across the line, measured along an axis intersecting the electrodes at a distance of 11.5cm (11.8m) from the line input. Bracketed quantities are the full scale field values corresponding to the model values.69
- 3.16: Sketch of the current lines generated by one upper/lower electrode pair within the array (see figure 3.13)70
- 3.17: Physical layout of model used to examine the dielectric coated line concept. Physical properties and dimensions of both the field and model are presented.....74
- 3.18: Measured temperatures in the scale model. Temperatures obtained during a dielectric coated electrode heating run. Temperature variation across the line, measured along an axis intersecting the electrodes at a distance of 10cm (14.5m) from the line input. Bracketed quantities are the full scale field values corresponding to the model values.76

- 3.19: Measured temperatures in the scale model.
Temperatures obtained during a dielectric coated electrode heating run. Horizontal temperature variation, measured along a line 0.5cm (.73m) below and perpendicular to the top electrode at a point 12cm (17.4m) from the line input. Bracketed quantities are the full scale field values corresponding to the model values.77
- 3.20: Measured temperatures in the scale model.
Temperatures obtained during a dielectric coated electrode heating run. Temperature variation into the formation, measured at a central point 1.5cm (2.2m) above the ground plane (above the midplane). Bracketed quantities are the full scale field values corresponding to the model values. Dotted line indicates expected energy deposition profile if no self leveling effects were present.78
- 3.21: Measured temperatures in the scale model.
Temperatures obtained during a heating run with self coating electrodes. Temperature variation across the line, measured along an axis intersecting the electrodes at a distance of 10cm (10.8m) from the line input. Bracketed quantities are the full scale field values corresponding to the model values.81
- 3.22: Measured temperatures in the scale model.
Temperatures obtained during a heating run with self coating electrodes. Horizontal temperature variation, measured along a line 0.5cm (.54m) below and perpendicular to the top electrode at a point 12cm (13m) from the line input. Bracketed quantities are the full scale field values corresponding to the model values.82
- 3.23: Temperatures obtained during a heating run with self coating electrodes. Temperature variation into the formation, measured at a central point 1.5cm (1.62m) above the ground plane (above the midplane). Bracketed quantities are the full scale field values corresponding to the model values.83
- 3.24: Attenuation rate versus electrode coating thickness at various operating frequencies.
Based on the conductivity value at 25°C.....84
- 3.25: Attenuation rate versus electrode coating thickness at various operating frequencies.
Based on the conductivity value at 100°C.....85

- 3.26: Required uniform potential $V(x)$ between the electrodes for uniform heating.....91
- 3.27: Measured and theoretical potential distribution on a low loss two wire line with no compensation. Operating frequency is 60 MHz.....93
- 3.28: Position and size of series compensating capacitors on a two wire line. Values will nominally resonate the line at 60 MHz.....94
- 3.29: Measured potential distribution on a compensated two wire line operated at the 60 MHz design frequency. Also shown is the least squares linear fit of the measured potential points and the theoretical potential distribution that would be on the line if it were not compensated. .95
- 3.30: Measured potential distribution on a compensated two wire line operated at 52.18 MHz. The line design frequency is 60 MHz. Also shown is the least squares linear fit of the measured potential points and the theoretical potential distribution that would be on the line if it were not compensated.96
- 3.31: Measured potential distribution on a compensated two wire line operated at 69 MHz. The line design frequency is 60 MHz. Also shown is the least squares linear fit of the measured potential points and the theoretical potential distribution that would be on the line if it were not compensated.97
- 3.32: Installation method used to place both the compensated and uncompensated transmission line electrodes in a lossy medium.99
- 3.33: Measured potential distribution on an uncompensated two wire line buried in a lossy medium. Operating frequency is 60MHz.101
- 3.34: Measured potential distribution on a compensated two wire line buried in a lossy medium. Operating frequency is the design frequency of 60 MHz. Also shown is the least squares linear fit of the measured potential points.102
- 3.35: Measured potential distribution on a compensated two wire line buried in a lossy medium. The operating frequency is 54 MHz but the design frequency is 60 MHz. Also shown is the least squares linear fit of the measured potential

	points.	103
3.36:	Measured potential distribution on a compensated two wire line buried in a lossy medium. The operating frequency is 66 MHz but the design frequency is 60 MHz. Also shown is the least squares linear fit of the measured potential points.	104
3.37:	Construction detail of electrode design which yields a transmission line with higher energy coupling over a section of its length. The bracketed quantities are the full scale field values corresponding to the model values.....	108
3.38:	Measured temperatures in the scale model. Temperatures obtained during a variable coupling electrode heating run. Temperature variation across the line, measured along an axis intersecting the electrodes at a distance of 10cm (9.9m) from the line input. Bracketed quantities are the full scale field values corresponding to the model values.	110
3.39:	Measured temperatures in the scale model. Temperatures obtained during a variable coupling electrode heating run. Horizontal temperature variation, measured along a line 0.5cm (0.49m) below and perpendicular to the top electrode at a point 12cm (11.9m) from the line input. Bracketed quantities are the full scale field values corresponding to the model values.	111
3.40:	Measured temperatures in the scale model. Temperatures obtained during a variable coupling electrode heating run. Temperature variation into the formation, measured at a central point 1.5cm (1.49m) above the ground plane (above the midplane). Bracketed quantities are the full scale field values corresponding to the model values.	112
3.41:	Sketch of the dried sand coating generated on the selective coupling electrode, showing a thicker generated coating in the region of higher initial coupling.....	114
3.42:	Production controlled heating demonstration. Construction detail of the test cell packed with the artificial oil sand.....	129
3.43:	Production controlled heating demonstration. Power level absorbed by the sample versus time. Sample is excited at a constant potential.	

	Numerical simulation results are shown as well as experimental results.	131
3.44:	Production controlled heating demonstration. Total fluid production versus time. Numerical simulation results are shown as well as experimental results.	132
4.1:	Geometry of a parallel plate transmission line in which the plates are separated by an insular zone and a conductive zone.....	139
4.2:	Representation of an electric field line generated on the parallel plate transmission line, at a number of different operating frequencies.....	147
4.3:	Distributed impedance representation of a short length of the parallel plate transmission line. .	150
4.4:	Sketch of the electric and magnetic field lines of a forward and reverse travelling wave on the parallel plate transmission line.....	156
5.1:	A two wire transmission line buried in a non-magnetic lossy medium. a) Geometry of the transmission line. b) Distributed impedance representation of a short length of the transmission line.....	162
5.2:	A coated two wire transmission line buried in a non-magnetic lossy medium. a) Geometry of the transmission line. b) Distributed impedance representation of a short length of the transmission line.....	163
5.3:	The shunting leg segment of the distributed impedance representation of a coated electrode transmission line, may be reduced to a single equivalent admittance pair (G,C) using phasor algebra.....	165
5.4:	Representation of a multi-section lossy transmission line, showing the pertinent attributes of each section.	167
5.5:	Impedance and reflection coefficient values at various points along a length of lossy transmission line.	168
5.6:	Translation of phasor potentials along a length of transmission line.....	170
6.1:	Model geometry for simulation of production	

	controlled electromagnetic flood.....	178
6.2:	Distributed impedance representation of a short section of transmission line.....	181
6.3:	Fluid flows between saturated elements in the numerical model of a production controlled electromagnetic flood.	189
6.4:	Base case model run of production controlled electromagnetic flood numerical model. a) Saturated zone temperature profiles at various times in the heating sequence. b) Location of the demarker between the saturated zone and the depleted zone at various times in the heating process. c) Production rate and cumulative production of fluids from the oil sand formation as the heating sequence progresses.....	196
6.5:	Production controlled electromagnetic flood simulation runs for two different operating frequencies. a) The effect on the saturated zone temperature profiles. b) The effect on the fluid production.....	198
6.6:	Production controlled electromagnetic flood simulation runs for two different applied power levels. a) The effect on the saturated zone temperature profiles. b) The effect on the fluid production.....	200
6.7:	Production controlled electromagnetic flood simulation runs for two different flow permeabilities in the formation. a) The effect on the saturated zone temperature profiles. b) The effect on the fluid production.....	203
6.8:	Production controlled electromagnetic flood simulation run for the case of a selected portion of the formation having a lower flow permeability. a) The effect on the saturated zone temperature profiles. b) The effect on the demarker location between the saturated and depleted zones.....	205
B.1:	Schematic diagram showing a structural model of Athabasca oil sand.....	231

C.1: Estimated cost range for the electrical pre-heat
portion of an in-situ recovery scheme.....234

List of Plates

Plate

page

- 1: The crust of dried sand formed around the
electrode during the heating run of a scale
model operating in the partial evaporation
boring mode.....235

Nomenclature

α	attenuation constant (nepers/metre)
$\Delta=1/\alpha$	skin depth (metres)
β	phase constant (radians/metre)
$\gamma=\alpha+j\beta$	propagation constant
ϵ	electrical permittivity (Farad/metre)
μ	magnetic permeability (Henry/metre)
λ	wavelength (metres)
σ	electrical conductivity (Siemens/metre)
$\omega=2\pi f$	angular frequency (radians/second)
f	frequency (Hertz)
j	the square root of negative one
R	transmission line distributed series resistance (Ohm/metre)
L	transmission line distributed series inductance (Henry/metre)
G	transmission line distributed shunt conductance (Siemens/metre)
C	transmission line distributed shunt capacitance (Farad/metre)
C_s	transmission line distributed series compensating capacitance (Farad/metre)
p	mechanical scale factor (Field/Model)

T	time scale factor (Field/Model)
Γ	transmission line reflection coefficient (potential ratio of reflected to incident wave)
Z_0	transmission line characteristic impedance (Ohms)
Z_{in}	equivalent impedance seen looking into a transmission line network. (Ohms)
k	fluid flow permeability (Darcy)
μ_m	fluid viscosity (g/m·s)
k_t	thermal conductivity (W/m·C°)
ρ	density (g/m³)
c	specific heat (J/g·C°)
E	electric field vector (V/m)
H	magnetic field vector (A/m)
A	magnetic vector potential (A)
F	electric vector potential (V)
ψ	scalar potential (V)

1. Background and Problem Identification

1.1 General Background

Alberta oil sand deposits are estimated to contain 1350 billion barrels ($215 \times 10^9 \text{ m}^3$) of bitumen resources, or about twice the amount of recoverable conventional reserves in the entire world'. At present, however, less than 10 percent of these reserves can be economically recovered by any current mining technique due to the great depth of the materials overlying the bitumen containing sands.

A great amount of research has been directed toward methods of recovering deeply buried bitumen directly from its native formation without mechanically removing the sand, and many "In-Situ" recovery methods have been proposed. Most of the proposed recovery methods operate on the premise, that if the tar like bitumen in a formation can be heated well above its ambient temperature of about 10 degrees Celsius, then the bitumen's viscosity will drop sufficiently for it to flow through its native sand bed and be collected.

The major difficulty encountered in thermal schemes is that of transferring energy into the oil sand formation. The sand bed holding the bitumen, while quite permeable when considered in isolation, has quite different properties when saturated with the tar like bitumen. Basically, oil sand has many of the properties of solid rock'. Oil sand is a relatively poor thermal conductor, and thus is difficult to heat by thermal conduction. Oil sand is also virtually

impermeable, and hence is difficult to inject with hot fluids or gases. While the poor thermal conductivity and low permeability of oil sand, thus, preclude or inhibit the use of conventional heating schemes, they pose no obstacle to heating by use of electromagnetic energy. Indeed, electromagnetic energy, in spite of its relatively high cost per unit of energy, shows exceptional promise for the in-situ heating of oil sand. The principal advantage attributed to electrical methods is that since they heat from within, they allow energy transfer deep into the formation at a much faster rate than thermal conduction would allow. Further, the electrode placement allows the energy to be deposited in a controlled manner thus minimizing wasted energy (ie. the heating of non-oil bearing overburden/underburden zones).

At present, electrical schemes are mainly directed toward pre-heating a large block of the oil sand material well above its original in-situ temperature, the concept being that once the viscosity of the bitumen has been lowered sufficiently for it to become mobile, the bitumen can be produced from the formation by, for example, a steam drive mechanism.

1.2 Electromagnetic Heating

1.2.1 Heating Mechanisms

When a time harmonic electromagnetic source is used to excite an oil sand formation; each unit volume in the formation is exposed to some degree of electrical potential gradient. In response to this drive an electrical current is established through the unit volume. The current generated is normally separated into two components. The component of current in time phase with the potential across the volume is termed the conduction current. The current in time quadrature with the potential is termed the displacement current. If the conduction current is greater than the displacement current in a material, the material will be called a conductor. If the displacement current is larger than the conduction current in a material, the material will be termed a dielectric.

In heating problems the conduction current component is of the most interest as the amount of energy transferred from the electromagnetic fields to the material (the ohmic volume heating) is dependent on the conduction current component but independent of the displacement current component. The conduction current passing through a unit volume of material is normally a linear function of the magnitude of the potential gradient established across the volume. In this situation the material may be assigned a property relating the in-phase current density passing

through a unit volume, to the magnitude of the potential gradient established across it. The property is called conductivity (σ). Any mechanism which transforms the applied electromagnetic field energy into thermal energy, in a material, contributes to the conductivity of the material.

In Athabasca oil sand a major contribution to conductivity comes about as a result of free ions being available in the naturally present or "connate" water (a description of the structure of Athabasca oil sand is included in appendix B). The ions are accelerated by the applied potential gradient and then they dissipate the gained kinetic energy through collisions which add to the amount of random thermal motion in the material. Temperature is a measure of the degree of this random motion and will therefore rise. Heating occurring as a result of the presence of free charge carriers may be termed *conduction* heating.

A second mechanism contributing to the conductivity of oil sand comes about as a result of the slightly polar nature of water molecules. When exposed to a potential gradient the molecules tend to rotate and align with the potential gradient. The rotational energy imparted to the polar molecules is eventually transferred to other molecules and thus adds to the degree of random thermal motion. A contribution to the overall average motion represents an increase in temperature. When a time harmonic potential is applied to a formation the polar molecules tend to rotate in

alternate directions in response to the cyclic potential gradient. The amount of motion added by this mechanism in any given time period increases as the number of potential cycles in the time period increase. The contribution of this mechanism to conductivity is thus small when a low operating frequency is used but much more pronounced if a high operating frequency is used.

In Athabasca oil sand the conductivity (see figure 1.2) is essentially constant with frequency up to about 1 MHz. Thereafter it gradually rises to higher levels at higher frequencies as the rotational losses associated with polar molecules increase. The contribution of this second mechanism to conductivity is thus small compared to the ionic contribution for frequencies below 1 MHz but can be identified as the dominant contributor at frequencies above about 10 MHz.

In materials which do not have free charge carriers the ratio of conduction current to displacement current is generally quite small and the material is termed a dielectric. Such materials are difficult to heat with low frequency electromagnetic energy. The potentials that must be applied to a low conductivity material before substantial heating takes place can easily exceed the electrical breakdown strength of the material. If the material has any polar molecules, however, its conductivity can be increased by operating at a higher frequency. The conductivity increase permits heating to occur with much lower applied

potential. Such an approach is termed *dielectric* heating and has been used to heat low moisture oil sands such as those found in Utah.

Having briefly reviewed the basic electromagnetic heat generating mechanisms in oil sand, one may now proceed to examine the heating process on a more macroscopic scale. Electromagnetic heating methods applied to oil sand bodies may be divided into two basic categories, low frequency methods and high frequency methods. Different limitations are experienced depending on the method used.

1.2.2 Low Frequency Methods

The availability of large amounts of electromagnetic energy at a frequency of 60 Hertz provides a considerable economic bias for heating a formation at this frequency. The heating methods at this frequency all involve the placement of a suitable array of electrodes directly into the formation to be heated. The electrodes are then excited to establish a conduction current flow through the formation. Bulk resistive heating of the formation structure occurs and the resulting temperature rise reduces the viscosity of the bitumen.

Heating at this frequency does, however, have some difficulties. Unless electrode structures with very large surface areas are used, the current density throughout the formation is highly non-uniform. Typically, the formation volume nearest the electrodes, where the current density is

highest, heats more rapidly than the rest of the formation, the result being a non-uniform temperature distribution across the block of formation being heated'. Indeed, the formation material immediately surrounding the electrodes can rapidly heat to the point where the connate water is flashed off. Once the water is lost the electrodes are surrounded by an insulating (water depleted) zone. At 60 Hz this depleted zone need only be a few millimetres thick to effectively stop all current flow, and heating of the formation could be terminated at a point in time when the central oil sand region between the electrodes has only risen a few degrees above its original temperature.

A number of suggestions have been put forward for overcoming this contact difficulty. These include pressurizing the electrodes to increase the temperature at which formation water turns to steam, cooling the electrodes to prevent flashing, artificially extending the electrode's effective surface area to lower the current density in the oil sand near the electrode and injecting conductive fluids to replace the flashed water.

1.2.3 High Frequency Methods

The heating of oil sand formations with frequencies greater than 60 Hertz has the economic disadvantage of requiring an additional energy conversion stage with its attendant capital costs and energy losses. The capital cost of a high power RF source is not, however, large compared

to the total capital costs associated with most in-situ recovery schemes and the efficiency of class C amplifiers can approach that of electric motors (85-95%). Thus, if any significant advantage can be shown for heating an oil sand

mation at a high frequency rather than 60 Hz, the former should be as economically viable as the latter.

The most obvious advantage of using a higher operating frequency is that the problems associated with an insular gap forming around the electrodes are reduced. At higher frequencies current may be capacitively coupled across the gap, thus maintaining contact with the formation to be heated. Further, this non-conductive transfer of current away from the electrode surface results in a larger effective electrode surface area than is obtained with 60 Hz excitation. This spreading effect should alleviate overheating of the oil sand near the electrodes and thereby improve the uniformity of the temperature distribution in the formation.

High frequency heating is also attractive for heating formations such as the Utah oil sands^{4, 5} which have a very low moisture content and, therefore, a very low electrical conductivity at low frequencies. The energy absorption of such material is very low, even if potentials approaching the material breakdown limit are applied. Since the electrical conductivity of oil sand increases with frequency, a high frequency excitation is desirable in this case in order to obtain significant energy absorption by the

formation material.

At high frequencies the typical volumes of Athabasca oil sand to be heated have dimensions that are large compared to the wavelength of the electromagnetic energy. The energy transfer mechanism must, therefore, be viewed as a wave propagating into the formation and being attenuated (giving up its energy) as it travels. The energy distribution tends to be as shown in Figure 1.1 and is described by a decaying exponential of the form $e^{-\alpha z}$, where z is the distance into the formation and α is the attenuation constant.

As a measure of the depth into a formation that a wave will propagate before giving up the bulk of its energy, it is typical to compare distances to the "depth of penetration". The "depth of penetration", Δ , is the distance that a uniform plane wave will propagate into a material before its field strength is reduced to 36.8 percent ($1/e$) of its initial value and the power density is correspondingly reduced to 13.5 percent of its initial level ($\Delta = 1/\alpha$).

For a uniform plane wave travelling in a lossy material for which the conduction current dominates, the depth of penetration can be approximated by

$$\Delta \approx (1/\pi f \mu \sigma)^{1/2} \quad (1.1)$$

in which case it is generally referred to by the more familiar term "skin depth". In the following sections the depth of penetration will generally be referred to as skin

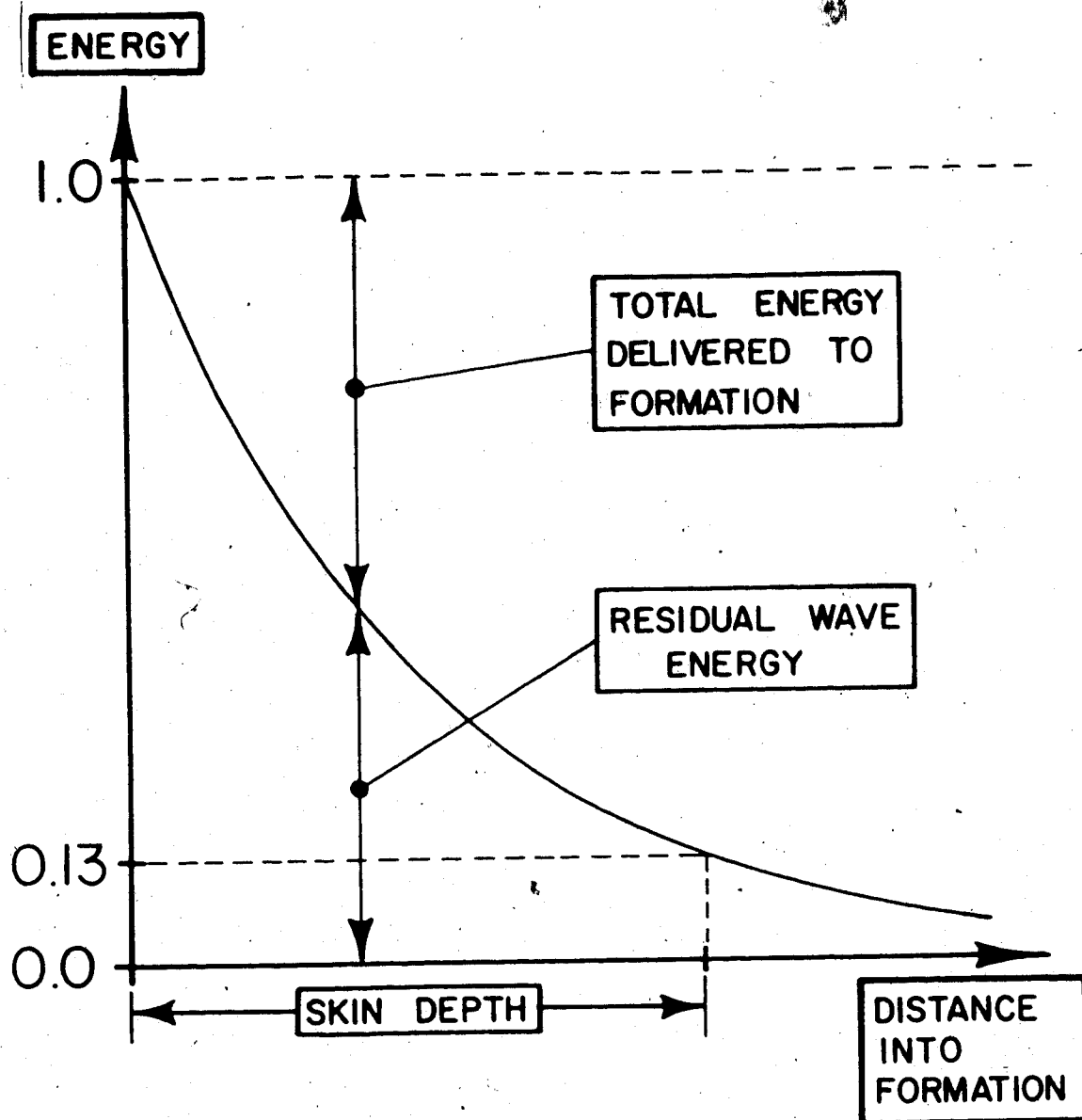


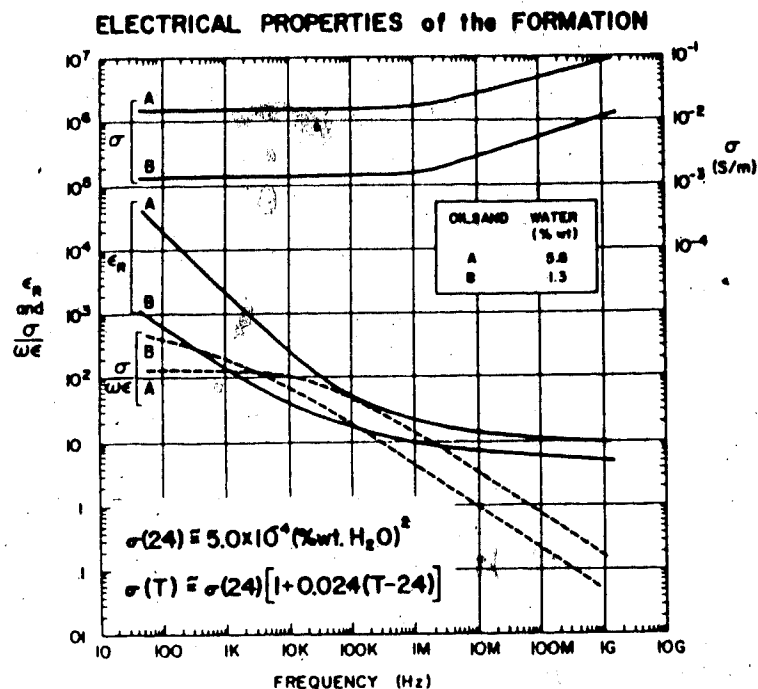
Figure 1.1: Energy deposition of an electromagnetic wave in a lossy oil sand formation.

depth, but in each case it should be taken to mean the reciprocal of the the attenuation constant rather than the approximation quoted above.

An examination of figure 1.1 would imply that very non-uniform heating of the formation would result unless all dimensions of the formation block to be heated are much less than the skin depth distance. If reasonably uniform heating of a formation block is desired a necessary requirement is that all dimensions of the block be restricted to be much less than the skin depth value. This size restriction can be met while still heating large blocks of material, if the formation is a low loss material such as the oil sands of Utah^{4, 5}, this being due to the large skin depth values associated with such materials. As an example, for the operating frequency of 1 MHz, the skin depth of the Utah Sunnyside⁴ deposit is about 470m at 22°C.

This dimensional size restriction is much more limiting if applied to more lossy materials such as the water wet oil sands of the Athabasca region. The skin depth distances for a range of Athabasca oil sand types are reproduced from reference 7 as figure 1.2. As an example consider a bitumen rich, low moisture, oil sand (type B on figure 1.2) at an operating frequency of 1 MHz. The skin depth value is about 15m. The largest dimension of a oil sand block to be heated would thus be restricted to about 3 to 4 metres. This size limitation must be overcome if high frequency heating is to be used for oil sands of the Athabasca type.

(a)



(b)

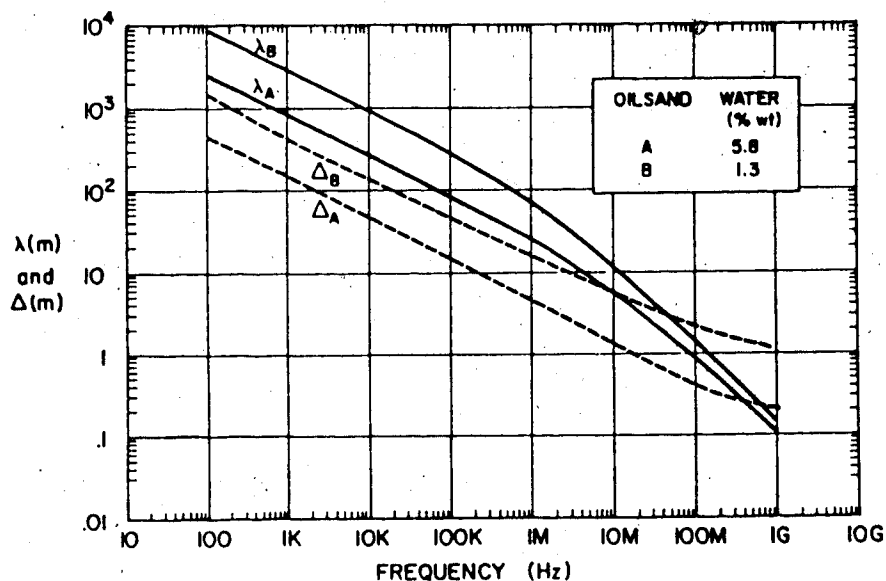


Figure 1.2: Electrical properties of Athabasca oil sand. Type A is low grade oil sand (high moisture, low bitumen). Type B is high grade oil sand (low moisture, high bitumen).

a). Conductivity σ , relative dielectric ϵ_r , and loss tangent $\sigma/\omega\epsilon$ for oil sand as a function of frequency and at a temperature of 24°C.

b) Wavelength λ and skin depth Δ for oilsand as a function of frequency at 24°C.

Both high frequency and low frequency electromagnetic heating require the placement of electrodes in or near the oil sand body to be heated. Two methods of electrode placement are currently under consideration by the industry. The first method is to sink electrode wells directly from the surface through up to 400 metres of overburden to contact the 20 to 40 metres of bitumen rich sand. The electrodes are insulated in the overburden regions. The second method is to sink a shaft through the overburden and then cut cross shafts either in the oil sand or in the underlying bedrock. Electrode wells are then drilled into the oil sand payzone from the tunnel system. The advantage of this "mine assisted" electrode placement scheme is that essentially 100% of the electrode well is in contact with the payzone area to be heated. For a given contact area the drilling costs for this latter scheme are much lower. The savings must, however, be considered against the additional cost of the shaft and tunnels. The mine assisted electrode placement scheme is preferable for high frequency electromagnetic heating since the wellbore losses associated with transferring large amounts of power through the overburden, to the payzone, increase with frequency and can become a limiting factor.

1.3 Guided Versus Unguided Electromagnetic Waves

There exists a multitude of conductor configurations for launching or guiding an electromagnetic wave. It is, therefore, first of all necessary to establish which configurations show the best promise for obtaining uniform heating of large blocks of oil sand of the Athabasca type.

First consider launching an unguided wave into the formation. This approach has the advantage of not requiring the placement of guiding conductors into the formation. Unfortunately, this is not a viable option for oil sands of the Athabasca type. An examination of figure 1.2 shows that the ratio of conduction current to displacement current is much greater than one, except at very high frequencies where the skin depth is prohibitively small. It is very difficult to generate an unguided electromagnetic wave in a conduction dominated medium. An antenna structure buried directly in the material would not generate significant radiation fields and the conductivity of the material is high enough that an externally generated wave would be largely reflected away from the surface of the formation rather than penetrating into it. Therefore, the use of unguided waves as a heating mechanism for oil sands of the Athabasca type is ruled out, except perhaps in instances where it is desirable to limit heating to the vicinity of the well-bore.

An alternative method of impressing an electromagnetic wave on the formation is to place conductors into the oil sand body such that a transmission line is formed to guide

the wave into the formation. With a suitable matching network between the source and the formation conductors, a propagating electromagnetic wave can be established in the oil sand material.

1.4 Research Objectives

The objective of the current line of examination is to analytically and experimentally examine a number of transmission line type electrode configurations to determine if large blocks of Athabasca oil sand can be heated reasonably uniformly and in a sufficiently short time so that thermal conduction losses to the surrounding formations are minimized. The greatest difficulty immediately foreseen is that this will require heating depths into the formation that are significantly greater than a "skin depth". A secondary effect is that these distances may in fact be a significant portion of a wavelength, in which case an irregular heating distribution can result irrespective of the formation conductivity. It will be necessary to circumvent these limitations if the advantages of high frequency electromagnetic heating are to be exploited.

1) The concept of establishing a transmission line structure in an hydrocarbonaceous formation and then heating the formation using high frequency electromagnetic energy is not new. The IIT Research Institute has proposed^{4, 5} such a scheme for the heating of oil shales and dry oil sands such as those found in Utah. The methods proposed by IITRI are,

however, oriented toward heating very low conductivity materials ($\sigma \ll \omega\epsilon$) by inducing dielectric losses through the use of very high operating frequencies. The methods put forward by IITRI are not viable in oil sands of the Athabasca type due to the very different electrical characteristics which are encountered. The water-wet oil sand of the Athabasca region tends to be a conduction current dominated ($\sigma \gg \omega\epsilon$) material which at any given frequency has a substantially smaller skin depth value than is found in the oil-wet oil sands of the Utah region (typical values were presented in section 1.2.3). The IITRI method calls for the maximum dimension of the formation block to be heated to be less than one-third of a skin depth. If this restriction is applied to Athabasca oil sand the size of the heated volume becomes unreasonably small.

The objective of this thesis is to propose and examine several novel high frequency transmission line heating configurations. These include the concepts of *partial evaporation boring, dielectric coated lines, series resonated lines, variable coupling electrodes, and production controlled heating.*

The general plan of the thesis is to present a brief description of these concepts in chapter 2 to give the reader a conceptual understanding of the ideas involved, followed by supporting experimental results in chapter 3. Subsequent chapters contain descriptions detailing subsidiary areas developed to support the main concepts.

These subsidiary areas include a description of a numerical model developed to aid in the selection of suitable scale model electrode configurations, a description of the scaling considerations required to construct a scaled electrothermal model which emulates a larger scale in-situ heating process, a description of a numerical model used to examine gravity production of bitumen from an electrically heated oil sand formation, and finally an analytical examination of the form of electromagnetic fields which can be established on a transmission line buried in an oil sand type of material. A reader interested in obtaining only an overview of the material may do so by reviewing chapters 1 to 3. It should be pointed out that the present work does not contain a definitive examination of any of the proposed configurations. The present work was directed toward examining as many promising configurations as possible, the objective being to establish the basic feasibility of each configuration and its relative merits compared to the other configurations. In this manner the configurations showing the most promise and warranting more detailed examination may be identified.

2. A Conceptual Discussion of Possible Electrode

Configurations and Modes of Heating

As previously mentioned a number of different electrode configurations and operating modes will be considered for in-situ heating of oil sand bodies using high frequency electromagnetic energy. In this chapter only a brief operational description is given for each configuration. Subsequent chapters expand and examine in more detail each of the individual concepts.

2.1 Total Evaporation Boring

In this first proposed scheme the field placement of electrodes would involve sinking a mine shaft from the surface through the oil sand bearing formation (payzone) and then driving out two cross shafts horizontally. From the cross shafts located at the top and bottom of the payzone, horizontal boreholes would be driven deep into the formation and cylindrical copper clad pipes would be inserted. This configuration is shown in figure 2.1. By attaching a high frequency source between the upper and lower electrodes an electromagnetic wave propagating horizontally away from the cross shafts and into the formation would be established.

The action of the multiple electrodes is expected to create the approximate equivalent to a parallel plate transmission line with the payzone sandwiched between the plates. As such, the heating of the payzone should be reasonably uniform across the width of the line except near

the edges where fringing will occur. The heating will not, however, be uniform along the length of the line (into the formation) due to the skin depth phenomenon.

For this first configuration the proposed method of overcoming the skin depth limitation is based on the relationship between the electrical conductivity of oil sand and its moisture content'. It has been found that the electrical conductivity drops very rapidly as the moisture content is reduced. Correspondingly, the wave attenuation rate falls and the skin depth increases as the electrical conductivity decreases. The postulated action is then as follows. When the source is first energized, the bulk of the heating will be near the line input with only limited deeper heating, as shown in figure 1.1. However, once the front end of the line reaches the boiling point of water, evaporation will cause the moisture level near the input to drop. This drop in moisture level will cause the conductivity of the material near the input to greatly decrease and to become, in effect, transparent to the electromagnetic wave. The wave may thus pass through the initial part of the line with little energy loss and impinge on progressively deeper portions of the formation. No standing wave heating irregularities (see section 2.3) are expected with this technique, since any pattern generated can be expected to shift along with the advancing wavefront and thus average out the heating effects. Note that virtually all the water in the formation must be heated and evaporated for the

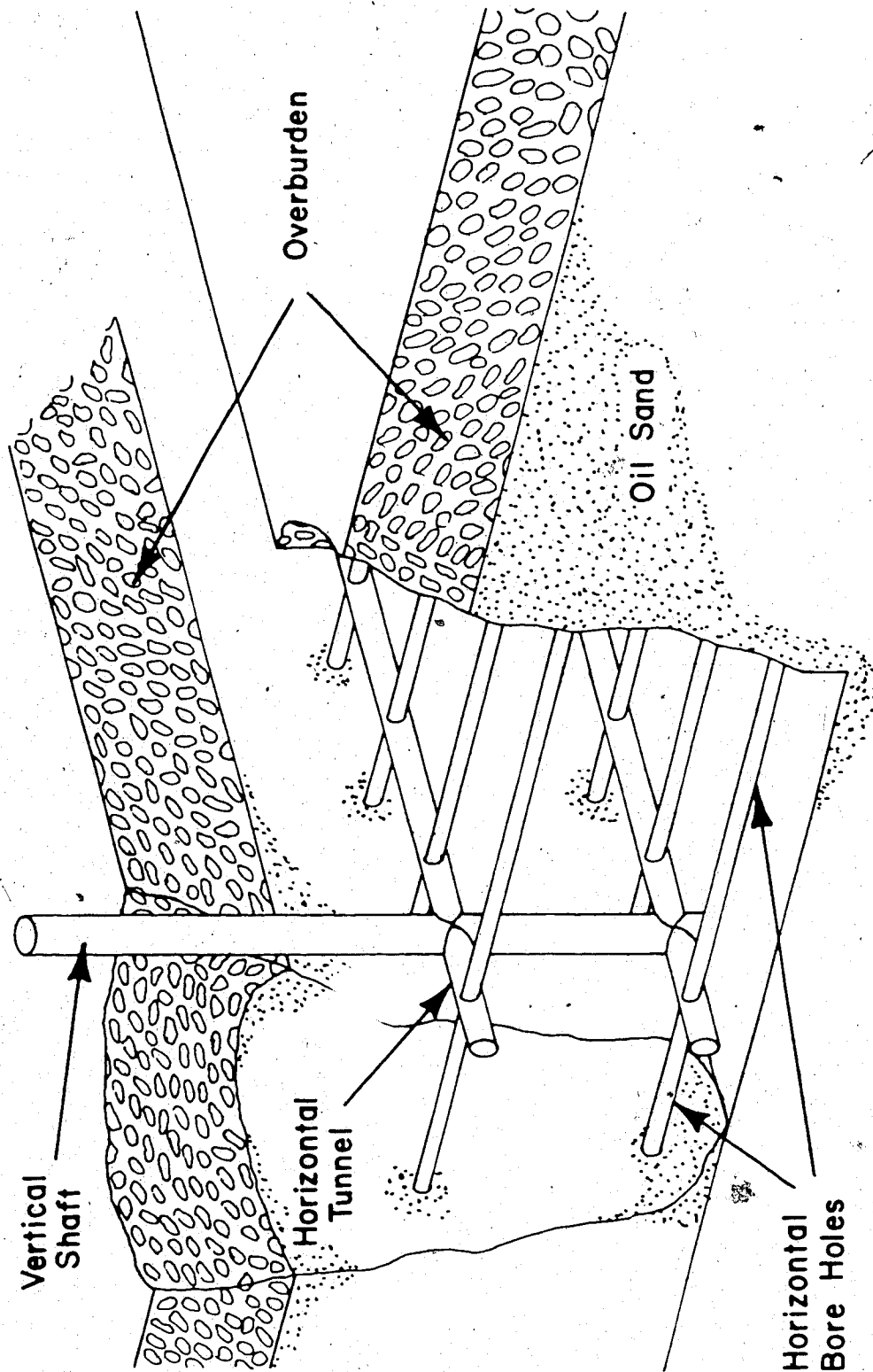


Figure 2.1: A sketch showing one possible means of placing electrodes into the oil sand formation. The electrodes are placed in horizontal bore holes drilled into the formation payzone from mined cross shafts.

wavefront to progress.

An unscaled experimental verification of the postulated boring action in Athabasca oil sand material was undertaken. A description of the experimental set up and the results obtained is presented in section 3.1.

It should be pointed out that there are a number of possible disadvantages foreseen for this basic method. First of all, a significant amount of energy is wasted by boiling off most of the moisture in the oil sand. For example, the energy needed to boil off the moisture in an oil sand in which the water makes up three percent of the weight would be about half of the energy expended to heat the oil sand up to 100°C from 10°C. The second possible disadvantage has to do with the oil sand structure. The Athabasca oil sands are termed "water-wet", which means that each sand grain has a thin film of water surrounding it and buffering it from the interstitial bitumen. This is an important property from a recovery point of view since the bitumen may be much more completely recovered from oil sand of this type than from oil sand in which the sand grains are bitumen wet. The water wet feature is maintained down to very low moisture contents since the volume of the thin film (15 nm) adsorbed on the surface of the sand grains is only a very small portion (0.05%) of the pore volume. The possibility, however, may exist that if the heating is severe enough this film would be destroyed and the sand would become bitumen wet.

The final unknown foreseen for this scheme has to do with the venting of the water vapor generated. The bitumen impregnated sand will have a fairly low relative permeability to gas flow. This raises the question of how fast the water vapour may be removed from the formation. Formation temperatures well above 100°C may be necessary to develop a high vapour pressure drive. It is expected that the electrodes would be perforated to allow vapour to escape. This would allow relatively easy drying of the oil sand immediately adjacent to the electrodes. The more distant oil sand in the central region between the electrodes may, however, be more difficult to dry.

2.2 Partial Evaporation Boring

The second technique proposed here would involve the same field arrangement of electrodes as presented in figure 2.1 which shows electrodes leaving the tunnel system horizontally above and below the payzone, resulting in the rough equivalent of a parallel plate transmission line with the payzone sandwiched between the plates.

In order to differentiate this method from total evaporation boring a more detailed consideration of the evaporation process is required. As was described in section 1.2 the formation heating is a result of conduction current passing through the oil sand material. There is a concentration of this current in the immediate vicinity of the electrodes and correspondingly the oil sand immediately

surrounding the electrodes experiences a larger heating rate than elsewhere. The moisture in this region is thus the first to be evaporated. The result is the creation of an insular (low moisture) zone around the electrodes. At high frequencies current will be capacitively coupled across this zone such that heating of the formation continues. Further, the thickness of this insular zone will grow with time as progressively more water is evaporated. In total evaporation boring, as described in section 2.1, the operating frequency is selected high enough that this process continues until the entire zone between the electrodes is depleted of moisture.

Consider, however, what occurs if a somewhat lower operating frequency is used such that current cannot be transferred across the insular zone. Specifically, consider an operating frequency selected such that current is coupled across the insular gap, that is developing around the electrodes, only so long as the gap width is less than a few percent of the distance between the upper and lower electrode arrays. The postulated operation is then as follows. On initial power application the heating would be largely confined to the line section nearest the wave source due to the skin depth effect. In time, however, the insular gap forming in this section will become large enough to significantly reduce the shunt current flow between the upper and lower electrodes. At this point the reduction of shunt current will imply that the wave is largely decoupled

from the formation in this section. Once decoupled, the energy in the wave will not be absorbed by this section, thus allowing the energy to be carried further along the line to heat deeper parts of the formation where the electrodes have not yet formed insular coatings of dry oil sand.

A relative advantage of this method over total evaporation boring is that only a small portion of the moisture in the formation is evaporated, thus improving the efficiency of the energy use. In addition, since only the oil sand in the immediate vicinity of the perforated electrode must be dried, considerably less difficulty may be expected in venting off the evolved water vapour.

An uncertainty in the method lies in determining the extent to which it is possible to attain a reasonably uniform temperature distribution between the upper and lower electrodes before the electrodes are decoupled.

In order to verify the postulated operation of this method, two experiments were performed. The first was an unscaled test to confirm that the postulated boring would occur (with only partial evaporation) in actual Athabasca oil sand material. A second experiment to determine the uniformity of the heating that could be obtained in the zone between the electrodes was performed by constructing and heating a properly scaled electrothermal model of the proposed electrode arrangement. The experimental setup and results obtained from these two experiments are presented in

sections 3.2 and 3.3.

2.3 Finite Length Dielectric Coated Line

The third proposed method would again have an electrode configuration essentially the same as shown in figure 2.1, except that the upper and/or lower electrodes would be uniformly coated with a dielectric material. The postulated operation would be as follows. The coating thickness and operating frequency would be selected such that the effective attenuation rate of the line is greatly reduced. For example, assume 10% of the wave energy is dissipated as the wave travels from the input matching network through the formation to the transmission line end. The abrupt impedance change at this point should cause the bulk of the wave energy to be reflected back from the line end. The reflected wave would then re-traverse the line, again losing 10% of its residual energy to the formation. The matching network would then in turn again reflect the residual wave back toward the line end. The steady state result of these multiple passes of the wave through the formation would be the eventual transfer of all of the wave energy into the formation to be heated.

The heating along the length of the transmission line would nominally be quite uniform since for low attenuation rates the wave energy deposited per unit length is essentially constant. There is, however, a limitation to this effect. If the total line length exceeds about

one-tenth of a wavelength, the forward and backward traveling waves on the line begin to have different relative phase shifts. The result is that at some points along the line the fields of the waves destructively interfere, reducing the local heating effect, while at other points the fields constructively interfere, increasing the local heating effect. This phenomenon is well understood and documented^{1,2} and the resulting electromagnetic field/heating distribution is referred to as a "standing wave".

Another electromagnetic heating effect not considered up to this point, but affecting all the schemes, comes about as a result of the temperature dependence of the oil sand conductivity. The conductivity of Athabasca oil sand increases with temperature (about 2 to 3 %/°C). A material with this property is normally considered a poor candidate for electromagnetic heating as thermal instabilities can occur. To expand on this point let us consider the simple arrangement of a conductive material, with a positive conductivity temperature relation, placed between two plate electrodes. Energizing of the electrodes would nominally lead to uniform ohmic heating of the conductive material. If, however, some volume of the material is slightly warmer, it will exhibit an increased conductivity and hence will draw a larger current through this select volume. The ohmic heating of this local volume will be higher than elsewhere and the local temperature will rise disproportionately. The local conductivity will therefore continue to rise,

compounding the effect. The heating pattern in this situation tends to break up into a number of localized hot spots, unless the material's thermal conductivity is high enough to damp out the instabilities.

In the specific case of coated electrodes, however, the effect is quite different. In the format postulated, a coating is introduced which is thick enough to greatly expand the skin depth of the transmission line. The expansion implies that the coating represents the dominant impedance to the flow of current between the electrodes. The current which passes through both the coating and the conductive material will not be significantly affected by changes in the conductivity of the conductive material. If a hot spot develops the local conductivity rises thereby decreasing the local resistance value. The local current level is, however, essentially unchanged and the local ohmic heating will be reduced. The net effect is now one which stabilizes the heating process. Hotter regions absorb less power and cooler regions absorb more power.

The magnitude of this self leveling effect is not immediately clear. However, the experimental results presented in section 3.4 suggest that the self leveling effect is effective enough to remove the heating irregularities expected from standing wave effects.

To examine the coated electrode configuration a simplified explicit numerical model of a coated two wire transmission line in a lossy medium was first developed (see

chapter 5). This model was used to examine the effects of line coatings on wave attenuation rates and phase velocity, as well as the wave energy deposition along the length of the line. Using the results of these studies as a guideline a number of scaled electrothermal models were then constructed to determine if the desired temperature uniformity could be obtained. The experimental results obtained using this concept are presented in section 3.4. This section also contains a description of a rather promising effect which is referred to as "self generated uniform coatings".

2.4 Series Resonated Line

In this fourth suggested scheme the proposed line configuration would again be essentially the same as shown in figure 2.1 except that the upper and lower electrodes would be periodically broken and a series capacitor inserted at each break in the lines. This could be accomplished by joining the threaded sections of the electrode wells with short insular sections containing the series capacitors. Assuming the spacing between the series capacitors is small compared to the skin depth and wavelength of a wave in the formation material, the capacitors may be treated as a continuously distributed capacitance (C_s). The effect of this distributed capacitance on the deposition of energy along the line can be described as follows.

Consider the potential developed between the electrodes by an electromagnetic wave propagating along the transmission line. The potential measured at successive points along the line would normally show a progressively larger lagging phase angle relative to the potential at the feedpoint. Series connected capacitors in the electrodes will, however, introduce a leading phase shift. If the leading phase shift generated by each capacitor can be made equal to the phase lag experienced by a wave as it propagates between the successive capacitors the potential across the line will have essentially constant phase at all points along the line. If this occurs, wavelength related effects such as a standing wave pattern will be eliminated.

In order to examine this effect in a more specific manner, one may make use of the distributed impedance representation of the transmission line. Consider the propagation characteristics of a wave traversing a transmission line with closely spaced series capacitors. The propagation constant of the wave travelling on the line becomes (see nomenclature section for definition of variables):

$$\gamma = \alpha + j\beta = [[R + j(\omega L - (1/\omega C_s))][G + j\omega C]]^{1/2} \quad (2.1)$$

For a good conductor

$$R \rightarrow 0$$

and for a resonant selection for C_s

$$\omega L - (1/\omega C_s) \rightarrow 0$$

Hence, at resonance, the attenuation rate (α) approaches

zero and the apparent steady state phase velocity (ω/β) and wavelength ($2\pi/\beta$) approach infinity. Typical plots of the effect of series resonating capacitance on attenuation and wavelength are shown in figures 2.2 and 2.3. These curves were generated using the numerical model described in chapter 5.

The heating mechanism postulated is then akin to the finite length coated line in that the wave traverses and re-traverses the line multiple times losing only a small portion of its energy in each pass through the formation. The major difference is that the wavelength value ($2\pi/\beta$) becomes very large, thus permitting the compensated line to avoid heating irregularities due to standing waves.

Unfortunately, an examination of figure 2.2 reveals that while an ideally infinite reduction in attenuation is possible, a large attenuation reduction would probably be very difficult to attain and maintain in a field situation. The reason is that the resonant drop in attenuation is very sharp near the perfect compensation point. The ability to maintain essentially perfect resonance over the required wide temperature range is questionable.

For this reason a slightly modified variation may be considered. The variation is to coat the line with an insulating coating as well as add series resonating capacitors. Two advantages are foreseen for this format. To describe these advantages it is first necessary to briefly review the wave propagation characteristics of an unmodified

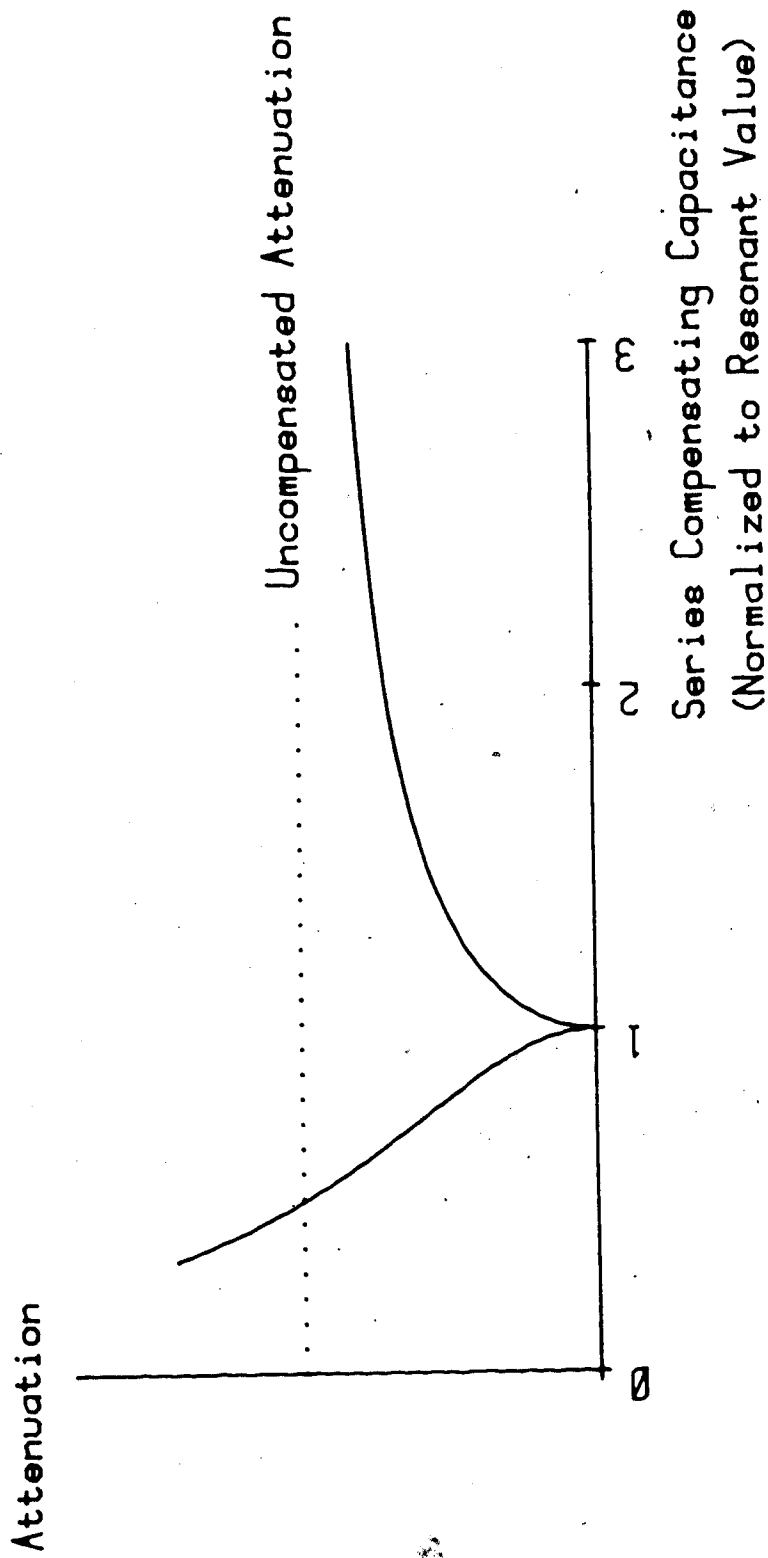


Figure 2.2: Effects of series compensating capacitance on wave attenuation rate, showing ideally zero attenuation when the line is resonated.

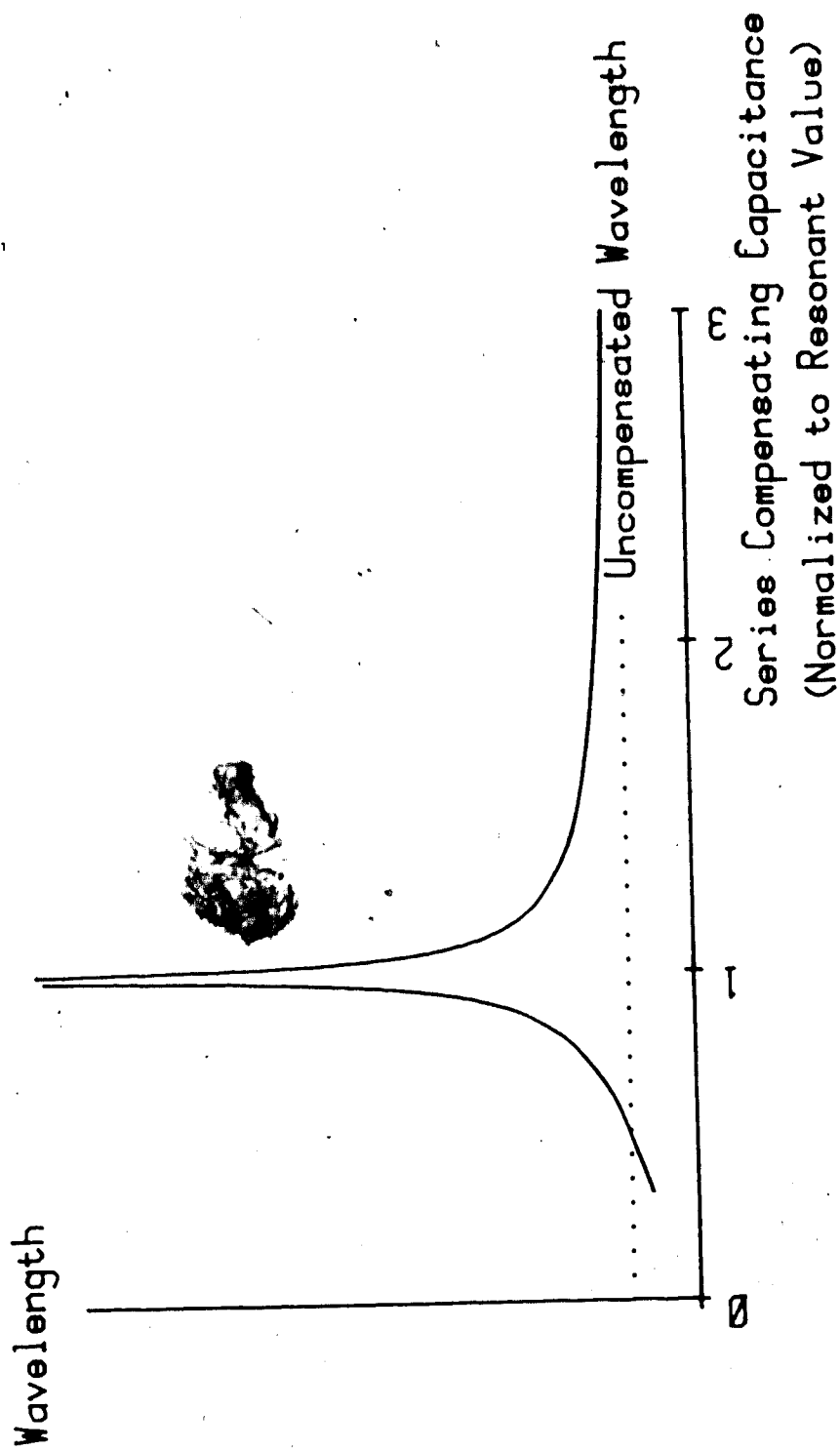


Figure 2.3: Effects of series compensating capacitance on wavelength, showing ideally infinite wavelength when the line is resonated.

line in oil sand. For the frequencies envisioned, the conduction current is much larger than the displacement current ($\sigma \gg \omega \epsilon$) for oil sands of the Athabasca type. In this situation the attenuation constant (α) and the phase constant (β) of the wave will be approximately equal. The wavelength ($2\pi/\beta$) is thus about 6.28 times the skin depth ($1/\alpha$). The requirements to obtain uniform energy deposition along a finite length line are that the line length be much less than the skin depth and the wavelength. Attenuation reduction is therefore a more critical requirement than wavelength expansion, when large depths into the formation are to be heated. Coating a line can greatly increase the skin depth, but it has very little effect on the wavelength. An advantage attributable to a coated and then compensated line is that the coating increases the skin depth and the series compensation then further increases the skin depth, but more importantly expands the wavelength which becomes the limiting factor to uniform heating along the line after attenuation is reduced. The attenuation reduction in this permutation is not critically dependent on maintaining nearly perfect resonance.

The second advantage attributable to this format over straight series compensation is that the placement of compensating capacitors is easier. The use of lumped element capacitors to simulate a continuously distributed series compensating capacitance requires that the spacing between the capacitors be much less than the skin depth and

wavelength of the wave on the line *before* the compensation is implemented. The spacing requirement arises out of the basic limitation of circuit theory analysis. Lumped element circuit theory analysis is only accurate if all portions of the circuit are much less than the wavelength and skin depth in physical extent. In this compensation scheme the required distributed series capacitance is gathered up over a finite length of line and simulated by a single lumped element capacitor. The desired resonance effect will only occur if the length of line compensated by each capacitor is short compared to the wavelength and skin depth values of the uncompensated line.

The skin depth increase of a coated line will generally be sufficient that the capacitor placements need only meet the lesser requirement that they be much less than a wavelength apart. The compensating capacitors may thus be spaced further apart (a smaller total number is required) and be of smaller size (doubling the distance between capacitors will halve the capacitor size required for a given C).

In order to examine the feasibility of series resonated lines, a number of simplified experiments were performed to verify the general effect postulated. A description of the experiments and samples of the results obtained are presented in section 3.5.

2.5 Variable Coupling Electrodes

A fifth proposed technique would involve essentially the same line configuration as shown in figure 2.1. The difference would be in the construction of the electrodes penetrating the oil sand formation. One electrode is envisioned as a copper clad pipe, the other electrode would have the physical form shown in figure 2.4.

The variable coupling electrode would involve placing or forming a dielectric sleeve along the bore hole for one of the electrodes. A smaller cylindrical conductor would then be placed in the sleeve and supported to form a coaxial arrangement. Over a portion of the line length an electrode extension bridges the air gap between the center electrode and the dielectric sleeve. The electrode extension is mobile inasmuch as its location along the length of the line is adjustable. The mobile aspect of the electrode extension can be accomplished in a number of ways. One possibility is to physically move a coaxially shaped metallic slug back and forth using a cable and pulley arrangement. Another possibility is to place a series of discs along the length of the line thereby forming a number of sealed compartments. The compartments could then be selectively flooded or drained of a conductive fluid via small feed lines passed through the inside of the centre electrode.

The envisioned operation of the line to obtain uniform heating along the length of the line is then as follows. The operating frequency of the line and the electrode geometry

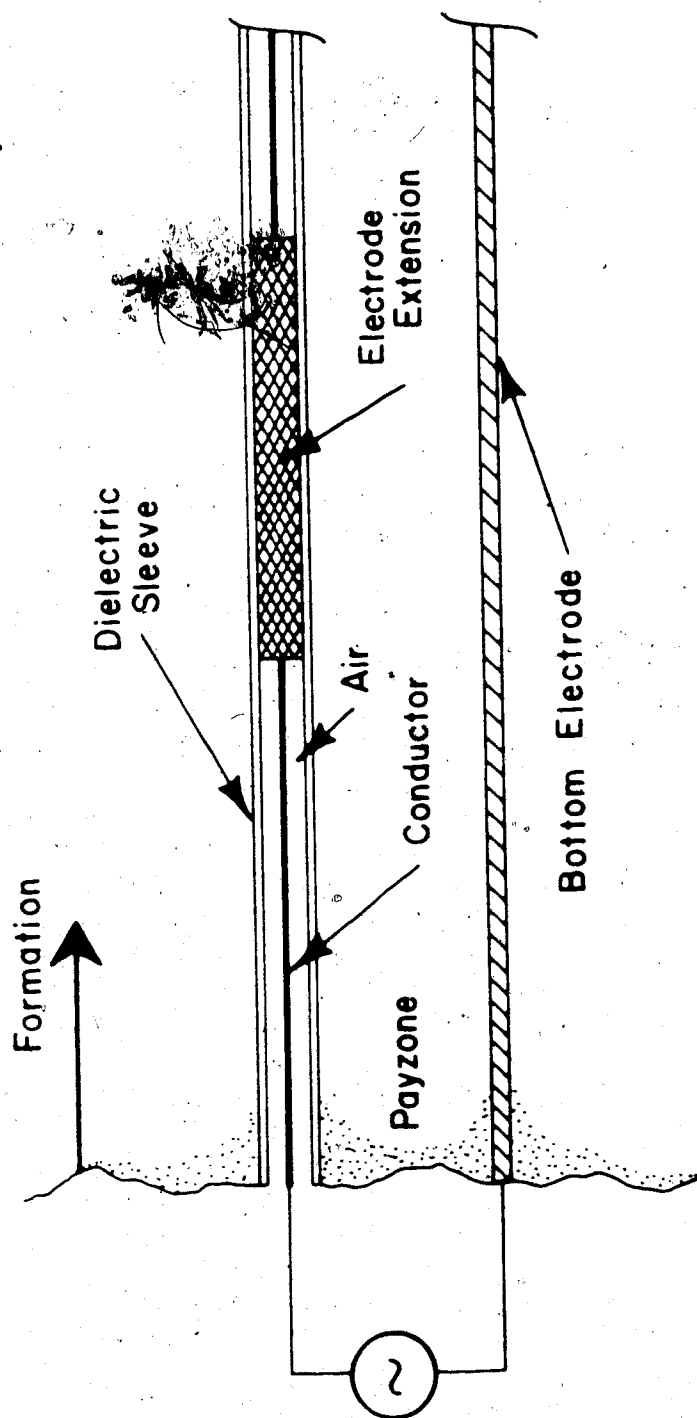


Figure 2.4: An electrode form in which high energy coupling to the formation occurs only over a selected section of the electrode length.

are selected such that the energy coupling from the center electrode to the formation is very small and in particular much less than the coupling that occurs over the line section that is provided with an electrode extension. The bulk of the wave energy entering the formation will thus be placed in the segment containing the electrode extension. This segment, being shorter than the total line length, may be more readily designed to have a length that is short compared to both the skin depth and the wavelength, such that formation heating will be uniform over the section of line with the extension. Uniform heating over the entire line length may be accomplished by cyclic movement of the electrode extension section along the total line length. A particular advantage foreseen for this arrangement is the additional controllability of energy placement introduced. Heterogeneities in the formation could be more selectively heated to attain a particular desired heating profile. The major disadvantage foreseen for this type of arrangement is that additional controllability is obtained at the expense of a considerable increase in the complexity of the electrode structures used.

A first examination of this concept using the numerical model described in chapter 5 indicated reasonable promise if an adjustable matching network was used between the RF source and the line. Some scale model work was done to illustrate this concept and the results are presented in section 3.6.

2.6 Production Controlled Heating

A sixth proposed method would involve a similar layout to that shown in figure 2.1, except that the bottom electrodes would be perforated and possibly filled with a coarse sand pack. The bottom electrodes would also all be joined to a central sump and pumping station. The rate of energy application in this configuration would be much lower than in, for example, the partial evaporation boring case. Operation to yield heating over distances large compared to a skin depth is envisioned as follows.

On initial application of power, penetration of the formation would be quite shallow and only oil sand near the source would be heated. As the temperature in this near zone rises the viscosity of the bitumen will drop rapidly and the bitumen will start to flow into the perforated lower electrode structure via gravity drainage (see section 3.7 for a more detailed discussion of drive mechanisms). This flow in turn would lead to the formation of a depleted zone near the upper electrodes (see figure 2.5). The moisture content of this depleted zone will be low due to the drainage and a limited amount of evaporation. Correspondingly the conductivity of this region will be very low. The electrode surface area and applied power levels are selected such that the fluid drainage, rather than evaporation, is the dominant effect creating this depleted zone.

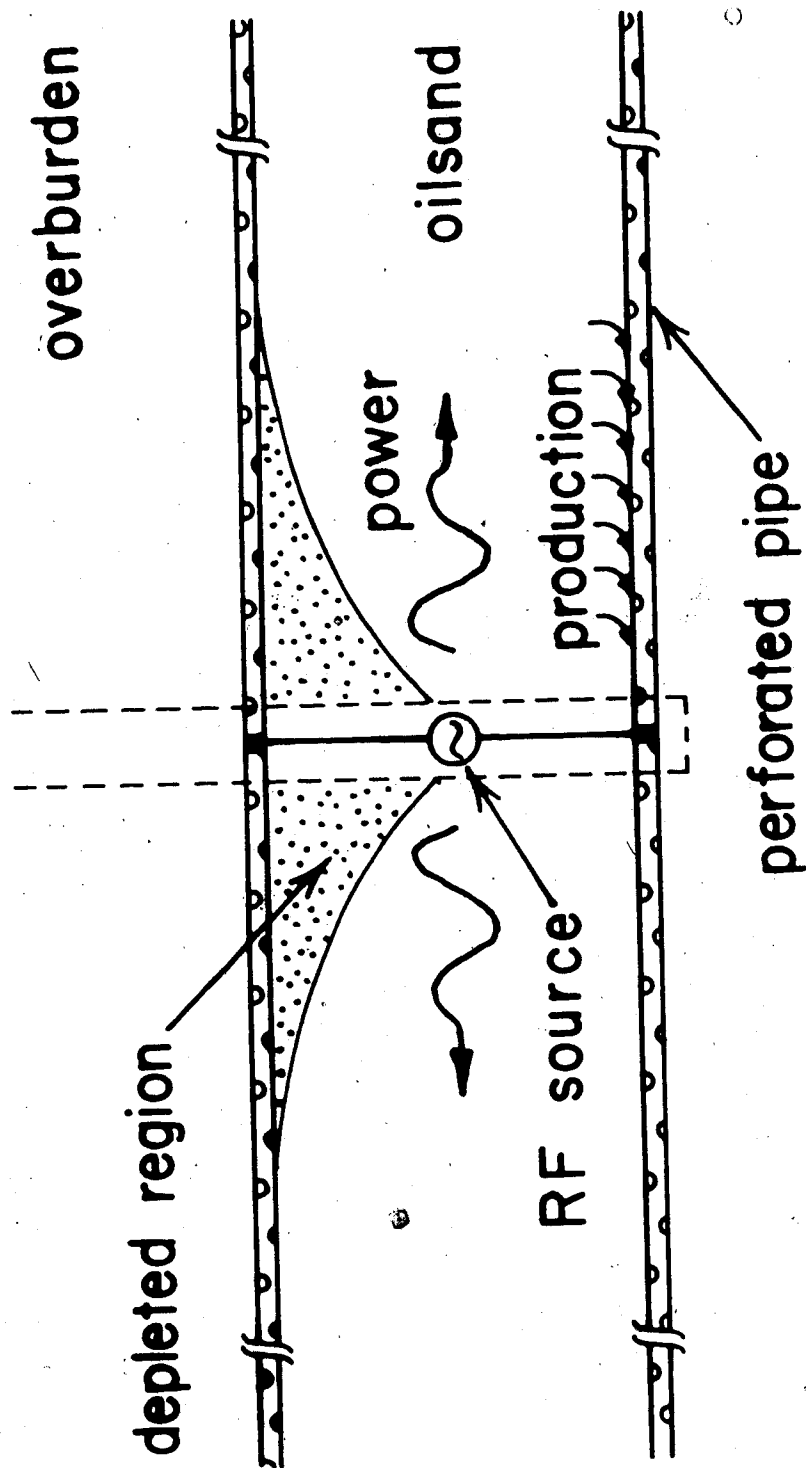


Figure 2.5: Representation of an oil sand body as production controlled heating is occurring, showing the generation of a depleted zone as production takes place.

With the suitable selection of operating frequency, the creation of this insular gap will greatly reduce the energy coupling to the formation immediately below it (the wave attenuation rate is reduced), thus allowing the energy from the source to propagate past this zone to begin heating the oil sand farther along the transmission line. The energy is thus transferred progressively deeper into the formation as more areas are heated and brought into production.

One unique aspect of this heating/production mechanism is that it may be expected to be reasonably "self-levelling". The concept is that variations in the material properties are not expected to greatly affect bitumen production. As an example of this self-leveling effect, consider the situation where, say, along a portion of the electrodes the flow permeability of the formation material is lower than elsewhere. When the electromagnetic wave impinges on this zone the initial production would be lower due to a reduced flow. The reduced flow would, however, also slow the formation of the depleted region. The electromagnetic wave would therefore stay coupled to this zone of the formation for a longer time than elsewhere and consequently raise it to a higher temperature. The bitumen viscosity is, however, a very strong function of temperature and the viscosity of the bitumen would therefore be much lower in this zone than in other zones. The reduced viscosity would increase the flow rate, thus compensating for the reduced permeability.

In order to examine the feasibility of this concept two avenues of investigation were undertaken, the first of which was to verify that the basic processes postulated actually occur. A series of experiments was executed to demonstrate that electromagnetic heating leads to fluid production and that this fluid production in turn causes a de-coupling of the electromagnetic wave. The experiments are described in section 3.7. In addition, a first order numerical model to explicitly represent the fluid flow, thermal conduction and electrical energy deposition for formation points between an ideal parallel plate line was developed (see chapter 6 for model description and assumptions). Temperature and production data from a number of simulated heating runs are presented in the same section. While care must be taken in interpreting this data due to the model limitations outlined in chapter 6, the results do show good promise and would suggest that the concept is a candidate for more detailed study at a future date.

3. Experimental Case Studies

Having discussed in principle the operation of six proposed schemes for in-situ heating of Athabasca oil sands using high frequency electromagnetic energy, this chapter now presents the results of a series of experiments conducted in order to elucidate the features and feasibilities of the various schemes.

*** 3.1 Total Evaporation Boring: Demonstration of Concept in Athabasca Oilsand**

The postulated operating mechanism for this concept (see section 2.1) calls for the wave attenuation rate of oil sand to be greatly reduced when its moisture content is lowered. To experimentally verify the validity of this assumption for Athabasca oil sand type material, the following experiment was performed.

A 1.6m length of S band rectangular waveguide was packed with a low grade, high moisture, oil sand. The waveguide was then mounted in a plywood box lined with styrofoam insulation. The insulation is required to ensure that the thermal losses from the waveguide are much smaller than the applied electrical power. A 2450 MHz microwave source was then used to generate an electromagnetic wave propagating into the oil sand. A series of thermocouples was used to monitor the midpoint temperature of the oil sand in the waveguide at various times as the heating occurred. The thermocouples could not be left permanently in place as

their presence in the guide would distort the electromagnetic fields. Temperatures were obtained by briefly turning off the source and inserting the thermocouples. The thermocouples were mounted on a jig to allow simultaneous insertion and were guided into position by small dielectric straws previously driven into the oil sand. The experimental setup is shown in figure 3.1. The source used was a Gerling Moore model 4003 microwave power source. The circulator was a Merrimac type FSCM 12457. Forward and reflected power levels were detected with a Gerling Moore model 4009 power monitor. The temperatures were measured using J type thermocouples (iron/constantan) attached to a Hewlett Packard model 3052A data acquisition system.

The skin depth of this material at 24 °C is approximately 15cm. The objective was to determine if distances significant compared to the skin depth could be heated. The temperature profiles during one of the heating runs are presented in figure 3.2.

The temperature profiles obtained are consistent with the postulated heating mechanism inasmuch as only limited depth heating occurs until the oil sand near the input reaches 100 °C and the moisture begins to evaporate. After this occurs deeper heating begins, which implies that the attenuation rate in the oil sand near the input has been reduced, thereby permitting wave energy to pass through to deeper regions.

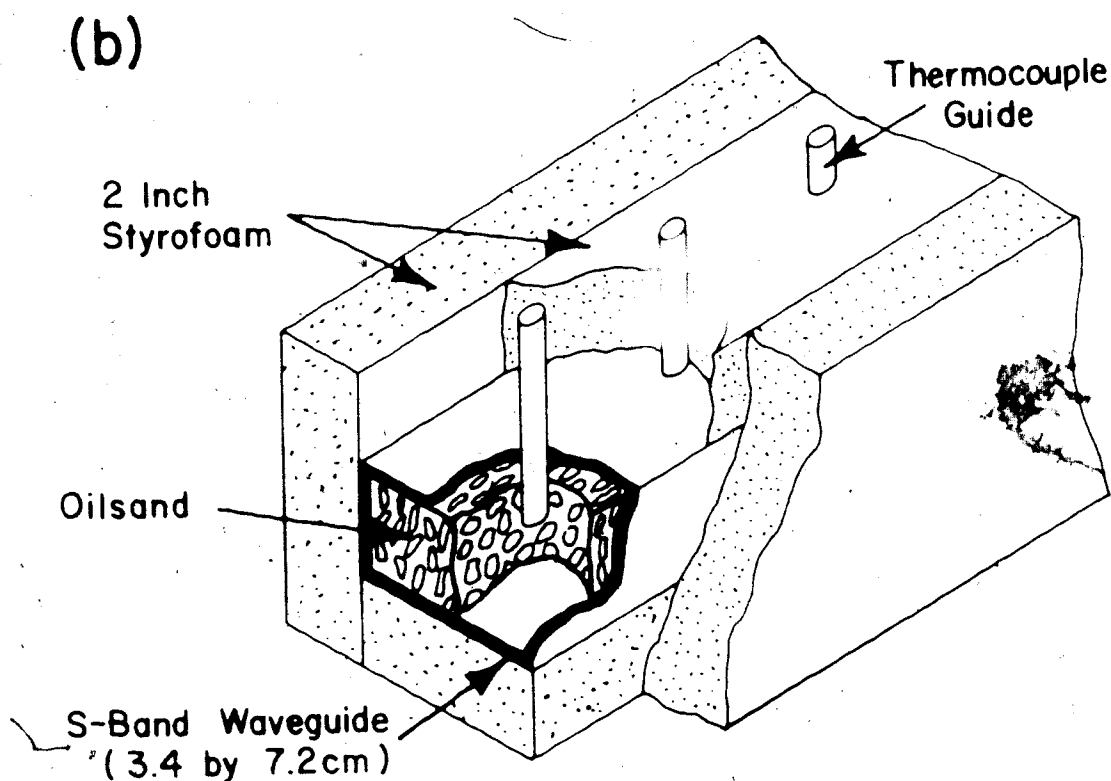
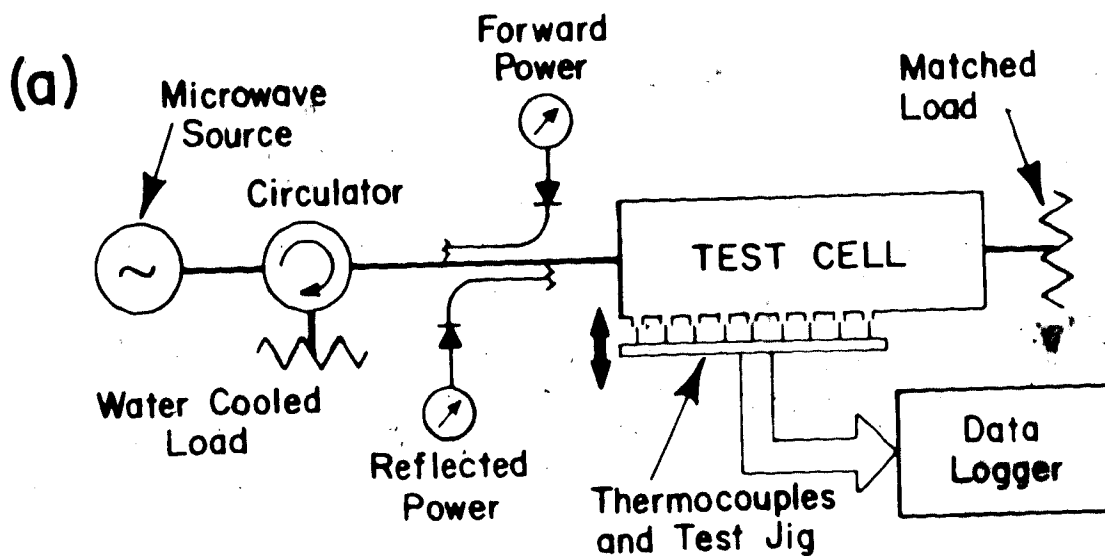


Figure 3.1: Experimental demonstration of total evaporation boring concept.

- a) Apparatus interconnection showing excitation and instrumentation connected to the test cell.
 b) Construction details of the test cell packed with oil sand. The oil sand is heated by passing an electromagnetic wave through it.

Power = 220W

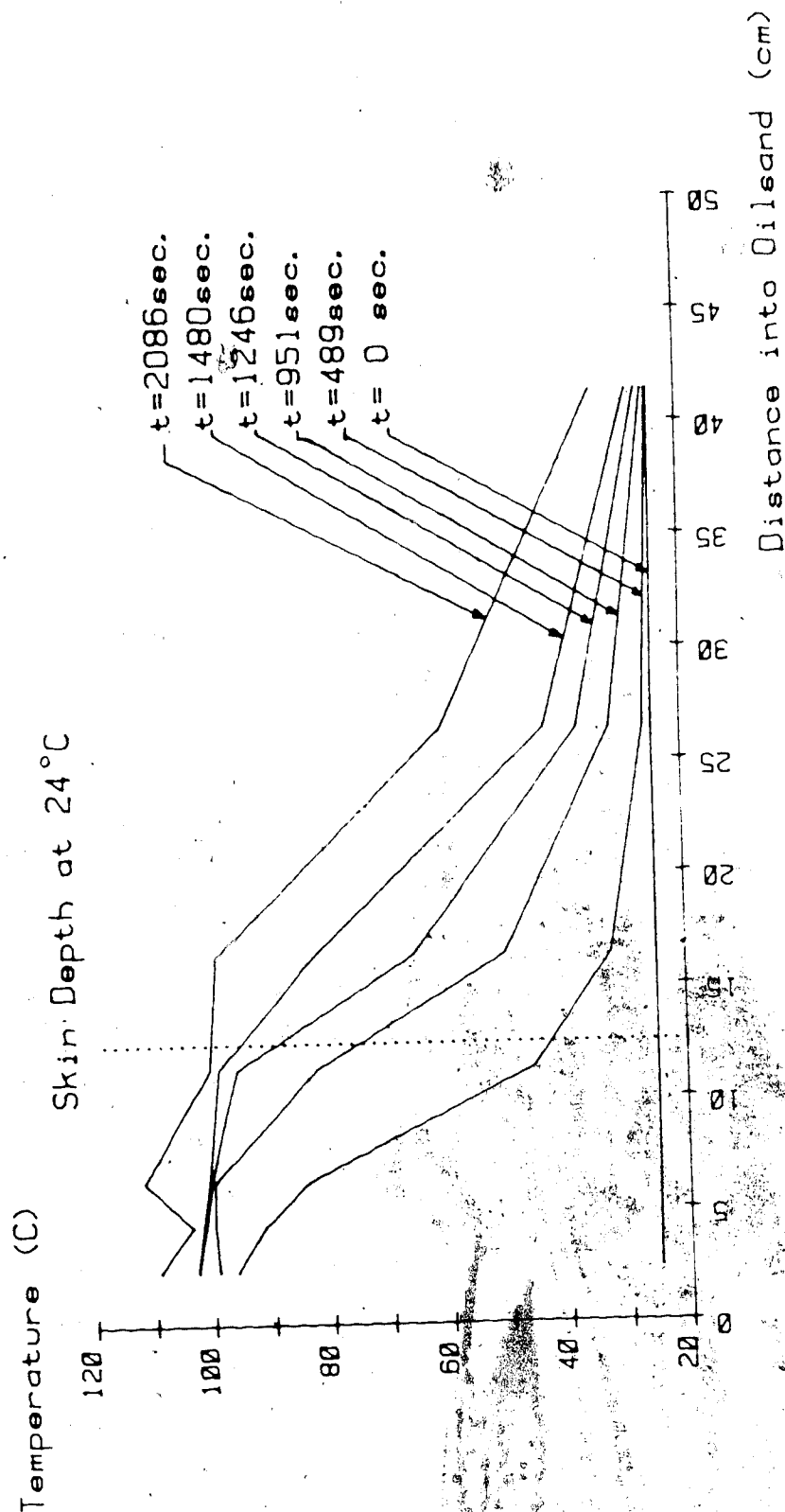


Figure 3.2: Total evaporation boring demonstration. Plot of midpoint temperatures obtained along the length of the waveguide, at various points in time as the heating run progresses.

An analysis of the percent moisture, by weight, of the oil sand was performed for both the source material used to pack the waveguide and the material dug out of the first few centimetres of the waveguide after the heating run. The weight percent water of the original oil sand was 7.6%. The weight percent water of the sample from the input region of the waveguide upon completion of the heating run was 0.25%.

One of the principal advantages postulated for electromagnetic heating was that it would allow an oil sand formation to be heated much more quickly and uniformly than any heating mechanism which is dependent on thermal conduction for energy transfer into the formation. In order to obtain an empirical comparison of the two effects a second experiment was performed as follows.

New oil sand was packed into the waveguide and an electric contact heater was placed in intimate contact with the oil sand across the face of the waveguide. The heater was fabricated by placing a stove top heating element in a machined brass holder and fixing it in place with a ceramic epoxy compound. Power was then supplied to the heater from a variac and the central oil sand temperature along the length of the guide was monitored with time. The power level to the heater was monitored using a Feedback model EW604 electronic wattmeter. Two experiments were tried. In the first case the heating plate temperature was held at 100 °C. The profiles obtained are shown in figure 3.3. In the second case the heater was heavily insulated with rock wool and a constant

Input Temperature 100 C

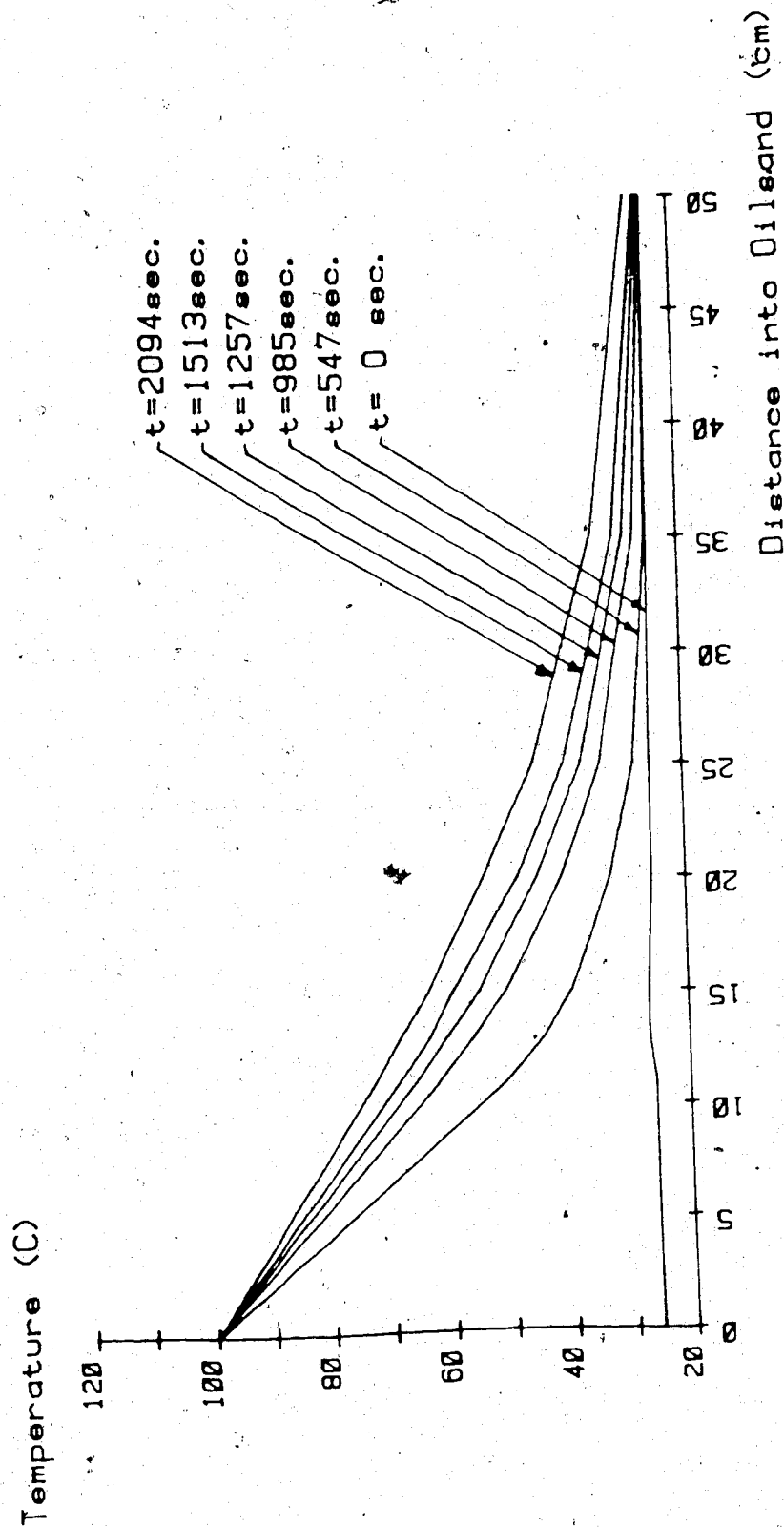


Figure 3.3: Conduction heating comparison to electromagnetic heating. Oil sand is packed in the same waveguide test cell as used for total evaporation boring experiment. Plots are of midpoint temperatures obtained along the length of the waveguide. The input heater was held at a constant 100°C.

220W (the same power as in the electromagnetic case) was supplied to the heater. The temperature profiles obtained are shown in figure 3.4. In both cases the results suggest that thermal conduction heating is much slower than electromagnetic heating in terms of depth heated in a given time. Further, the temperature distributions obtained are highly non-uniform.

The total evaporation boring experiments demonstrated that the energy absorption of an electromagnetic wave in Athabasca oil sand decreases as the moisture in the sand is evaporated. The postulated boring action of the wave was observed, as evidenced by the advancing heat front visible on the temperature profile graphs. Distances into the oil sand which are significant compared to the skin depth value have been heated. The experiment was, in summary, a reasonable success. The total evaporation boring concept was not, however examined in any more detail. The reason for this action was that the partial evaporation boring experiment described in the next section showed equally good results with much less moisture evaporation being required (better efficiency). This latter concept was deemed more promising (for reasons previously mentioned) and efforts were directed toward examining it in more detail through the use of scaled electrothermal models operating in the partial evaporation mode.

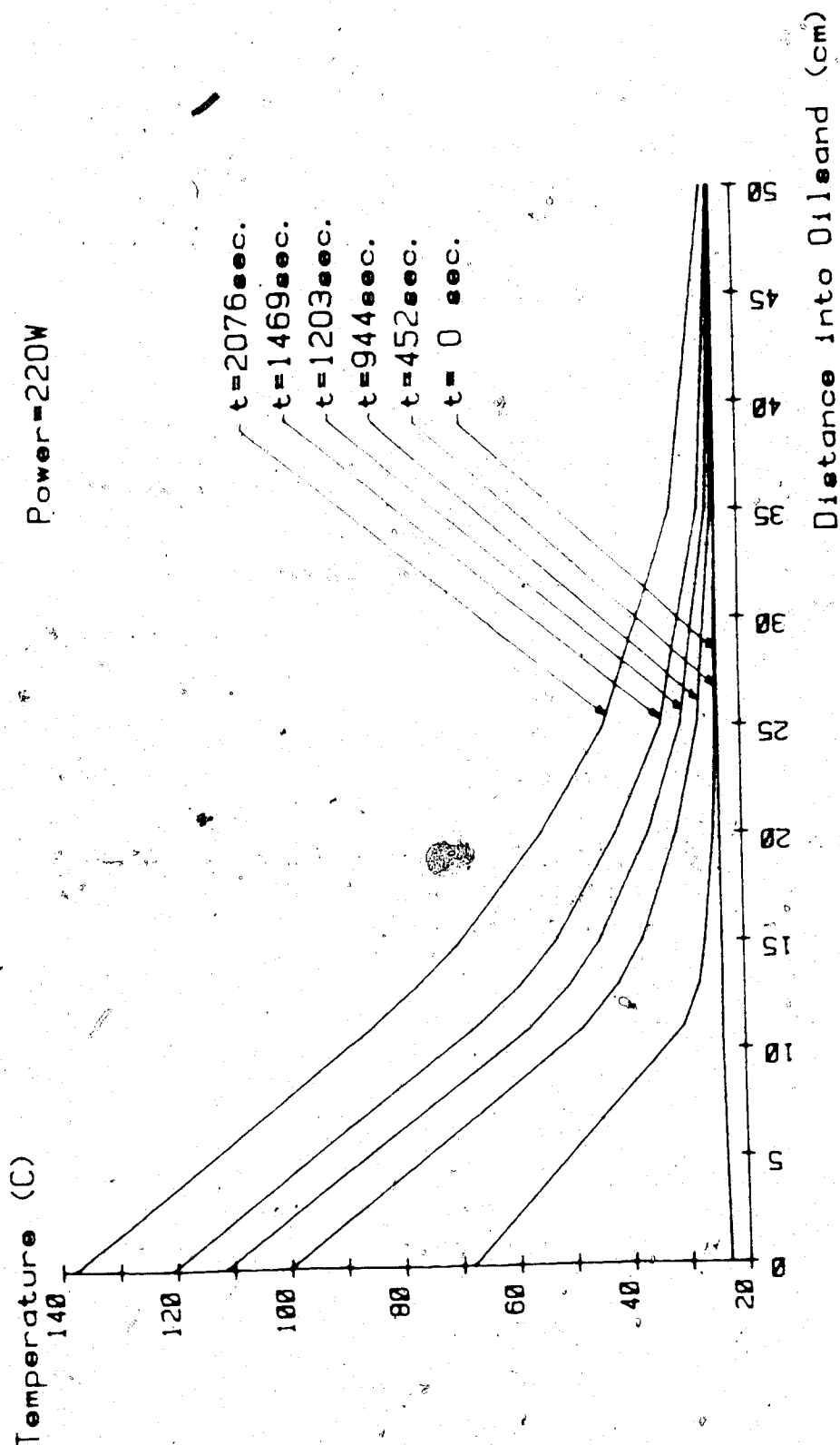


Figure 3.4: Conduction heating comparison to electromagnetic heating. Oil sand is packed in the same waveguide test cell as used for total evaporation boring experiment. Plots are of midpoint temperatures obtained along the length of the waveguide. The input heater was supplied with a constant 220W.

3.2 Partial Evaporation Boring: Demonstration of Concept in Athabasca Oilsand

The postulated operating mechanism for this concept (see section 2.2) calls for the wave attenuation to be reduced as a relatively thin insular zone of dried oil sand forms around the electrodes penetrating the oil sand formation. Nominally the moisture lost as this insular zone is formed should not be a large percentage of the moisture present in the total volume to be heated.

In order to examine this concept the following experimental setup was assembled (see figure 3.5). The test cell consisted of a two wire line with 5.1cm separation placed in a 10.2cm inside diameter PVC tube. The tube was wrapped in fiberglass insulation to minimize thermal losses to the air. The tube was packed with a high moisture, low grade, Athabasca oil sand. The electrical properties of the oil sand are shown in figures 3.6 to 3.8. The electrical properties of this material, as well as of all the materials used in subsequent experiments, were determined using a custom built measurement cell. In order to determine the electrical properties of a material at high frequencies a length of coaxial line was packed with the material of interest. By use of electric field and magnetic field sampling probes attached to a vector voltmeter it was possible to obtain signals proportional to voltage and current as well as the phase angle between voltage and current. These values were obtained at the input point of

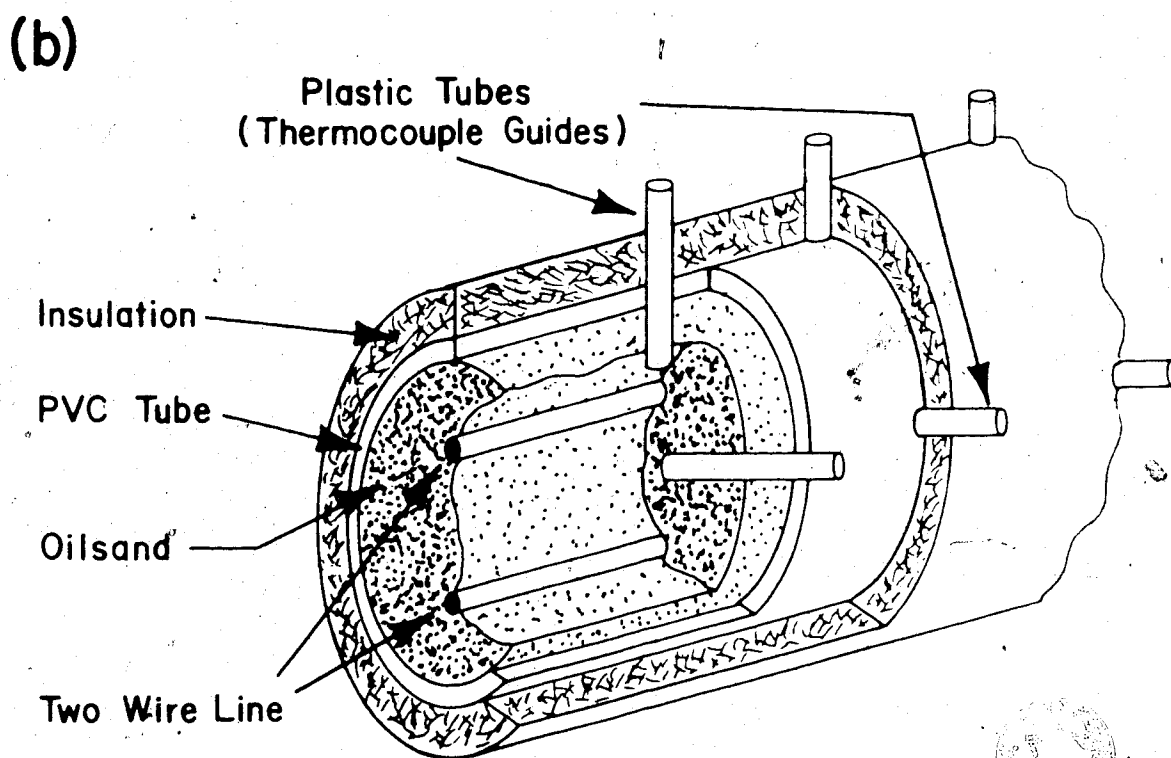
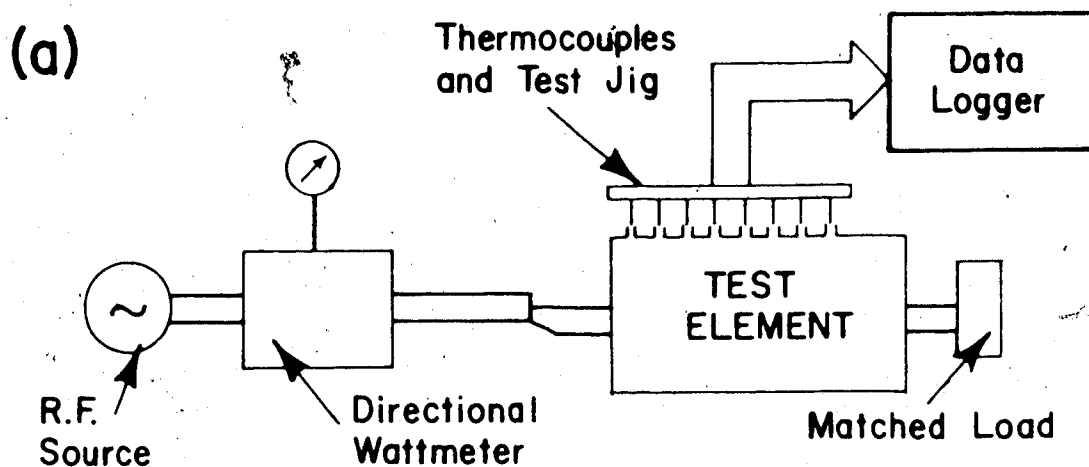


Figure 3.5: Experimental demonstration of partial evaporation boring concept.

a) Apparatus interconnection showing excitation and instrumentation connected to the test cell.
 b) Construction details of the test cell packed with oil sand. The oil sand is heated by passing an electromagnetic wave through it.

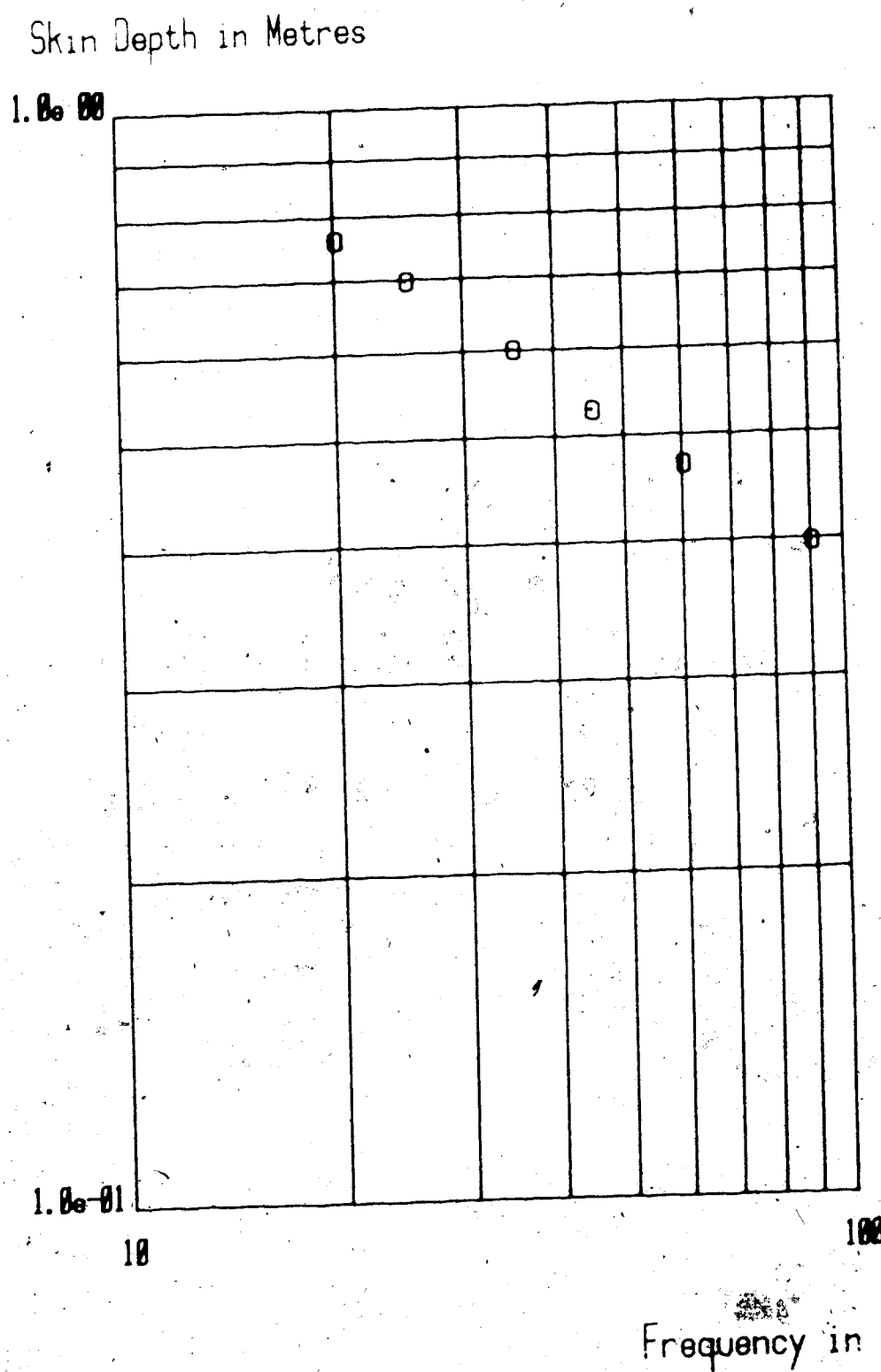


Figure 3.6: Skin depth versus frequency of the oil sand used in the thermal evaporation boring demonstration.

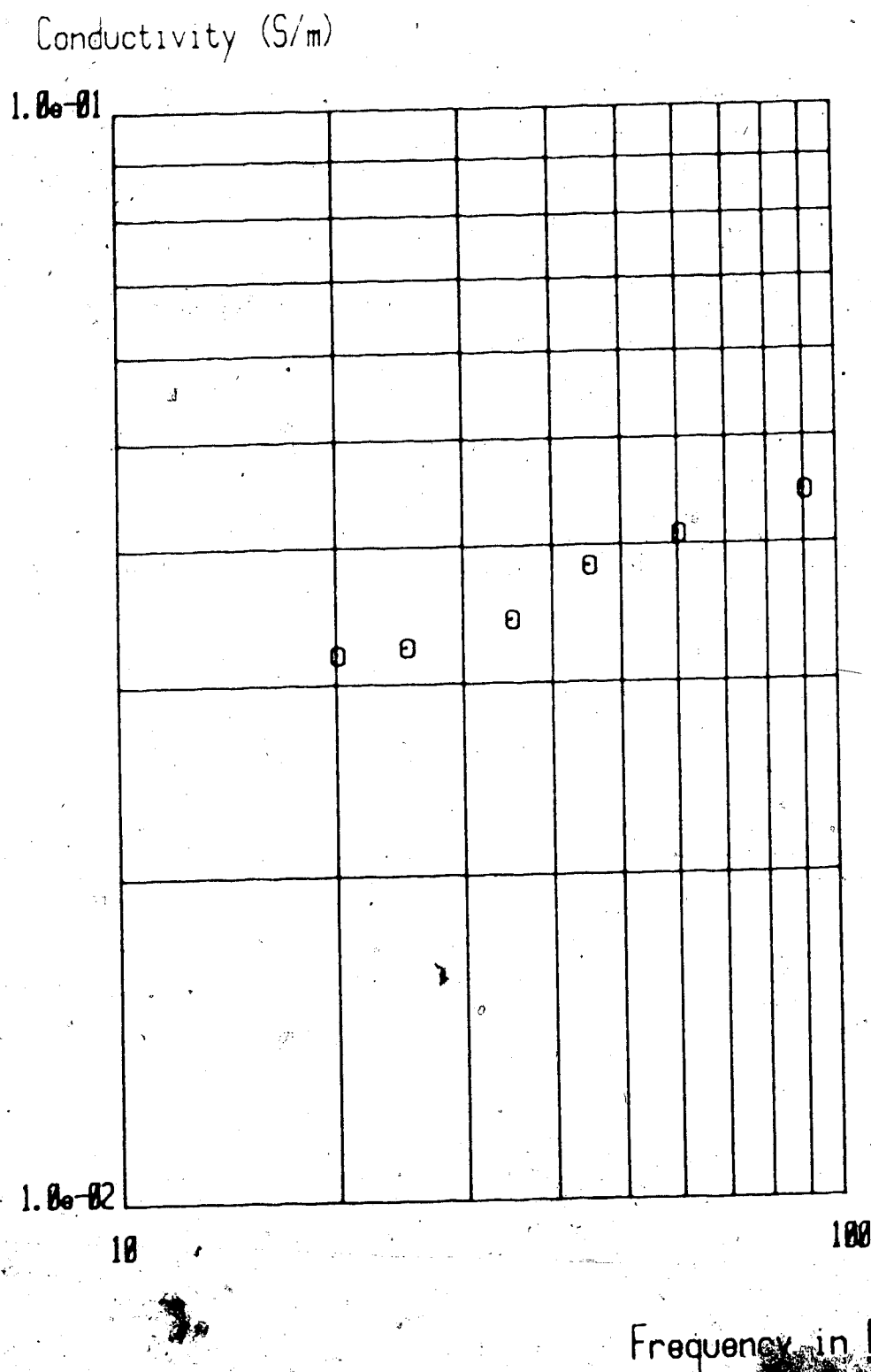


Figure 3.7: Conductivity versus frequency of sand used in the partial evaporation demonstration.

Conduction to Displacement
Current Ratio

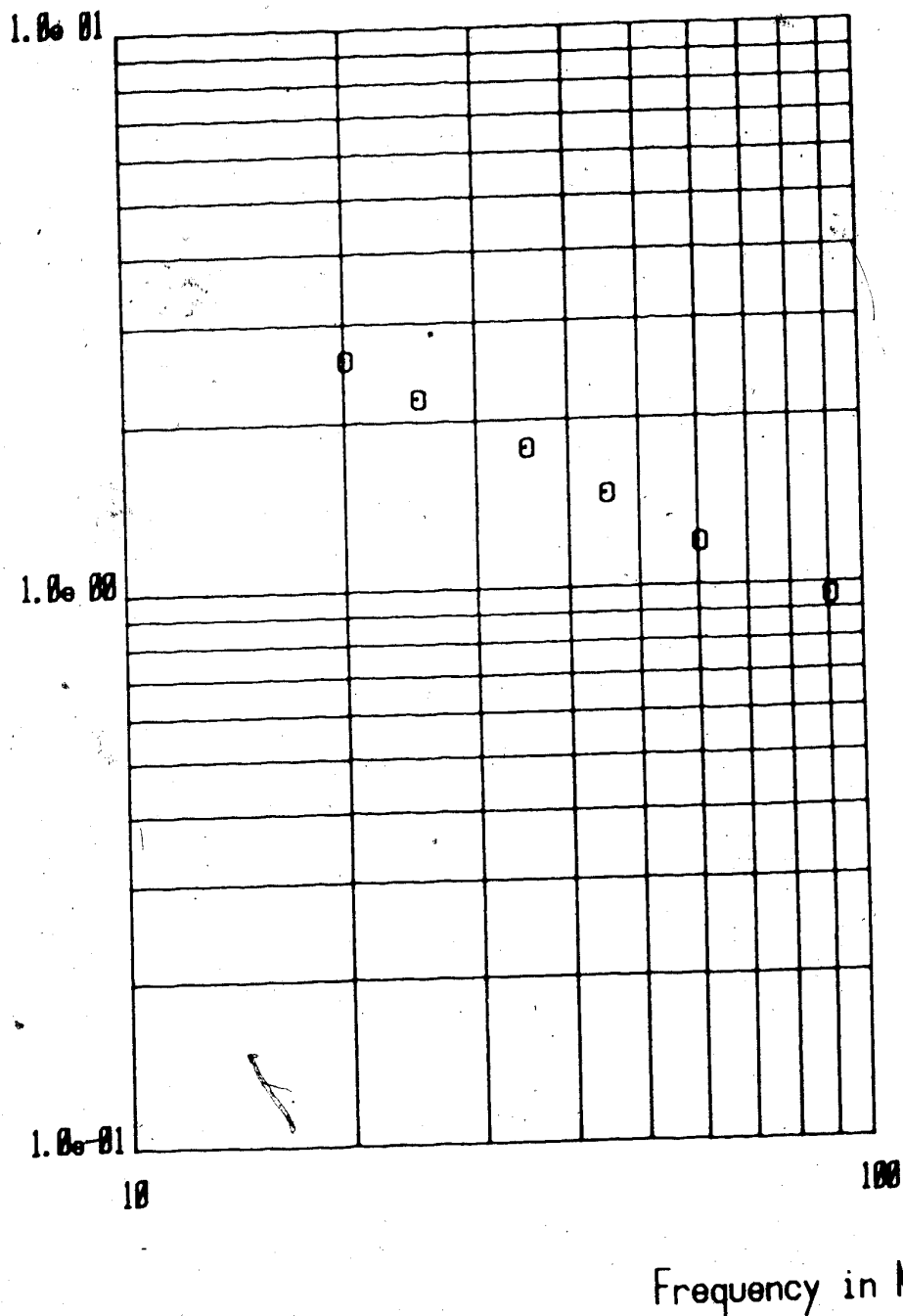


Figure 3.8: Conduction to displacement current ratio versus frequency, of the oil sand used in the partial evaporation boring demonstration.

the coaxial line packed with the sample material. From these readings it was possible to obtain a measure which was proportional to the impedance seen looking into the coaxial transmission line. At each test frequency the impedance value was determined for both an open circuit and short circuit termination on the transmission line. From these two impedance values it is possible to determine the electrical properties of the material packed in the coaxial line. A more detailed explanation of the measurement system may be found in reference 20.

The two wire transmission line was energized at 35 MHz and the temperatures at points along the line were measured by briefly turning off the RF source and inserting thermocouples with a test jig, at various times throughout the run. A Hewlett Packard 8656A signal generator driving an ENI model A-300 RF power amplifier acted as the power source. Forward and reflected power was monitored using a Bird Electronics model 4715-200 Truline RF directional power measurement system. Temperatures were recorded for a central point between the electrodes at eleven locations along the line. Temperatures were also recorded at a point close to one of the line conductors at eleven locations along the line (see figure 3.9) Temperatures were measured with J type thermocouples (iron/constantan) attached to a Hewlett Packard model 3052A data acquisition system.

The temperature profiles obtained are presented in figure 3.10 and 3.11. The profiles obtained suggest that the

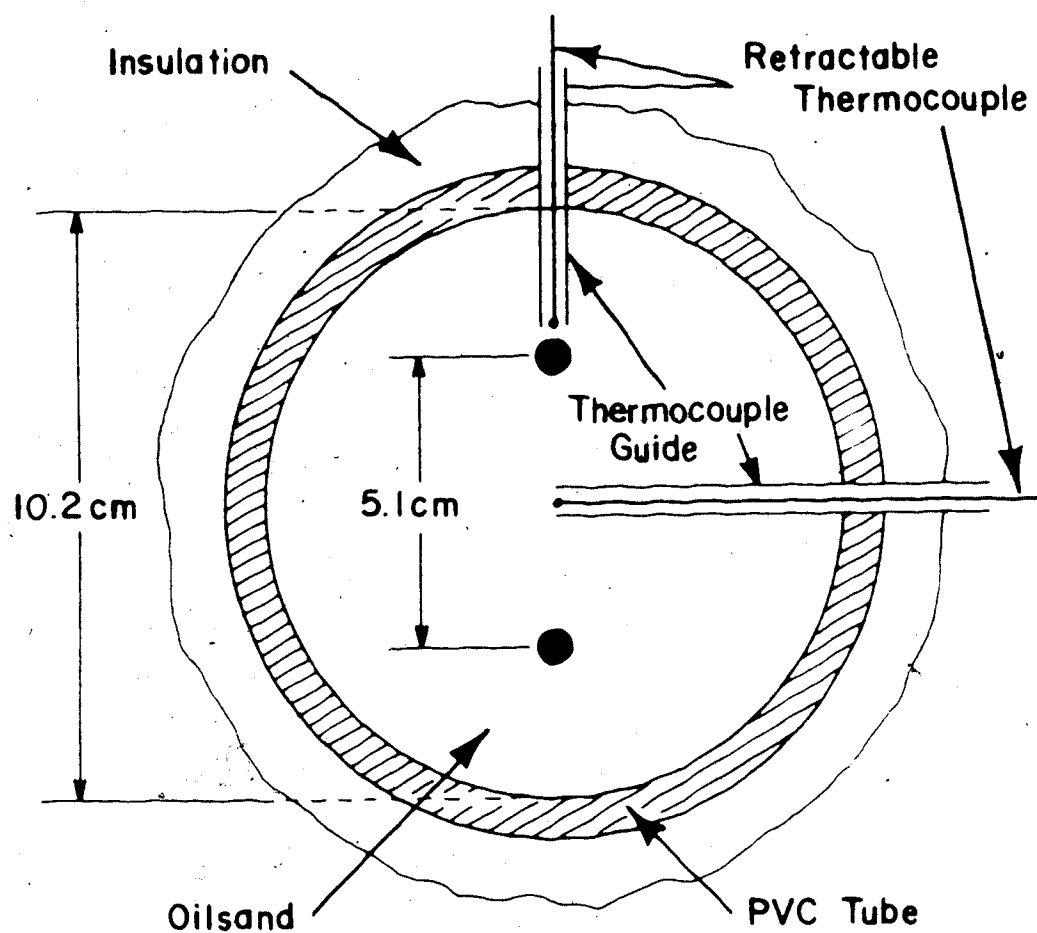


Figure 3.9: Temperature measurement locations in the partial evaporation boring demonstration.

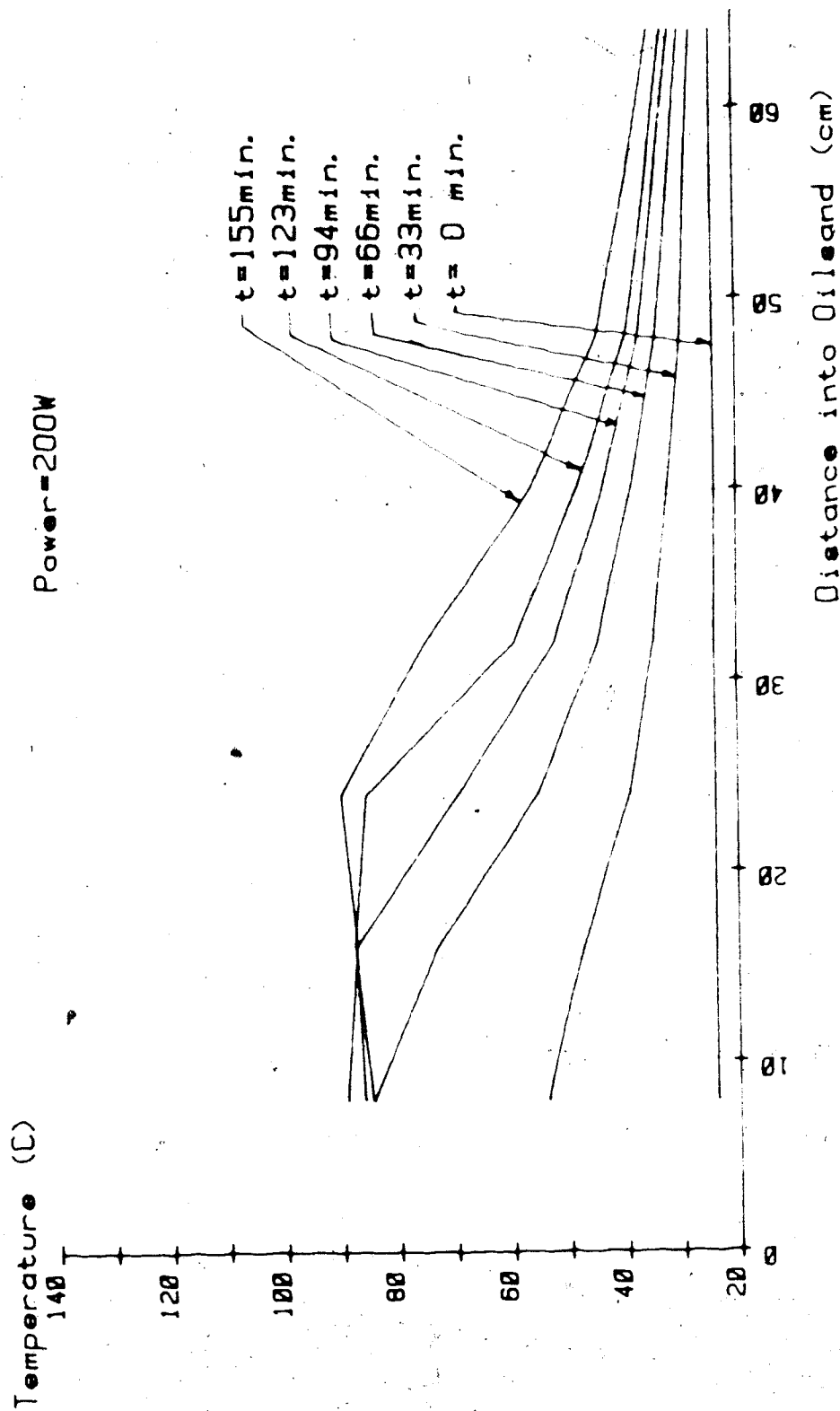


Figure 3.10: Partial evaporation boring demonstration. Plot of midpoint temperatures obtained along the length of the transmission line, at various points in time, as the heating run progresses.

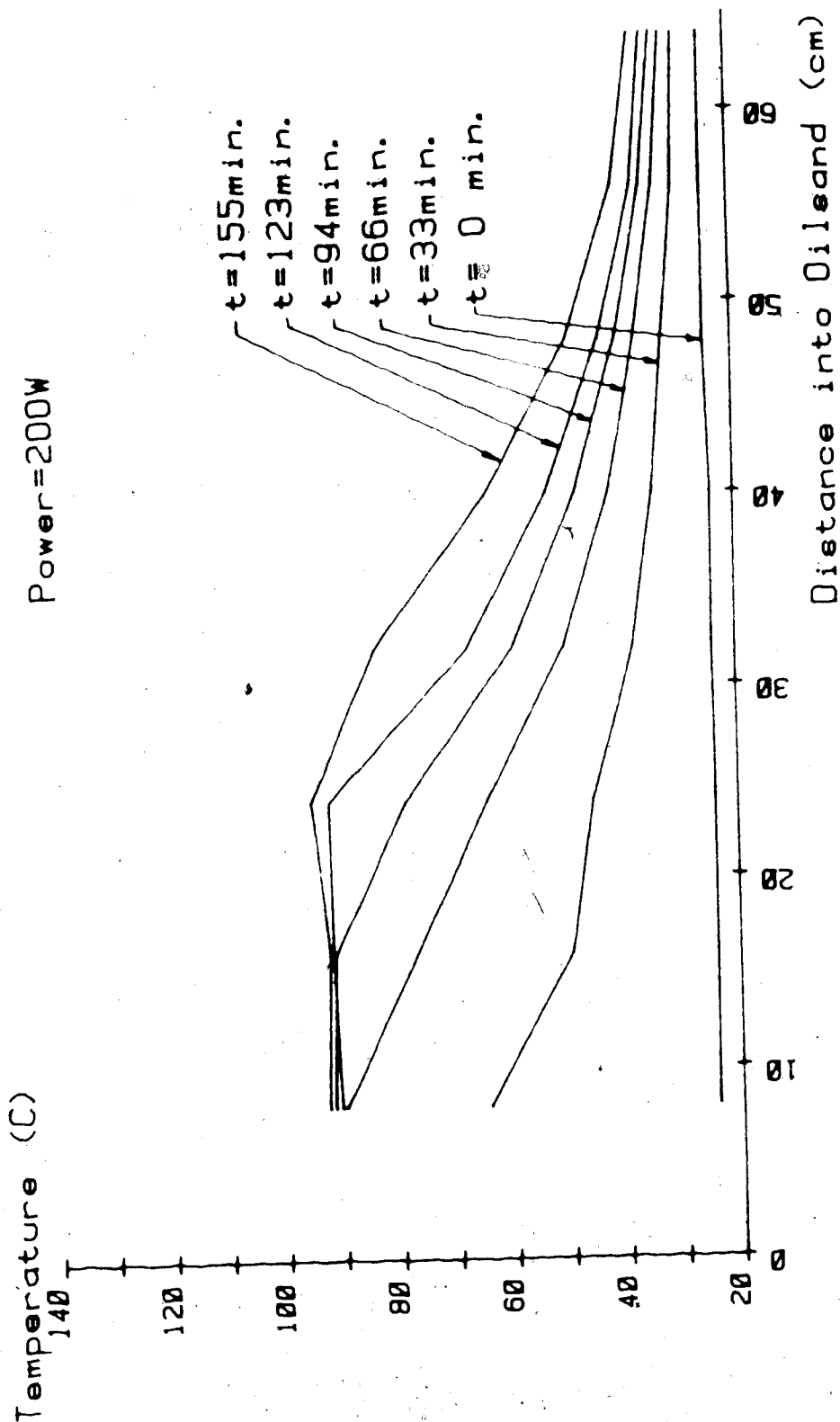


Figure 3.11: Partial evaporation boring demonstration. Plot of near electrode temperatures obtained along the length of the transmission line, at various points in time, as the heating run progresses.

postulated boring action is occurring, inasmuch as deeper heating into the formation occurs only after the zone near the input approaches 100 °C and evaporation begins.

One of the advantages postulated for partial evaporation boring over total evaporation boring was that the boring action would occur without having to evaporate the bulk of the oil sand moisture. Nominally only a reasonably small sleeve around each electrode would be totally depleted of moisture. The first several centimetres of oil sand were dug out of the tube after the run and an analysis (Dean-Stark method) performed. The volume of material involved was too small to allow a detailed cross-sectional determination of the moisture profile. However, by blending the sample it was possible to establish the average water content of the oil sand that had been heated. It may be recalled that in the total evaporation experiment the post run moisture level of the heated zone oil sand was 0.25% by weight, whereas the original oil sand packed in the guide had a moisture content of 7.6% by weight. The original oil sand packed in the partial evaporation experiment also had an average moisture content of 7.6% by weight. There are, however, some natural fluctuations in the moisture content of the oil sand material. The 7.6% is an average and fluctuations in the order of $\pm 1\%$, by weight, occur. The average moisture content of the heated zone oil sand dug out after the partial evaporation run was slightly higher than 7.6%. The exact

degree of moisture loss is thus masked by the natural fluctuations in the source material. The results do, however, demonstrate that the evaporation loss is minimal compared to the total evaporation case.

As was done in the waveguide case, a second experiment was performed to provide a direct comparison to thermal conduction methods. A contact heater plate was placed in intimate contact with the face of the oil sand packed in the PVC tube. The balance of the heater was heavily insulated with rock wool. The same power was supplied to the heater as was used in the RF case. The temperature profiles obtained are presented in figure 3.12. It is interesting to note that after 126 minutes the oil sand 25 cm from the input had barely risen above ambient even with a 360 °C temperature differential present between the plate heater at the input and the 25 cm point. Thus, again the temperature profiles suggest that electromagnetic heating provides much deeper energy penetration, in a given time, as well as a more uniform heating pattern.

The temperature profiles obtained in the electromagnetic heating case demonstrate that the postulated boring action occurs in Athabasca oil sand and the moisture analysis suggests that the boring action occurs without having to expend a great deal of energy to evaporate connate water. The experiment does not, however, address the type of temperature profile that develops in the formation region between the electrodes of the transmission line. It is

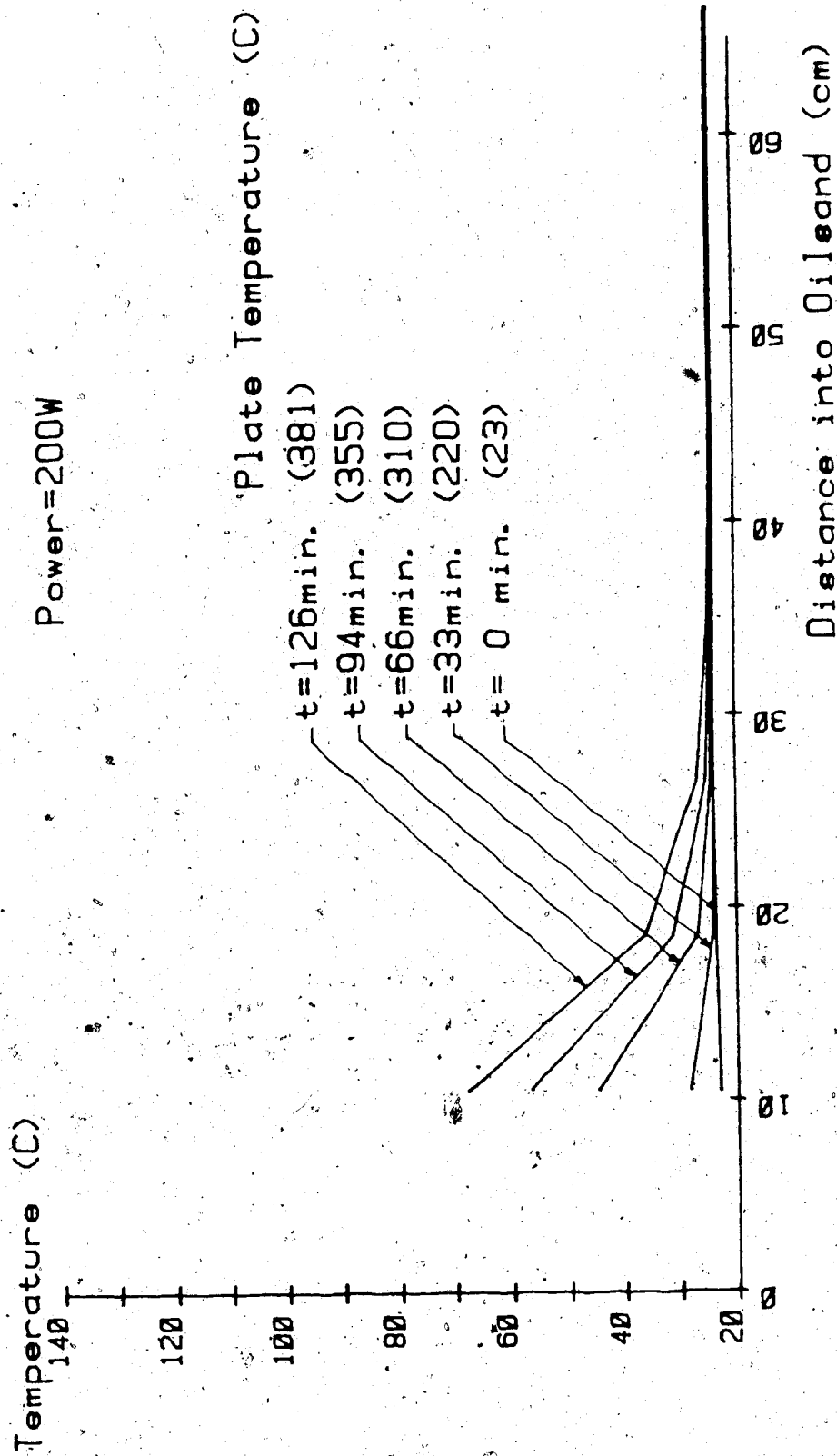


Figure 3.12: Thermal conduction heating comparison to electromagnetic heating. Oil sand is packed in the same transmission line test cell as used for partial evaporation boring experiment. Plots are of midpoint temperatures obtained along the length of the line. The input heater was supplied with a constant 200W. Note that the plate temperature given is the temperature at zero cm.

desirable for not only the regions close to the electrodes to be heated but also for the regions more central between the electrodes to undergo substantial heating. The wave decoupling which occurs should not take place until these central regions reach an adequate temperature. The next step in examining the partial evaporation boring concept is thus to determine the cross-sectional temperature profiles that can be obtained. This aspect may be investigated by electrically heating a scale model representation of the field electrode configuration. Experiments of this type have been done and are presented in the next section.

3.3 Partial Evaporation Boring: Scaled Electrothermal Models

The electrode array shown in figure 2.1 is symmetrical about a number of planes as shown in figure 3.13 a). A plane of symmetry is defined as a plane where the gradients of electric potential and temperature have no component normal to the plane. In this situation no current or heat flows across the plane. These planes are convenient positions to establish as boundaries in a scale model, as insular walls may be placed at these points without disturbing the boundary conditions. If the array of electrodes is large enough that edge effects do not significantly distort the electromagnetic field distribution, the heating pattern generated will be duplicated in each zone designated as an element in figure 3.13 a). It is therefore sufficient to model only one element to establish the heating pattern of

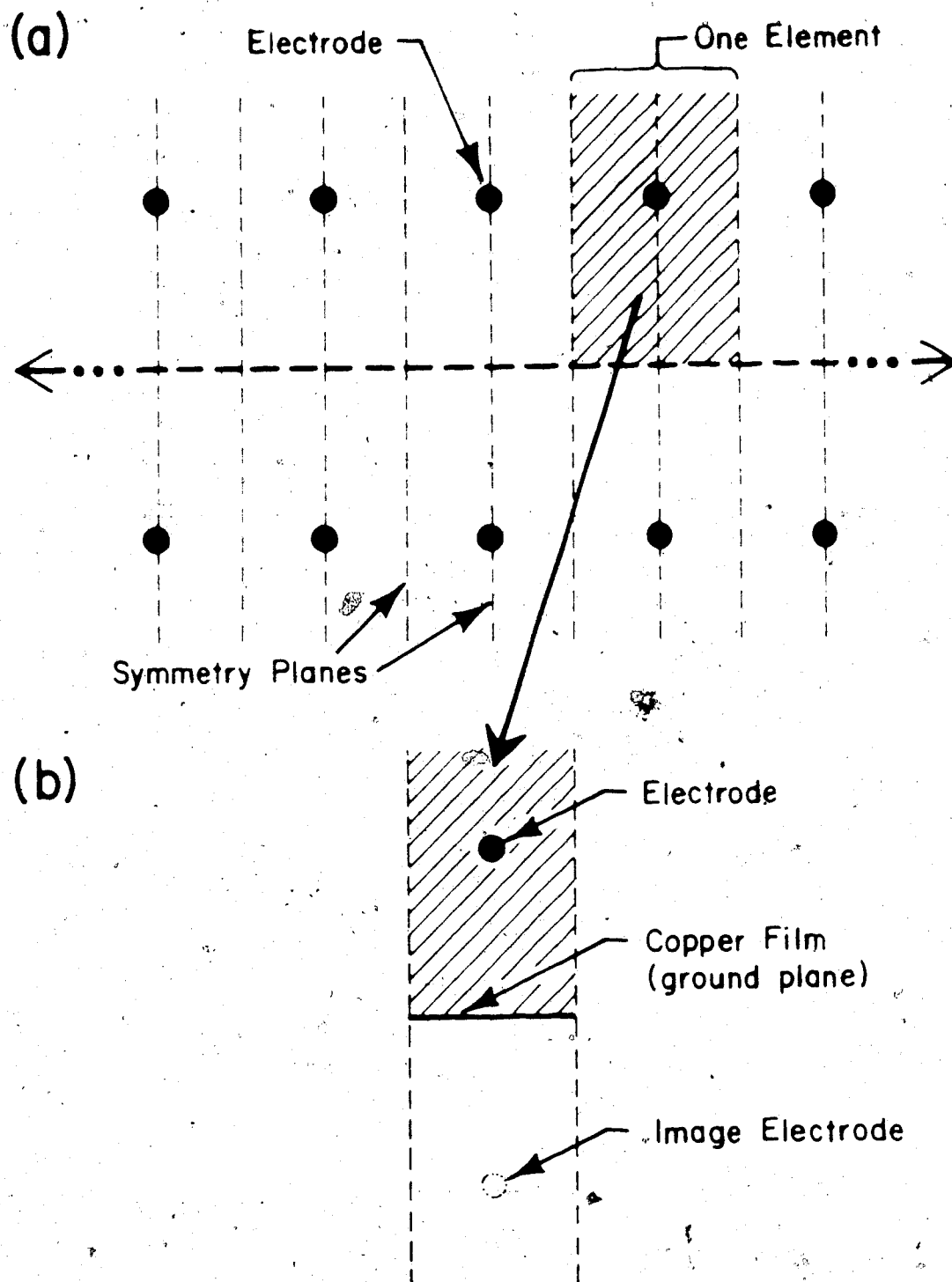


Figure 3.13: Scaled electrothermal model of field heating situation.

- a) End view of electrode array in the field with planes of symmetry shown.
- b) Half element of the field array. Represents the geometry selected for the scale model.

the overall array. Further, the heating pattern above the centre line of the element should mirror the heating pattern below the centre line such that a half element contains all the required heating pattern information. The model form selected is the half element shown in figure 3.13 b).

A half element using a ground plane, rather than a full element, was selected as the modelling unit. This selection allows for a more compact model that is easier to pack. In terms of electromagnetic fields present, image theory would predict that the ground plane will not modify the form of the fields found in the upper half element. In terms of transmission line parameters some differences between the half element and full element formulations come to light. The half element transmission line will have half the distributed series electrode inductance and both the distributed capacitance and conductance between the electrodes will be doubled. The characteristic impedance of the half element line will therefore be different from that of a full element line. The effects are, however, self cancelling in their effect on the propagation characteristic. The skin depth and wavelength values will be the same for both the half element and full element format. In summary, the half element formulation should accurately display the same electromagnetic heating pattern as the full element, but the impedance value presented to the driving source will not be representative of the impedance presented by a full element.

The medium packed into the model was clean tailings pond sand from the Syncrude plant. The sand was saturated with sufficient saline solution to obtain the desired scaled electrical properties. The scaling criteria required for an electrothermal model are summarized in chapter 7.

The model and field values for all of the pertinent electrical, thermal, and geometric factors are summarized in Table 3.1. The field values given for the electrical and thermal properties are typical for rich, low moisture, oil sand.

The model was energized and the temperature variation at a number of points was monitored as the heating occurred. The power source used was an Amplifier Research model 2000L RF amplifier. Forward and reverse power levels were monitored using a Bird Electronics model 4715-200 Truline RF directional power measurement system. Temperatures were measured using J type thermocouples (iron/constantan) attached to a Hewlett Packard model 3052A data acquisition system. At the frequency used it is not possible to leave the thermocouples permanently in place without distorting the electromagnetic fields in the medium. The temperatures were thus obtained by briefly powering down the RF source and then inserting the thermocouples with a test jig at various times throughout the run.

Two sets of temperatures were recorded. The first set was measured 2 cm (field 2.05m) above the ground plane (above the midplane) at various distances along the

	MODEL	FIELD
Frequency MHz	52	0.505
Conductivity (S/m)	0.205	0.002
Conduction ratio $\sigma/\omega\epsilon$	12	5.6
Density (g/cc)	1.62	2.1
Specific heat (J/g·°C)	0.86	0.915
Thermal conductivity (W/m·°C)	1.40	1.65
Vertical Electrode Separation (cm)	0.216 (0.108 above ground plane)	22.2
Horizontal Separation (cm)	0.108	11.1
Electrode diameter (cm)	0.066	6.8
Total line length (m)	0.61	62.7
Input power (kW)	0.8 (to a half element)	194 (to a full element)

Mechanical scale factor $p = 0.205 / 0.002 = 103$

Time scaling (thermal) $\Gamma = 12353$

TABLE:3.1 Full scale field quantities corresponding to the model values in the scale model heating demonstration of the partial evaporation boring concept.

transmission line. The temperatures obtained are presented in figure 3.14, and indicate that the postulated boring action is occurring.

The second set of temperatures was obtained for the region along an axis between the upper and lower electrodes at a distance of 11.5 cm (field 11.8m) from the line input. The heating profile (see Figure 3.15) indicates that the heating is initially very similar to 60 Hz heating. The regions near the electrodes heat very quickly but the central region is left relatively cooler. Note, however, that once the electrodes approach 100°C, where 60 Hz heating would normally stop due to the generation of an insulating gap around the electrodes, the heating continues in the RF case and the central portion between the electrodes is brought up to 100°.

It may also be noted that a distance of about 20% of the electrode separation is heated above and below the electrode pair. This heating is likely due to current emanating from the back of the electrodes, rather than due to any thermal conduction mechanism. (see Figure 3.16).

It should be noted that the operating frequency used in this run may be somewhat higher than optimum. The concept of partial evaporation boring requires the selected operating frequency to be high enough that coupling is maintained long enough for significant heating of the central region between the electrodes to occur. The frequency should not, however, be so high that an excessive amount of moisture must be

Power = 800W (194kW)

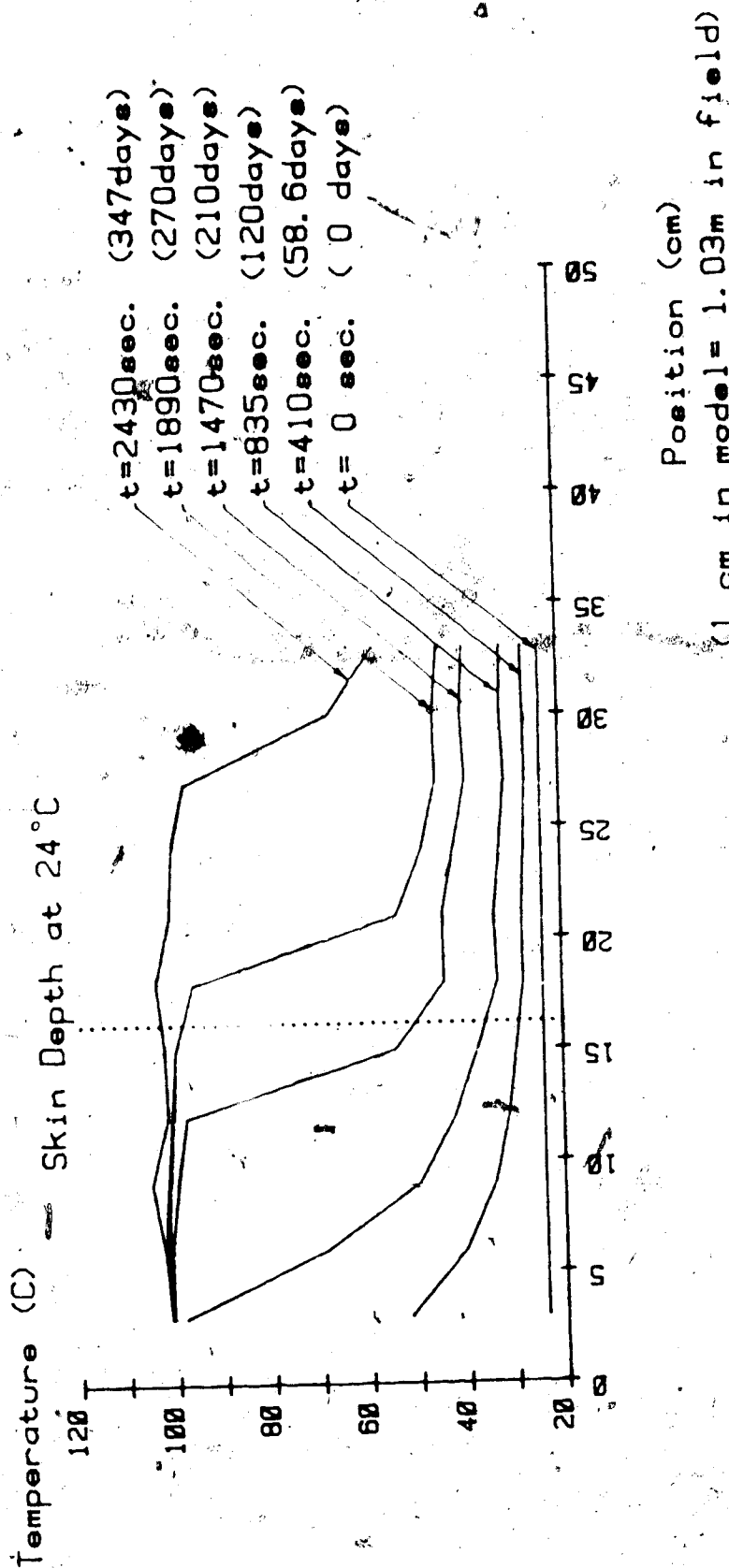


Figure 3.14: Measured temperatures in the scale model. Temperatures obtained during a partial evaporation heating run. Temperature variation into the formation, measured at a central point 2cm (2.05 m) above the ground plane (above the midplane). Bracketed quantities are the full scale field values corresponding to the model values.

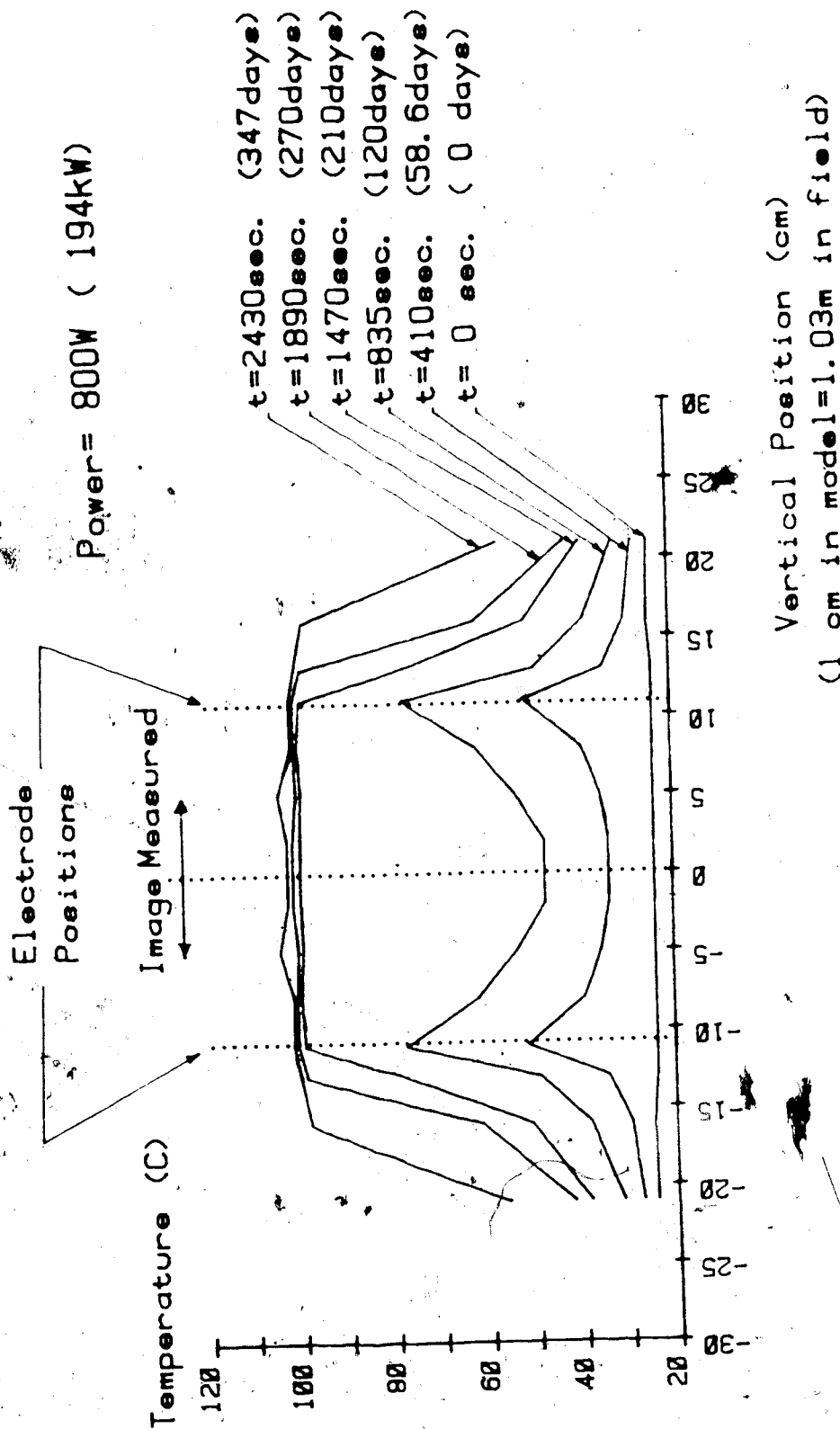


Figure 3.15: Measured temperatures in the scale model. Temperatures obtained during a partial evaporation heating run. Temperature variation across the line, measured along an axis intersecting the electrodes at a distance of 11.5cm (11.8m) from the line input: Bracketed quantities are the full scale field values corresponding to the model values.

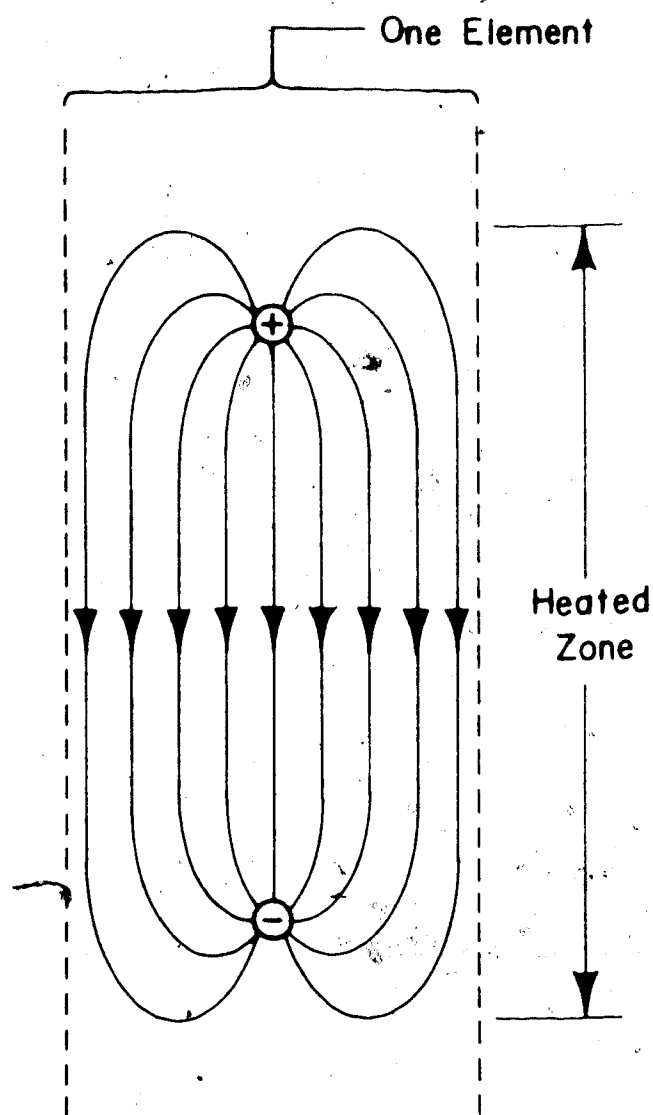


Figure 3.16: Sketch of the current lines generated by one upper/lower electrode pair within the array (see figure 3.13)

evaporated before decoupling occurs. An examination of figure 3.15 shows that the entire region between the electrodes reaches 100°C . This implies that evaporation is occurring not only near the electrode but also to some degree in the central regions.

Included in this report is a photograph of a partially unpacked model from one of the Partial Evaporation runs (see plate 1 appended to end of this thesis). It was interesting to note during the unpacking of these models that a hard crust of dried sand had formed around the electrode. By carefully removing the softer moist sand from around the crusted area it was possible to obtain a visual representation of the evaporated gap postulated (see also discussion in section 3.4). A small taper may be noted, with the thicker region occurring at the line input. This taper is consistent with the concept of the wave progressively becoming more decoupled in the input regions and thus allowing the wave energy to be carried deeper into the formation.

An examination of figure 3.14 indicates that the heat front progressed approximately 30 cm along the transmission line. The heated volume of sand from this run was dug out and separated into four lots; the 30 cm being divided into four 7.5 cm sections. Each lot contained a heterogeneous collection of sand ranging from soft moist sand obtained from the central region to hard dried crusts obtained from around the electrode. Each lot was carefully blended and

then a sample was drawn for moisture analysis. The original packing material was 4.15% water by weight. The average weight percent water of the four sections, starting from the input, were 2.9%, 3.6%, 3.8% and 4.0%. These results show that for the heated zone in total about 14% of the water in place was evaporated in the heating process. This level of evaporation supports the proposition, put forward in section 2.2, that the partial evaporation boring mode of heating would make more efficient use of the applied energy than heating using the total evaporation boring mode.

The results of this section are very promising in that the temperature profiles generated suggest that a very uniform zone of hot (low viscosity) bitumen can be created in the oil sand deposit. Subsequent production of this zone could take place by, for example, the injection of steam into the upper electrode wells and the collection of bitumen through the lower wells. Whatever production method is ultimately used, an initially uniform temperature/viscosity profile is desirable in terms of efficiently sweeping the bitumen from the formation.

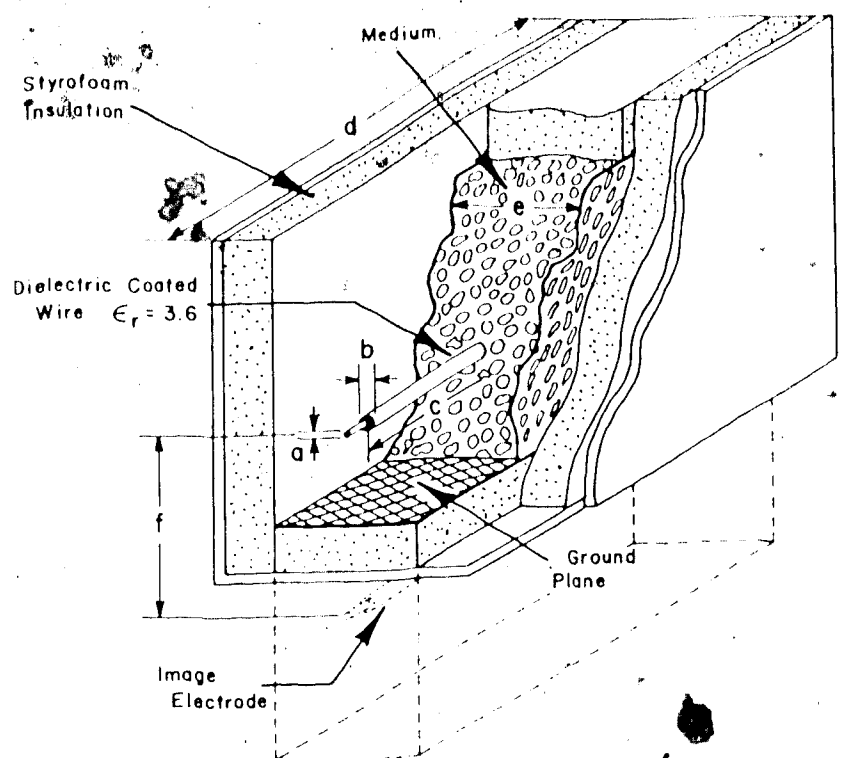
3.4 Dielectric Coated Transmission Line: Scaled Electrothermal Models

3.4.1 Applied Coating

A scaled electrothermal model was assembled to simulate the heating effects which can be obtained with an electrode array such as shown in figure 2.1. The particular objective was to see if the addition of a suitable dielectric coating to the electrodes would allow essentially uniform heating to be obtained over the entire depth that the electrodes penetrate the formation. An end view of the model layout is shown in figure 3.17. Again, the scaled up field distances are noted in brackets. The general format is to model a half element of the overall array as was done in section 3.3. The equipment used was the same as that described in section 3.3. The scaling criteria are as outlined in chapter 7 and this specific case of scaling is used for the sample calculation shown in section 7.3. For both model and field the conduction current is dominant in the media to be heated ($\sigma \gg \omega \epsilon$).

The net power input supplied to the model was 715 watts (to a half element), at an operating frequency of 12 MHz (82.8 kHz). The corresponding field power level would be 244kW (per full element of 15.7m width) or about 325 hp.

Using the numerical model described in section 5 it is estimated that the initial (25°C) depth of penetration along the line was increased to 24.9m (3611 m) from 27.4 cm (39.7



Physical Properties		Model	Field
Wire Diameter	(a)	1.65 mm	0.239 m
Wire & Coating	(b)	3.2 mm	0.464 m
Electrode Length	(c)	90 cm	130.5 m
Box Length	(d)	106 cm	153.7 m
Medium Width	(e)	10.8 cm	15.7 m
Electrode Spacing	(f)	18 cm	26.1 m
Medium Properties		Model	Field
Density	(ρ)	1.62 g/cm ³	2.1 g/cm ³
Specific Heat	(c)	0.86 J/g·°C	.915 J/g·°C
Thermal Conductivity	(k)	1.40 W/m·°C	1.65 W/m·°C
Electrical Conductivity (σ) ($\sigma \gg \omega\epsilon$)		.289 S/m at 12 MHz	.002 S/m at 82.8 kHz

Figure 3.17: Physical layout of model used to examine the dielectric coated line concept. Physical properties and dimensions of both the field and model are presented.

m) by the addition of the coating. The wavelength ($2\pi/\beta$) with the coating in place is estimated as 4.63 m (670 m). The total line length of 90 cm (130.5 m) is thus short compared to the depth of penetration, but not short compared to a wavelength. In this situation some irregularities in the heating pattern may be expected due to standing wave effects. Recall, however, that in section 2.3 a temperature induced self leveling mechanism was described which may be expected to reduce heating pattern irregularities. The uniformity of the heating profile obtained in the experiment should give some indication as to the strength of this leveling mechanism.

The temperature profiles obtained are presented in figures 3.18, 3.19 and 3.20. The temperature profiles suggest that a reasonably uniform temperature rise occurs along the transmission line with the only disturbance being some slump near the line end. Considering the high temperature gradient that is being established between the heated zone and the cold zone beyond the line end, some slump of temperatures due to thermal conduction may be expected. The degree of thermal slump, both off the line end and above and below the electrodes, suggests that a higher heating rate would be appropriate. An increase in the applied power level would also reduce the total heating time to a more reasonable period.

The absence of any standing wave irregularities in the heating pattern suggests that the self leveling mechanism

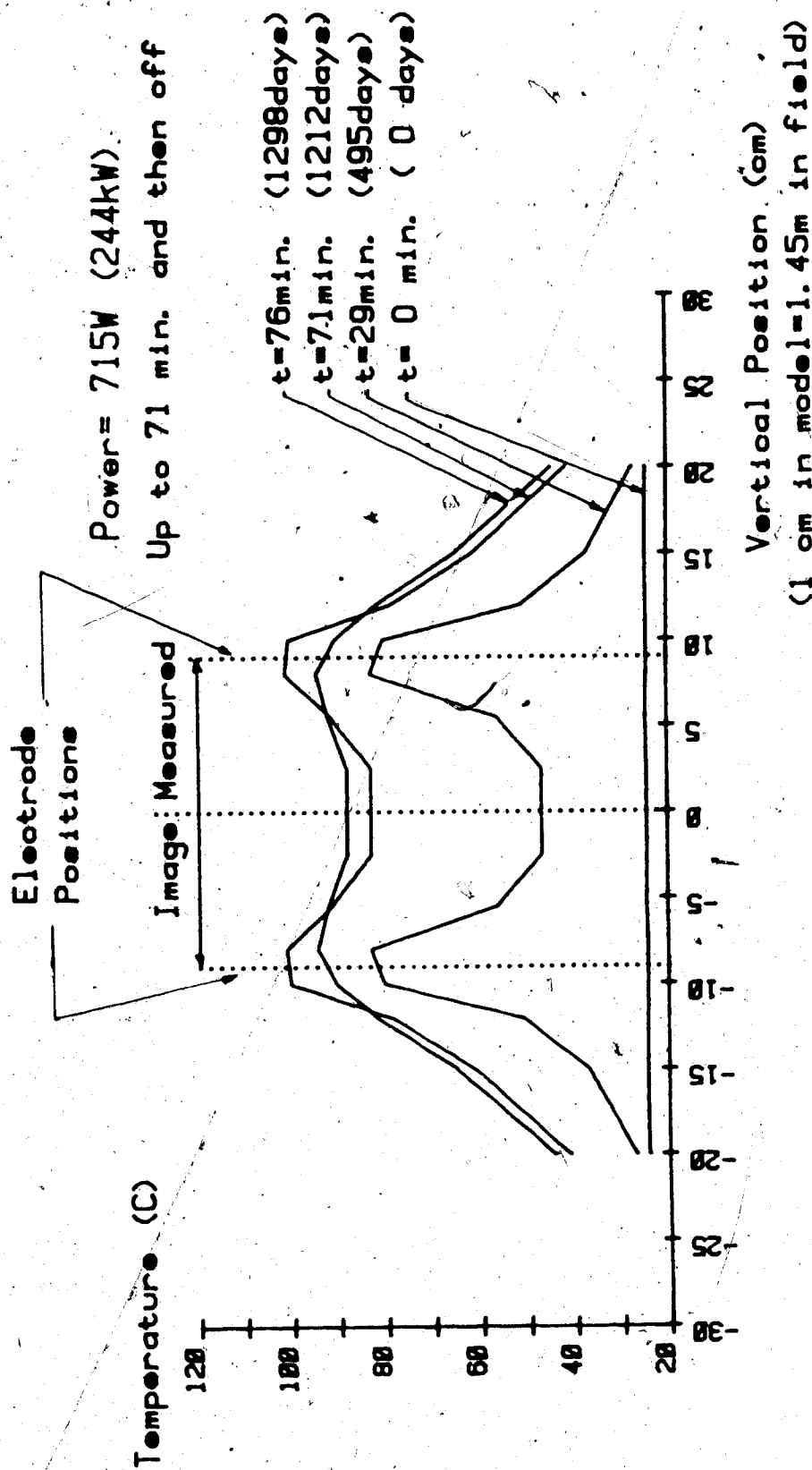


Figure 3.18: Measured temperatures in the scale model. Temperatures obtained during a dielectric coated electrode heating run. Temperature variation across the line, measured along an axis intersecting the electrodes at a distance of 10cm (14.5m) from the line input. Bracketed quantities are the full scale field values corresponding to the model values.

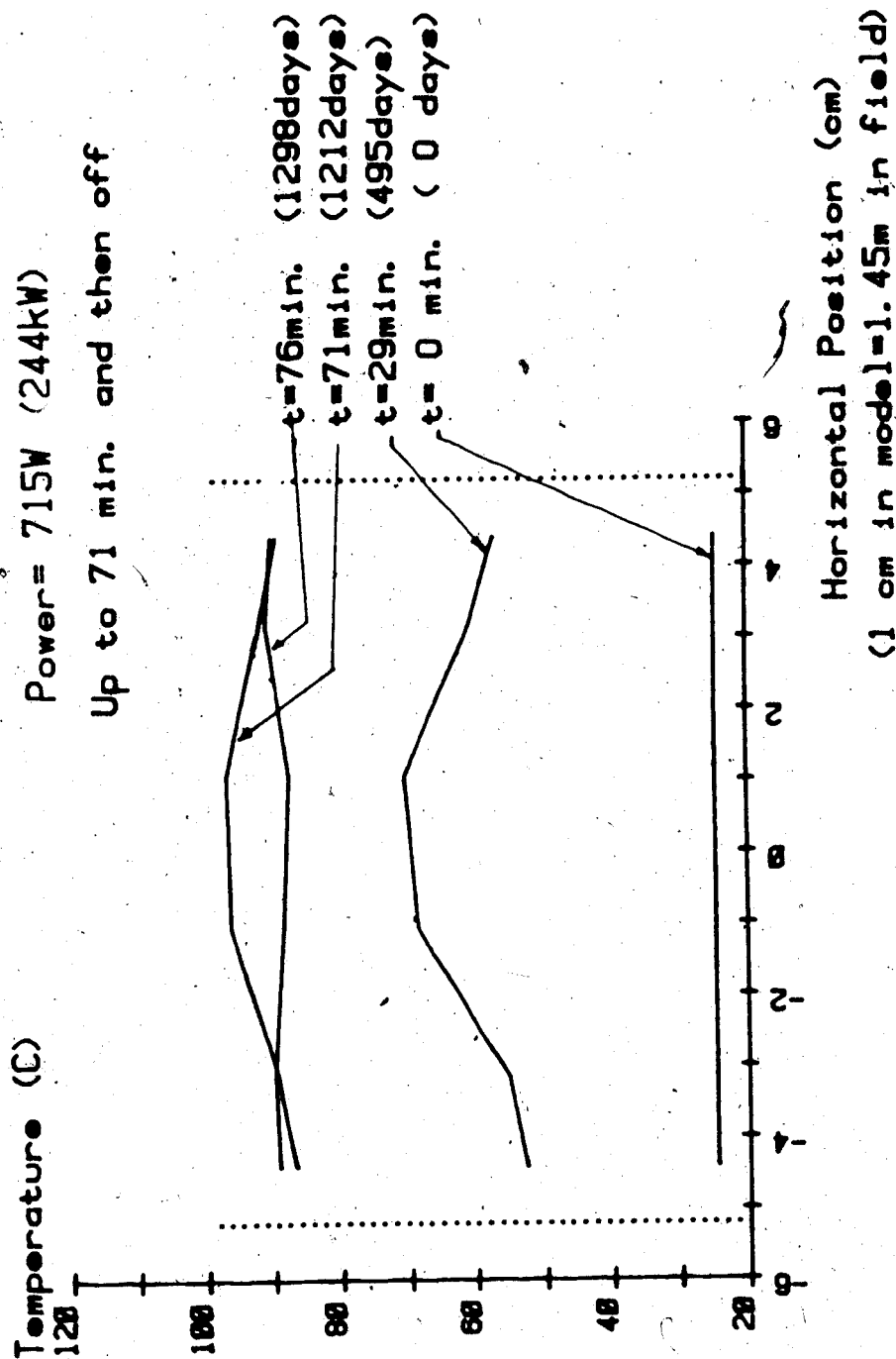


Figure 3.19: Measured temperatures in the scale model. Temperatures obtained during a dielectric coated electrode heating run. Horizontal temperature variation, measured along a line 0.5cm (.73m) below and perpendicular to the top electrode at a point 12cm (17.4m) from the line input. Bracketed quantities are the full scale field values corresponding to the model values.

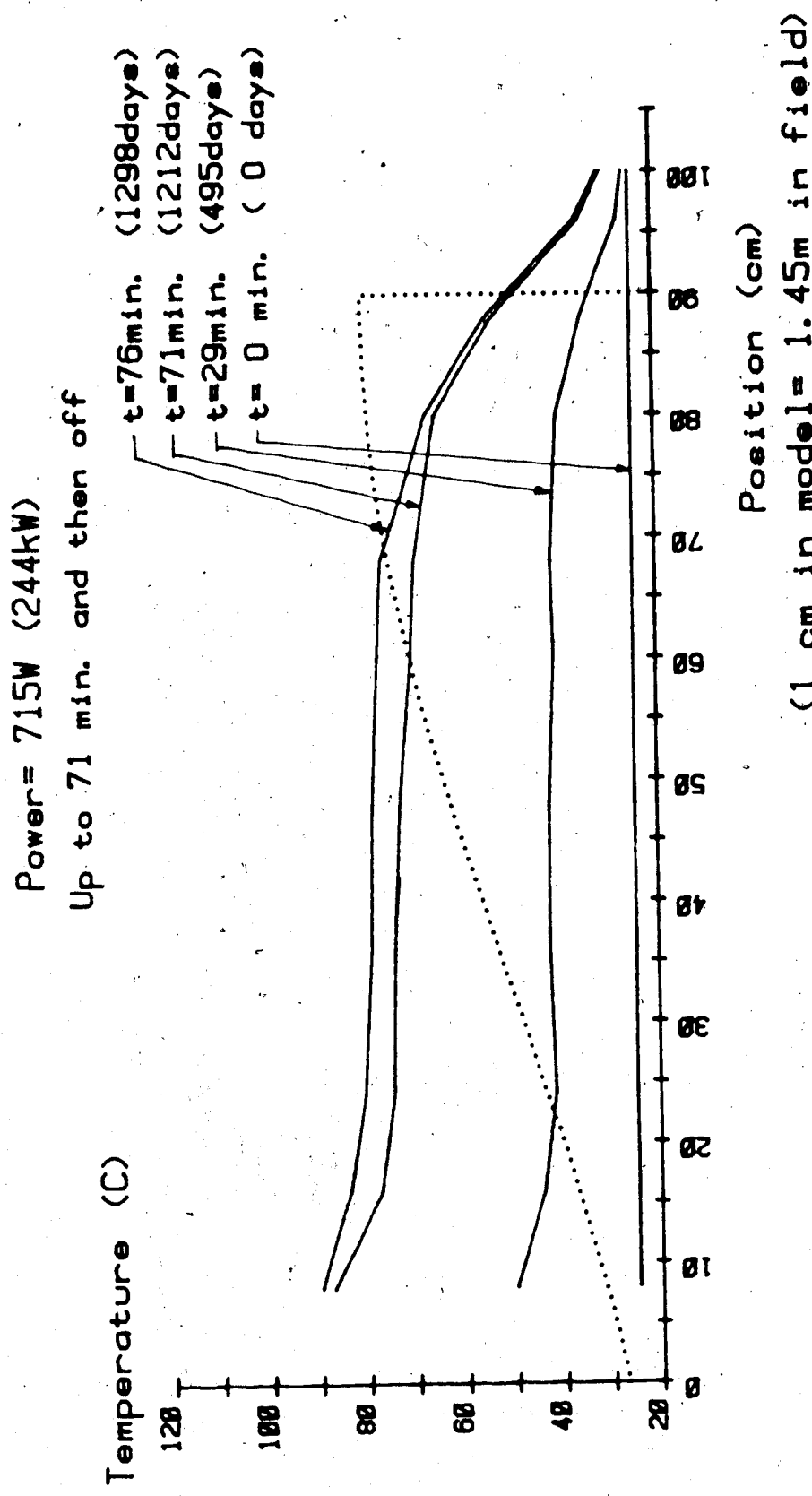


Figure 3.20: Measured temperatures in the scale model. Temperatures obtained during a dielectric coated electrode heating run. Temperature variation into the formation, measured at a central point 1.5cm (2.2 m) above the ground plane (above the midplane). Bracketed quantities are the full, scale field values corresponding to the model values. Dotted line indicates expected energy deposition profile if no self leveling effects were present.

5 1 79

outlined is strong enough to overcome any standing wave effects. Note that superimposed on figure 3.20 is a dotted line. This line is obtained by squaring the initial (25°C) standing wave potential distribution expected on the electrodes ($\lambda=4.63\text{m}$). The curve is representative of the energy deposition profile expected when no self leveling effects are present.

In summary, the uniformity of the thermal profiles obtained in this section support the original hypothesis that the use of suitably coated electrodes would allow the skindepth and standing wave effects to be circumvented. Further the cross-sectional temperature profiles obtained for points between the electrodes suggest that a zone of uniformly hot (low viscosity) bitumen can be created in the formation. As has been pointed out before, this is a desirable feature in terms of permitting efficient production of the bitumen subsequent to the electric pre-heat stage. The final temperature profile generated with the coated electrode configuration is similar to the final temperature profile obtained in the partial evaporation boring experiment. The principal difference is that in the present case the entire line length is brought up to temperature simultaneously whereas in the partial evaporation boring case a heat front sweeps the length of the line.

3.4.2 Self Generated Uniform Coating

The physical setup, operating frequency and power level for this experiment were essentially similar to the case described in section 3.4.1, which deals with an applied coating, except that a slightly smaller mechanical scale factor is obtained. The only major difference is that *no coating* was applied to the electrode. The heating profiles obtained are shown in figures 3.21, 3.22 and 3.23. An examination of these figures shows heating profiles which have the same essential aspects as those obtained for the uniformly coated line. This was an unexpected effect. An additional point noted during the heating run was that the degree of mismatch, and therefore the line input impedance, changed rapidly for the initial few minutes of the run and then stabilized. In the coated line case the degree of mismatch was relatively more constant. From these observations and results, a modified heating mechanism may be postulated.

As has been demonstrated earlier (see section 3.3) a coating can be generated on the electrodes by the partial evaporation mechanism. The results in the present section suggest the possibility that an essentially uniform coating of dried material is being generated on the electrodes early in the heating run. As an aid to comprehending why such an effect would occur figures 3.24 and 3.25 have been prepared. The figures were generated using the numerical model developed for predicting the energy deposition along a

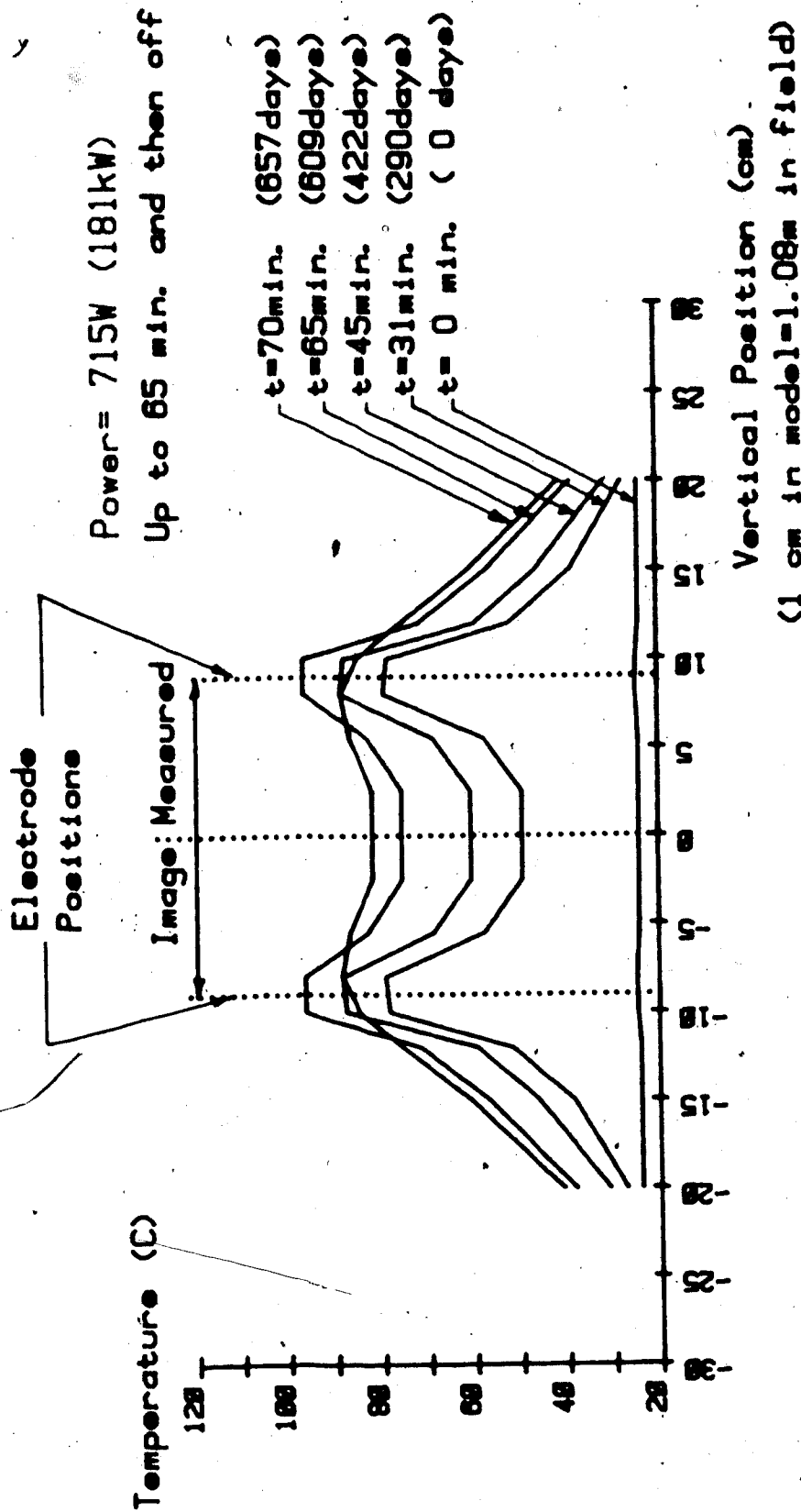


Figure 3.21: Measured temperatures in the scale model. Temperatures obtained during a heating run with self coating electrodes. Temperature variation across the line, measured along an axis intersecting the electrodes at a distance of 10cm (10.8m) from the line input. Bracketed quantities are the full scale field values corresponding to the model values.

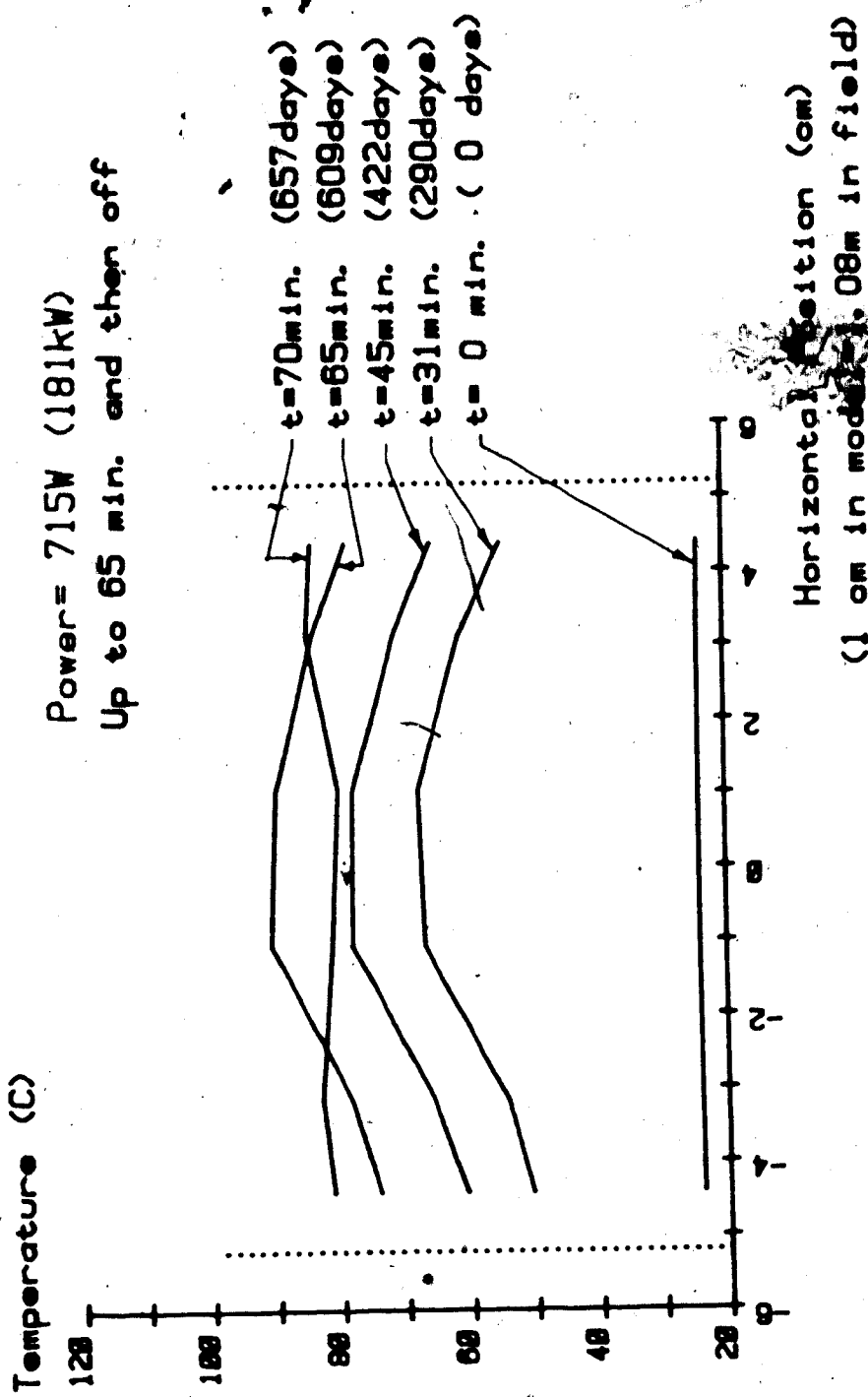


Figure 3.22: Measured temperatures in the scale model. Temperatures obtained during a heating run with self coating electrodes. Horizontal temperature variation, measured along a line 0.5cm (.54m) below and perpendicular to the top electrode at a point 12cm (13m) from the line input. Bracketed quantities are the full scale field values corresponding to the model values.

Power= 715W (181kW)

Up to 65 min. and then off

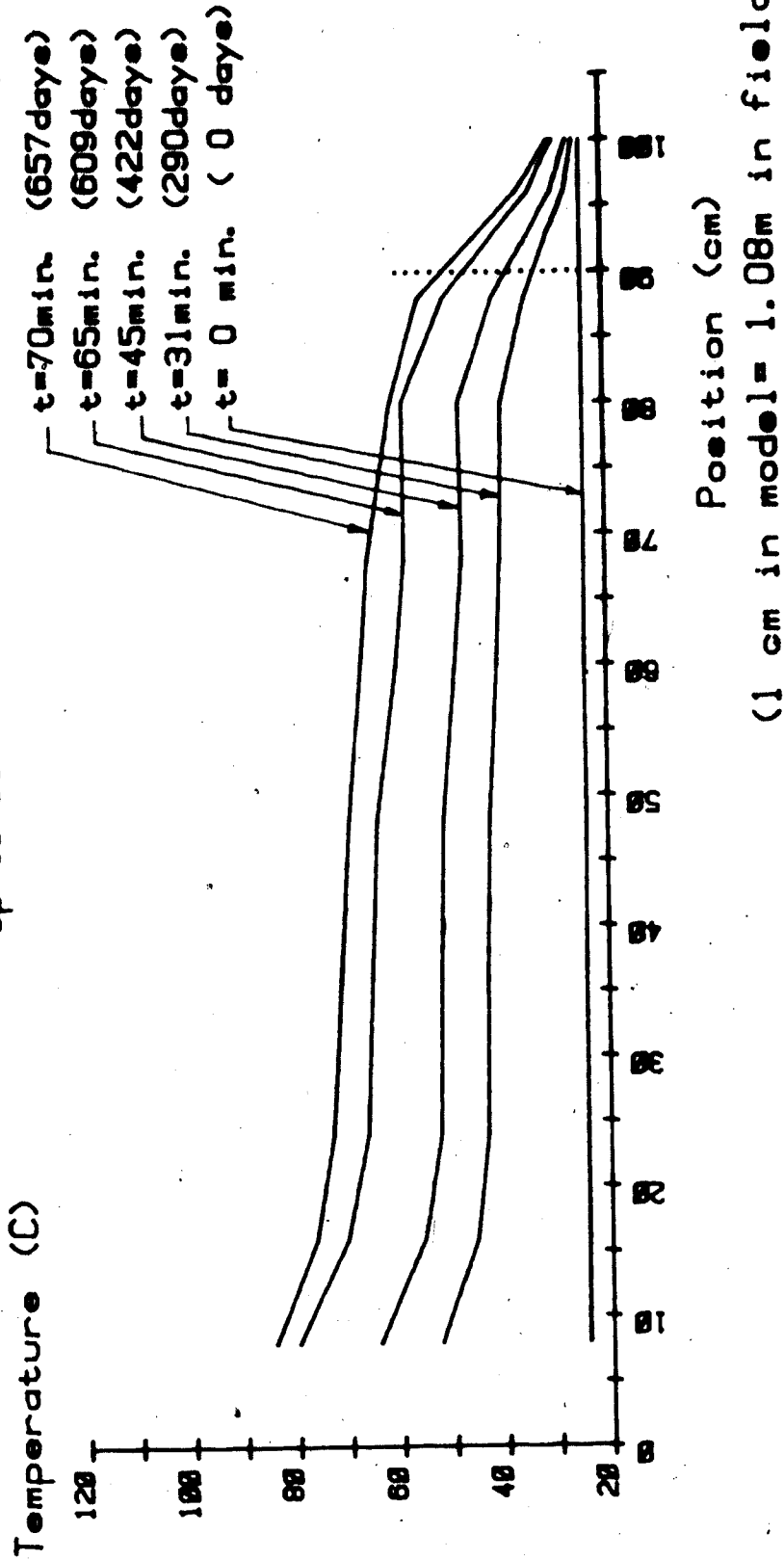


Figure 3.23: Temperatures obtained during a heating run with self-coating electrodes. Temperature variation into the formation, measured at a central point 1.5cm (1.62m) above the ground plane (above the midplane). Bracketed quantities are the full scale field values corresponding to the model values.

Attenuation (Nepers/metre)

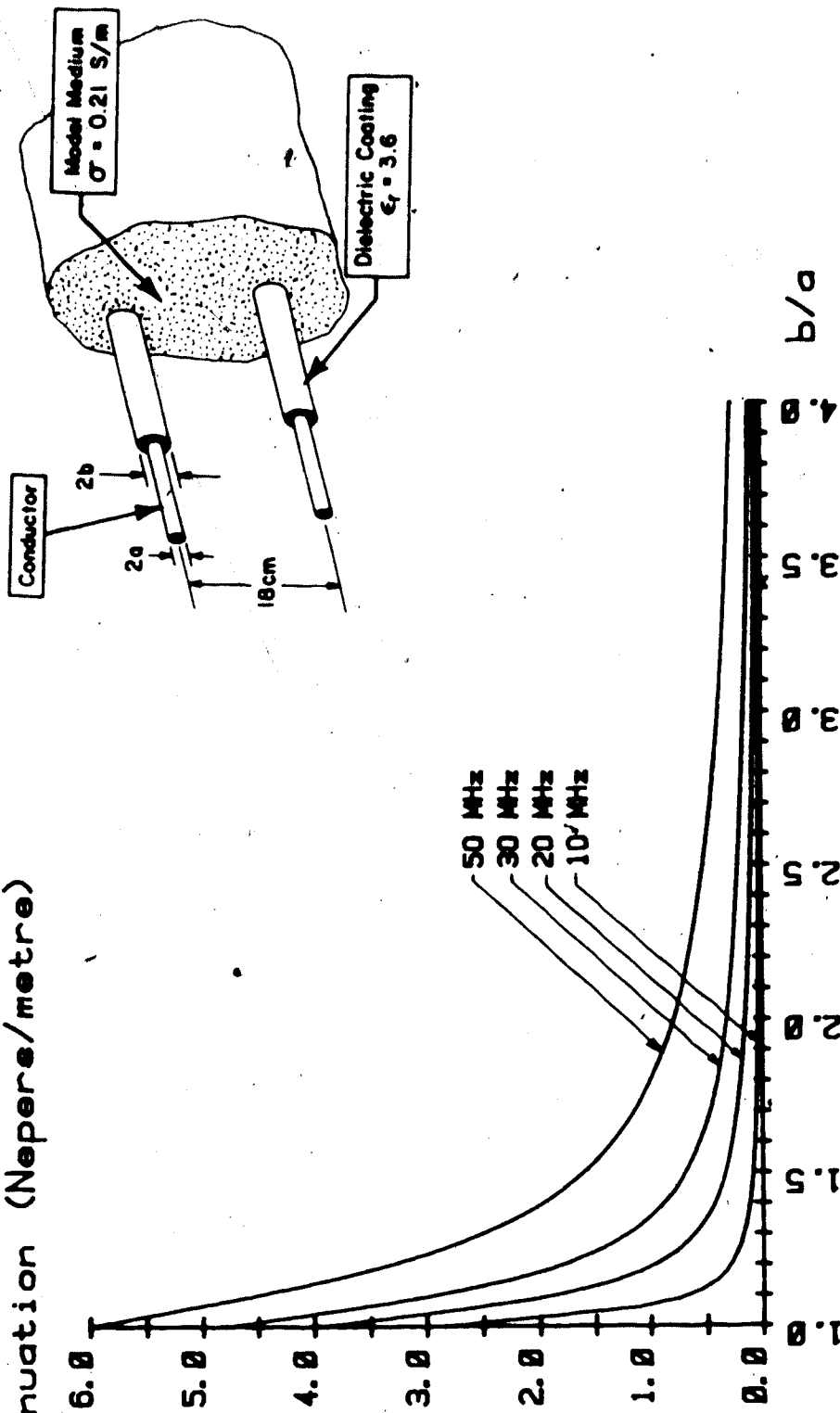


Figure 3.24: Attenuation rate versus electrode coating thickness at various operating frequencies. Based on the conductivity value at 25°C.

Attenuation (Nepers/metre)

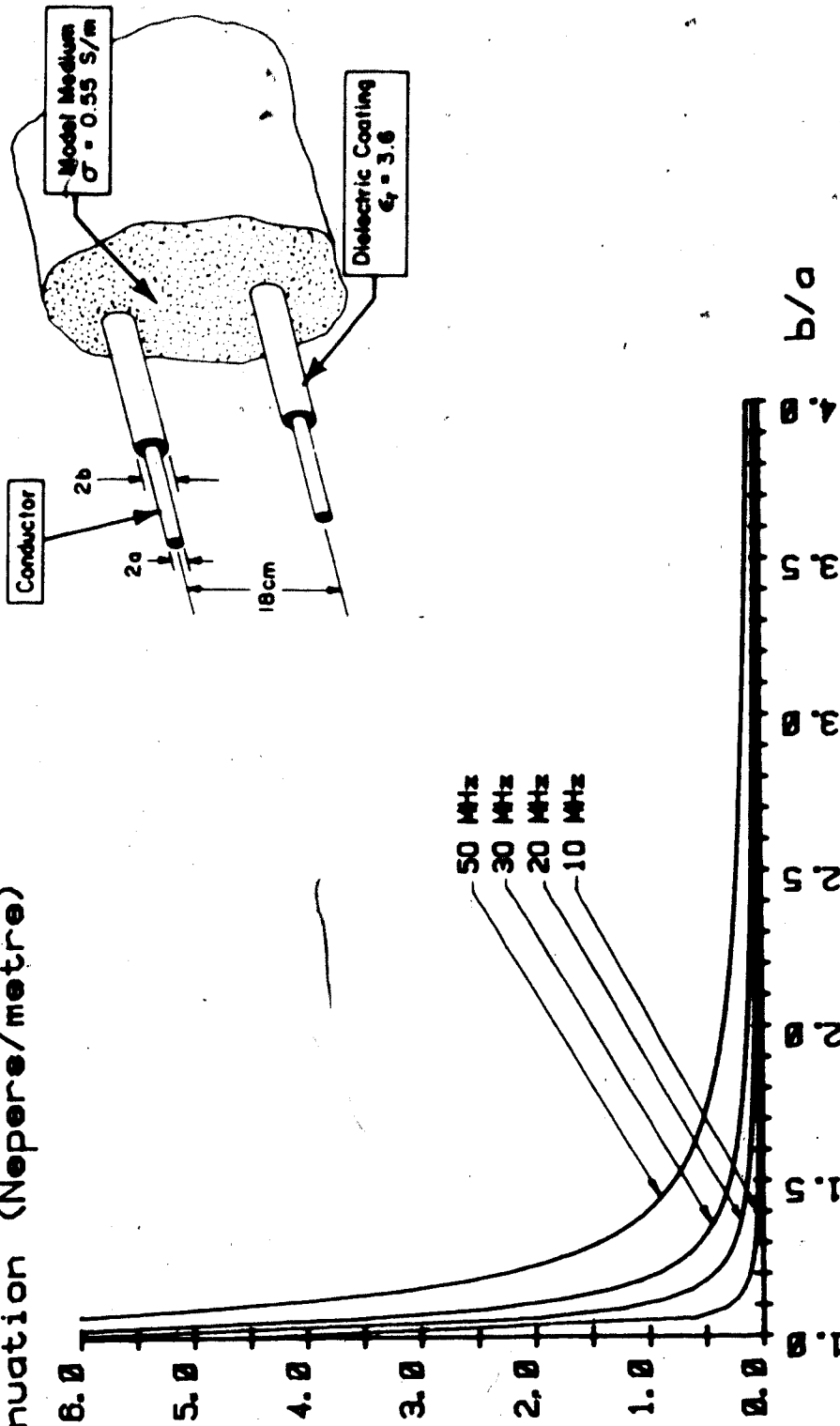


Figure 3.25: Attenuation rate versus electrode coating thickness at various operating frequencies. Based on the conductivity value at 100°C.

dielectric coated transmission line in a lossy medium. A description of the numerical model formulation is given in chapter 5. The figures are plots of the transmission line attenuation (depth of penetration = $1/\text{attenuation}$) versus coating thickness. The change in attenuation, as a coating is built up, is shown for a number of frequencies. The geometric sizing and material properties used in the numerical model were those of the physical experiment currently under consideration. Two figures are shown. The first shows the attenuation for the initial (25°C) material conductivity and the second is for the case of the conductivity approaching the 100°C value. An interesting aspect of these curves is that they show a distinct knee point. The attenuation reduction wrought by increasing coating thickness is quite large up to the knee point, but the change is much more gradual beyond this point.

The heating sequence is believed to develop in the following manner. On initial power application partial evaporation boring occurs creating a growing coat on the electrodes. Since the decoupling/coating thickness relation initially changes very rapidly, there will be a strong tendency for the electrode coating to rapidly reach the knee point. If, for example, a part of the line has a coating even slightly thinner than elsewhere, it will have a significantly higher attenuation rate. Power absorption and therefore the current density around the electrodes would be higher in this section such that a more rapid generation of

the dried coating may be expected. A line section with an initially thinner coating will have its coating grow more rapidly until its thickness is comparable to the coating on other portions of the line.

The heating profile generated in the formation may be expected to develop in different ways according to the operating frequency used. In the present example the model operating frequency is 12 MHz (111 kHz in the field). From figure 3.24 the knee point attenuation rate is about 0.4 nepers/m. The model line length is 0.9m. Following a short transition period during which the coating reaches the knee point value, a wave travelling the length of the line may be expected to lose about half its energy each time it traverses and re-traverses the line length. As the temperature rises the loss per pass will decrease (see figure 3.25). It may be expected that the coating generated on the line electrodes will be of equal thickness at all points along the line. The heating along the line will be essentially uniform because of the relatively low end to end attenuation on the coated line. The experimental temperature profiles obtained in this section support this postulated heating sequence.

Consider what happens if a higher operating frequency is used. In the scale model partial evaporation boring experiment (see section 3.3) the operating frequency was 52 MHz. An examination of figure 3.24 shows that in this frequency range the knee point is considerably less

distinct. A typical value of attenuation would be about 1.6 nepers/m. The attenuation rate will not drop to this point until a considerably thicker coating is generated than is the case at 12 MHz. At this higher attenuation rate a wave will lose the great bulk of its energy far before it reaches the end of the transmission line. Rather than a wave traversing and re-traversing the line multiple times and depositing its energy evenly, an incoming wave is absorbed in the first part of the line. Eventually when a sufficiently thick coating is generated the first part of the line will de-couple and deeper portions will heat. The expected result is an advancing heat front type of temperature profile. The experimental temperature profiles obtained in section 3.3 indicate this form of heating sequence.

Both heating modes considered are generated by the evaporation of connate water from the immediate vicinity of the electrodes. The higher frequency case would appear to be somewhat less energy efficient since a thicker zone of oil sand would have to be evaporated. The lower frequency case is not, however, without its own limitations. During the lower frequency run described in the present section, the electromagnetic heating was continued until the central regions between the electrodes were brought up to temperature. It was noted that, particularly toward the end of the heating run, the drive potential had to be increased to maintain the power level selected. The effect is due to

the increasing degree of de-coupling that occurs as the electrode coatings grow. The effect, however, places a lower limit on the operating frequency. Given some maximum operating potential the frequency must be selected high enough that the central regions may be heated adequately before essentially complete de-coupling occurs. One possible variation for obtaining uniform heating while reducing the de-coupling problem might be to initially operate at a lower frequency and then shift to a higher frequency later in the heating run after the uniform coating has been generated.

3.5 Series Resonated Transmission Line: Experimental Results

3.5.1 General

The electrode configuration under consideration would involve coupling lengths of coated electrode pipe together using short capacitor sections. As previously described two desirable effects were foreseen for this arrangement. The first of these is an increase in the skin depth due to the electrode coating. The second is that a resonant (or near resonant) selection of the series coupling capacitors would further increase the skind depth, and more importantly, increase the effective wavelength such that distortions in the heating pattern due to standing wave effects can be reduced.

In order to provide some experimental verification of these postulated effects two unscaled transmission line experiments were performed.

3.5.2 Wavelength Expansion: Demonstration of Effect

The basic configuration under consideration is a finite length, coated electrode, transmission line driven horizontally into the formation. The payzone to be heated is sandwiched between the upper/lower electrode pairs. The operating frequency and coating thickness are selected such that the line length is small compared to the skin depth obtained with the coating in place. Uniform heating of the payzone along the length of the line may be expected if the overall length is much less than a wavelength (no standing wave pattern). If the length involved is not much less than a wavelength, it may be postulated that the proper addition of series capacitors to the electrodes will greatly increase the wavelength and thereby improve the uniformity of the heating. Note that uniform heating of the area between the upper and lower electrodes, for all points along the line, implies a constant potential between the electrodes for all points along the line (see figure 3.26).

Experimentally then, one may examine the wavelength expanding effect if one examines a low loss transmission line, which has a significant length compared to a wavelength. If the addition of series capacitors improves the uniformity of the voltage profile along the line, an

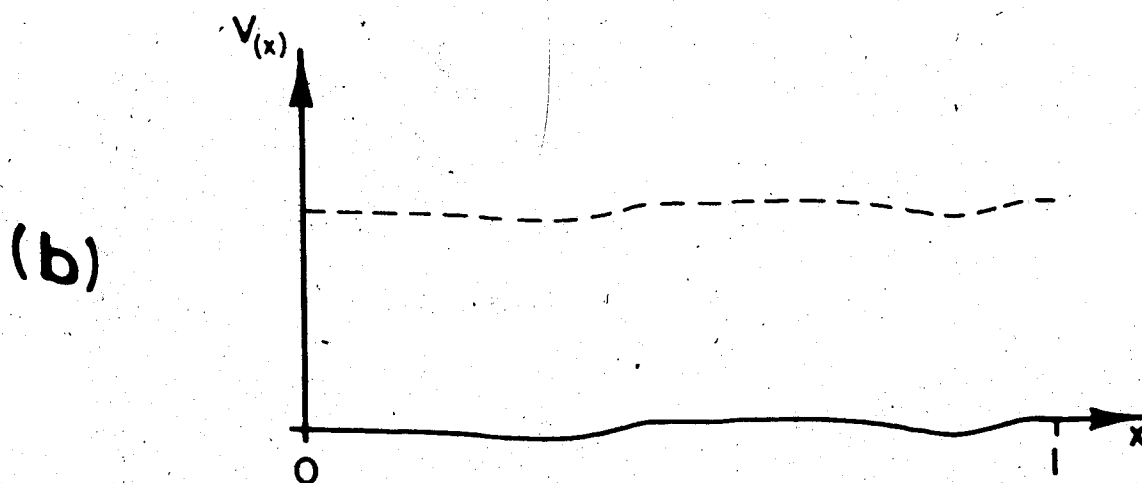
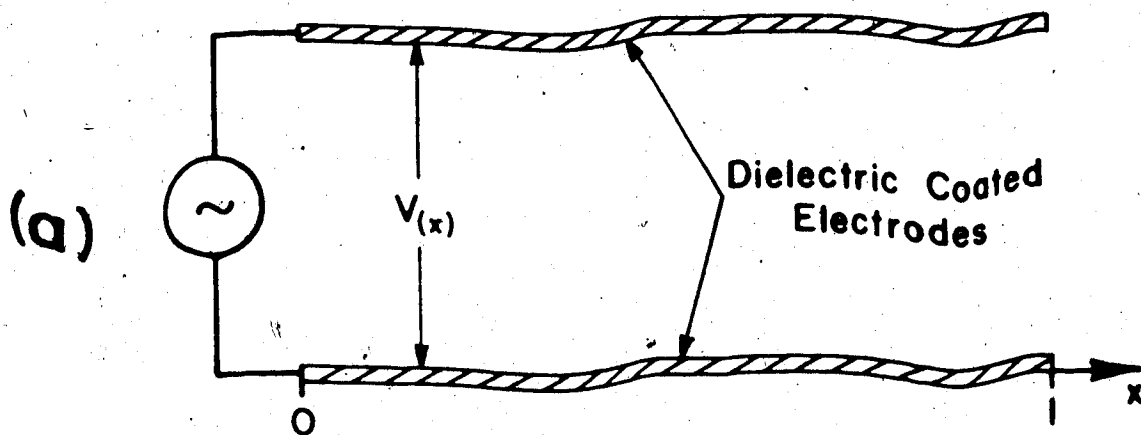


Figure 3.26: Required uniform potential $V(x)$ between the electrodes for uniform heating.

improved heating profile may also be expected.

In this first demonstration a very basic configuration was assembled. Two cylindrical electrodes 6.35 mm in diameter and 104.4 cm long were supported 39 mm apart in air thus forming a low loss transmission line. The line was excited at 60 MHz and fed through a balun. The potential across the line, at various points along the line, was measured. The results are shown in figure 3.27. One may note that the line is somewhat less than a quarter of a wavelength long at this frequency and that the measured potential distribution follows the expected (theoretical) standing wave distribution except for some distortions at the line feedpoint and end.

An essentially identical set of electrodes was then constructed, except that the line was broken at four points to insert capacitors. The line spacing and capacitor sizes were selected to approximate a distributed series capacitance (for both electrodes combined) of 7.04 pF/m (or 27 pF/26.1cm). This series capacitance will nominally resonate with the line inductance at 60 MHz. The distances and capacitance values used are shown in figure 3.28.

The potential distribution along the line was measured at 60, 52.2 and 69 MHz. The results are shown in figures 3.29, 3.30 and 3.31. Three curves are shown on each figure. One curve is the measured potential distribution along the compensated line. The second curve is the theoretical distribution one would obtain with no compensation. The

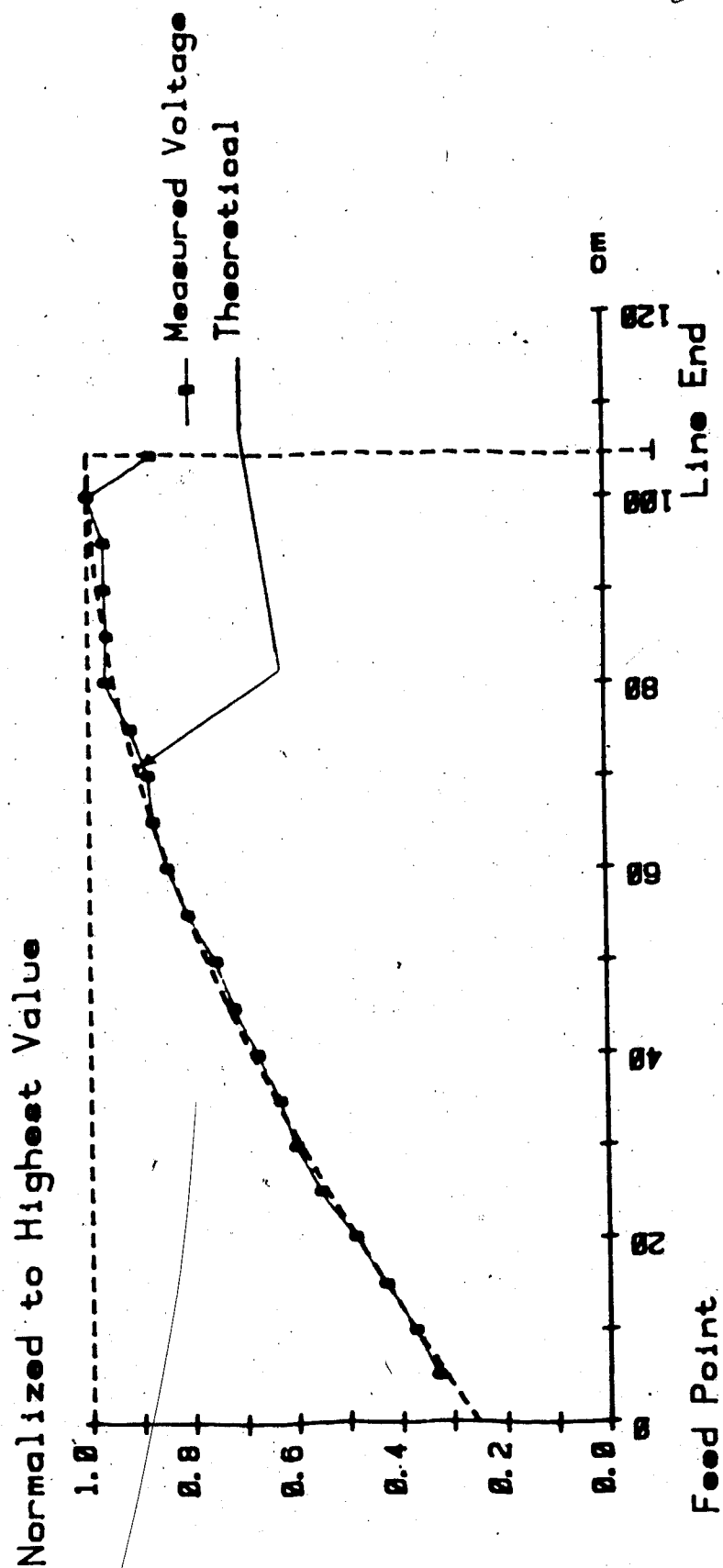


Figure 3.27: Measured and theoretical potential distribution on a low loss two wire line with no compensation. Operating frequency is 60 MHz.

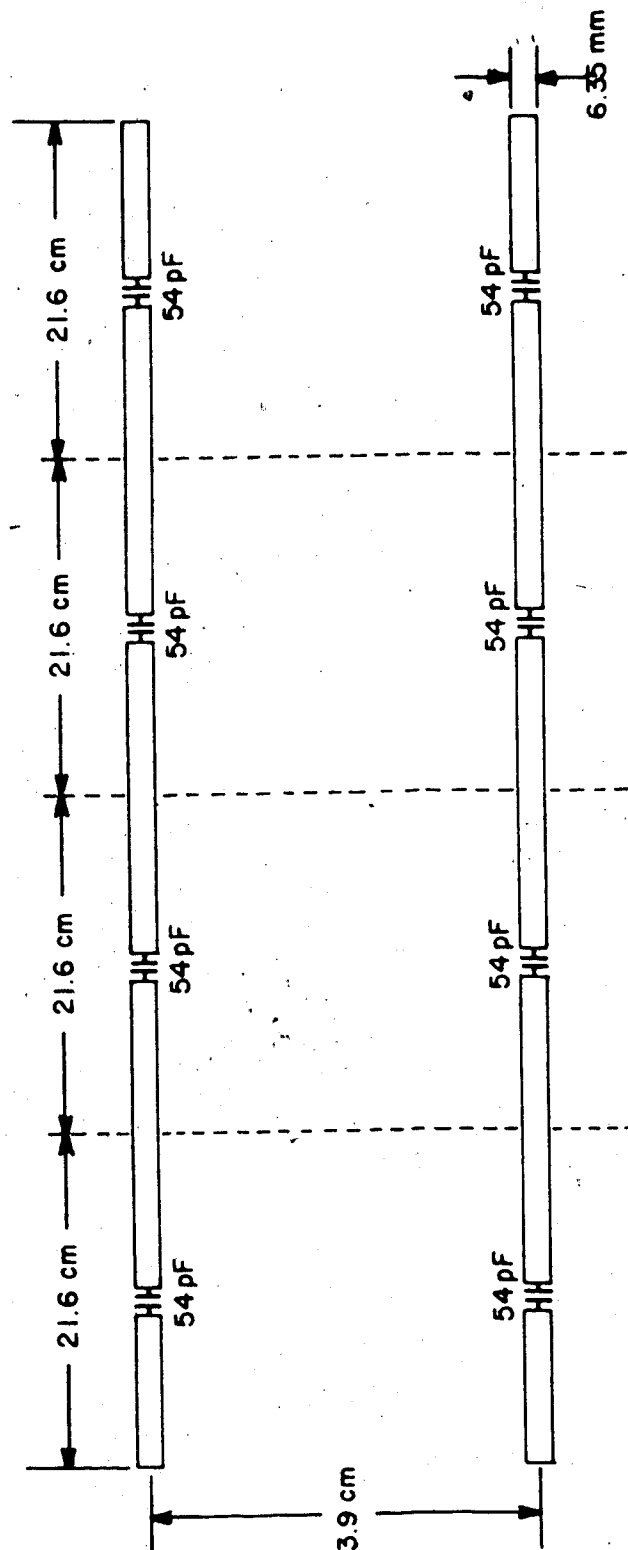


Figure 3.28: Position and size of series compensating capacitors on a two wire line. Values will nominally resonate the line at 60 MHz.

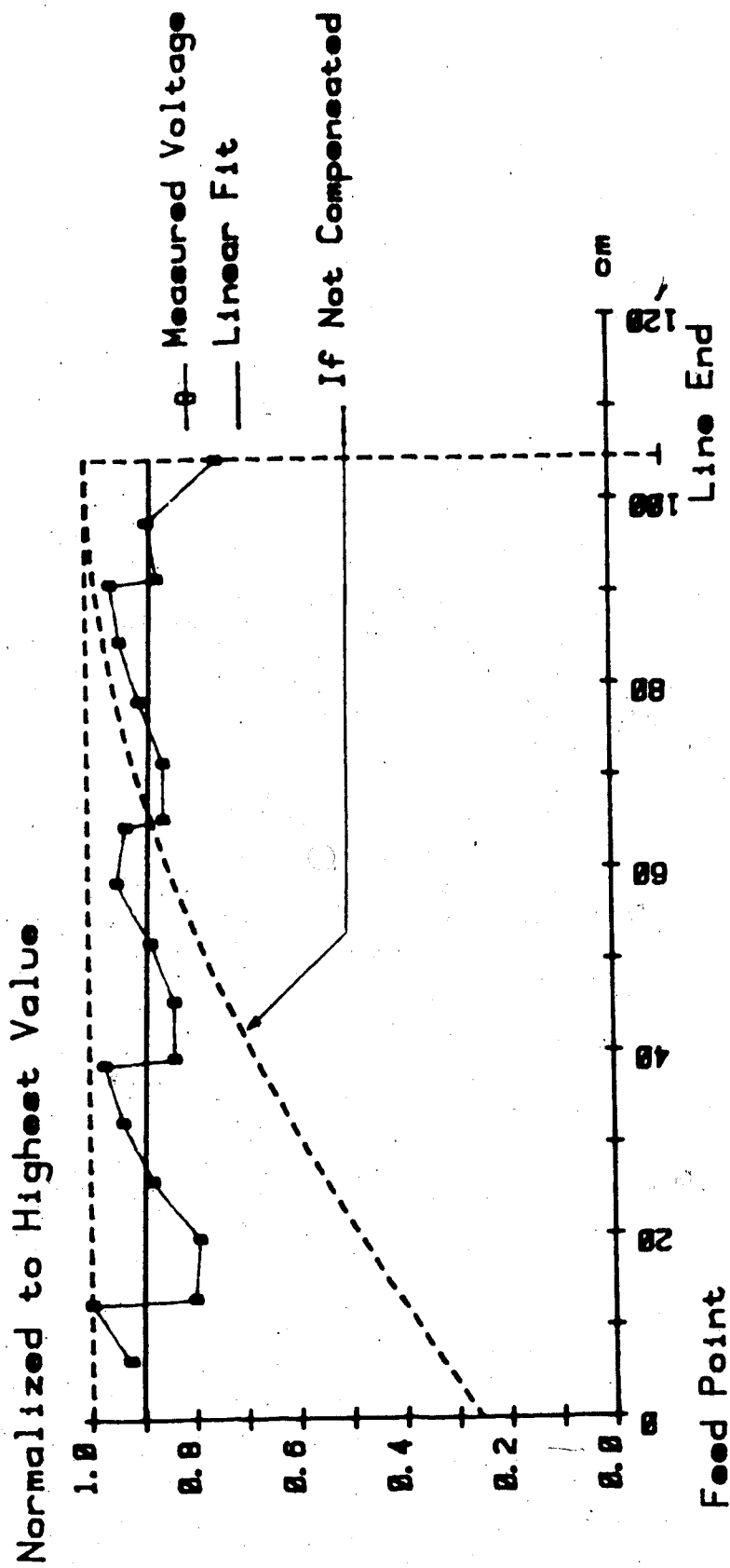


Figure 3.29: Measured potential distribution on a compensated two wire line operated at the 60 MHz design frequency. Also shown is the least squares linear fit of the measured potential points and the theoretical potential distribution that would be on the line if it were not compensated.

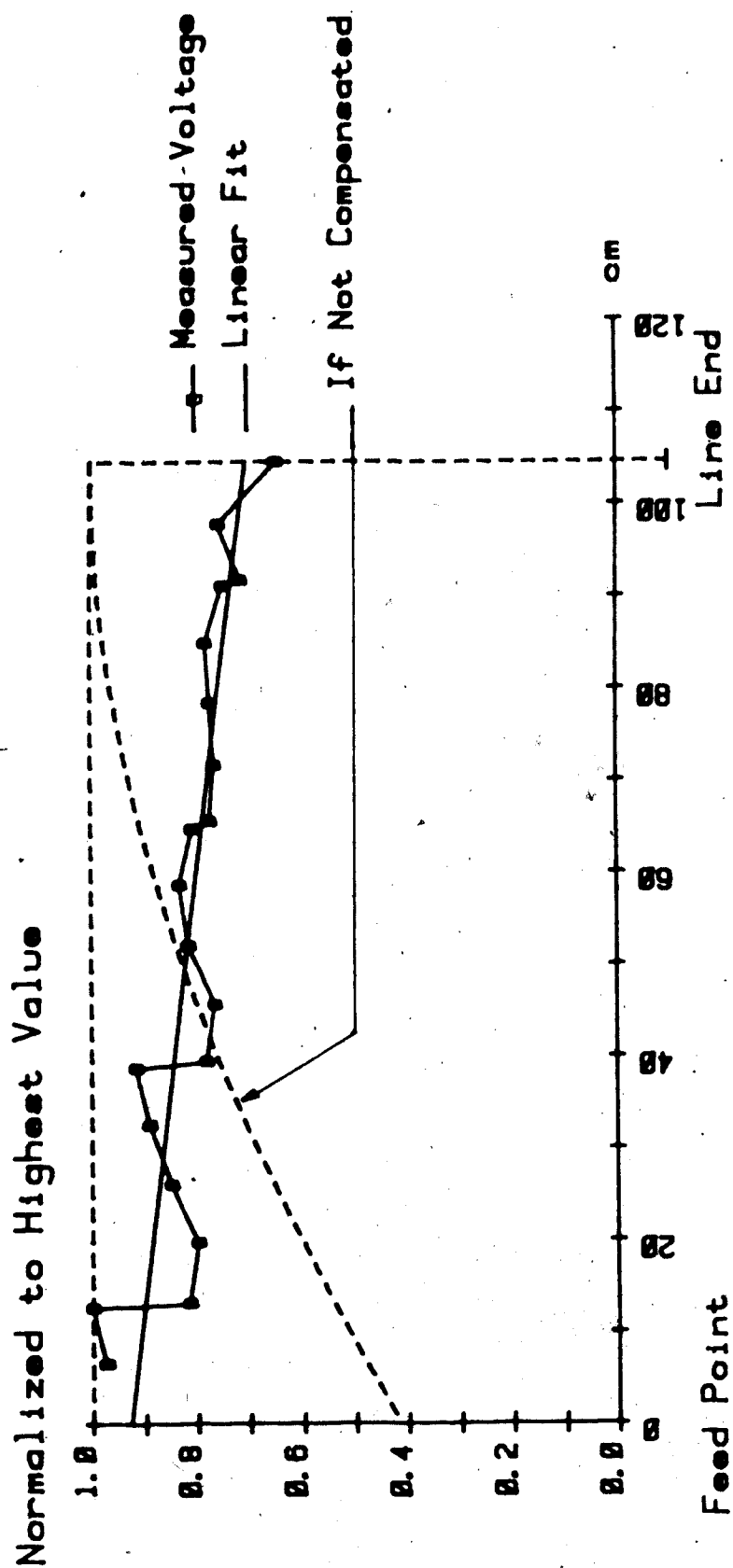


Figure 3.30: Measured potential distribution on a compensated two wire line operated at 52.18 MHz. The line design frequency is 60 MHz. Also shown is the least squares linear fit of the measured potential points and the theoretical potential distribution that would be on the line if it were not compensated.

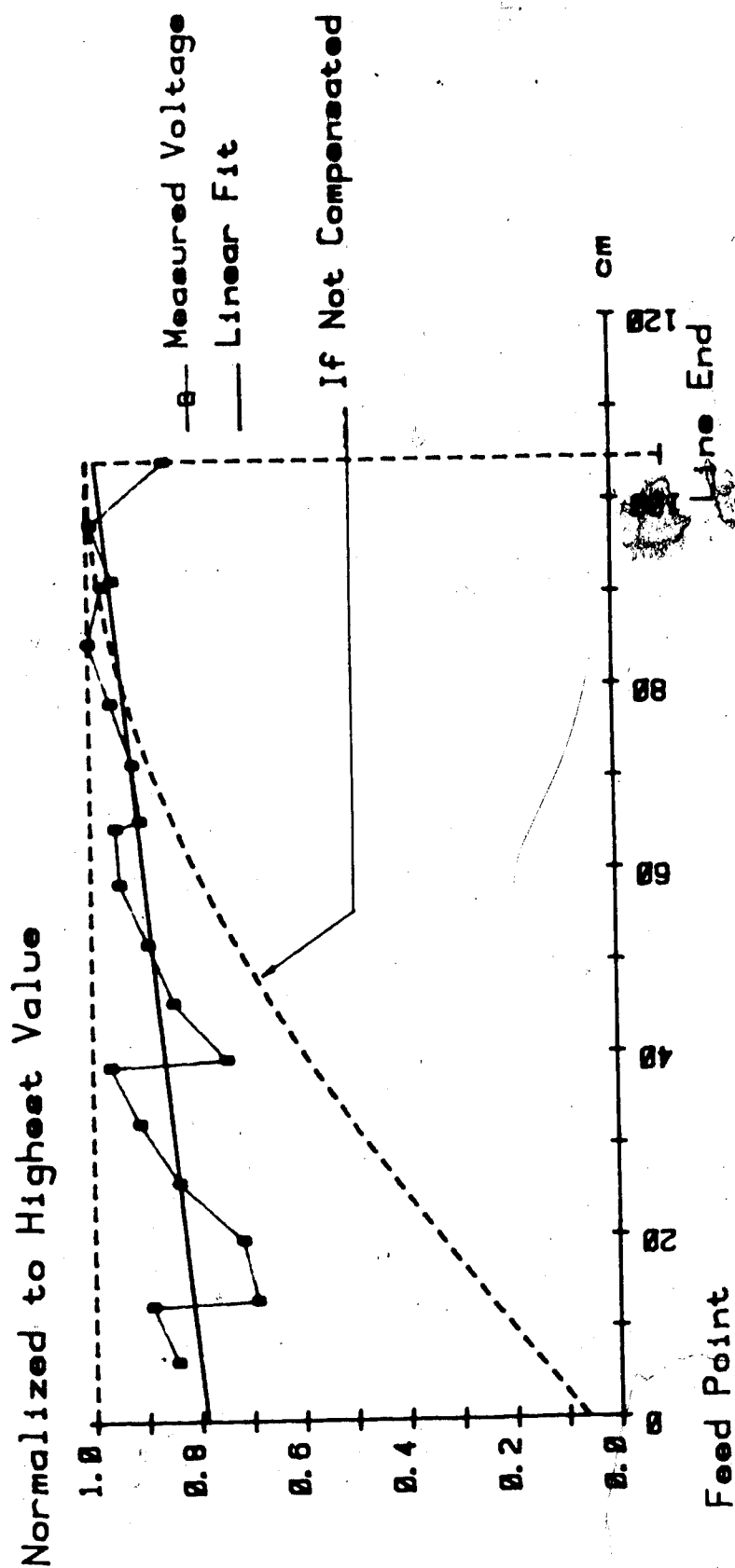


Figure 3.31: Measured potential distribution on a compensated two wire line operated at 69 MHz. The line design frequency is 60 MHz. Also shown is the least squares linear fit of the measured potential points and the theoretical potential distribution that would be on the line if it were not compensated.

final curve was generated by doing a least squares fit of the compensated line measurements, its purpose being to establish the general trend of the potential distribution. It is interesting to note that the potential distribution trend appears to be the most uniform at the design frequency. A comparison of the compensated and uncompensated results obtained, suggests that a substantially more uniform heating pattern will be obtained with the compensated line.

3.5.3 Skin Depth Expansion: Demonstration of Effect

It has been postulated that the addition of suitable series resonating capacitors to transmission line electrodes, will in addition to expanding effective wavelength, increase the depth of penetration as well. To test for this effect both the uncompensated and compensated electrodes described in the preceding section were alternately installed in a lossy medium as shown in figure 3.32.

The spacing requirement postulated for the compensating capacitors (see section 2.5) was that the length between the capacitors must be much less than the uncompensated skin depth and wavelength on the transmission line. Since the introduction of a lossy medium reduces both the wavelength and skin depth, while the capacitor spacing has remained fixed, we are in effect expanding the electrical spacing

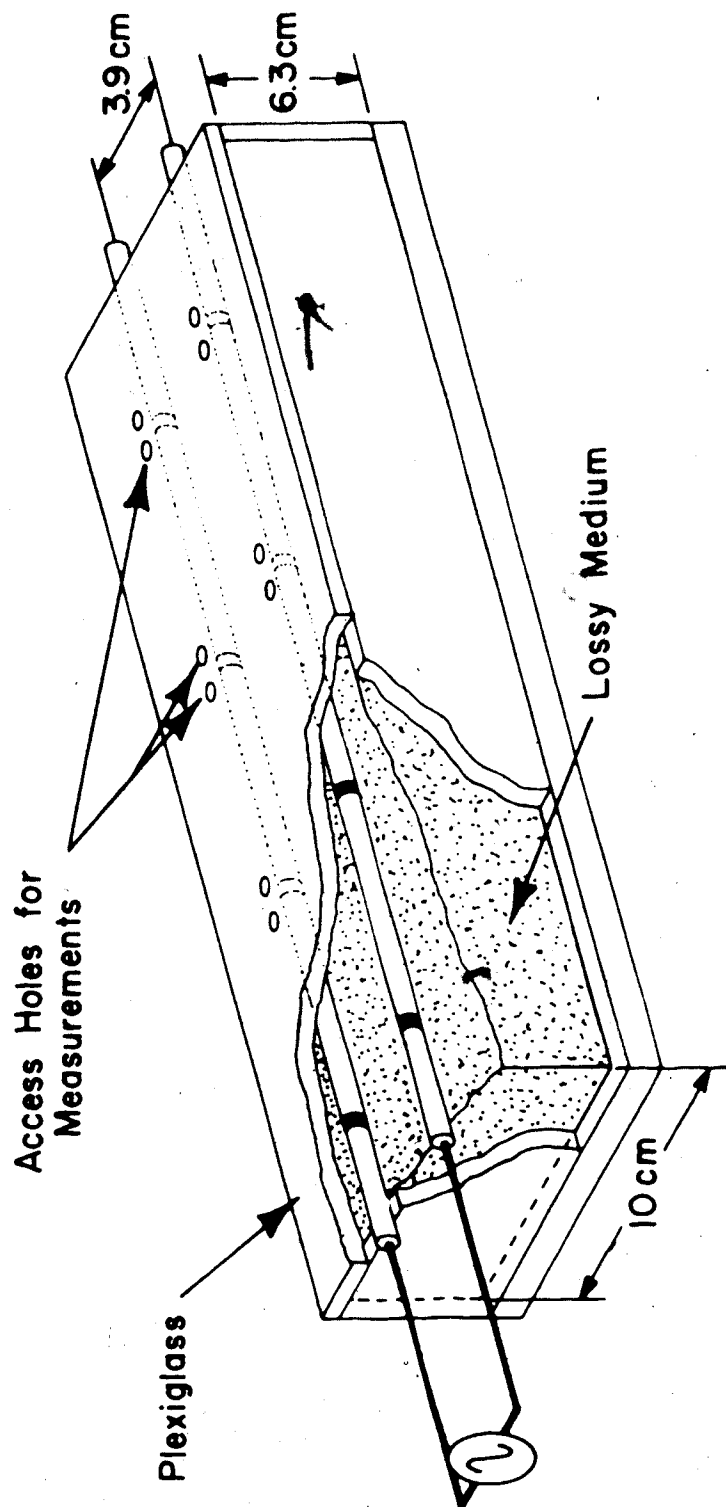


Figure 3.32: Installation method used to place both the compensated and uncompensated transmission line electrodes in a lossy medium.

between the capacitors. This being the case, each capacitor must make a larger adjustment to the potential distribution and somewhat larger fluctuations in the measured potential distribution may therefore be expected.

The lossy medium was assembled by blending Syncrude tailings pond sand with a saline solution. At 60 MHz the medium's conductivity was 2.3×10^{-3} S/m, and its relative permittivity was 4.6. The uniform plane wave skin depth in this medium is 59 cm for 60 MHz excitation. As the transmission line is only a little more than half buried in the medium, the skin depth on the uncompensated line can be expected to be about 30% to 40% larger.

The potential distribution obtained with uncompensated electrodes operated at 60 MHz is presented in figure 3.33. The results appear consistent with what would be expected on a fairly high loss open circuited transmission line; namely a decaying potential in the input region, with some standing wave effects visible but only near the line end.

The compensated electrodes were then buried in the same arrangement and measurements taken at 60, 54 and 66 MHz. The results obtained are shown in figures 3.34, 3.35 and 3.36.

As postulated earlier the potential fluctuations are higher than in the previous compensated line example. An examination of the potential distribution obtained for the 60 MHz design frequency shows an unexpected distortion in the potential distribution near the feedpoint. If the potentials obtained after the first compensating capacitor

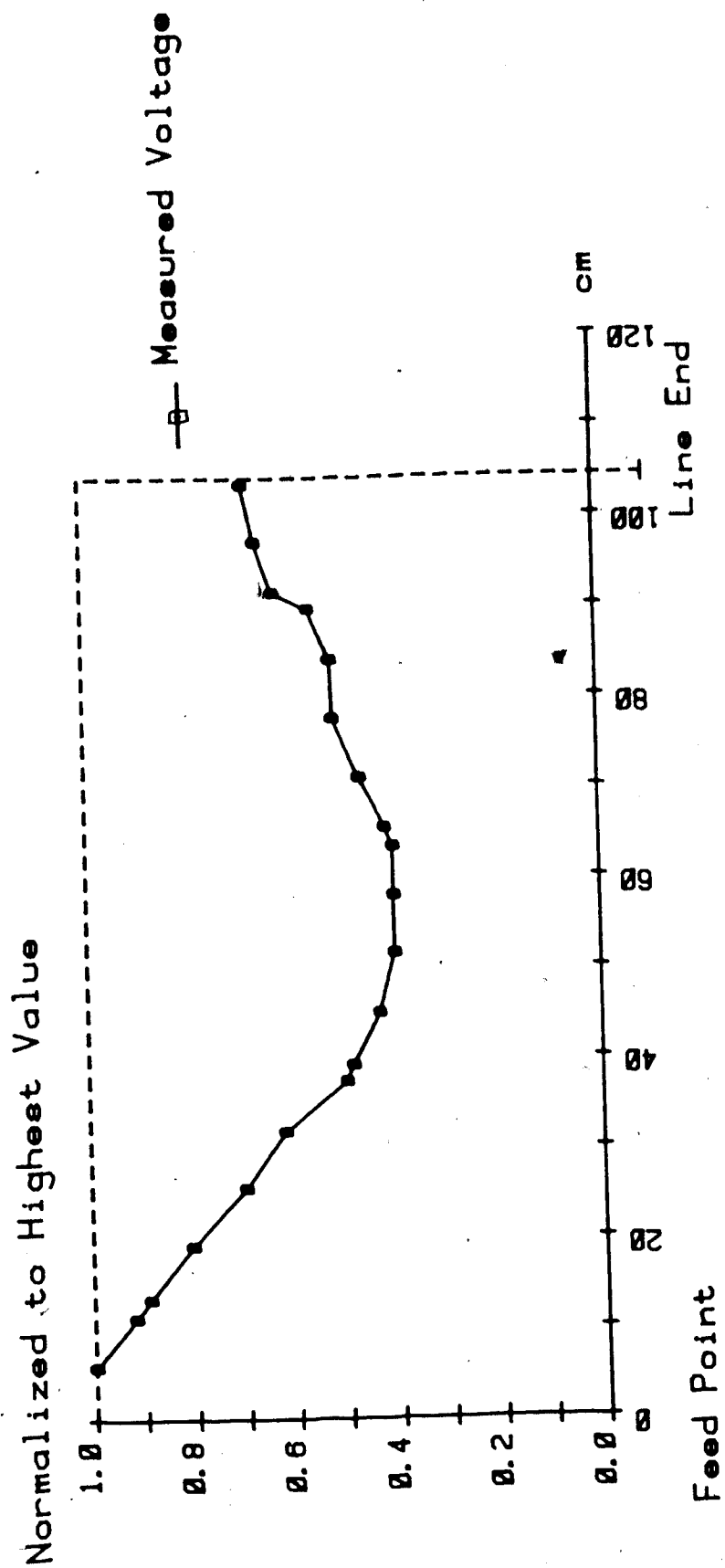


Figure 3.33: Measured potential distribution on an uncompensated two wire line buried in a lossy medium. Operating frequency is 60MHz.

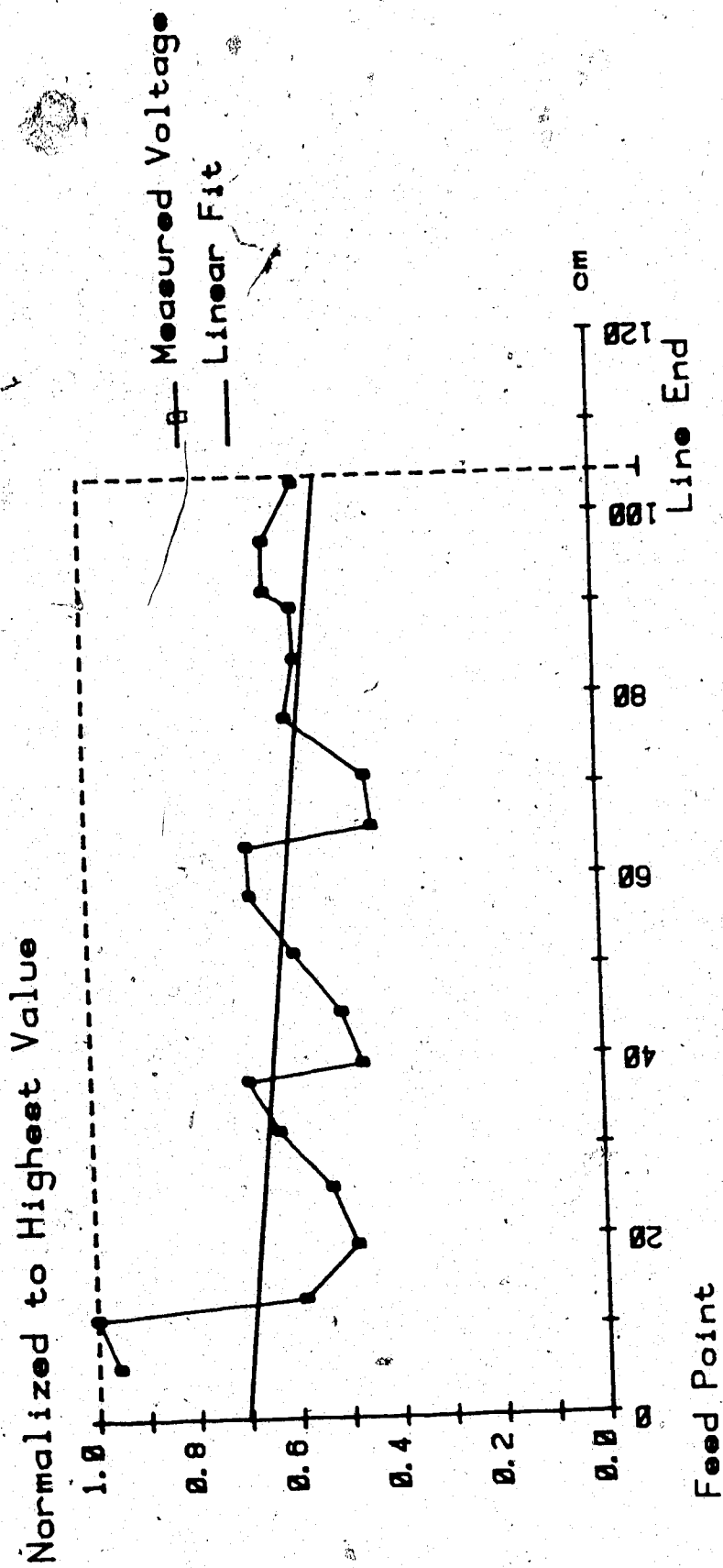


Figure 3.34: Measured potential distribution on a compensated two wire line buried in a lossy medium. Operating frequency is the design frequency of 60 MHz. Also shown is the least squares linear fit of the measured potential points.

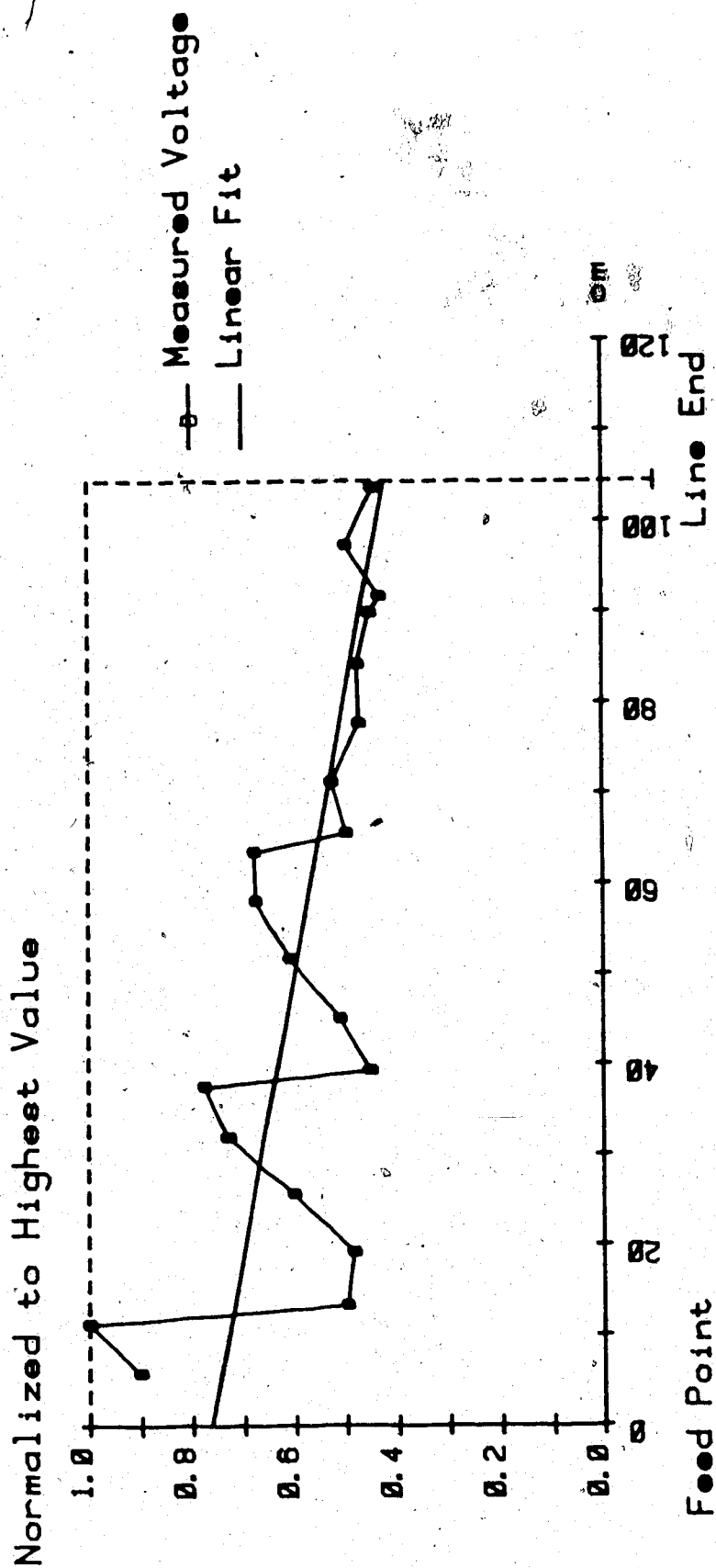


Figure 3.35: Measured potential distribution on a compensated two wire line buried in a lossy medium. The operating frequency is 54 MHz but the design frequency is 60 MHz. Also shown is the least squares linear fit of the measured potential points.

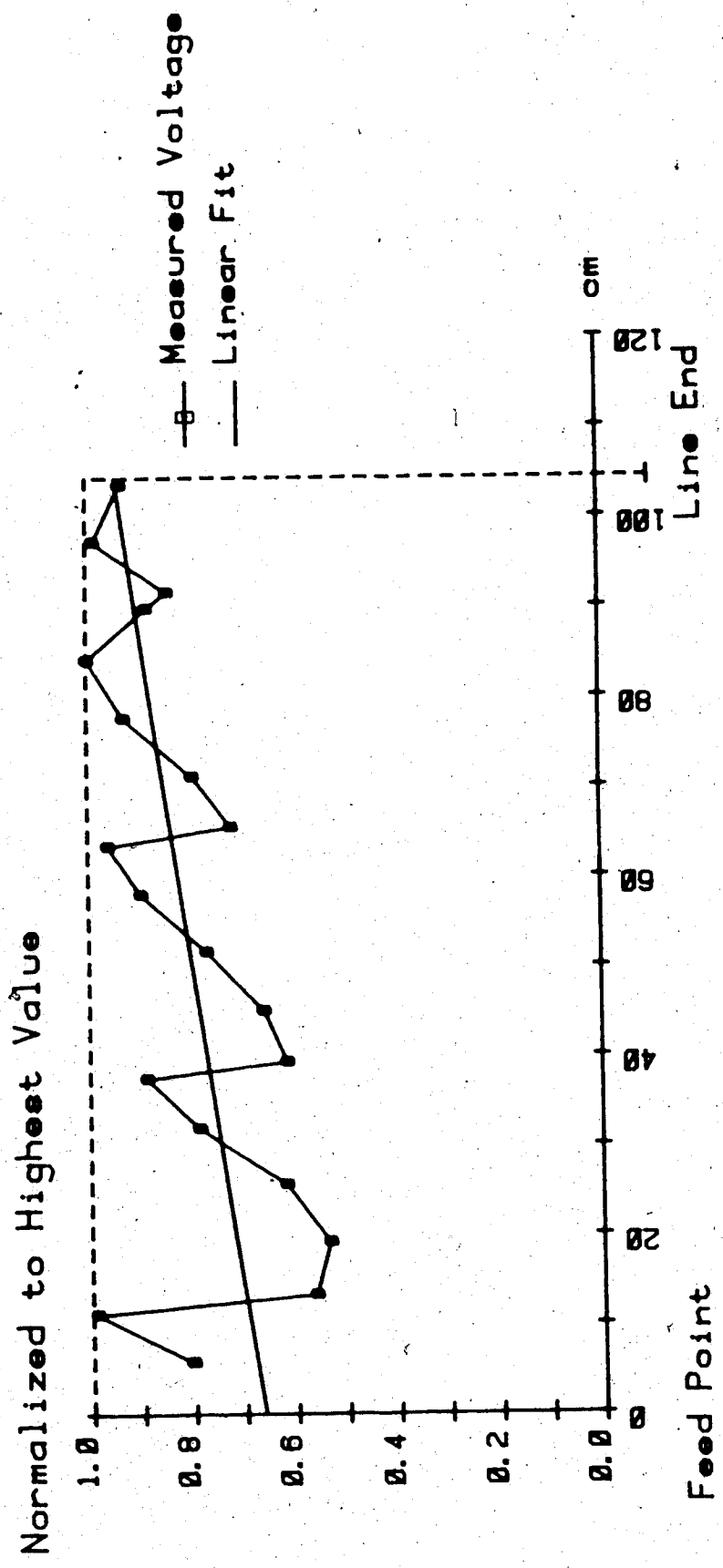


Figure 3.36: Measured potential distribution on a compensated two wire line buried in a lossy medium. The operating frequency is 66 MHz but the design frequency is 60 MHz. Also shown is the least squares linear fit of the measured potential points.

(at 13 cm) are considered in isolation, the average potential is uniform as desired. The higher potentials in the immediate area of the feedpoint are believed to be due to stationary modes established to meet the input boundary conditions. Considering the large abrupt change in characteristics that occurs at the feedpoint, some distortion of the field patterns in the immediate vicinity of the boundary does not seem unreasonable.

3.5.4 Conclusions

In summary, the results suggest that the postulated wavelength and skin depth expansion effects are in fact occurring as evidenced by the improved uniformity of the potential profiles obtained over the bulk of the transmission line length. Some tapering of the feedpoint transition may be desirable if a hot spot in the heating pattern is to be avoided.

An attempt was made to execute a scale model heating run using electrodes with series compensating capacitors. The attempt was unsuccessful. After considerable investigation it was established that the series capacitors were changing value substantially during the heating run. The capacitors used were Centralab type N750. These are low loss, temperature compensated ceramic capacitors. The principal difficulty was that these capacitors were buried

along with the electrodes in the thermally insulating model medium. In this environment the capacitor losses were adequate to heat the capacitors beyond their compensated range such that a substantial change in their reactance value took place. No permanent capacitor damage occurred, however, and the capacitors dug out after a failed heating run, were found to be undamaged.

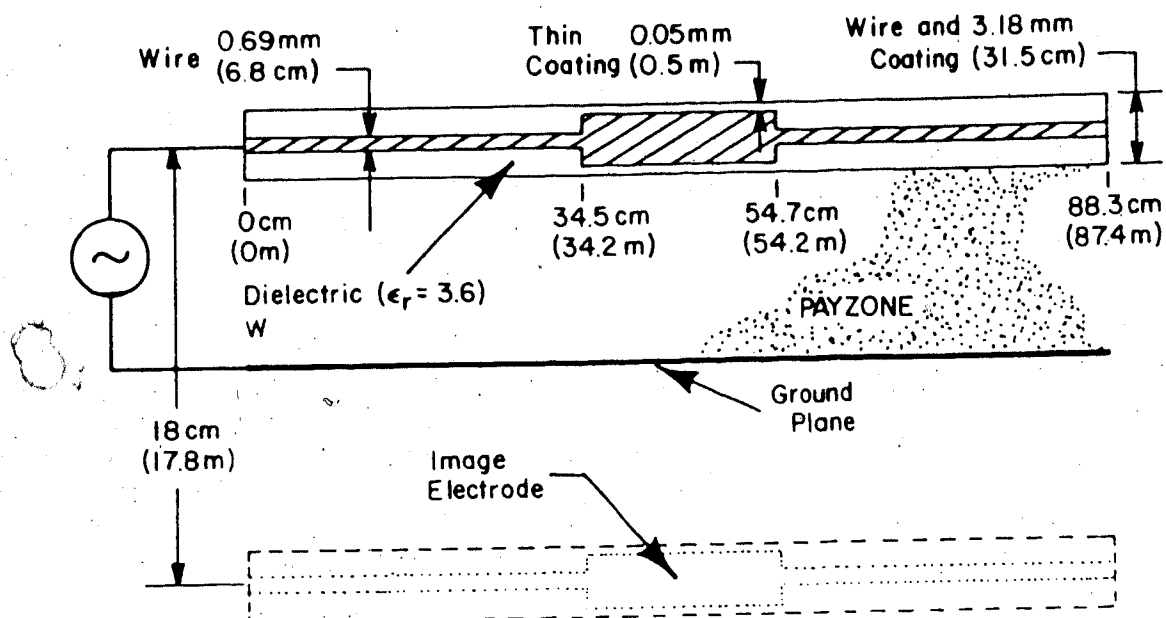
No additional work was performed to resolve this experimental difficulty. The principal reason for this was that the coated electrode heating runs described earlier showed no signs of a standing wave pattern in the thermal profile because of the presence of self leveling effects. The use of series compensating capacitors to expand the effective wavelength became, therefore, of questionable value.

3.6 Variable Coupling Electrodes: Experimental Results

The concept under examination involves constructing electrodes which have a much higher energy coupling factor over a selectable portion of their length, with the objective of gaining more specific control of the heating profile established in the formation. Two possible electrode construction formats to obtain this variable coupling feature were outlined in section 2.5. Unfortunately the construction of such variable electrodes in miniature for a scale model heating run is impractical due to the sizes involved. The construction of electrodes with a fixed region of higher coupling is, however, feasible. A partial heating run to examine the degree to which wave energy may be selectively placed in a specific section of a formation with such an electrode, should provide a good estimate as to the viability of the overall concept.

To that end, a scale model heating run was made using an electrode which has, over a portion of its length, a higher coupling factor. The general layout is the same as that used for the electrothermal scale model runs described in sections 3.3 and 3.4 dealing with partial evaporation boring and dielectric coated lines. The only major difference is in the construction of the electrode used.

The electrode used is detailed in figure 3.37. Note that the corresponding field scale distances are presented in brackets. The electrode has a relatively thick dielectric coating over the bulk of its length. For the frequency used



Medium Properties	Model	Field
Density (ρ)	1.62 g/cm ³	2.1 g/cm ³
Specific Heat (c)	0.86 J/g·°C	0.91 J/g·°C
Thermal Conductivity (k)	1.40 W/m·°C	1.65 W/m·°C
Electrical Conductivity (σ) ($\sigma \gg \omega\epsilon$)	0.198 S/m at 12 MHz	0.002 S/m at 121 kHz

Figure 3.37: Construction detail of electrode design which yields a transmission line with higher energy coupling over a section of its length. The bracketed quantities are the full scale field values corresponding to the model values.

the wave attenuation rate of this line type is small, leading to little attenuation when considering the total electrode length. Over a shorter portion of the electrode length the electrode has been radially extended and is only coated by a relatively thin dielectric layer. The wave attenuation rate on a transmission line with the latter cross-section is much higher than on the sections with thicker coatings and no radial extension.

A scaled electrothermal model was assembled using this electrode. The field electrical and thermal properties assumed were the same as in the heating runs described in 3.3 and 3.4 dealing with scale model electrothermal heating runs. The measured electrical properties of the model media were used in conjunction with these field values to establish the scaling relations. The methodology is outlined in chapter 7.

The heating run was made under the following conditions (field values in brackets). The drive and matching were monitored to maintain a constant net power level into the model of 200 W. The model is only a half element and therefore the corresponding drive to each electrode pair was 400 W (46 kW). The operating frequency was 12 MHz (121 kHz). Temperatures were obtained at various points in the model during the heating run. The temperature profiles obtained are presented in figures 3.38, 3.39 and 3.40.

Of particular interest is the thermal profile which develops in the formation for various points along a line

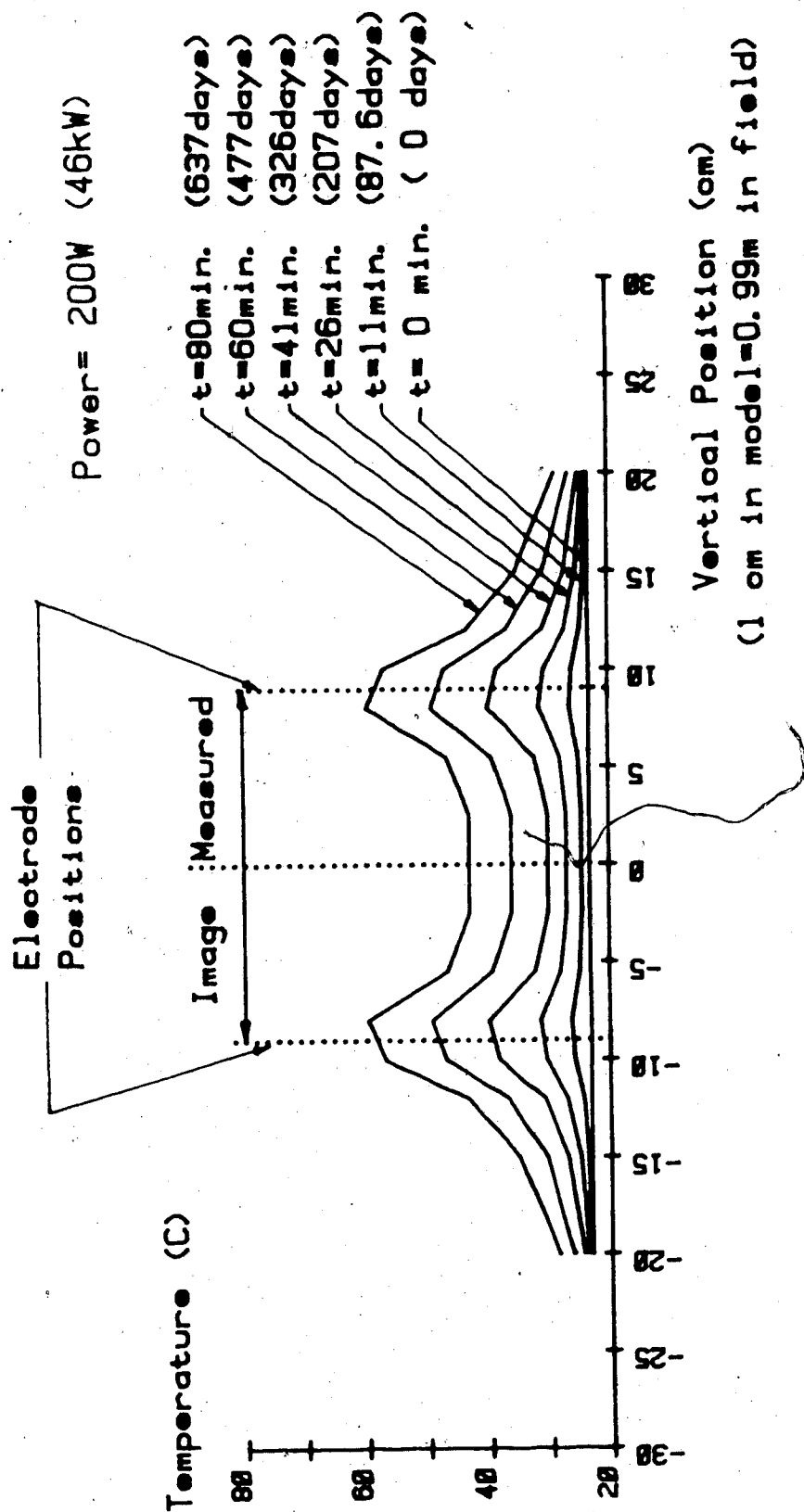


Figure 3.38: Measured temperatures in the scale model. Temperatures obtained during a variable coupling electrode heating run. Temperature variation across the line, measured along an axis intersecting the electrodes at a distance of 10cm (9.9m) from the line input. Bracketed quantities are the full scale field values corresponding to the model values.

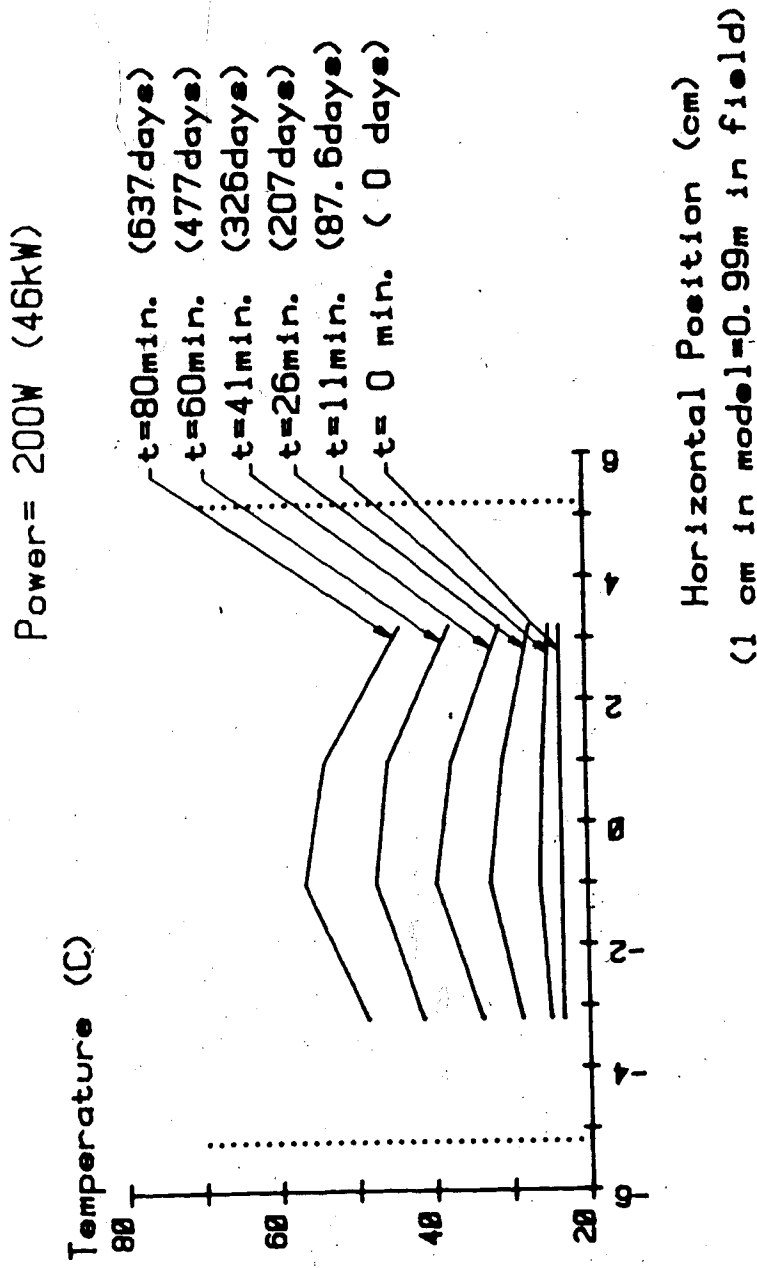


Figure 3.39: Measured temperatures in the scale model. Temperatures obtained during a variable coupling electrode heating run. Horizontal temperature variation, measured along a line 0.5cm (0.49m) below and perpendicular to the top electrode at a point 12cm (11.9m) from the line input. Bracketed quantities are the full scale field values corresponding to the model values.

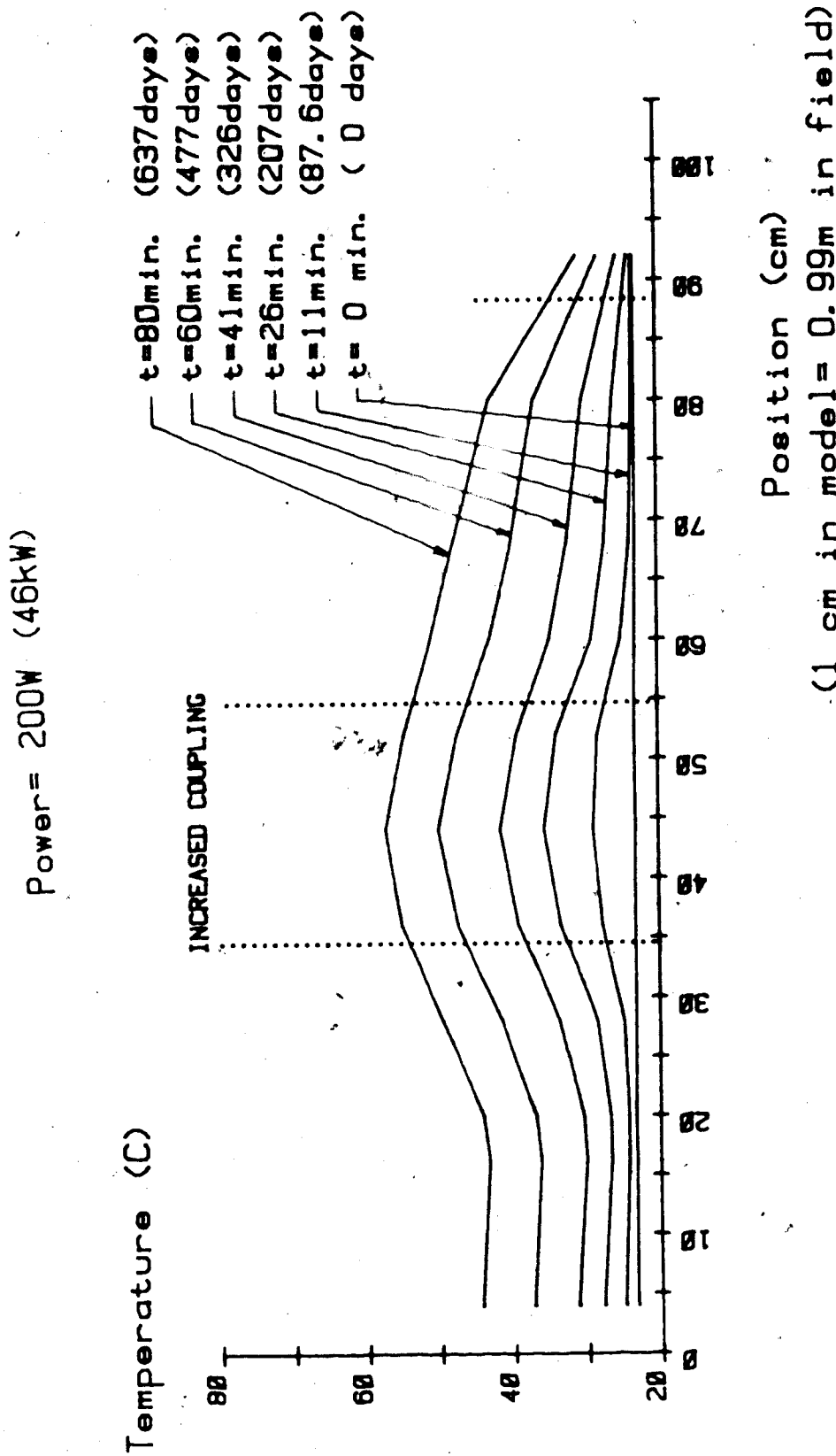


Figure 3.40: Measured temperatures in the scale model. Temperatures obtained during a variable coupling electrode heating run. Temperature variation into the formation, measured at a central point 1.5cm (1.49m) above the ground plane (above the midplane). Bracketed quantities are the full scale field values corresponding to the model values.

parallel to the electrodes (see figure 3.40). Bearing in mind that for any given point the temperature change between subsequent measurement times is representative of the energy added, a number of phenomena may be noted in the temperature profiles. If one examines the thermal profile after the first time step it may be noted that a much larger temperature rise occurs in the region of higher coupling, than is observed elsewhere in the formation. This result is consistent with our expectations of selective energy placement. Further into the heating run, however, this effect decreases. Near the end of the run the higher coupling zone still shows a somewhat higher temperature but an examination of the temperature change between readings shows an essentially constant temperature rise for all points along the line. This result would suggest essentially uniform coupling of energy is occurring along the line.

Mechanisms have been previously identified which tend to equalize energy deposition (see section 3.4 with regard to coated electrodes and self generated coatings). When the model was unpacked, considerable care was taken in digging out the electrode. The electrode was found to be encrusted with a layer of dried sand. By carefully brushing away the softer (moist) sand it was possible to obtain a reasonable idea of the self generated coating profile. A sketch of the profile is shown in figure 3.41.

The results of this experiment suggest that the temperature leveling effects associated with coated and self

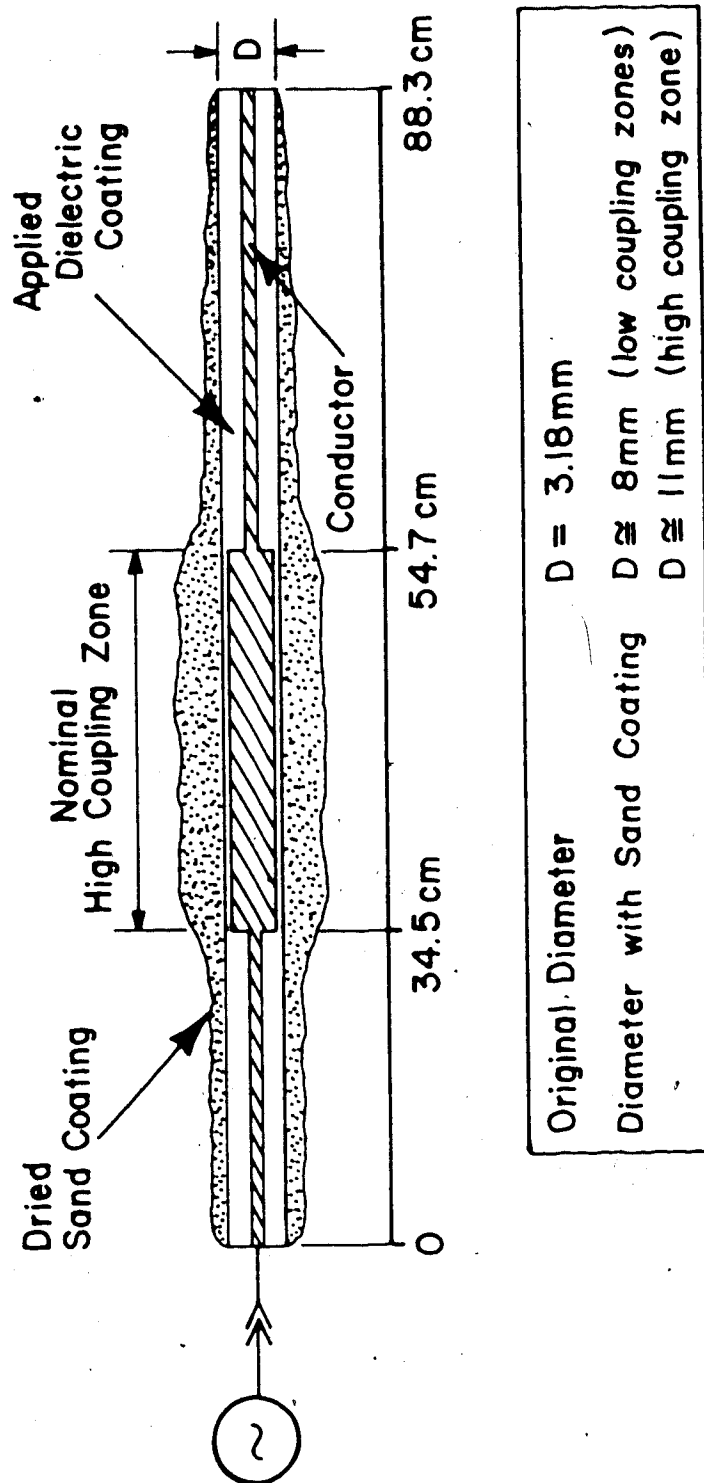


Figure 3.41: Sketch of the dried sand coating generated on the selective coupling electrode, showing a thicker generated coating on the region of higher initial coupling.

coated electrodes are sufficiently strong to largely counteract the selective energy placement effect of variable coupling electrodes. Considering this result and the innate complexity of the electrode structure, it was concluded that this format did not show sufficient promise to proceed with any further tests.

3.7 Production Controlled Heating: Experimental Demonstration of Effect

3.7.1 General

The concept and expected behaviour of the production controlled heating process were outlined in section 2.6. Briefly, when the input zone of oil sand, between the upper and lower transmission line electrodes, is heated by an impinging electromagnetic wave, formation fluids will flow into the lower electrodes and be removed from the system. The production of these fluids will lead to a decoupling of the electromagnetic wave from the oil sand formation in the input zone. The wave energy is thus freed to penetrate further into the formation and heat deeper parts of the formation. Starting from the feed point, successively deeper formation zones are heated and brought into production by the impinging electromagnetic energy.

The pivotal point to the heating process developing in the postulated manner is that the production of fluids takes place and that *this production leads to a substantial*

reduction of the wave energy absorption by the formation.

Significant fluid production is not expected from any oil sand zone until the zone has undergone some heating. This expectation is due to the very high viscosity of the bitumen (a few million centipoise) at the initial formation temperature of about 10°C. The viscosity, however, reduces very rapidly with temperature (to ≈ 1000 centipoise at 80°C) and fluid production becomes much more feasible as a zone is heated. A number of different drive mechanisms may contribute to the ejection of fluids from the formation. In conventional oil fields high initial production is often obtained due to the evolution of dissolved gases from the oil. The gases form a cap over the reservoir and provide a pressure drive that forces the oil into the well. Unfortunately, there are minimal dissolved gases in Athabasca bitumen and no significant contribution to production can be expected from this mechanism. A second drive mechanism comes about as a result of bitumen undergoing thermal expansion as it is heated. Bitumen can be expected to expand about 8 to 9 percent if heated from 10°C to 100°C. The amount of production from this drive is thus quite limited. A third drive mechanism can develop if the upper portions of the formation can be heated past the flash point of the connate water. The flashing will result in the depleted zone containing pressurized steam which will force the bitumen into the lower electrode wells in a manner similar to a gas cap in a conventional oil reservoir. It is

unclear, however, how long this steam drive mechanism can be maintained in a production controlled heating scheme. Examining the depleted zone/saturated zone demarker shown in figure 2.5, it may be expected that at some point the steam in the depleted zone would break through to the lower electrode wells in the input region where the saturated zone is least thick. A steam breakthrough into the lower wells, or possibly into the tunnel system, would release the pressure and terminate the drive available through this mechanism. A final drive mechanism is for the heated bitumen to simply drain into the lower electrode wells by the action of gravity. This final drive mechanism is considered the most reliable, very inexpensive, but, unfortunately relatively weak compared to the previous drive mechanisms.

In order to obtain an initial estimate of the viability of the production controlled heating concept a number of unscaled physical experiments were undertaken to demonstrate the salient feature of production leading to decoupling. A description of these experiments follows this section. In addition, a first order numerical model was developed to simulate production controlled heating occurring in an Athabasca oil sand deposit. The model is conservative in that it assumes the only drive mechanism available is gravity. The numerical model and some of the simulation results obtained are presented in chapter 6.

3.7.2 Experimental Setup

A reasonably straightforward experimental configuration to demonstrate the fundamental processes of heating, production and wave decoupling was sought. The selected configuration consists of a parallel plate arrangement packed with an oil sand type of material. The bottom plate is perforated to allow the passage of fluids while blocking the sands. If it can be shown that energizing these plate electrodes gives rise to heating, followed by production and a subsequent large reduction in wave coupling, the critical aspects of the production controlled heating concept will have been demonstrated. This configuration can be considered to be representative of a short segment of the transmission line that is embedded in the formation.

The next consideration is what form of excitation a line segment would experience if it were part of a transmission line operating in the production controlled heating mode. Consider the potential that would be measured between the upper and lower electrodes, at various points along the length of the transmission line, during production controlled heating. The amplitude of the potential would be essentially constant in the input areas where decoupling has taken place. Further into the formation the potential will rapidly decrease in the first zone that is still coupled, and deeper than that the potential will be essentially zero. At any given point in the formation the potential experienced is essentially zero until the wave bores into

that point and then the potential rises rapidly to a particular value and stays constant. The excitation for the experiment consisted, therefore, of energizing the plates with a constant potential. The power absorbed by the test cell was then monitored to verify if indeed the power absorbed decreased as fluid was produced.

The construction of a suitable parallel plate test cell is dependent on the properties of the medium to be packed in it. The medium selected will thus be considered first. The most logical choice is to use actual Athabasca oil sand. A drainage analysis was performed using the technique outlined by Dykstra¹¹ and typical Athabasca oil sand properties. This analysis revealed that for the drainage of oil sand columns, which have a height substantially larger than the residual capillary height, significant drainage would occur for periods up to several months. Given the time frame available for work on this particular scheme and the difficulty of maintaining controlled experimental conditions for this length of time, direct use of Athabasca oil sand in this initial experiment was rejected. A medium which would drain in a much shorter time period was sought. In order for the medium to reasonably simulate a bitumen saturated sand the viscosity of the saturating fluid should drop rapidly with increasing temperature. In oil sand the two qualities affecting the drainage rate are the permeability of the sand and the viscosity of the bitumen. These two properties were varied to obtain a decreased drainage time.

The experimental medium selected was an artificial oil sand constructed in the laboratory. The artificial oil sand was assembled in the following manner. A 40-60 "frac" sand from the Ottawa Industrial Sand Company was used as a base. The permeability of this sand was established as 70 ± 5 Darcies by flowing constant temperature water through a tube packed with the sand and monitoring the pressure drop across the tube. The variations indicated were due to some natural spread in the product consistency. The permeability of Athabasca oil sand fluctuates considerably and is particularly dependent on the amount of clay fines present. For comparison purposes, however, a value of about two Darcies can be taken as representative. A drainage rate gain of about 35 may thus be expected for this material over actual oil sand. To construct the artificial oil sand the frac sand was first partially saturated with a saline solution and then stored for 24 hours. A gear oil (Gulf Ultima EP460) was then blended in to bring the mixture up to about 97% fluid saturation. The intended purpose of the time delay in adding the oil was to induce some water wetting of the sand grains. The success in obtaining this feature is questionable since subsequent drainage experiments executed to determine residual capillary height demonstrated a residual oil saturation in the order of 15% in the drained areas. The initial fluid saturations used in the experiments were 65% oil and 32% saline solution. The 15% residual saturation level was somewhat higher than expected²³ and

suggests the sand may be oil wet since a higher residual saturation would be expected in this circumstance. A discussion of the effects of different residual saturation levels on the production controlled heating process has been included in chapter 6.

The published viscosity properties of the gear oil were 426 centistokes (centistokes times density equals centipoise) at 40°C and 30.2 centistokes at 100°C. If these points are put on an ASTM (American Society for Testing Methods) standard viscosity-temperature chart for liquid petroleum products the oil appears to fit the viscosity profile of about 15°API (American Petroleum Institute) crude oil. If 8°API oil is assumed for bitumen, the viscosity of the gear oil is about 100 times less than that of bitumen at any given temperature. A corresponding increase in the drainage rate can therefore be expected.

The electrical properties of the resulting mixture were measured and various permutations of the two saturating fluids were tried to determine what electrical properties were obtainable. From these measurements a particular mix was selected for the drainage experiment. The fluid saturation in this mixture was about 65% oil and 32% saline solution by volume. This amount of saline solution was higher than desired in terms of keeping the oil as the dominant saturating fluid but was required in order to obtain a conduction to displacement current ratio significantly greater than one. This conduction property

exists in Athabasca oil sand at operating frequencies below about a megahertz.

Heating and drainage effects which take place in this artificial medium should reasonably simulate actual oil sand. In both cases drainage is predominately regulated by the dominant saturating fluid which is a liquid petroleum product. The viscosity of both oils (EP460 and bitumen) have a similar viscosity-temperature relation in which viscosity drops off very rapidly with temperature.

Prior to construction of a parallel plate drainage cell a number of simple experiments were performed to establish the residual capillary height in the medium. The residual capillary height is the minimum level to which a column of fluid will drain under a gravity drive. The vertical plate separation in a drainage experiment should be much larger than the residual capillary height if significant fluid production and energy decoupling is to be observed. The residual capillary height was measured by two methods. The first method was to pack a 20 cm length of 5.1 cm inside diameter PVC tubing with the artificial oil sand. A screen was placed over the bottom of the tube and fluids were allowed to drain out into a large plate. The drainage column was placed in a Delta Design MK6300 convection oven and held at 80°C for 24 hours. The tube and sample were then frozen and the tube cut away. The demarker between the fluid saturated zone at the bottom of the sample and the depleted zone was visible and its height was measured as 5 cm. The

second method used to estimate the residual capillary height was to fill a tube with the frac sand and place it in a dish of the gear oil and to let the oil be drawn up the column by capillary action. This arrangement was left in the oven at 80°C for 16 hours. The dry sand above the demarker was then vacuumed off and the capillary height measured was 4.5 cm. It was concluded that the parallel plate drainage box requires a vertical plate separation which is substantially larger than 5 cm.

3.7.3 Experimental Runs

Two series of drainage experiments were run using two different parallel plate arrangements. The first series was, by and large, a learning experience which established the construction and instrumentation requirements. The information presented from these experiments has been limited to a description of the apparatus used and the observed phenomena. More detailed experimental results are presented from the second series.

In the first drainage test cell a 20.3 cm square by 25.4 cm high sample of artificial oil sand was packed in a plywood box lined with 5.1 cm thick styrofoam. The upper and lower plate electrodes were fabricated from a fine stainless steel mesh. The lower electrode was supported on a 1.3 cm thick plastic grill cut from a fluorescent light diffuser. The test cell was excited by an Amplifier Research model

2000L RF amplifier. The potential on the plates was monitored, through a 220 to 1 step down capacitive divider, on a Tektronics model 2465 oscilloscope. The current through the sample was measured on the oscilloscope by monitoring the potential developed across a capacitor mounted in series between the lower electrode and the supply ground. The capacitor size was selected such that the potential across it was much less than the potential drop across the sample. By monitoring these two signals and the phase between them, the impedance across the sample and the power absorbed by the sample could be determined.

The whole assembly was then mounted on top of a second plywood box containing an insulated beaker and a funnel arrangement to direct any fluid produced into the beaker. A small vertical strip on one side of the beaker was exposed so that the fluid level obtained at various times could be observed. Thin dielectric straws were inserted through the upper electrode to various depths in the sample to act as guides for inserting thermocouples. These thermocouples were mounted on a test jig which allowed them to be inserted and retracted from the sample with the straws acting as guides. A 5.1 cm thick styrofoam block was placed over the top electrode to insulate it. The bottom electrode could not be insulated without interfering with the fluid flow.

During the heating run the test cell was excited from the RF amplifier and the drive to the amplifier was continually adjusted to maintain a constant potential across

the plates. Power, impedance, fluid production and temperatures were monitored during the course of the run. The temperatures were obtained by briefly powering down the test cell and inserting the thermocouples. The temperatures were read using a ten channel Fluke model 2176A digital thermometer. The first series of runs were operated at various frequencies between 2 MHz and 10 MHz. The numerical model described in chapter 6 was modified to simulate the physical form of the test cell. Various operating frequency and voltage level combinations were run using the numerical model. The results of these runs were used as a guide in selecting the experimental voltage/frequency values.

As previously mentioned, a number of phenomena were experienced that led to modified arrangements for the second series of experiments. For example, during the first heating run it was noted that the support grill for the bottom electrode lost all structural integrity when exposed to hot oil. The grill was therefore replaced by one fabricated from copper strips. It was also found that the two kilowatt RF amplifier used would occasionally burst into oscillation at some very high frequency in excess of 500 MHz as a result of feedback between the amplifier and the experimental apparatus. Suitable re-positioning of the test cell further from the amplifier effectively suppressed the oscillations. Unfortunately, the oscilloscope inputs were damaged in this process as the permissible signal levels to the oscilloscope are much lower at very high frequencies than at lower

frequencies. In consideration of the costs involved, modifications were made in the electrical measurement procedure. The changing test cell impedance was monitored during the course of a heating run by briefly disconnecting the power source and connecting a Hewlett Packard 4815A RF Vector Impedance meter to the test cell. The power absorbed by the test cell was determined as follows. An Amplifier Research model DC2000 50db dual directional coupler was mounted between the source and the test cell. The forward and reverse sampled signals were applied to a Hewlett Packard 8481A power sensor connected to a Hewlett Packard 435A power meter. The power absorbed by the test cell could then be determined by subtracting the reverse power from the forward power. The potential across the plates was sampled with a resistive divider, rectified and then filtered before being applied to a Fluke model 8000A digital voltmeter. The filter was designed with a series inductive element to protect the voltmeter input if oscillations occurred.

An examination of the temperature profiles developed during the first series of drainage experiments indicated that the temperature throughout the sample was reasonably uniform except for points very close to the top and bottom electrodes which were cooler. When the central region approached 100°C the plate regions were 12 to 14 degrees cooler. A slightly cooler region near the top electrode was expected since this region is decoupling. A cooler region near the uninsulated bottom plate and copper support grill

suggested that thermal heat losses to the environment were sufficient to slightly cool the zone near the bottom plate. The energy loss, while not significant compared to the total energy input, did imply one difficulty. The oil viscosity changes very rapidly with temperature and a 12 to 14°C temperature difference implied a viscosity near the bottom of the sample about four times higher than in the middle of the sample. A viscosity plug is thus formed at the outlet which restricts the production. In order to partially compensate for this effect a resistance heater was bolted to the grill supporting the bottom electrode. It was experimentally determined that supplying the heater with 15 watts resulted in a steady state grill temperature of about 58°C. This temperature was about half way between the initial 23 °C sample temperature and 100°C. The heater power level was generally much less than the RF power level except at the terminal stages of heating when almost complete decoupling had occurred.

The final phenomenon noted was that fairly soon after a heating run was initiated, thermal expansion of the fluids would occur as evidenced by not only fluid production out the bottom but also by the appearance of fluids welling up over the top electrode. The fluids above the top electrode would cool and the oil/water mix tended to separate. In time the fluids would eventually drain back into the interplate region. The power absorbed by the drainage cell did not, however, fall off significantly until these fluids had

drained back in. Energy coupling was maintained much longer than expected. In the proposed field configuration the only outlet for the fluids would be the bottom collector electrode wells, as there is no place for the oil to expand above top electrodes. In this situation expansion can be expected to provide a strong initial production drive followed by a much more rapid formation of a depleted zone with its attendant decoupling. In order to circumvent this overflow phenomenon a different form of parallel plate drainage cell was designed and a second series of heating runs executed.

In the second series of heating runs a cylindrical sample 20 cm in diameter and 25 cm high was packed between the two plate electrodes. The bottom electrode was again a fine steel screen supported by a copper grill. The grill had an attached resistance heater. Thermal tests showed that a heater power level of 15 W would maintain the grill at about 60°C. The construction details of this second drainage cell are shown on figure 3.42. It may be noted that the top electrode is entirely sealed except for a tall thin tube attached to the top of the test cell. The objective of this arrangement was to insure that any fluid expanding over the top electrode would be forced up the tube. The tube diameter was small so that very little fluid expansion would lead to a large rise in the fluid level in the tube. The concept was that any expansion over the top electrode would lead to a significant increase in the gravity drive due to the fluid

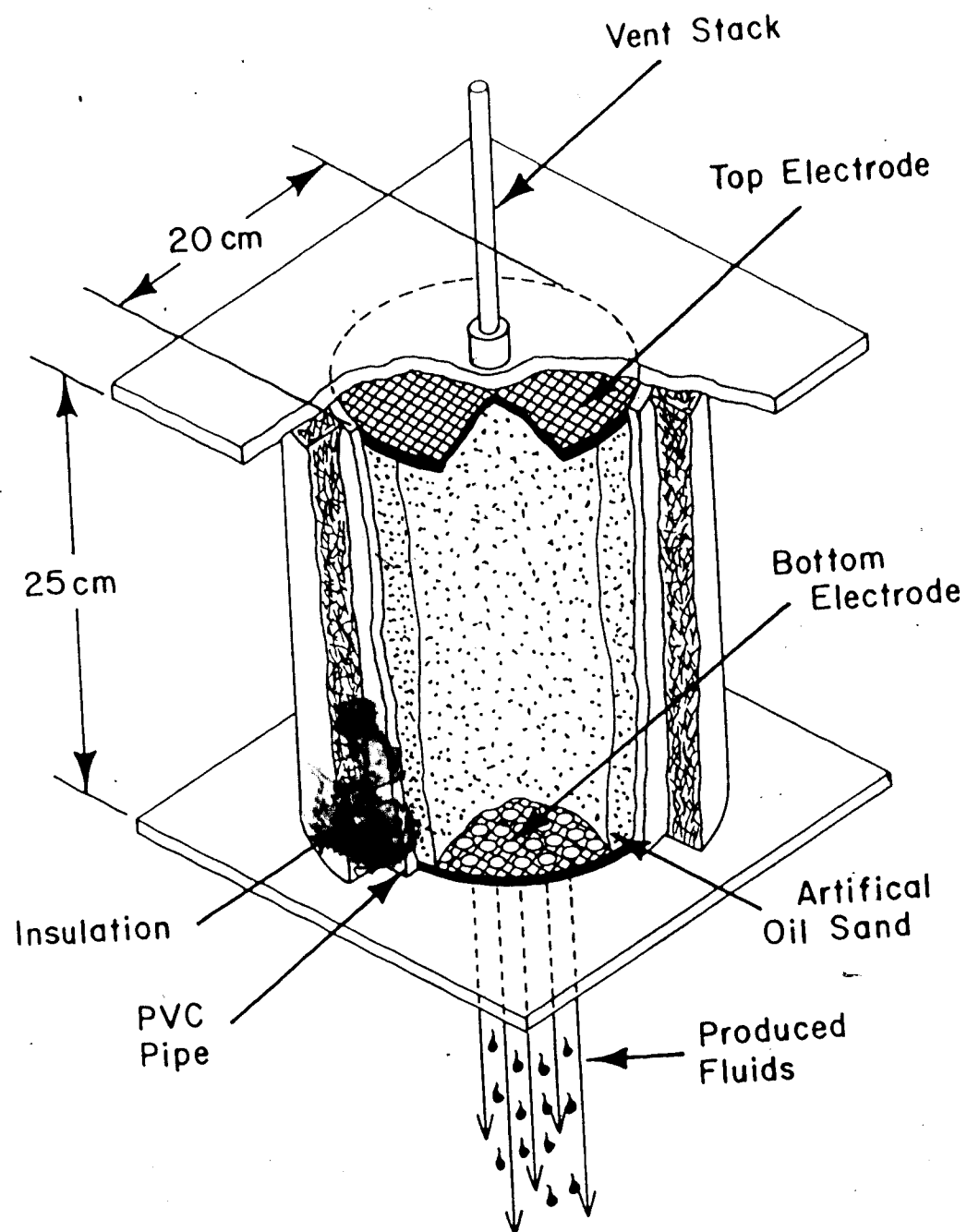


Figure 3.42: Production controlled heating demonstration. Construction detail of the test cell packed with the artificial oil sand.

head in the tube. In this manner the initial drive derived by the fluid expansion would not be entirely lost and since the tube diameter was small only a small amount of fluid would have to drain back into the test cell following the initial expansion.

In practice the fluid tended to break up and become lodged in the tube due to capillary forces. At later points in the heating run when evaporation would occur the vapour generated tended to pump the lodged fluid out of the tube. The vapour also tended to condense in the tube and drain back into the depleted zone. The coupling, as implied from the level of absorbed power, tended to be erratic due to this effect. Given the difficulties, the vent stack concept was abandoned.

The final combination examined was to execute the heating run with the top electrode entirely sealed. In this situation the drive mechanisms of thermal expansion and evaporation pressure supplement the gravity drive. The test cell was excited at 1 MHz and the potential across the cell maintained at a constant level. The RF power absorbed by the artificial oil sand was recorded throughout the heating run. A graph showing the power delivered to the test cell is presented in figure 3.43. Note that the energy coupling drops off in a time that is small when compared to the total production time. The fluid production from the test cell is shown in figure 3.44.

Power Absorbed (W)

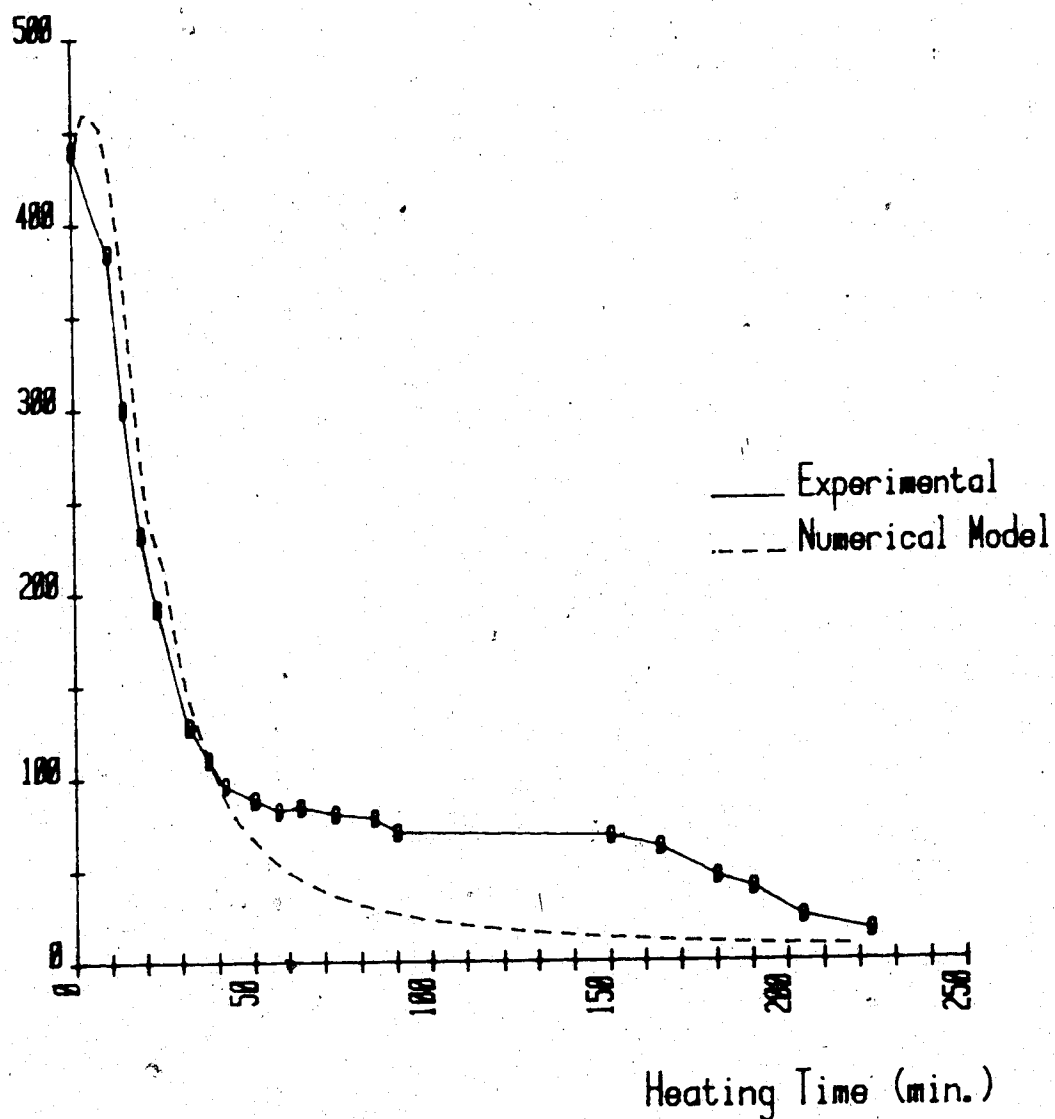


Figure 3.43: Production controlled heating demonstration. Power level absorbed by the sample versus time. Sample is excited at a constant potential level. Numerical simulation results are shown as well as experimental results.

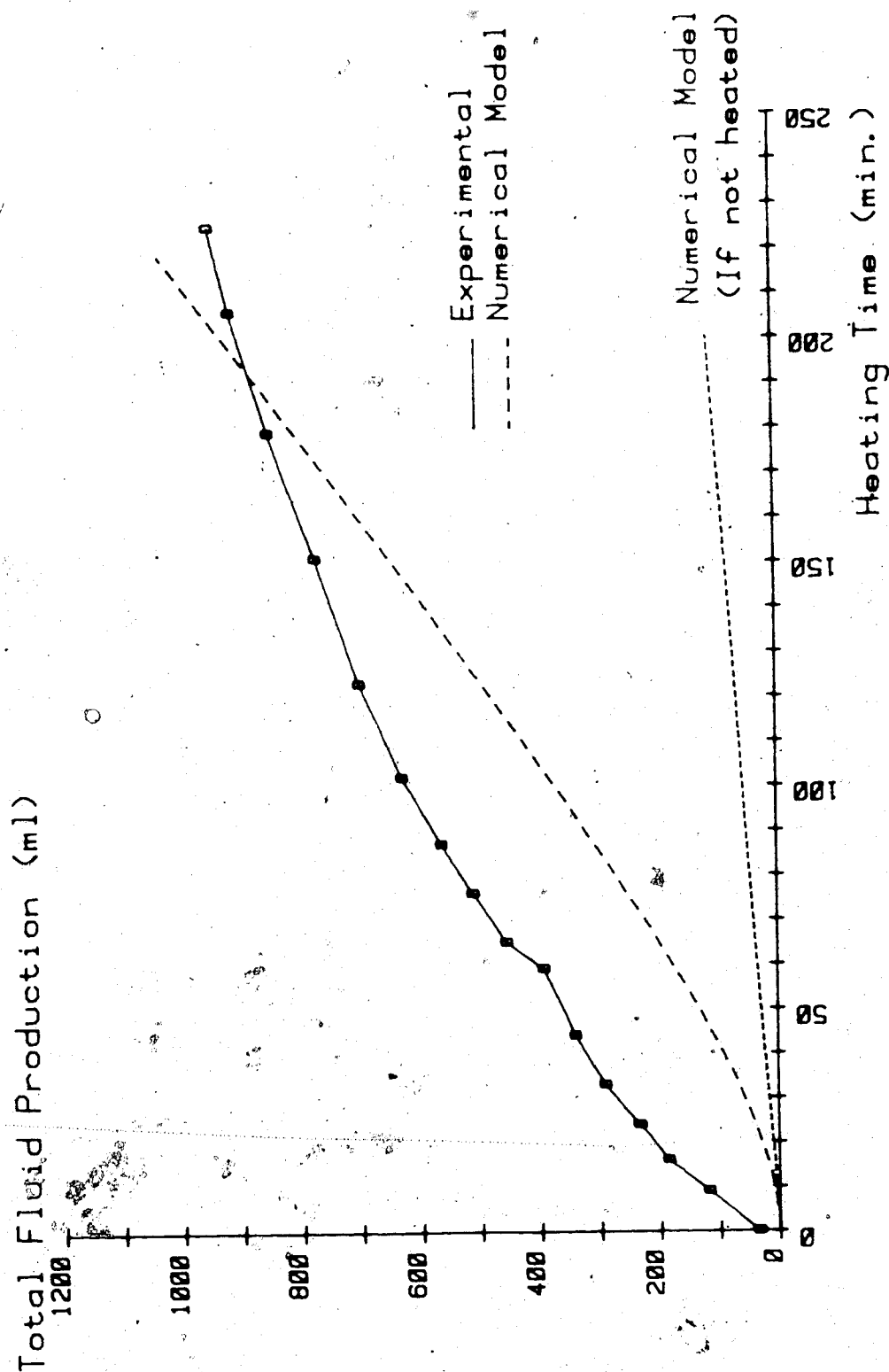


Figure 3.44: Production controlled heating demonstration. Total fluid production versus time. Numerical simulation results are shown as well as experimental results.

The production rate from the test cell is undoubtedly higher than the rate that would be obtained if only a gravity drive were available. In order to obtain some estimate of the difference involved, the numerical model described in chapter 6, which assumes only a gravity drive, was modified to simulate the experiment. The numerical model was reduced to a single slice with no fluid cross flow components. This ~~model~~ more accurately simulates the physical form of the experimental drainage box. The material properties used in the model are summarized in table 3.2. The electrical properties of the saturated zone were derived from the initial test cell impedance measured before any heating was begun. The electrical properties of the depleted zone were obtained by digging out a sample of the depleted zone after the run and measuring its impedance when packed in a small test cell. The numerical model uses a single fluid approximation and the presence of the saline solution in the sand reduces the effective permeability of the sand to the oil. To simulate this relative permeability effect the permeability of the artificial oil sand was derated by a factor of 0.6 from the 70 darcy level measured. This is a first order correction drawn from a graph presented in Craft and Hawkins². The graph relates various oil/water saturation mixes to the relative permeability of a porous medium.

The power level and total production values obtained from the numerical model are also shown on figures 3.43 and

Property	Saturated Zone	Depleted Zone
ELECTRICAL		
conductivity σ (S/m)	$7.12 \times 10^{-2} f(T)$ (*)	4.85×10^{-4}
relative permittivity	343	14
THERMAL		
density ρ (g/m ³)	1.95×10^3	1.66×10^3
specific heat c (J/g·°C)	1.0	1.0
thermal conductivity (W/m·°C)	1.6	1.6
FLOW		
permeability k (m ²)	4.2×10^{-11} (0.6x70 Darcy)	--
saturation S	0.97	0.15
porosity ϕ	0.33	0.33
viscosity (g/m·s)	$A \exp(B/T)$ (**)	--
	(*)	$f(T) = 1 + 0.0224(T - 24)$ T in °C
	(**)	$A = 3.03 \times 10^{-5}$ $B = 5154.3$ T in °K

TABLE:3.2 Material properties used in numerical model simulation of production controlled heating experiment.

3.44. The two situations (experimental and numerical model) are not entirely comparable since the numerical model assumes, rather conservatively, that only gravity drive is available. Further, the numerical model uses a number of first order approximations which limit its accuracy. With regard to the drive mechanisms, it may be noted from figure 3.44 that, as expected, the production rate predicted by the model is, at least initially, lower than the level obtained in the experiment. The difference is likely attributable to the thermal expansion drive. By the end of the heating time the theoretical production regains the difference and actually exceeds the experimental value. This sort of effect may be expected as the numerical model can be expected to yield optimistic results for recovery levels exceeding about 40% of the total fluid present in the test cell. A description of the flow model limitations may be found in section 6.2.5. In brief, the numerical model assumes a clean demarker between the saturated and depleted zones. In actual practice a partial saturation profile will develop above the demarker and the accurate prediction of production beyond about 40% recovery requires a much more involved numerical model formulation. Based on initial fluid saturations, the infinite time fluid recovery level for this system was determined assuming 100% fluid saturation in the bottom 5 cm (residual capillary height) and 15% residual saturation in the top 20 cm. At the end of the experimental heating time the fluid recovered represented 54% of the infinite time

value. Production beyond this point is, however, substantially slower^{15, 16}.

The experimental and theoretical electrical power curves shown on figure 3.43 are much more closely related than the corresponding production curves, except that the experiment did not decouple to quite the degree predicted by the numerical model. The difference may again be attributed to the saturation profile being more complex than is assumed in the model.

In summary, the experiments in this area were reasonably successful in demonstrating the pivotal effects of RF heating leading to production and this production subsequently de-coupling the formation. Similar work using an elemental model packed with actual Athabasca oil sand would be an important next step in examining this concept. Unfortunately the drainage times required for this type of experiment precluded such an examination in this study. A further alternative would be to demonstrate the decoupling and boring action postulated using artificial oil sand. This would require the construction of a sealed test chamber several metres long and would require assembling five to six hundred kilograms of artificial oil sand for each heating run. A project of this magnitude was not feasible in the present study.

4. Fields of a Lossy Parallel Plate Line

4.1 Introduction

Throughout this thesis, a number of schemes for high frequency electromagnetic heating of Athabasca oil sand formations are examined both experimentally and numerically. The electrode configurations postulated all involve the creation of some form of transmission line penetrating the formation in the payzone. Some numerical modelling has been undertaken for the schemes involving dielectric coated lines (chapter 5) and production controlled heating (chapter 6). Prediction of the electromagnetic heating in these numerical models is accomplished using transmission line analysis involving the use of the distributed impedance representation of the transmission line. An implicit assumption inherent in the distributed impedance representation is that the actual electric and magnetic field lines established in the formation have a particular transverse electromagnetic (TEM) form. If a single homogeneous medium exists between the electrodes of a transmission line the fields established between the electrodes will be TEM. In the cases of dielectric coated lines and production controlled heating the medium between the electrodes is not homogeneous due to the introduction of an insulating material in addition to the oil sand. The material is the coating in the dielectric coated line case and the depleted zone in the production controlled heating

case. As will be shown, the field form obtained from an analysis of a transmission line with an insular gap, as well as an oil sand zone, is not TEM.

A substantially non-TEM solution, therefore, brings into doubt the validity of using the distributed impedance representation. It will be shown that, for purposes of predicting wave energy deposition and propagation along the length of a lossy line, the distributed impedance representation is accurate, provided that the vertical separation between the electrodes is much less than the skin depth of a uniform plane wave in the oil sand between the electrodes. This result occurs in spite of the fact that even under these circumstances the field solution is still distinctly different from the form assumed by the distributed impedance representation.

The geometry under consideration is shown in figure 4.1. This formulation is of interest as it is representative of the geometry that is expected to develop in the production controlled electromagnetic flood process. In addition, some of the basic effects established here should also apply in the partial evaporation boring and coated line schemes.

In the case of a parallel plate transmission line with no depletion layer, the dominant field mode is a Transverse Electromagnetic (TEM) field that is essentially a uniform plane wave between the plates. The introduction of a depleted (insular) layer will, however, substantially alter

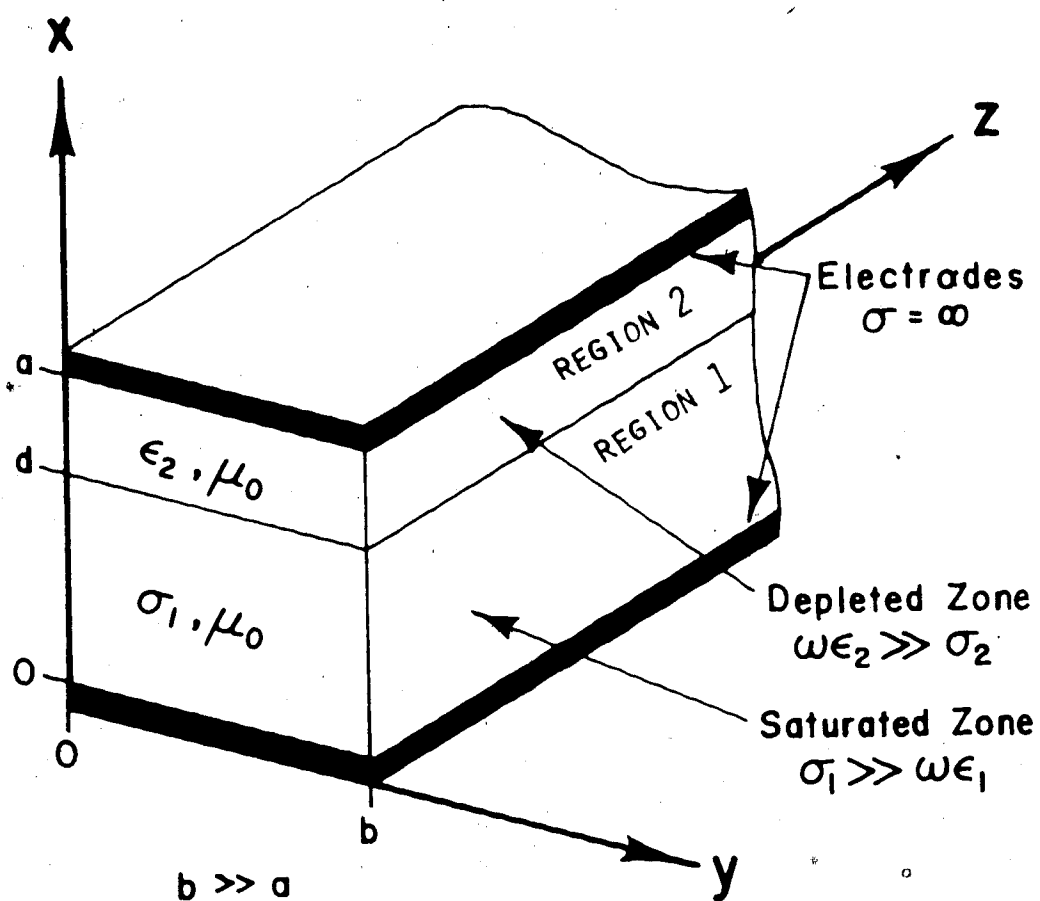


Figure 4.1: Geometry of a parallel plate transmission line in which the plates are separated by an insular zone and a conductive zone.

the field configuration necessary to meet the modified boundary conditions created by the introduction of an insular (depleted) layer.

It is necessary to determine the form of the electromagnetic fields possible for a two zone transmission line of the form shown in figure 4.1. For the present purposes, it will be adequate to determine the dominant mode formulation only.

Field boundary conditions must be met at the upper and lower plates as well as at the interface point between the zones. The continuous matching of the interface boundary conditions will require the z component of the wave velocity to be the same in both zones. This latter requirement allows one to immediately discard the TEM field configuration as a possible solution as the phase velocities of TEM waves would be vastly different in the two zones.

The geometry presented is somewhat similar to a two dielectric rectangular waveguide problem examined by Harrington¹¹. A similar line of attack will therefore be used in seeking a solution. A short description of the terminology used is included, prior to a description of the solution to the boundary value problem of interest. The reader is, however, directed to Harrington for greater background on the overall methodology.

4.2 Electromagnetic Field Solution

4.2.1 Terminology

In a homogeneous source-free region the phasor-vector representation of Maxwell's equations is:

$$\begin{aligned}\nabla \times \mathbf{H} &= (\sigma + j\omega\epsilon)\mathbf{E} \\ \nabla \times \mathbf{E} &= -j\omega\mu\mathbf{H} \\ \nabla \cdot \mathbf{E} &= 0 \\ \nabla \cdot \mathbf{H} &= 0\end{aligned}\tag{4.1}$$

Since any divergenceless vector may be expressed as the curl of some other vector, the divergenceless character of the electric and magnetic fields allows one to express the fields in terms of either a magnetic vector potential (\mathbf{A}), or in terms of an electric vector potential (\mathbf{F}), or, if more convenient, as some combination of each with the resulting fields determined by superposition. Further, it is the common, although not mandatory practice, to select the divergence properties of the vector potential used, such that the selected vector potential satisfies the Helmholtz equation. If, for example, a magnetic vector potential is selected then the potential must meet the Helmholtz relation:

$$\nabla^2 \mathbf{A} + k^2 \mathbf{A} = 0\tag{4.2}$$

$$\text{where } k^2 = -(\sigma + j\omega\epsilon)(j\omega\mu)$$

If one further restricts consideration to vector potentials which in cartesian coordinates (x, y, z) follow a

constant direction, some simplification will result. Consider, for example, the selection:

$$\mathbf{A} = \mathbf{u}_x \psi \quad (\mathbf{F} = 0) \quad (4.3)$$

where \mathbf{u}_x = a unit vector in the x direction

ψ = some scalar expression which satisfies the scalar Helmholtz equation

Determination of the electromagnetic fields arising out of this form of magnetic vector potential reveals that no H_x field component is generated. The resulting field formulation is thus termed transverse magnetic (TM) to x. Alternately, the selection of an electric vector potential of the form:

$$\mathbf{F} = \mathbf{u}_x \psi \quad (\mathbf{A} = 0) \quad (4.4)$$

leads to an electromagnetic field formulation in which no E_x component is generated. The field formulation is thus termed transverse electric (TE) to x.

These two special cases are of interest since it can be shown that an arbitrary field configuration in a source-free homogeneous region may be expressed as the sum of a TE and a TM field. Theoretically any electromagnetic field solution can be constructed from a suitable combination of TE and TM field solutions. The fields may be selected to be TE and TM to x as in the present example, or to any other constant vector direction selected. While the selection is nominally arbitrary, in practice the proper selection will often greatly simplify the solution process.

4.2.2 Solution

Consider the parallel plate line arrangement shown in figure 4.1. In the limiting case of the region between the plates being filled with only one medium, the fields between the plates are essentially the same as those of a uniform plane wave (a constant E_x and H_y) propagating in the z direction. Such a field form is TE to z and y , as well as TM to z and x . The solution in the perturbed case of two media is therefore likely to contain E_x and H_y components. One may thus discard looking for solutions TE to x , or TM to y .

Further, consider the currents that might be expected to flow on the plates. Current will pass from the source outward (z direction) on one plate and back on the other. In effect then, there is a current circulating around the conductive medium (region 1), which is insulated from direct contact with both plates by an insular layer (region 2). Such a formulation normally leads to the induction of flux cancelling currents (Eddy currents) in the conductive region. One may postulate then that the solution could contain a z directed electric field component. This would eliminate solutions TE to z .

One is then left with the possible forms TE to y , TM to z , or TM to x . As it turns out the final solution reached has all three properties. However, the solution was obtained by first seeking a solution TM to x , as is outlined in the following text.

A solution is sought which is transverse magnetic (TM) to x and therefore an x directed magnetic vector potential is selected.

$$\mathbf{A} = \mathbf{u}_x \psi \quad (4.5)$$

The scalar potential ψ is determined in the usual manner. A form of solution is postulated which is the product of harmonic functions. Each function has only one of the spatial coordinates in its argument. This solution format is compatible with the separation of variables solution method. The harmonic functions are selected such that the boundary conditions at the conductor walls are met. The solution is then tested to see if the balance of the boundary conditions can be satisfied. Following this line of attack, separate scalar potentials are selected for each of the two regions (see figure 4.1) as follows:

$$\begin{aligned} \psi_1 &= C_1 \cos(k_{x1} x) \exp(-jk_z z) \\ \psi_2 &= C_2 \cos(k_{x2} (a-x)) \exp(-jk_z z) \end{aligned} \quad (4.6)$$

This selection insures no tangential electric field components at the conductor plates, as is evident from equations 4.8 below. Further, it has been anticipated that a common z direction propagation term will be required to continuously match the fields at the interface between the regions. Substitution of these potentials into the Helmholtz equation leads to the separation parameter equations.

$$\begin{aligned} k_{x1}^2 + k_z^2 &= k_1^2 = -j\omega\mu\sigma \\ k_{x2}^2 + k_z^2 &= k_2^2 = \omega^2\epsilon_2\mu \end{aligned} \quad (4.7)$$

The fields generated in a general medium (σ, ϵ, μ) by the

selected magnetic vector potential (A) are given by''.

$$E_x = (1/\xi) [\partial^2 \psi / \partial x^2 + k^2 \psi]$$

$$E_y = (1/\xi) \partial^2 \psi / \partial x \partial y$$

$$E_z = (1/\xi) \partial^2 \psi / \partial x \partial z$$

$$H_x = 0$$

$$H_y = \partial \psi / \partial z$$

$$H_z = -\partial \psi / \partial y$$

(4.8)

where $\xi = \sigma + j\omega\epsilon$

and $k^2 = (-j\omega\mu)(\sigma + j\omega\epsilon)$

These relations can be applied to equations 4.6 to obtain expressions for the field components in the two regions. Comparison of the field expressions at the boundary ($x=d$) leads to the following requirements. Matching of tangential magnetic field components ($H_{y,1} = H_{y,2}$) and continuity of current across the interface ($\sigma_1 E_{x,1} = j\omega\epsilon_2 E_{x,2}$) both lead to the requirement that:

$$C_1 \cos(k_{x,1} d) = C_2 \cos(k_{x,2} (a-d)) \quad (4.9)$$

The requirement for matching tangential electrical field components ($E_{z,1} = E_{z,2}$) at $x=d$ leads to:

$$-[k_{x,1} C_1 \sin(k_{x,1} d)] / \sigma_1 = [k_{x,2} C_2 \sin(k_{x,2} (a-d))] / j\omega\epsilon_2 \quad (4.10)$$

These last two relations may be combined to form:

$$-[k_{x,1} \tan(k_{x,1} d)] / \sigma_1 = [k_{x,2} \tan(k_{x,2} (a-d))] / j\omega\epsilon_2 \quad (4.11)$$

The relations 4.11 and 4.7 represent a set of three transcendental equations which can be solved numerically for the three complex propagation constants $k_{x,1}$, $k_{x,2}$, and k_z . The numerical method used was as follows. Initial values for the three complex propagation constants were obtained from the

approximate relations derived in a succeeding section, section 4.4, and labelled 4.14. The two separation relations labelled 4.7 can be combined to eliminate k_z and thereby relate k_{x1} to k_{x2} . The resulting expression may be substituted into 4.11 to reduce it to an expression containing k_{x1} only. The resulting expression was then solved numerically for k_{x1} , using the Newton-Raphson technique. The other two propagation constants could then be determined by back substituting. As a final check the two sides of expression 4.11 were evaluated in polar form and compared. Typically after one hundred iterations the amplitude and phase values would agree to the first four or five significant digits.

4.3 Field Lines

The three complex values k_{x1} , k_{x2} and k_z can be determined numerically for a given geometry. Once this is done, it is possible to plot the trajectory of an electric field line and thus obtain a visual representation of the current flow in the formation.

This has been done and is presented in figure 4.2. The field line was generated by determining the E_x/E_z ratio at fifty values of x and then using these ratios to successively extend an electric field line starting from an arbitrary point at the interface. Bearing in mind that the tangential components of the electric field match at the interface, the abrupt directional change at the interface

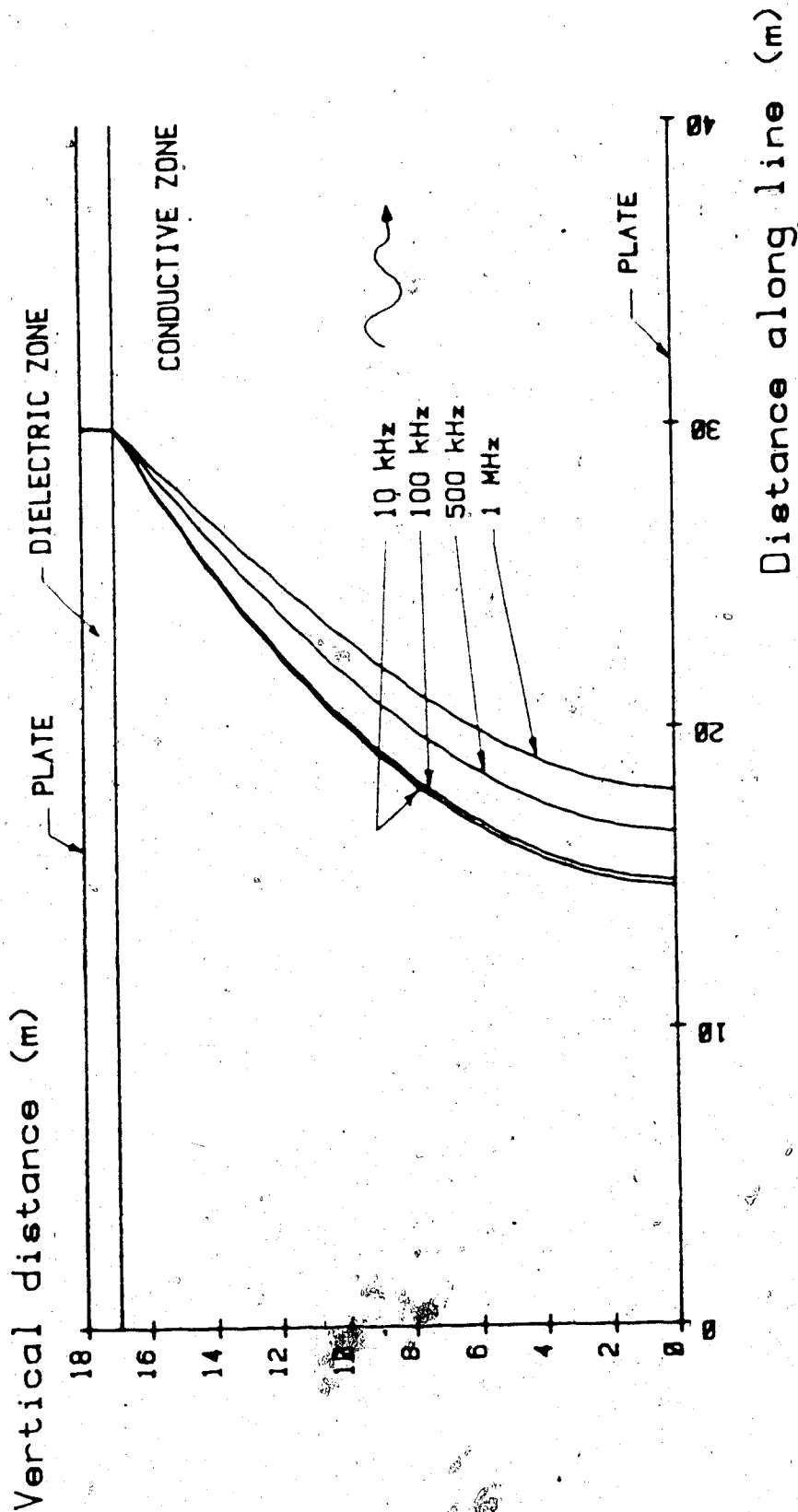


Figure 4.2: Representation of an electric field line generated on the parallel plate transmission line, at a number of different operating frequencies.

indicates that the electric field is much stronger in the depleted zone than it is in the conductive zone, for this configuration.

The electric field line derived for a number of different operating frequencies is shown in figure 4.2. At high frequencies, where the capacitive impedance of the depleted zone approaches zero, the electric field lines should approach the vertical form of the TEM mode that may be expected if no depleted zone were present. The electric field lines shown support this expectation by becoming progressively more vertical at higher frequencies. At low frequencies the electric field lines derived appear to asymptotically approach a form which is not vertical. In fact, it is possible to determine from the field expressions that as frequency approaches zero the ratio of the electric field components at the interface ($x=d$) is:

$$|E_z/E_x| \rightarrow \sigma_1((\mu/\epsilon_2)(a-d)d)^{1/2} \quad (\text{in the conductive zone})$$

and

$$(4.12)$$

$$|E_z/E_x| \rightarrow 0 \quad (\text{in the dielectric zone})$$

The result is that even at low frequencies, the electromagnetic field form in the conductive material is quite different from TEM.

4.4 Validity of Distributed Impedance Representation

One may now address the original problem stipulated, this being the validity of the distributed impedance representation for the transmission line. When the region between the plates is entirely filled with either of the two media, a uniform TEM field solution is obtained. In terms of the previous formulation this corresponds to the k_x terms being zero. Therefore, one may examine the case where $k_{x1}d$ and $k_{x2}(a-d)$ are both small such that :

$$\begin{aligned}\tan(k_{x1}d) &\cong k_{x1}d \\ \tan(k_{x2}(a-d)) &\cong k_{x2}(a-d)\end{aligned}\quad (4.13)$$

The substitution of these terms into equation 4.11 allows the three transcendental equations to be solved algebraically for the complex propagation constants. The results are:

$$\begin{aligned}k_{x1}^2 &= (-j\omega\mu\sigma_1 - \omega^2\epsilon_2\mu) / (1 + (1/M)) \\ k_{x2}^2 &= (j\omega\mu\sigma_1 + \omega^2\epsilon_2\mu) / (1 + M) \\ k_z^2 &= (-j\omega\mu\sigma_1(a/d)) / (1 + M)\end{aligned}\quad (4.14)$$

where $M = \sigma_1(a-d) / (j\omega\epsilon_2d)$

One may now examine the same problem using a distributed impedance approach. Consider the same physical arrangement (see figure 4.3) but assume (incorrectly) uniform TEM fields.

The shunt impedance between the plates for a one metre length is:

$$Z_s = (d/\sigma_1 b) + (1/j\omega(\epsilon_2 b)(a-d))\quad (4.15)$$

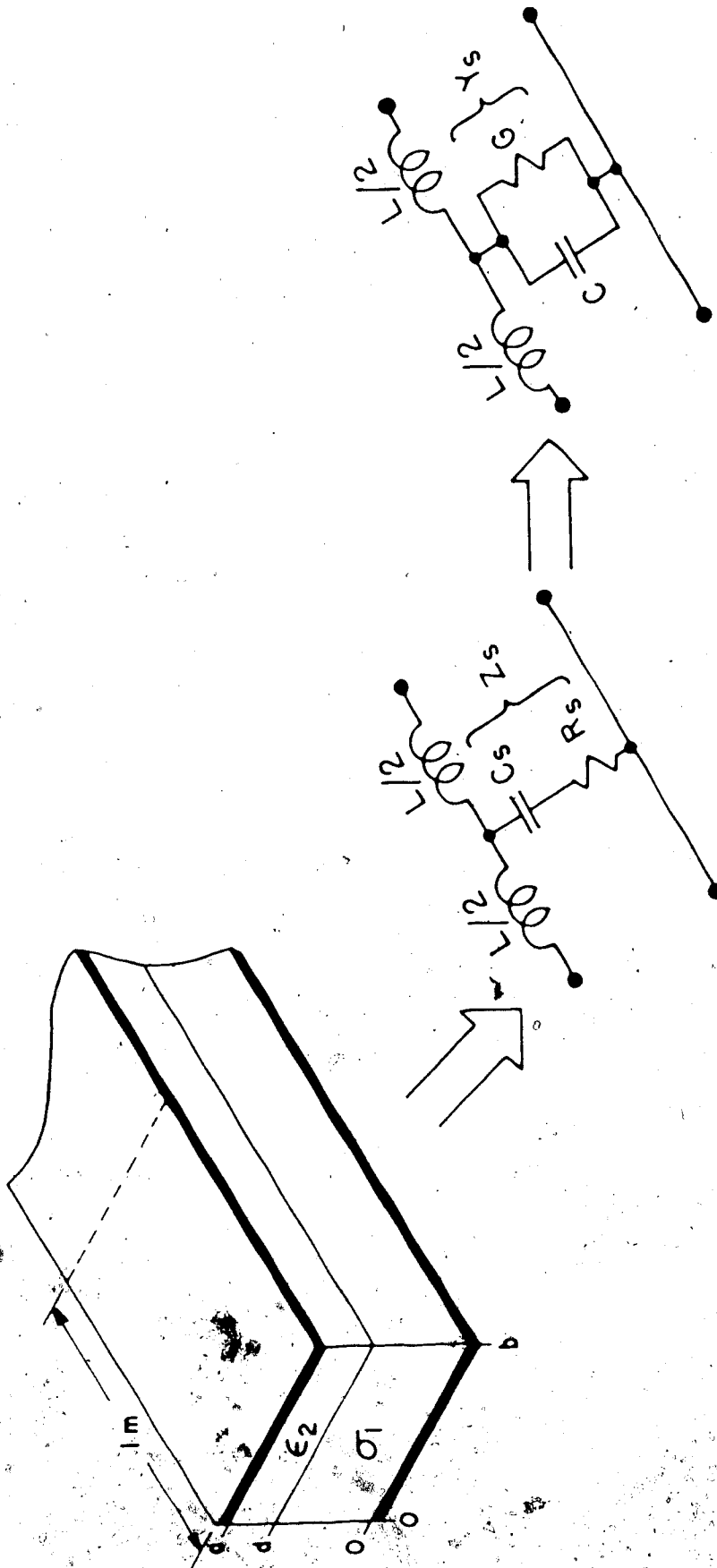


Figure 4.3: Distributed impedance representation of a short length of the parallel plate transmission line.

The distributed shunt admittance is therefore:

$$Y_s = 1/Z_s \quad (4.16)$$

The distributed series reactance of a parallel plate line is:

$$j\omega L = j\omega \mu a/b \quad (4.17)$$

For perfectly conducting plates the propagation constant

($\gamma = \alpha + j\beta$) is determined as:

$$\gamma^2 = j\omega L Y_s = j\omega L / Z_s \quad (4.18)$$

By substitution of 4.15 and 4.17 into 4.18 we may obtain the term:

$$k_z^2 = -\gamma^2 = (-j\omega \mu \sigma_1 (a/d)) / (1+M) \quad (4.19)$$

where M is as defined in equation 4.14.

This is the same expression for k_z as was obtained in 4.14.

The net result is that the wave propagation characteristics along the transmission line (energy dissipation and wavelength) can be predicted by the distributed impedance representation, even though the field formulation is not of the form assumed for the distributed impedance representation. There exists of course a limitation to this result, since it is predicated on the small argument approximation of the tangent function, and therefore requires both $k_{x1}d$ and $k_{x2}(a-d)$ to be much less than one.

The principal reason for examining this configuration is to establish the validity of the distributed impedance representation in the numerical simulations. To this end, consider what this limitation means in terms of the production controlled Electromagnetic Flood simulation presented in chapter 6. For the frequency range under

consideration ($\approx 100\text{kHz}$ to 250kHz) the depletion zone thickness ($a-d$) that develops before essentially complete decoupling occurs is much less than the saturated zone thickness (d). Considering this and the electrical properties used, the requirement for $k_{x1}d$ to be small is more restrictive than the requirement that $k_{x2}(a-d)$ be small.

To recast this requirement into a more familiar form, consider the point where, say, the depleted zone is about 10% of the plate separation. Using the same electrical properties as the production controlled electromagnetic flood simulation, the k_{x1}^2 expression of equation 4.14 reduces to:

$$k_{x1}^2 \approx -j\omega\mu\sigma_1 \quad (4.20)$$

and therefore

$$|k_{x1}d| \approx (\omega\mu\sigma_1)^{1/2}d = 1.414(d/\Delta) \quad (4.21)$$

where Δ is the skin depth of a uniform plane wave in the conductive material between the electrodes. For a real argument the $\tan(x) \approx x$ representation is accurate within 10% for values of x up to about 0.5. Thus as a coarse rule of thumb, one may consider the distributed impedance representation as adequate for frequencies up to the point where the electrode separation becomes about one-third of the plane wave skin depth in the conductive material. For electrode separations greater than this a more detailed representation of the full field solution would have to be used. Up to that point, however, one has the rather

surprising result that the propagation characteristics of a distinctly non-TEM wave are accurately predicted by a model predicated on a TEM form for the fields.

The distributed impedance representation shown in figure 4.3 may also be used to predict a second transmission line property, that property being the characteristic impedance of the transmission line. The characteristic impedance is the ratio of the potential developed between the electrodes, to the current induced along the electrodes, by an electromagnetic wave propagating along the line in the z direction. The potential between the electrodes may be determined by integrating the expression for the x component of the electric field between $x=0$ and $x=a$. The current in the electrodes may be determined from the expression for the y component of magnetic field. A combined expression relating the ratio of voltage to current may then be subjected to the same small argument approximation put forward for the propagation constant derivation. If this is done the resulting expression for characteristic impedance is the same as the one that can be derived directly from the distributed impedance representation shown in figure 4.3.

4.5 Discussion of Field Lines Generated

The electric field trajectories presented in figure 4.2 indicate a z directed component in the field line even in the case of low operating frequencies. For operating frequencies low enough that all dimensions of the transmission line are much less than a wavelength, the two zones may be treated simply as a lumped capacitor and resistor connected in series. The quasi-static field solution of this arrangement would predict only an x directed electric field. The reason for this apparent inconsistency in the electric field form is that the solution obtained in section 4.2 is not complete. The solution is for the lowest order mode propagating along an infinite length transmission line in the $+z$ direction. The transmission line end and feedpoint represent two additional boundary conditions which must be met to obtain a complete field solution.

The determination of the complete solution from the exact form of the boundary conditions, including the end points, is a very involved problem. Some estimate of the field formulation may, however, be obtained using less elegant techniques. In normal transmission line analysis (with TEM waves) the line endpoint boundary conditions are met by postulating the existence of two waves of similar form but propagating in opposite directions with the relative magnitude and phase of the two waves being determined from the endpoint boundary conditions. Following

this line of attack, one may postulate the existence of two waves with the field form shown in figure 4.4. The line end is an open circuit and the net electric field at this point should contain no z directed component (neglecting fringing). This condition can be met if the two waves shown are of equal magnitude and in phase at the line end. In this situation the z directed components of the electric fields will cancel, as will the y directed components of the magnetic field. The only resultant net field will be the x directed electric field. Consider again the low frequency case, where the line length is much less than a wavelength. In this case it may be expected that this cancelling effect will occur over the entire line length. Hence, the only net field anywhere on the line will be the x directed electric field. This form is consistent with the quasi-static solution.

If one extends this two wave concept to lines which are not short compared to a wavelength, a somewhat unusual standing wave/heating pattern can be expected to develop. The z components of the electric field in effect experience a reflection coefficient of -1 at the line end, while the x components experience a reflection coefficient of $+1$. The standing wave/heating pattern could thus be expected to have alternating relative peaks every quarter wavelength as the x and z components alternately come into phase. This sort of effect would assist in obtaining more uniform heating along the length of a coated line.

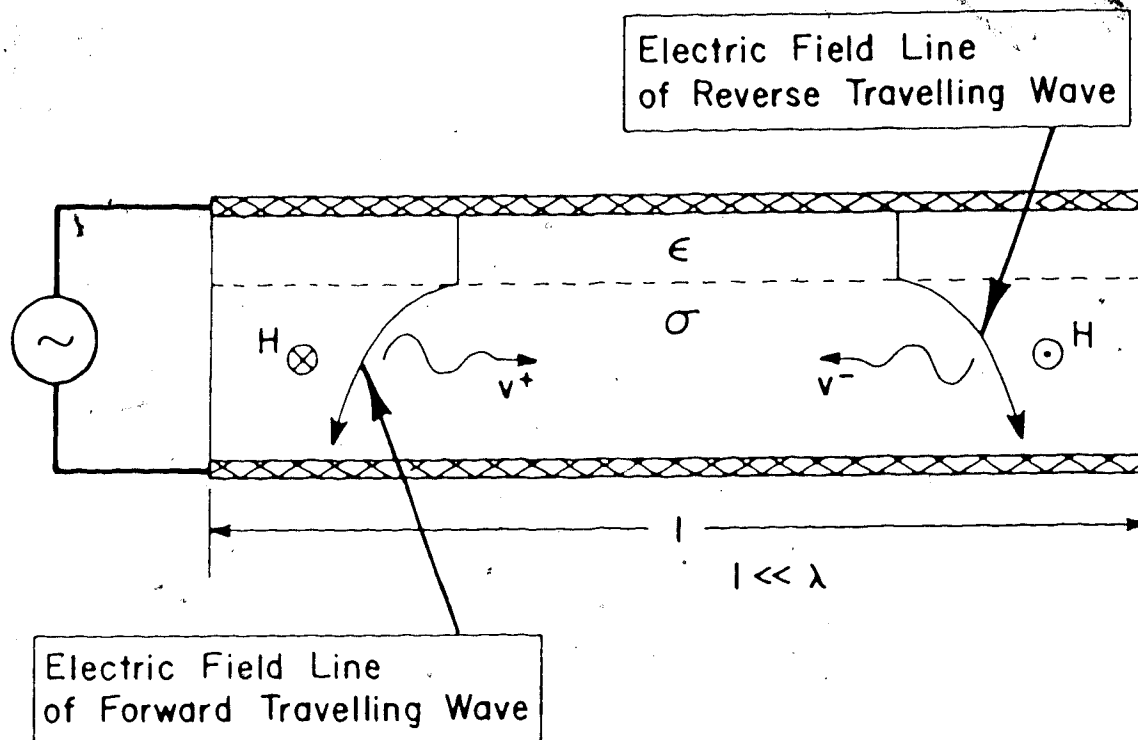


Figure 4.4: Sketch of the electric and magnetic field lines of a forward and reverse travelling wave on the parallel plate transmission line.

Unfortunately, in this more general case, the two wave concept is not sufficient to meet all the boundary conditions. The feedpoint boundary also precludes any net E_z component. In general the two waves which cancel at the line end will not also cancel at the feedpoint. A complete solution would, therefore, require the addition of some stationary field components in the vicinity of the feedpoint. Some distortion of the heating pattern may thus be expected in the vicinity of the line feedpoint.

In summary, the results of this chapter suggest that the distributed impedance representation, of an insulated electrode transmission line in a lossy medium, can accurately predict the propagation characteristic of the electromagnetic wave traveling on the line, if the conductor separation is not large compared to the uniform plane wave skin depth of the lossy medium. Knowledge of the propagation characteristic, particularly the wave attenuation rate, should allow an accurate description of the wave energy distribution along the length of the line with the possible exception of the portion of the line near the feed point.

A more complete solution involving feedpoint and endpoint boundary conditions was not sought. An examination of the simulation results in chapter 6 suggests that a very involved and heterogeneous situation will develop, as heating and production occur, due to the temperature dependence of oil sand conductivity and the changing demarker location. The determination of a full field

solution under such conditions is considerably beyond the range of the present study.

5. Approximate Numerical Model of a Coated and/or Compensated Transmission Line

5.1 General

As was discussed earlier, it is possible to increase the depth an electromagnetic wave can penetrate into and heat a formation by suitably coating and/or resonating the electrodes used. The question arises, however, of what values to use for coating thickness, operating frequency and resonating capacitance. Further, the presence or absence of standing wave effects are of interest. As a guide to finding suitable ranges for these values, for subsequent examination of formation heating using scaled electrothermal models, the following numerical model was developed.

Referring to figure 3.13, the electromagnetic field distribution about the electrodes, and, therefore, the transmission line distributed parameter values cannot be exactly determined except by numerical solution of the boundary value problem specified by the electrode placement and the applied drive potentials. If, however, the horizontal separation between each upper/lower electrode pair is large compared to the diameter of the electrodes, the near fields of each upper/lower electrode pair will be essentially the same as those of a single two wire line buried in an infinite medium. It is only the relatively weaker far fields that are significantly modified due to the presence of the other electrode pairs.

A transmission line's distributed parameter values are established by the total electric and magnetic field flux generated by the electrodes of the line. This total flux value of any given electrode pair will, however, be only minimally affected by neighbouring electrode pairs in the aforementioned circumstances. As a good first approximation for analysis, one may model a single upper/lower electrode pair and consider it in isolation of the other pairs.

Further, the normal two wire distributed parameter transmission line representation will be used. The results from chapter 4 suggest that this formulation should be reasonably accurate as long as the operating frequency is low enough that the vertical separation between the electrodes is not significant compared to the plane wave skindepth of the lossy material between the electrodes.

5.2 Model Formulation

A brief introduction to the concepts and terminology of transmission line theory is included in Appendix A. The case to be considered is a two wire transmission line buried in a lossy medium. Variations are to include the electrodes having a dielectric coating, which may change thickness at various points along the line, as well as the presence of closely spaced series resonating capacitors. The problem may be broken into two parts. The first part is to establish the propagation characteristics and characteristic impedance of each line segment with a particular coating or series

resonating capacitance. The second part is to cascade these segments together and determine how the incoming wave energy is distributed along the length of the total line.

5.2.1 Line Segment Parameters

Let us consider two conductors of conductivity σ and radius a , separated by distance d , buried in a nonmagnetic lossy medium with conductivity σ_m and permittivity ϵ_m (see figure 5.1). At high frequencies, where most of the electrode current flows on the surface of the line conductors, the transmission line distributed parameters are known to be represented^{2,2} as:

$$G_m = \pi \sigma_m / (\cosh^{-1}(d/2a)) \quad \text{S/m} \quad (5.1)$$

$$C_m = \pi \epsilon_m / (\cosh^{-1}(d/2a)) \quad \text{F/m} \quad (5.2)$$

$$L = (\mu_0 / \pi) \cosh^{-1}(d/2a) \quad \text{H/m} \quad (5.3)$$

$$R = [(\mu_0 \sigma) / (a^2 \pi \sigma)]^{1/2} \quad \Omega/\text{m} \quad (5.4)$$

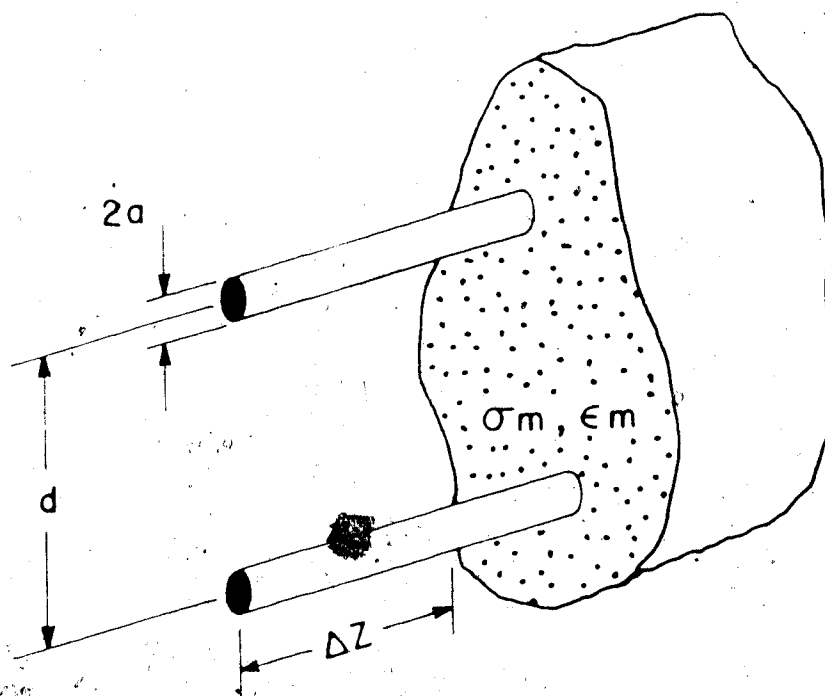
The addition of a coating to the line (see figure 5.2) modifies the shunt admittance between the electrodes. In any practical case the total electrode and coating radius b will be much less than the electrode separation d . In that case the added admittance components may be closely determined using the impedance relations for a coaxial line. The net admittance values contributed by the coatings on both electrodes are then:

$$G_d = (\pi \sigma_d) / \ln(b/a) \quad \text{S/m} \quad (5.5)$$

$$C_d = (\pi \epsilon_d) / \ln(b/a) \quad \text{F/m} \quad (5.6)$$

Further, the G_m and C_m expressions must be modified by

(a)



(b)

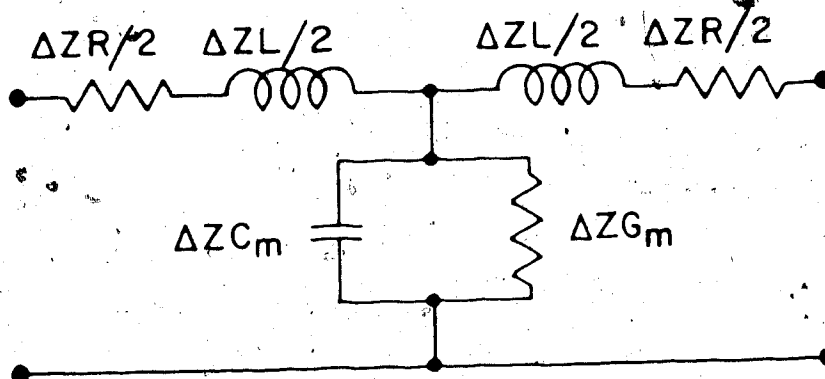
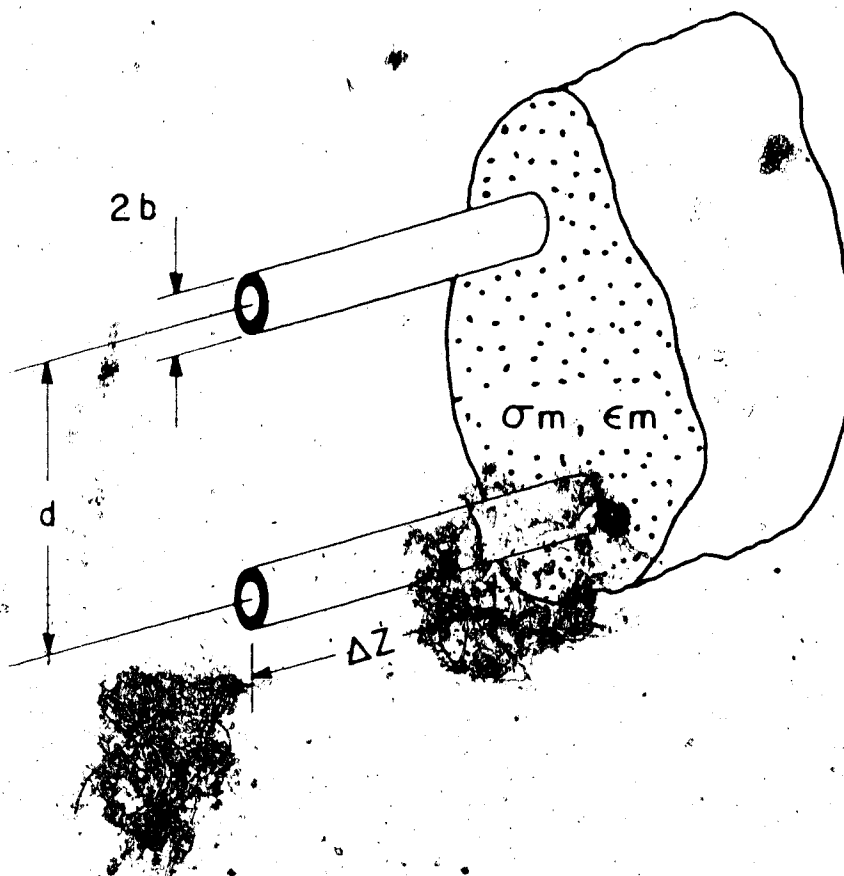


Figure 5.1: A two wire transmission line buried in a non-magnetic lossy medium.

- a) Geometry of the transmission line.
- b) Distributed impedance representation of a short length of the transmission line.

(a)



(b)

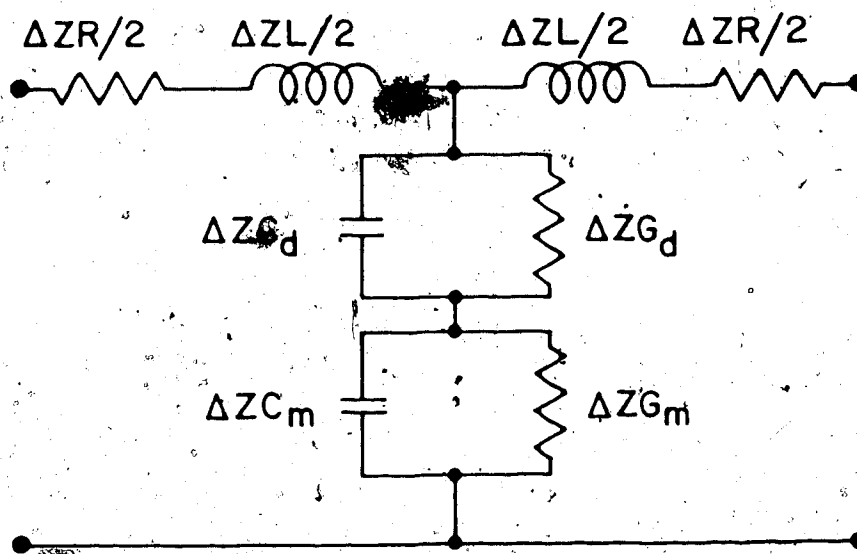


Figure 5.2: A coated two wire transmission line buried in a non-magnetic lossy medium.
 a). Geometry of the transmission line.
 b). Distributed impedance representation of a short length of the transmission line.

substituting b for a .

The modified shunt leg can be reduced to a single equivalent term (see figure 5.3).

The propagation and impedance characteristics of the transmission line may then be calculated as follows:

Propagation

$$\gamma = \alpha + j\beta = [ZY]^{1/2}$$

(5.7)

where $Z = R + j\omega L$

and $Y = G + j\omega C$ (equivalent)

Characteristic Impedance

$$Z_0 = [Z/Y]^{1/2}$$

(5.8)

If series compensating capacitors are to be added, their spacing along the electrodes must be much less than the skindepth ($1/\alpha$) and the wavelength ($2\pi/\beta$) present on the line before the series compensating capacitors are added. If these criteria are met and the equivalent series capacitance added per metre is C_s , then 5.7 and 5.8 may be modified by changing the Z expression to:

$$Z = R + j(\omega L - (1/\omega C_s))$$

(5.9)

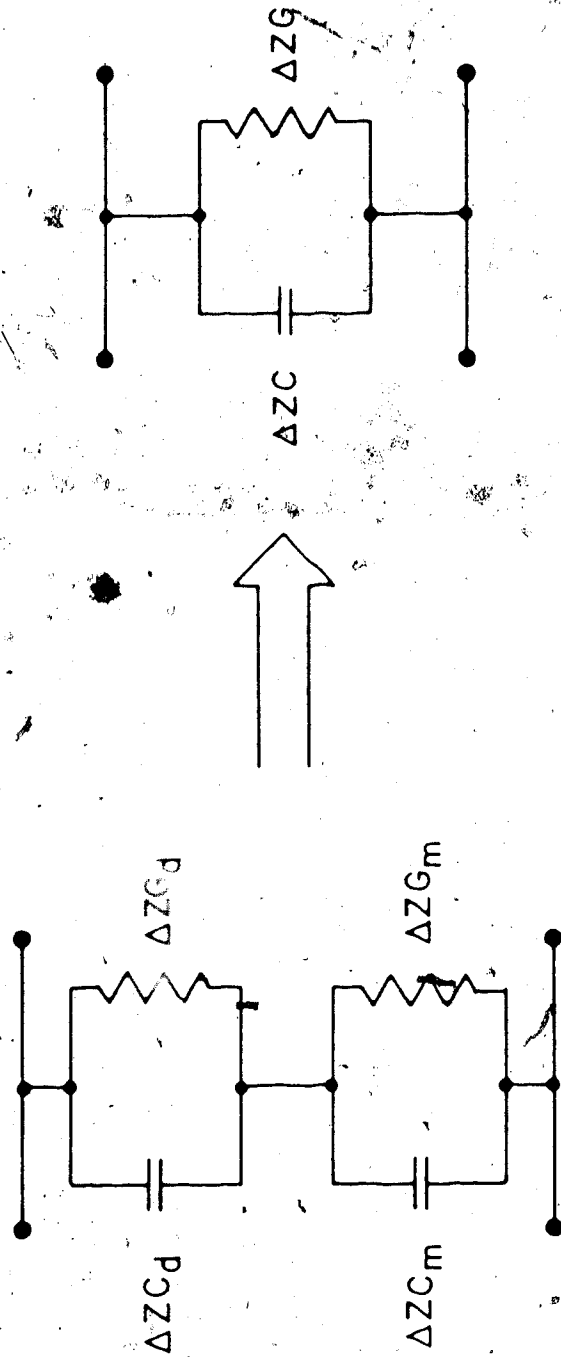


Figure 5.3: The shunting leg segment of the distributed impedance representation of a coated electrode transmission line, may be reduced to a single equivalent admittance pair (G,C) using phasor algebra.

5.2.2 Energy Deposition Along the Line

The basic configuration to be examined is shown in figure 5.4. The transmission line into the formation is broken into n sections each of which may or may not have different characteristics from the adjacent sections. The objective is to determine what portion of the input wave energy is deposited in each section. As a minimum a new section must be specified at each point where, say, the electrode coating thickness is changed. However, each section so specified may be further subdivided into a number of sections and thus allow better resolution in the calculation of the energy deposition.

The computational sequence is then as follows. First, assume that the coating, compensation, length and medium characteristics for each line section are given, and that the propagation and impedance characteristics for each section have been calculated. Then, starting at the line end (see figure 5.5), the apparent input impedance seen looking into the n 'th line section is calculated as²²:

$$Z_{in} = Z_{o_n} [(1 + \Gamma_n \exp(-2\gamma_n l_n)) / (1 - \Gamma_n \exp(-2\gamma_n l_n))] \quad (5.9)$$

$$\text{where } \Gamma_n = (Z_L - Z_o) / (Z_L + Z_o)$$

This impedance is then used to replace the load impedance in equation 5.9 to permit the calculation of the input impedance and reflection coefficient for the $(n-1)$ th line section. These operations, can thus be sequentially performed until the input line section is reached. From these operations information about the impedance seen at

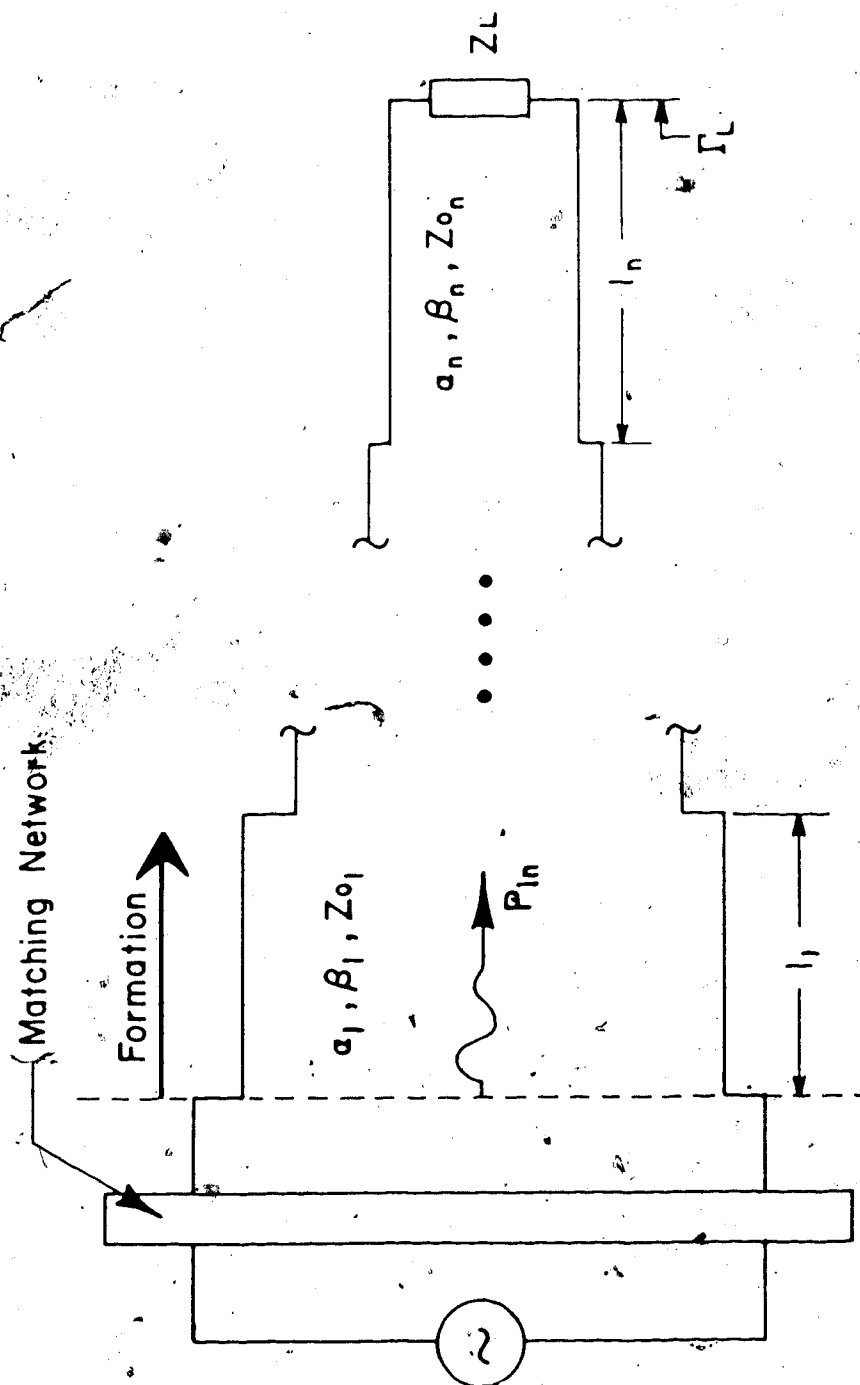


Figure 5.4: Representation of a multi-section lossy transmission line, showing the pertinent attributes of each section.

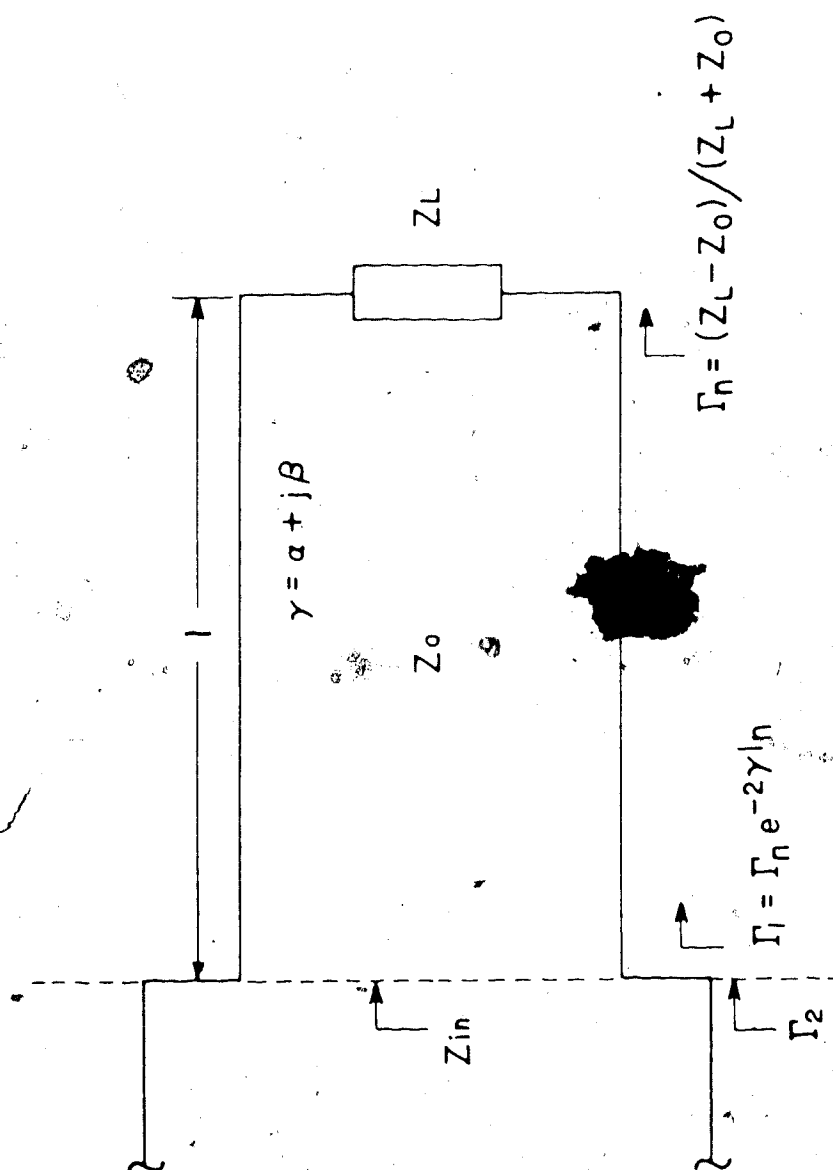


Figure 5.5: Impedance and reflection coefficient values at various points along a length of lossy transmission line.

each junction and the value of the reflection coefficient on either side of each junction is obtained. The deposition of the wave energy can then be determined with this data.

In the steady state the total phasor potential between the electrodes (V_t) at any given point can be considered to be the vector sum of two potentials V^+ and V^- . V^+ represents the net potential generated by all the waves travelling toward the line end and V^- represents the net potential of all the waves travelling back toward the line input. At any given point on the line the ratio of the two potentials is the reflection coefficient. In other words

$$V^-/V^+ = \Gamma$$

and

(5.10)

$$V^+ + V^- = V_t$$

The reflection coefficients at various points on the line are available from the previous calculation sequence.

Assume for normalization purposes that one volt rms at zero phase is applied across the line input junction. From the reflection coefficient value determined for the load side of this junction the values of V^+ and V^- may be found. These two potentials may then be translated to the next junction toward the load using the propagation characteristic of the line section (see figure 5.6). The total potential across the line at the second junction can be determined by performing a phasor addition of the forward and reverse potentials present at this point on the line. Given the potential across the line at the input and the

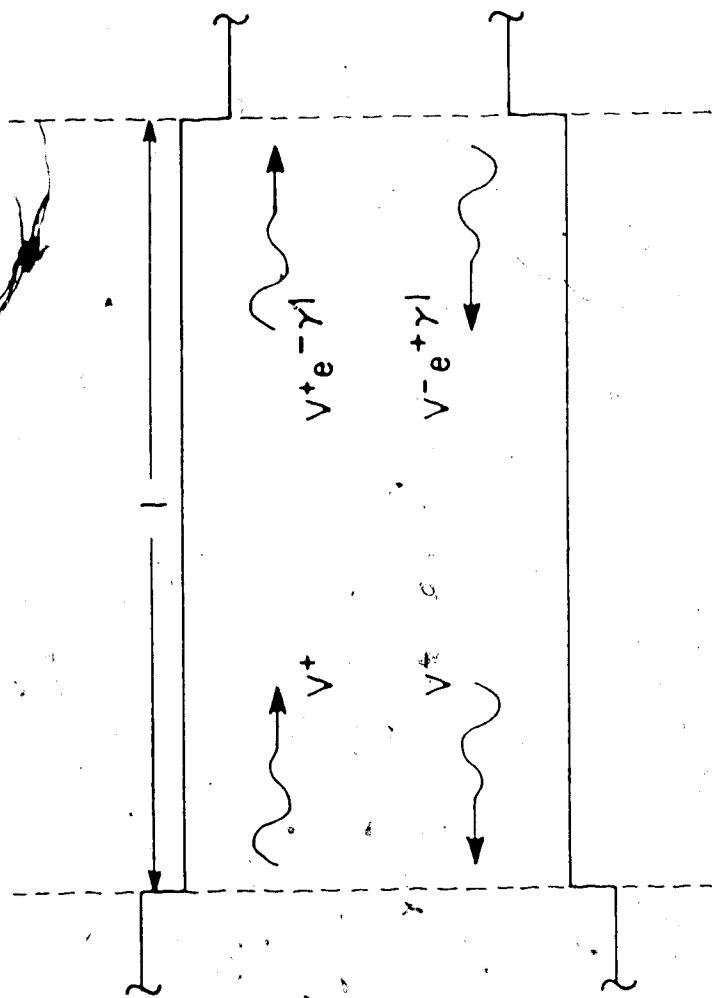


Figure 5.6: Translation of phasor potentials along a length of transmission line.

impedance seen looking into the line it is possible to determine the power being delivered into the first line section. Now knowing the potential across the second junction and the impedance seen looking into it, the power leaving the first section can be determined. The difference in power levels can be compared to the input power level to determine what portion of the input power is deposited in the first line section.

Subsequently the potential at the second junction can be similarly split into V^+ and V^- components and translated to the third junction using the propagation characteristic of the second line section. The total potential across the third junction may be determined and subsequently the power leaving the second line section. This sequence of calculations is repeated until the line end is reached. At that point the power deposition to all line sections has been determined.

The calculations involved are straightforward but somewhat tedious, particularly since most of the variables are complex numbers. The operations were therefore implemented in a computer program which runs on the datalogging system (HP 9825 Calculator) maintained in the Applied Electromagnetics Laboratory.

5.2.3 Model Limitations

The numerical model described in the previous sections was used extensively as a guideline in the selection of

electrode and coating sizes for the electrothermal model experiments described in section 3. The model formulation does not, however, consider a number of the physical phenomena which occur in the heating process and as such was only used as a guideline in selecting the most promising electrode configurations for scale model experimental heating runs. A brief description of some of the various phenomena foreseen is therefore presented along with an estimate of the effect they will have on the validity of the calculated results.

A significant deficiency in the model is the implicit assumption that the electromagnetic field lines around the electrodes of each line segment are transverse and have the same form as the electromagnetic fields found around an infinitely long line with the same physical cross-section. The assumption of transverse fields on a dielectric coated transmission line is incorrect, as pointed out in chapter 4, but the analytical results obtained in that chapter suggest that the propagation characteristic of a wave on a line and the characteristic impedance of the line, may be accurately predicted from the transverse field based formulation. The only restriction is that the vertical distance between the electrodes should not be a significant portion of Δ , where Δ is the plane wave skin depth of the lossy material between the electrodes.

A further limitation of the model is the failure to account for the "fringing" fields that will be established

to meet the boundary conditions at every discontinuity in the cross-section, such as when the coating thickness changes or the line end is reached. The contribution by these additional field components to the heating profile is difficult to estimate. It should be noted that a number of the results in chapter 3 show distortions of the heating pattern in the vicinity of the transmission line feedpoint. It may be expected that the predicted heating distributions will be inaccurate in the vicinity of junctions where large changes occur in the line characteristics.

A third phenomenon not considered in the model representation is the temperature dependence of the lossy medium's conductivity. It has been found that the conductivity of most earth type materials has a temperature dependence of the form given in table 6.1. The shunt parallel equivalent conductance G , of the transmission line representation, may be expected to change significantly as the heating occurs. For the particular applications of interest, namely transmission lines where the attenuation has been greatly reduced by the presence of an electrode coating, the capacitive term introduced by the coating is the dominant shunt admittance ($j\omega C \gg G$). This being the case the wavelength and characteristic impedance are essentially independent of G and therefore temperature. The attenuation rate will, however, vary significantly with temperature. Even so, as long as the attenuation rate is small such that the end to end attenuation over the line length is small,

the energy deposition tends to be uniform and is not greatly affected by the absolute value of the attenuation rate. The temperature dependence of the lossy medium's conductivity is, therefore, not expected to greatly modify the heating profiles for the particular coated electrode forms of interest.

The numerical model described in this section was used to estimate appropriate operating frequency and coating thickness combinations for use in the scale model heating runs described in section 3.4.1. In addition a variation of this model was used to generate the coating thickness versus attenuation graphs used in section 3.4.2.

6. Production Controlled Heating: A First Order Numerical Model

6.1 General

In chapter 2 a number of schemes were proposed to obtain high frequency electromagnetic heating of an Athabasca oil sand formation, over distances which are large compared to the nominal skin depth of the material. One of the schemes was referred to as production controlled heating. In this scheme a heat front is generated which sweeps through the formation in a manner akin to a fire flood and is thus referred to as a production controlled electromagnetic flood in this section. The scheme is similar to partial evaporation boring in that the electromagnetic wave is driven progressively further into the formation by the creation of an insular depleted zone which decouples the transmission line electrodes. The major difference is that in a production controlled electromagnetic flood the heating rate is low enough that the formation fluids have time to flow by gravity drive into the lower electrode array and be removed. This flow of fluids, rather than evaporation, is expected to be the dominant effect leading to the formation of a depleted zone below the upper electrode array. On initial application of power the heating is expected to be limited to the formation nearest the feedpoint due to the skin depth effect. In time, however, a depletion zone is created which decouples the input section of the line and

permits progressively deeper penetration of energy into the formation.

The process of production controlled electromagnetic flooding involves the interaction of a number of electromagnetic, thermal and viscous flow phenomena. It is not immediately obvious if economically viable production rates can be obtained using only a gravity drive or what selection of operating frequency and power level is best for a particular type of formation. In order to obtain an estimate of such parameters, a first order numerical model was assembled to simulate the electromagnetic flooding process. A brief description of the model formulation is given in the following sections. In addition, using Athabasca oil sand properties as a basis, the results of a few model runs are presented to demonstrate the effects of various power/frequency selections.

The numerical model briefly outlined in the following text makes use of a number of simplifying assumptions and approximations as outlined in the methodology sections. The purpose of the model was twofold. Its primary purpose was to determine if the postulated operating mechanism, of the heating pattern being regulated by the fluid production, was viable for materials which have electric, thermal and flow properties such as might be encountered in the Athabasca oil sands. The second objective was to obtain first order estimates as to the effect, on the heating profile and production rate, of various frequency and power level

selections. Interpretation of the model results beyond these rather broad effects must, however, be considered with caution.

6.2 Methodology Descriptions

6.2.1 Geometry

Figure 2.5, depicting the production controlled electromagnetic flood process, shows the payzone area of the formation between the electrodes divided into two basic zones: a depleted zone that has been drained of the bulk of its fluids and a saturated zone which still retains its fluid content. The division between the two zones changes with position along the electrodes and with time as the electromagnetic heating occurs. A third region of the formation is the material above and below the payzone. The material distribution in figure 2.5 was approximated by a two dimensional grid which separated the horizontal distance the wave propagates into the formation into fifty sections and then subdivides each section into six elements vertically. As the process is expected to be symmetrical on both sides of the source shown in figure 2.5, only the right hand side of the system is modelled. An example of the layout for three adjacent sections is shown in figure 6.1.

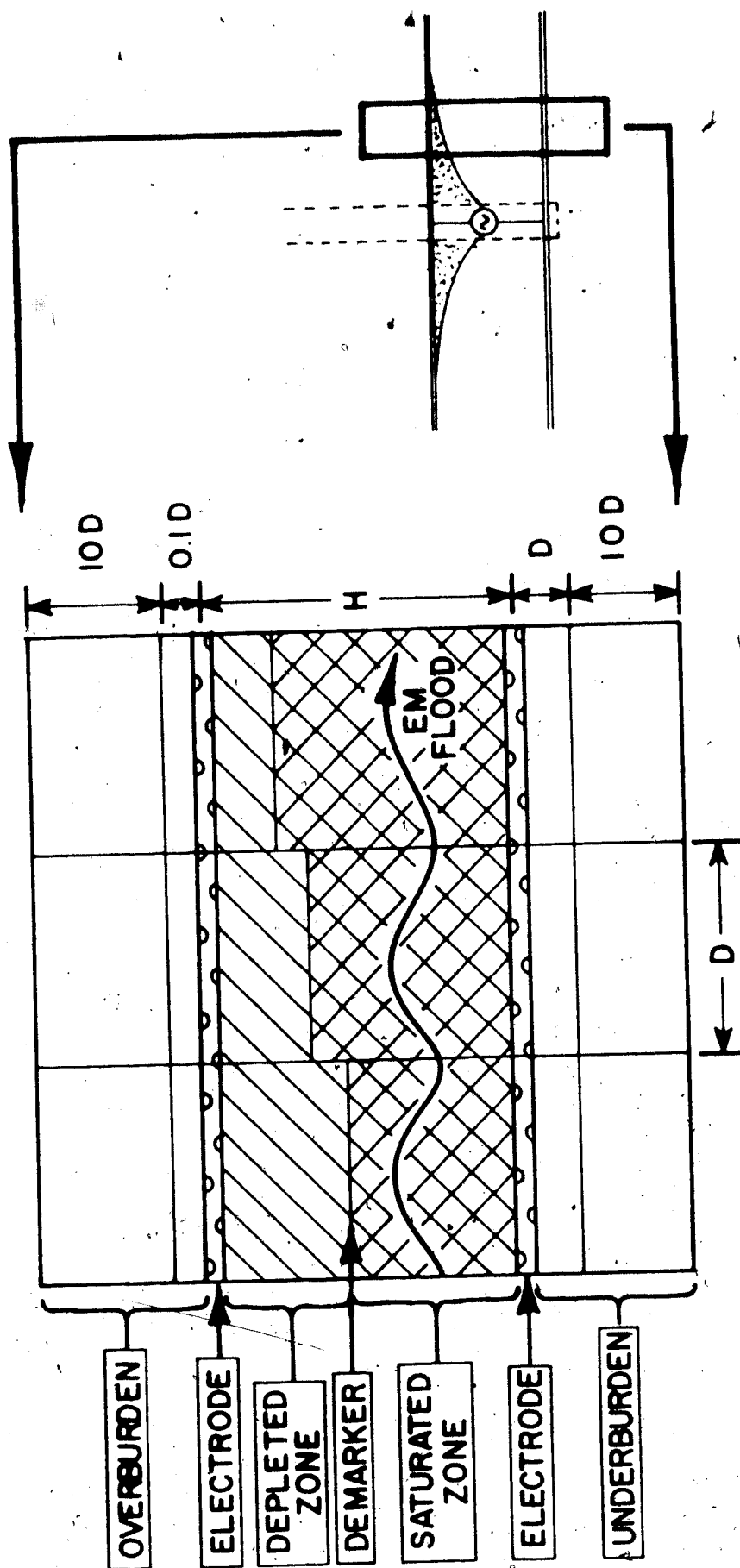


Figure 6.1: Model geometry for simulation of production controlled electromagnetic flood.

6.2.2 Energy and Flow Balances

The temperature variation of each element with time is determined as follows. Starting from a specified initial temperature distribution the net power flow into each element due to RF heating, thermal conduction and hot fluid flow is calculated. This power is then multiplied by the time step value to determine added energy. The added energy term is translated to a temperature change using the specific heat and mass of the element. The temperature of each element is then updated. The size and form of the depleted region is similarly determined by establishing the net fluid flow out of a section in a given time step and then-adjusting the demarker position between the depleted and undepleted zones.

A more specific description of the individual calculation processes and of the simplifying approximations made is presented in the following sections.

6.2.3 Distribution of Electromagnetic Wave Energy

Two approximations are made which simplify the description of the wave energy deposition. The first approximation deals with the representation of the formation electrodes. The upper/lower electrode pairs shown in figure 2.1 form two planar arrays of electrodes, one near the top of the payzone and one at the bottom. A first order estimate for the electrical effect of this discrete array of electrodes is to treat the upper and lower arrays as two

continuous horizontal plate conductors forming a parallel plate transmission line. The line progresses into the formation and has the payzone sandwiched between the plates. The second approximation is that as the wave travels into the formation the changes created by the varying thickness of the depletion region are gradual enough that negligible wave energy is reflected from the section boundaries. Such reflections are characteristic of wave propagation through a region with sharp discontinuities in the electrical properties.

Provided that the section depth selected (D) is much less than the skin depth value and the wavelength value of the electromagnetic wave, each section may be represented electrically by a "T" network equivalent circuit^{13, 14} as shown in figure 6.2. In this network both the saturated and (more insular) depleted zone materials between the electrodes are represented as parallel conductance/capacitance pairs. The actual values are calculated from the geometric distances involved and the temperature dependent electrical properties of the formation materials. Circuit theory may then be used to reduce the shunt elements to a single equivalent conductance/capacitance (G, C) pair. The values calculated are obtained on a distributed (per metre length into the formation) basis. The distributed inductance of the electrodes (L) is approximately that of a parallel plate transmission line and may be calculated from the geometry. For purposes of determining deposition of wave

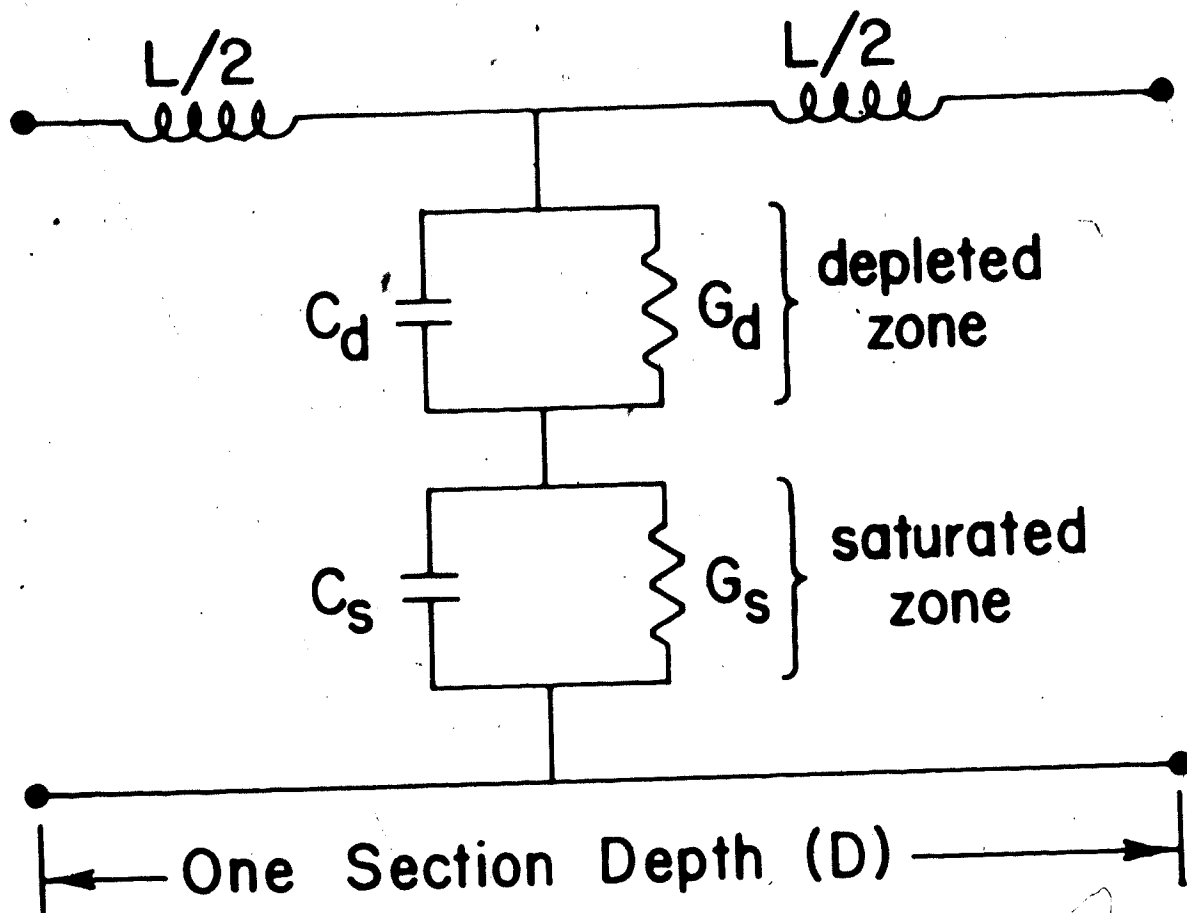


Figure 6.2: Distributed impedance representation of a short section of transmission line.

energy, the equivalent electrical representation is a cascaded series of these "T" sections.

Analysis of distributed networks of this type may be undertaken using transmission line theory^{13, 14}. A brief description of transmission line theory has been included as Appendix A in this thesis.

Subject to the negligible reflected wave approximation discussed earlier, the electromagnetic energy deposition in each section can be ascertained by the following sequence. The transmission line distributed shunt admittance values (G,C) are found for each section. Using these values and the electrode inductance (L) value, a wave attenuation constant (α) may be determined for each section. The attenuation constant is determined from the relation:

$$\alpha + j\beta = [j\omega L(G + j\omega C)]^{1/2} \quad (6.1)$$

where

α = attenuation constant

β = phase constant

$\omega = 2\pi$ times the operating frequency

j = the square root of -1

Starting from the line input, the power level entering and leaving each section of length D may be determined by sequentially applying the relation:

$$P(\text{out}) = P(\text{in}) \exp(-2\alpha D) \quad (6.2)$$

The difference between power entering and leaving each section may then be multiplied by the time step value to determine the electromagnetic energy deposited in the

section. The energy is assumed to be deposited entirely between the electrodes and is therefore split between the depleted and saturated zones. The appropriate split may be determined from the shunt admittance values of the two elements in the section.

Analytical investigations by the author (see chapter 4) indicate that this electrical representation is reasonably accurate as long as the vertical separation between the electrodes is less than approximately one-third of the skin depth value of the formation material. For rich (low moisture) Athabasca oil sand with a 20 metre separation between the electrodes, this places an upper frequency limit on the representation of about 250 kHz (see figure 1.2). Operating at frequencies above this level would require a more involved representation for the electromagnetic heating.

6.2.4 Thermal Conduction Energy Flows

The thermal energy flows considered were the horizontal and vertical transfers occurring between adjacent elements in the region between the electrodes (see figure 6.1). In addition the vertical heat leakage into the over/underburden areas was considered. The power levels were determined using the temperature difference between adjacent elements and a thermal resistance term. The thermal resistance term was established by the midpoint to midpoint distance between the elements, the cross sectional area joining the elements and

the thermal conductivity of the materials.

$$P_i = \Delta T / R_i \quad \text{where } R_i = \ell / k_i A$$

(6.3)

and k_i → thermal conductivity ($\text{W/m} \cdot \text{C}^\circ$)

ℓ → centre to centre distance between
two adjacent elements (m)

A → cross sectional area joining the two adjacent
elements in the case of vertical heat flow
and the average cross sectional area joining
the two elements in the case of
horizontal heat flows. (m^2)

(see figure 6.3, A_v and A_h respectively)

ΔT → centre to centre temperature difference
between adjacent elements (C°)

For simplicity a constant value of thermal conductivity was used for all elements. This approach was felt to be adequate since electromagnetic heating is the dominant energy transfer mechanism in the cases of interest.

The calculation process above is predicated on the assumption that the total energy interchange between elements in any given time step does not significantly modify the differential temperature between the elements (ie. suitably small time steps must be selected). For most of the model elements this presents no particular problem. The thermal capacity of the depleted zone elements is however initially very small as the zone has a nominal zero thickness to start with. To overcome numerical instabilities that can occur in these elements, unless vanishingly small

time steps are used, the above power term is modulated by a term :

$$(R_t C_t / \Delta t) (1 - \exp(-\Delta t / R_t C_t)) \quad (6.4)$$

where

Δt → time step value

$R_t C_t$ → effective thermal time constant of the two adjacent elements.

$$1/C_t = 1/C_1 + 1/C_2$$

C_1, C_2 → thermal heat capacities of the adjacent elements
($\rho c V_1, \rho c V_2$)

This yields the time averaged thermal heat flow for the two elements considered in isolation. The term reduces to unity if the time step is much less than the effective time constant. If the time step is significant compared to the time constant then the term reduces the energy flow rate in a manner consistent with the reduction which occurs with a diminishing differential temperature.

Thermal cross (horizontal) flows in the overburden/underburden areas were neglected. In addition, the number of elements used in those regions is very small even though a high temperature gradient is expected. The purpose of including those elements was, however, only as a means of obtaining a first estimate of the significance of thermal losses from the payzone as a function of the electromagnetic heating rate. The number of elements used is felt to be sufficient for that purpose.

In addition to thermal conduction power flows, the movement of fluids between elements results in some convective energy transfer. The power flow due to this effect is small compared to the electrical heating. However, estimates of the power flow involved were made and included in the energy balance calculations. Two effects were considered. The first effect may be examined if one considers the case of a saturated element losing energy due to a cross flow of fluid which increases in temperature as it crosses the element. Referring to figure 6.3, an estimate for the rate of energy loss (P) from the jth saturated element is given by:

$$P = q_j \rho c_o \Delta T$$

(6.5)

where q_j → horizontal volume flow rate
into the element (m^3/s)

ρ → fluid density (g/m^3)

c_o → specific heat of the fluid. ($J/g \cdot C^\circ$)

ΔT → temperature change the fluid undergoes
between elements (C°) ($T_j - T_{j+1}$)

The second energy transfer effect which occurs due to the fluid flow comes about as the result of the depleted zone volume increasing slightly with each time step. This results in a small volume at the saturated zone temperature being added to the depleted zone element. The thermal capacity of this volume change times the difference in temperatures. (saturated to depleted) represents an energy transfer to be diffused into the depleted zone element.

6.2.5 Flow Calculations

Again, a number of approximations were made to keep the model's complexity within reasonable bounds. First of all it is assumed that a rich homogeneous oil sand, essentially 100% fluid saturated, is being heated. Further, the bitumen is assumed to be the dominant saturating fluid such that its relative permeability is close to unity. The connate water saturation is assumed to be low such that its relative permeability is very small. The net result is that the system is treated as a single fluid system (bitumen) in which the water is blocked by the bitumen and thus restricted to flow at a rate limited by the bitumen. Fluid flow is assumed to follow Darcy's law which is akin to Ohm's law in electrical current flow. Fluid flow through a saturated porous medium is equal to the differential pressure established across the medium, divided by a flow resistance term. The flow resistance term is proportional to the length the differential pressure is applied over and inversely proportional to both the cross-sectional area the flow takes place through and a flow conductivity term. The flow conductivity term is equal to the permeability divided by the viscosity. Permeability is a property of the porous medium. It is a measure of how easily a fluid may pass through the porous medium. Viscosity is a fluid property. It is a measure of how difficult the fluid will be to force through a porous medium.

It is assumed that, except for a thin layer adsorbed to the surface of each sand grain, the bulk of the connate water is free to flow with the bitumen. The depleted zone, if deprived of most of its moisture content, may be expected to have an electrical conductivity much lower than the electrical conductivity of the saturated zone.

The flows considered are shown in figure 6.3. Both the vertical and horizontal flows are calculated using Darcy's law with gravity drive and assume a clean demarker between the saturated region and the depleted region, which was assigned a residual fluid saturation of 6 percent.

$$q_i = (k\rho g / \mu_m) (1 - H_0/h) A_i \quad (6.6)$$

$$q_j = (k\rho g / \mu_m) (\Delta h/D) A_j \quad (6.7)$$

where k → permeability (m^2)

ρ → fluid density (g/m^3)

μ_m → viscosity (temperature dependent) ($g/m \cdot s$)

g → gravitational acceleration (m/s^2)

h → demarker height (m)

H_0 → residual capillary height (m)

indicates the minimum level that a fluid may drain to under a gravity drive.

A_i, A_j → cross-sectional areas (see diagram) (m^2)

Δh → difference in the midpoint demarker heights (m)

D → horizontal depth of a section into the formation. (m)

The production rate predicted in this way would appear¹⁵ to

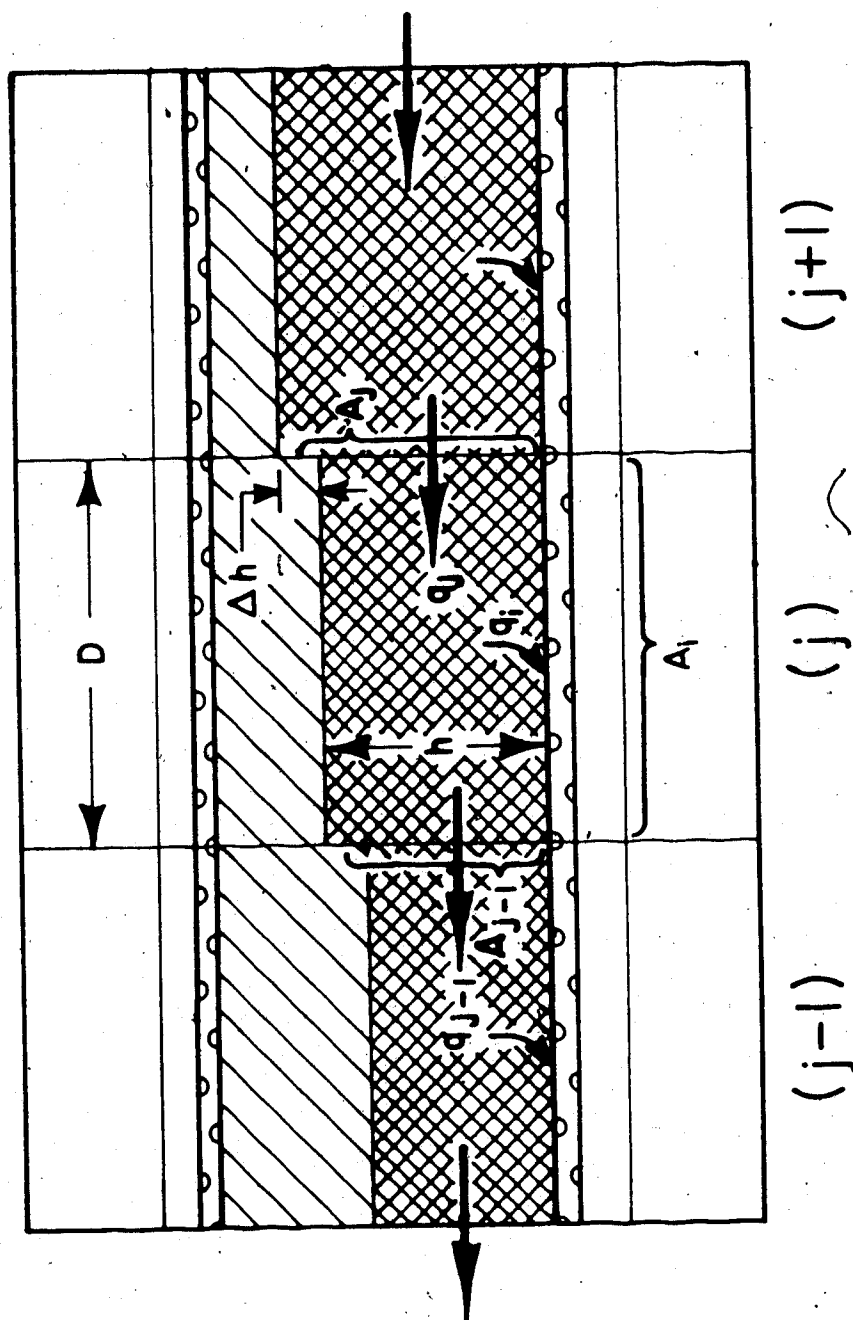


Figure 6.3: Fluid flows between saturated elements in the numerical model of a production controlled electromagnetic flood.

be reasonable up to the point where about 40 percent of a model section has been drained. Beyond this point, however, the rate is optimistic as the effects of partial saturation profiles above the demarker are not considered. The final assumption was that the gravity head loss created by the need to direct the bitumen flow into the perforated electrodes and then horizontally back to the gathering sump, was negligible (ie. a constriction coefficient of one). The demarker position in each section was adjusted at the end of each time step by dropping the demarker by an amount sufficient to allow for the net fluid flow out of the element in the time step.

$$\Delta X_i = q_{n,i} \Delta t / ((S_i - S_d) \phi A_i) \quad (6.8)$$

where ΔX_i → change in demarker position (m)

$q_{n,i}$ → net flow rate out of the element (m^3/s)

$$(q_i + q_{j-1} - q_j)$$

$S_i - S_d$ → difference in saturation below

and above the demarker

ϕ → porosity

Δt → time step (s)

Flow is affected by viscosity, and viscosity, in turn, is strongly affected by temperature. The viscosity of the bitumen in each element was set by the temperature of the element. The viscosity temperature relation used was of the form:

$$\mu_m = A \exp(B/T) \quad (6.9)$$

where T is temperature in °K. The constants A and B were

selected to yield a viscosity of 1000 centipoise at 80°C, and 300 centipoise at 99°C. These values are representative of an 8° API oil and the temperatures represented the range where significant production began in the model runs.

6.3 Model Runs

6.3.1 Material Properties Used

The electrical, thermal and flow characteristics used for the various regions within the model are summarized in table 6.1. The values are representative of a rich Athabasca oilsand material^{17, 18}. The assumed sand was 1.6 percent H₂O and 13.4 percent bitumen by weight with original water and bitumen saturations of 10 percent and 90 percent respectively.

Note that for most of the model investigations outlined below the depleted or drained region above the demarker was assumed to have a residual fluid saturation of 6 percent P.V. (pore volume). However, the model was also used to simulate recovery with residual saturations up to 40 percent P.V. with similar results (see frequency variation case which follows). Examinations by Morrow¹⁹ suggest that residual fluid saturations for a wide variety of fluids and porous media range from about 6 to 10 percent P.V.

The depleted zone was assumed to exhibit an electrical conductivity several orders of magnitude smaller than the saturated formation to reflect the generally disconnected nature of the irreducible water retained in the formation.

6.3.2 Base Case

The numerical model was used to establish suitable operating frequencies and power levels for the selected

Property	Saturated Zone	Depleted Zone	Over/Under Burden
ELECTRICAL			
conductivity σ (S/m)	$1.8 \times 10^{-3} f(T)$ (*)	10^{-4}	--
relative ϵ permittivity	11	3	--
THERMAL			
density ρ (g/m ³)	1.95×10^4	1.66×10^4	1.95×10^4
specific heat c (J/g·°C)	1.0	1.0	1.0
thermal k conductivity (W/m·°C)	1.6	1.6	1.6
FLOW			
permeability k (m ²)	1.98×10^{-12} (2 Darcy)	--	--
saturation S	1.0	0.06	--
porosity ϕ	0.33	0.33	0.33
viscosity (g/m·s)	$A \exp(B/T)$ (**)	--	--

(*) $f(T) = 1 + .0224(T - 24)$
T in °C

(**) $A = 2.296 \times 10^{-7}$
 $B = 7807.5$
T in °K

TABLE:6.1 Material properties for base case model run

formation. The simulations showed that in order to obtain significant production using gravity temperatures in the saturated zone had to exceed approximately 80°C. At very low frequencies such temperatures could not be achieved in the bulk of the formation lying between the electrode well pairs before the electromagnetic wave would decouple and move further into the formation. Formation temperatures and the rate of advance of the heat front were also strongly influenced by the choice of power level.

For the candidate formation described above these simulations identified a rather broad range of suitable frequencies in the LF band (30-300 kHz) with power levels of the order of 10 kW/m to 40 kW/m width of formation, based on a payzone vertical thickness of 20 m.

A 'typical' or base case was selected to illustrate the potential of the process. In this base case the operating frequency was selected as 250 kHz and the power supplied was 2 MW (2700 hp). This power is applied to the payzone section of the formation by a series of upper/lower electrode well pairs which have a vertical separation of 20 metres. The electrode well pairs are assumed to be distributed along a 100 metre length of the horizontal tunnels shown in figure 2.1. The number of actual well pairs required along this hundred metre interval is variable and depends upon the vertical separation. In the present example it is estimated that five well pairs should produce heating with satisfactory uniformity along the array. The applied power

is split between the two horizontal waves established (see figure 2.5). As the numerical model only simulated one half of this mirror image situation, its production results have been scaled to yield the equivalent full system results. Selected results of the simulation run made using the base case parameters are presented in figure 6.4.

Note that formation temperatures behind the heat front are maintained at about 100°C although some cooling is evident well behind the front which is advancing at about 75 m per year. The gradual increase in the size of the production interval, as the electromagnetic flood progresses, is clearly indicated by the changing demarker location in figure 6.4b.

The production figures given in figure 6.4 represent the total production from the 100 m width of formation modeled. The production is gathered by a set of five electrode-well pairs extending horizontally in both directions from the central tunnel system. (see figures 2.5 and 6.1). After approximately six months it is seen that the production per electrode-well pair has risen to about 70 bbls/day. By the end of the two year period shown about 300 metres of formation are contributing to production at a rate in excess of 200 bbls/day. The average energy cost is approximately \$3.25/bbl for electrical energy at 4 cents per kWh over the two year period.

In assessing the production figures given in figure 6.4c it should be recalled that the results are somewhat

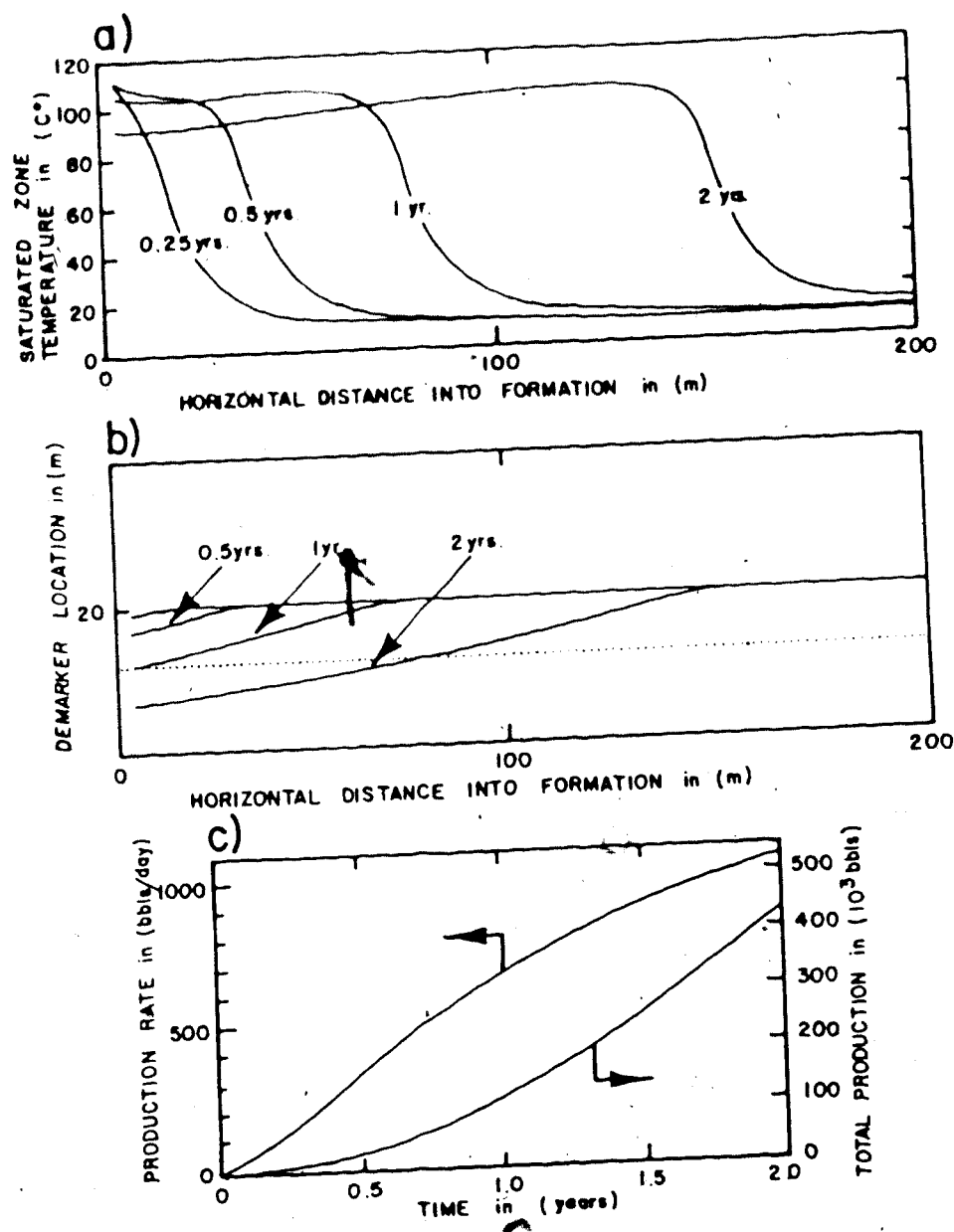


Figure 6.4: Base case model run of production controlled electromagnetic flood numerical model.
 a) Saturated zone temperature profiles at various times in the heating sequence.
 b) Location of the demarker between the saturated zone and the depleted zone at various times in the heating sequence.
 c) Production rate and cumulative production of fluids from the oil sand formation as the heating sequence progresses.

137

optimistic because of the clean demarker assumption. Indeed the figures for production from any of the fifty sections in the model are realistic only up to the point where about 40% of the section has been drained. The dotted line on figure 6.4b indicates the 40% recovery mark. The model overestimates production from those portions of the formation where the demarker has dropped below this line. Thus, the total production for the two year period shown is overly optimistic by some 40 to 80 thousand barrels out of the 430 thousand barrels produced.

6.3.3 Frequency Variation

The effect on the development of the electromagnetic flood of changing the operating frequency is illustrated in figure 6.5. All parameters for this simulation were the same as for the base case except that the operating frequency was reduced to 150 KHz from 250 KHz. A comparison of the saturated zone temperatures between the two runs shows two very similar temperature profiles. The higher frequency case, since the wave remains coupled somewhat longer, has a higher temperature over the bulk of the formation but the electromagnetic flood does not penetrate quite as far in a given time. The production figures for the higher frequency case are much larger, this being due to the relatively large change in the bitumen viscosity which attends the small temperature difference observed. It would appear then that a higher operating frequency is preferable in terms of

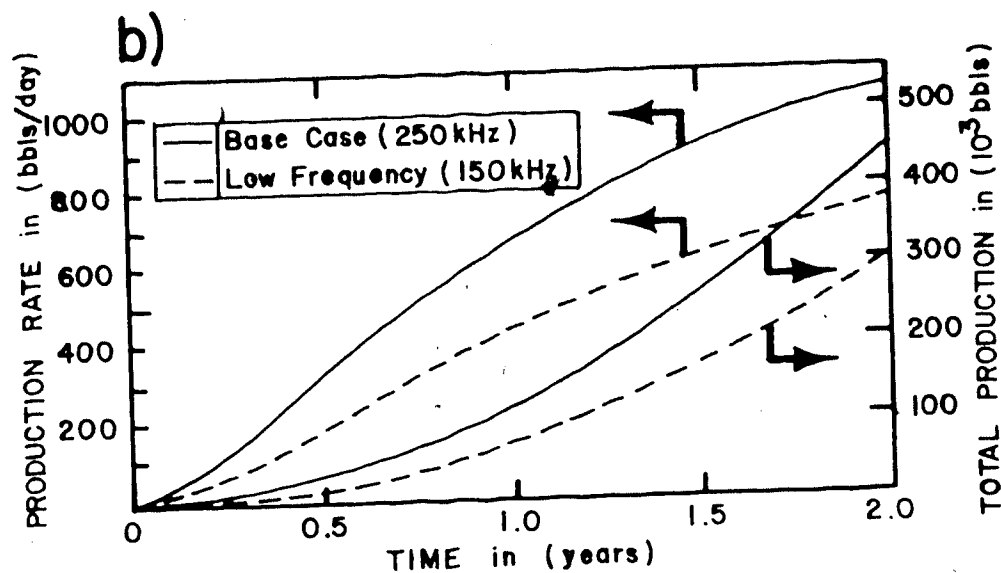
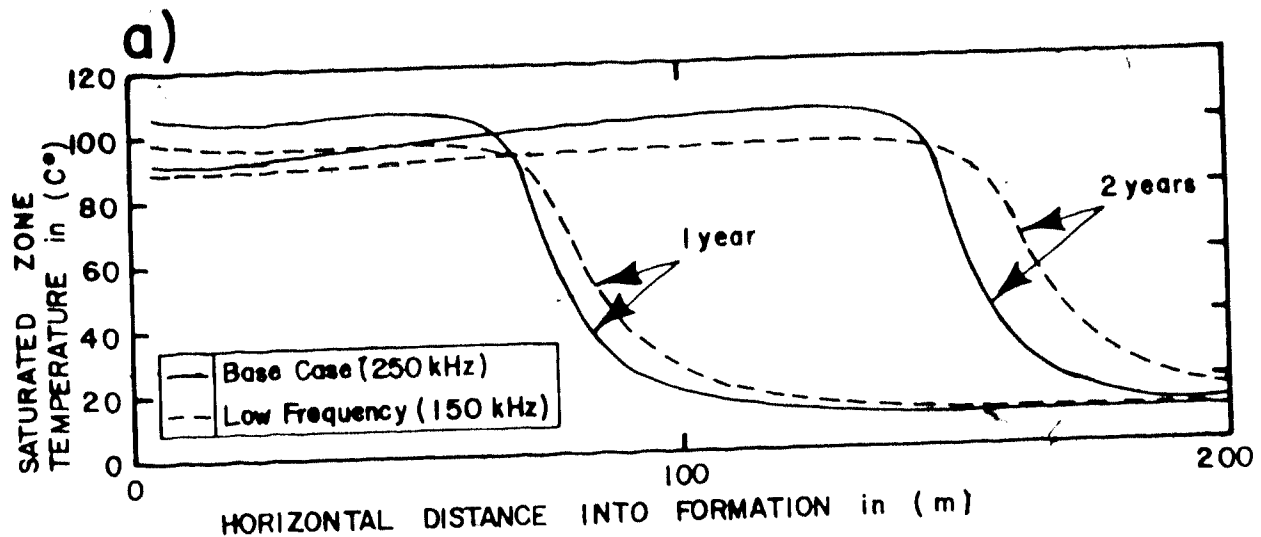


Figure 6.5: Production controlled electromagnetic flood simulation runs for two different operating frequencies.

- a) The effect on the saturated zone temperature profiles.
- b) The effect on the fluid production.

obtaining higher initial production rates. This advantage can, however, be expected to decrease in the longer term as the lower frequency case, while producing at a lower rate per metre depth into the formation, will produce at any one time over a deeper total range (the electromagnetic flood augers deeper), thereby decreasing the initial relative advantage of the higher operating frequency.

It is interesting to note that a model run with all parameters the same as the base case, except for the residual fluid saturation which was taken as 40 percent P.V. (pore volume), yielded results virtually identical to the low frequency simulation illustrated in figure 6.5. In this situation the demarker between the saturated zone and depleted zone dropped more rapidly causing the electromagnetic wave to decouple and move into the formation more quickly. In the longer term (beyond the two year production period shown) the high residual saturation would of course significantly effect the total recovery potential. The present model runs are, however, limited to estimating the initial production levels and are thus not strongly influenced by the assumed residual saturation level.

6.3.4 Power Variation

The effect of doubling the base case input power is illustrated in figure 6.6. The resulting temperature profiles show only a relatively small increase in the peak temperatures obtained. The higher heating rate tends to

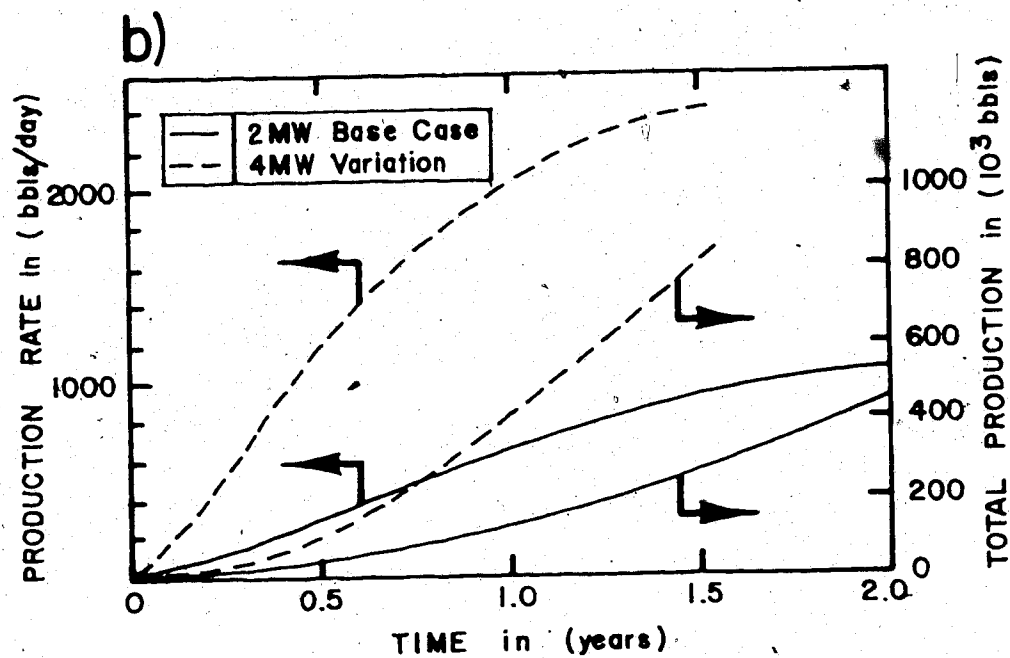
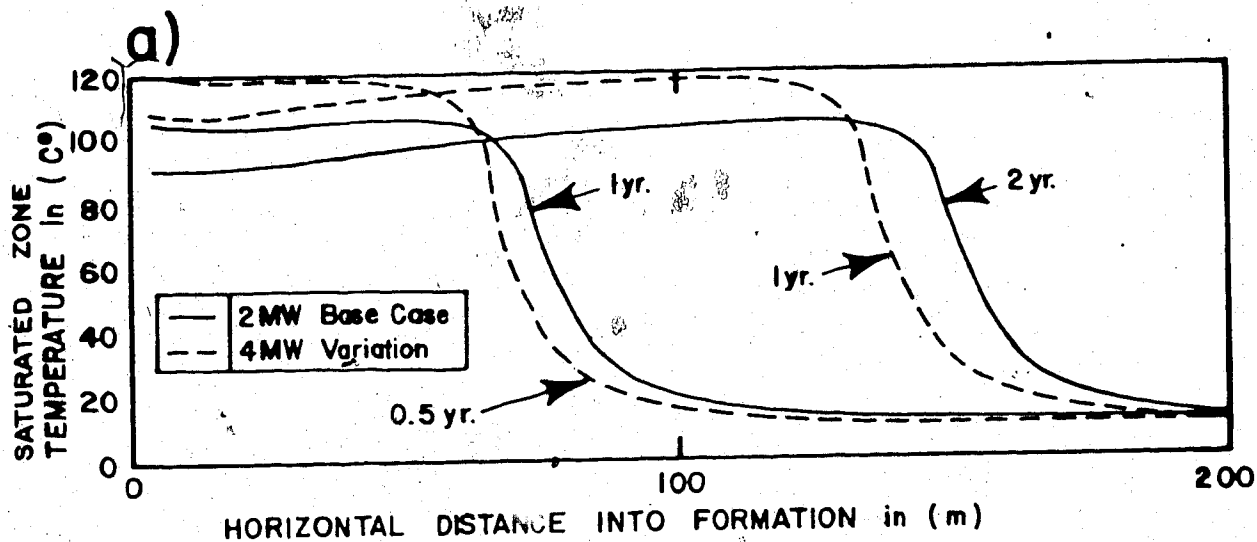


Figure 6.6: Production controlled electromagnetic flood simulation runs for two different applied power levels.

- a) The effect on the saturated zone temperature profiles.
- b) The effect on the fluid production.

increase the formation temperatures, but the corresponding decrease in bitumen viscosity increases the flow rate so that a given section remains coupled for a shorter time and thus tends not to obtain as high a temperature as might be expected.

Examining the production rate of the two cases at points of equivalent total energy input (for example the 2MW case at 2 years versus the 4MW case at 1 year) shows that the higher power case yields a higher production rate. The volumes of formation brought into production by the electromagnetic flood at this point are approximately equal. However, the somewhat higher temperature obtained in the higher power case leads to a significantly higher production rate. The conclusion to be drawn then is that the use of as high a heating rate as possible is desirable from the viewpoint of obtaining higher initial production rates. There will exist, however, a limitation to the maximum allowable power level for any given operating frequency and electrode surface area design configuration.

It may be noted that at this higher power level some of the average element temperatures exceed 100°C . Considering that a more detailed modeling of the formation volumes near the cylindrical electrodes would undoubtedly show even higher temperatures occurring near the electrodes, some formation water evaporation is likely. The numerical model, however, assumes that growth of the depletion region due to moisture loss by evaporation is negligible compared to the

flow generated depletion zone generation. The representation is therefore probably only valid for the case where the upper/lower electrode system is maintained at a moderate positive pressure relative to atmospheric pressure, such that formation moisture loss via evaporation is minimal. To prevent the venting of this pressure back into the tunnel system, the first several metres of each electrode could be coated with a dielectric layer. The coating would reduce the coupling such that this input zone would remain cold and thus could form a low permeability zone to block the pressure release.

The generation of steam in the depletion zone presents the possibility of operating an electromagnetic flood at elevated power levels so as to generate an autogenous steam drive which would assist the gravity drive. Significant alterations to both the electrical and flow modelling of the process would be required to simulate such a situation.

6.3.5 Permeability Variation

In this final case the permeability of the entire formation is reduced to one Darcy from the base case value of two Darcies. The simulation results for this variation are presented in figure 6.7. Recalling the earlier discussion of the self-leveling effect, one should expect an increase in formation temperatures so that the production reduction is considerably less than a factor of two. The production rate data from this run confirms this expectation

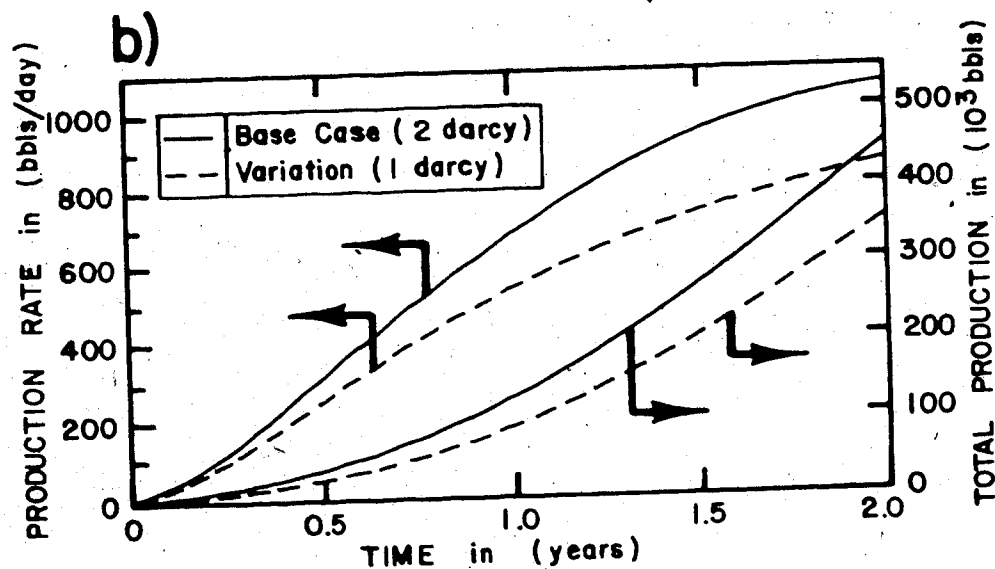
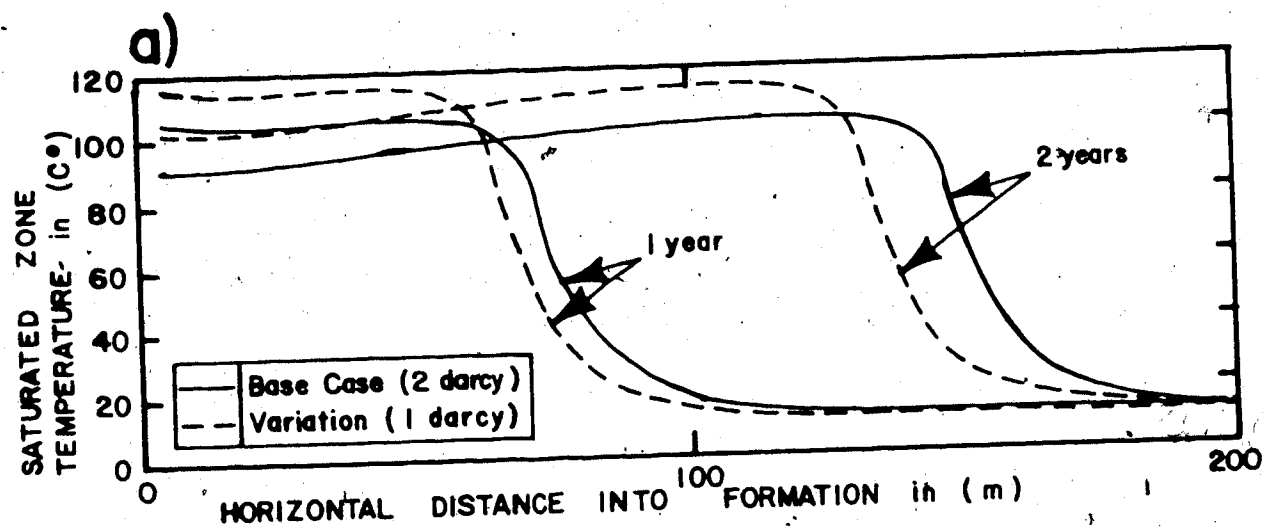


Figure 6.7: Production controlled electromagnetic flood simulation runs for two different flow permeabilities in the formation.
 a) The effect on the saturated zone temperature profiles.
 b) The effect on the fluid production.

in that the reduction is only about 20%.

In a similar vein the model was run for all parameters being the same as the base case, with the exception of the formation region between 40 and 60 metres having a permeability of 0.5 darcies (2 elsewhere). The temperature and demarker results for this case are presented in figure 6.8. The self leveling effect discussed in the production controlled electromagnetic flood section is evident in the selective temperature rise of the reduced permeability zone. At two years, the production rate in this case was only slightly lower than for the base case.

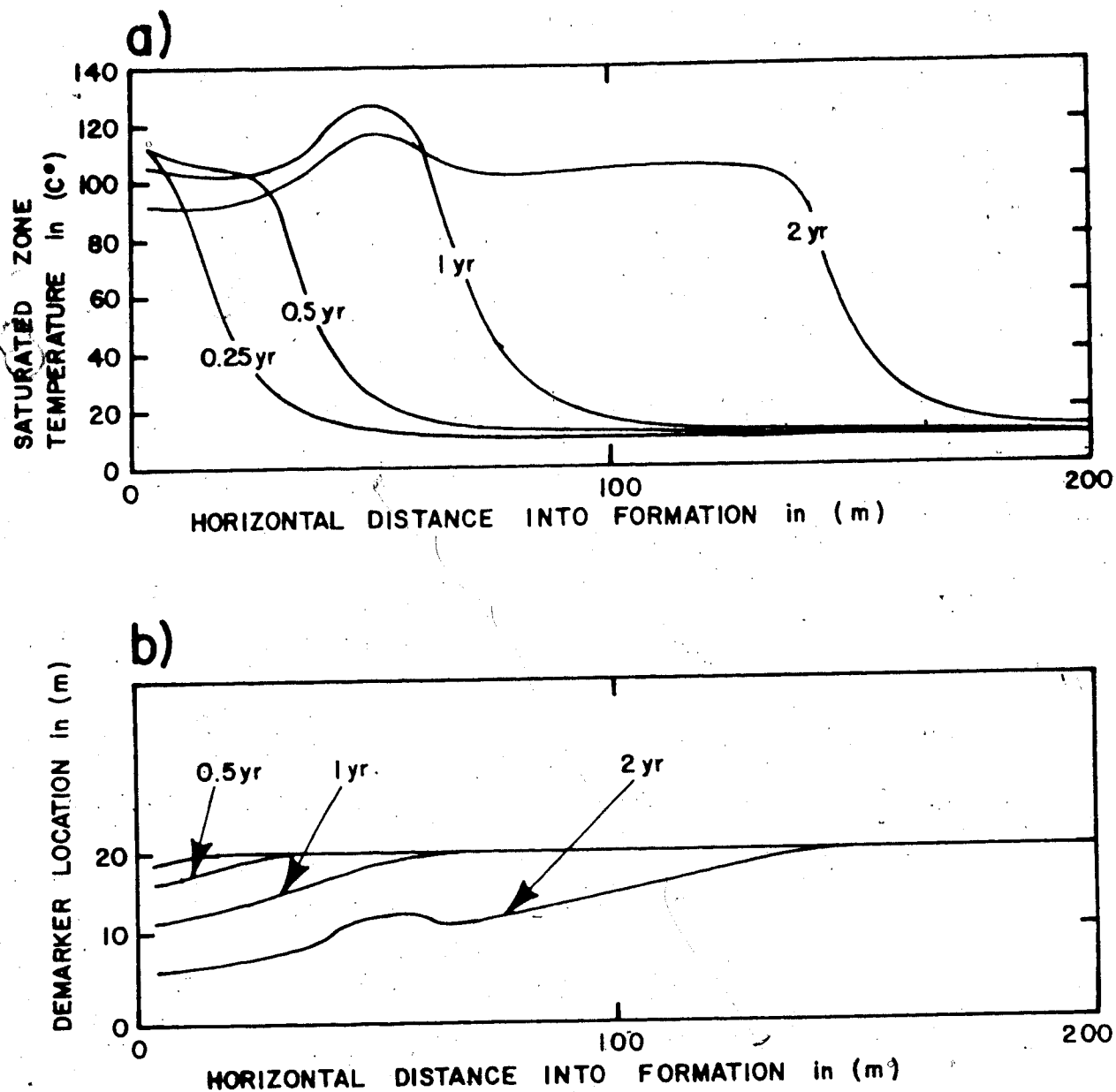


Figure 6.8: Production controlled electromagnetic flood simulation run for the case of a selected portion of the formation having a lower flow permeability.

- a) The effect on the saturated zone temperature profiles.
- b) The effect on the demarker location between the saturated and depleted zones.

7. Scaling Criteria for Electrothermal Models

An objective of this thesis has been to determine the heating patterns that can be obtained in an Athabasca oil sand formation using a variety of electrode configurations. The methodology used to accomplish this objective was to construct a physical scale model of the actual (field) electrode/oil sand arrangement and to heat the model using electromagnetic energy. The temperature changes which occur at any point in such a scale model can accurately simulate the temperature changes that would occur in the field if certain criteria can be met. The criteria are discussed in section 7.1.

To be of practical value a scale model should have physical dimensions substantially smaller than the field situation and the heating time required to reach any given temperature in the model should be shorter than the corresponding field heating time. To quantify these attributes two parameters may be defined. The first parameter is the mechanical scale factor P , which is the ratio of any linear distance in the field to the corresponding distance in the model. A mechanical scale factor greater than one implies a model that is physically smaller than the corresponding field configuration. The second parameter is the thermal time scale factor T , which is the ratio of the field heating time to the model heating time for a particular temperature rise to be obtained in both the field and the model. A thermal time scale factor

greater than one implies that the model heating run will take less time than the time required to heat in the corresponding field situation.

As was previously pointed out a number of criteria must be met for similitude to exist between the field situation and the scale model. These criteria are briefly outlined in the following section and then expanded upon to cover the particular case of a dielectric coated transmission line. Following that section a specific example of the scaling used in one of the experimental runs is presented.

7.1 Relations

The requirements to be met to obtain simultaneous scaled results for both electromagnetic fields and thermal conduction phenomena are described in detail in reference 6. The reader is directed to this reference for a detailed derivation of the scaling relations. For the convenience of the reader a brief summary of the scaling criteria is presented here.

It is necessary for the electric and magnetic fields to have the same geometrical configurations and relations to one and another in both the model and the field. This will occur if Maxwell's equations (see equation 4.1) are invariant under the transformation from full scale system to the model system. This invariance criterion can be met if two relations between the model and field variables are met. (Refer to the nomenclature section for definition of the

symbols used. Model parameters are distinguished from the corresponding field parameters by designating the model parameters with the superscript symbol '.') The first of the two relations is that the mechanical scale factor, expressed in terms of the model and field material properties, must be:

$$p = (\sigma' / \sigma) ([(\mu' \epsilon) / (\mu \epsilon')]^{1/2}) \quad (7.1)$$

The second relation required is that the ratio of conduction current to displacement current must be the same in both the model and the field.

$$\sigma / \omega \epsilon = \sigma' / \omega' \epsilon' \quad (7.2)$$

These two criteria ensure electromagnetic similitude between model and field.

The establishment of the same thermal profiles in both model and field, requires more than the establishment of the proper relative electromagnetic fields. It is necessary to construct a model for which the change in temperature in the model at a scaled down time t' , is identical to the change in temperature achieved in the full scale system after time t , at every geometrically similar point in the model and the full scale systems. To this end it is first of all necessary that the ratio of the electrical energy deposited per unit volume to the volumetric heat capacity be identical in the model and full scale system at corresponding times t' and t . Secondly, it is necessary that at corresponding times t' and t the ratio of the rate at which heat is delivered to a given region to the rate at which heat is lost from the same

region by thermal conduction is the same in the model and the full scale systems. One further requirement is that the operating frequency in both the model and the field must be high enough that temperatures do not change significantly in the course of a cycle of the electromagnetic fields. This allows the average or "RMS" heating effect of the fields to be considered rather than the instantaneous heating rate. In this situation the thermal time scale factor T is distinct from the electromagnetic time scale factor which is implied by the ω and ω' terms in equation 7.2.

The requirement that the ratio of heat delivered per unit volume to heat lost by thermal conduction from the same unit volume be the same in full scale and model systems may be addressed by considering the heat equation, with an electromagnetic heating term, and requiring the equation to be invariant under the transformation from the full scale system to the model system. It can be shown that the invariance criterion will be met if the thermal time scale factor is selected as follows:

$$T = p^2 (k' \rho c) / (k \rho' c') \quad (7.3)$$

where the variables are defined in the nomenclature section. From this sequence it is also possible to show that the electrical power delivered to the model P' is related to the full scale power level P as:

$$P/P' = p(k/k') \quad (7.4)$$

The three relations 7.1, 7.2 and 7.3 establish a unique mechanical scale factor, operating frequency and thermal

time scale factor for a model of a given field arrangement, once the model medium is selected. This result is, however, somewhat restrictive. If, for example, a particular mechanical scale factor is desired, a model medium with very specific electrical properties must be found in order to satisfy both equations 7.1 and 7.2.

Fortunately for the frequencies considered and the model types presented in the case studies of this thesis, the ratio of conduction current to displacement current in the lossy medium is much greater than unity for both the model and the field situation. If the displacement current is negligible it may be deleted from the curl \mathbf{H} expression in Maxwell's equations (see equation 4.1, neglect the $j\omega\epsilon\mathbf{E}$ term compared to the $\sigma\mathbf{E}$ term). This approximation is referred to as the "induction approximation" in reference 6. It can be shown that this simplified version of Maxwell's equations will be invariant under transformation if the mechanical scale factor is selected such that it is equal to the ratio of the skin depth Δ in the field to the skin depth Δ' in the model.

$$p = \Delta / \Delta'$$

(7.5)

$$\text{if } \sigma / \omega\epsilon \gg 1$$

$$\text{and } \sigma' / \omega'\epsilon' \gg 1$$

For a transverse electromagnetic wave propagating along a transmission line in a lossy medium ($\sigma / \omega\epsilon \gg 1$) the skin depth is given by:

$$\Delta = 1/\alpha = [1/\pi f \mu \sigma]^{1/2}$$

(7.6)

For non-magnetic media in both model and field the mechanical scale factor may thus be expressed as:

$$p = \Delta / \Delta' = [f' \sigma' / f \sigma]^{1/2} \quad (7.7)$$

or as

$$p^2 = f' \sigma' / f \sigma \quad (7.8)$$

Note that the single expression 7.8 replaces the two criteria equations 7.1 and 7.2. Mechanical scale factor selection under these circumstances is much easier since a particular size factor may be obtained by simply altering the model frequency and therefore Δ' to obtain the mechanical scale ratio desired. The requirements on thermal time scaling presented in equation 7.3 still apply.

For a single medium filling the space between the electrodes of a transmission line in an oil sand formation, the previous scaling criteria derived from Maxwell's equations will allow simultaneous electromagnetic and thermal modeling. In many of the experimental heating runs, however, an insular coating is either generated on (partial evaporation boring) or directly applied to (dielectric coated electrodes) the formation electrodes. In the case of a coated transmission line the introduction of a second medium (the coating), in which the conduction current is negligible, violates the assumption of the displacement current being an insignificant term compared to the conduction current for all points in the formation. The scaling criteria expressed by equation 7.8 are not, a priori, correct in this circumstance. It becomes necessary

to review the scaling criteria to see how they will be affected by the presence of this second medium. Further, it may be recalled that in partial evaporation boring the transmission line is a dynamically changing mix of coated and uncoated electrodes. If a scale model is to be a valid representation of both the single media case, encountered initially in partial evaporation boring, and the coated electrode (two media) case encountered later in the heating run the scaling criteria for both cases must be compatible.

The following section extends the scaling criteria developed in reference 6, and summarized here, to the specific case of dielectric coated electrodes placed in a conductive ($\sigma \gg \omega\epsilon$) oil sand formation to form a transmission line.

7.2 Scaling Criteria for Dielectric Coated Lines

The scaling criteria expressed by equations 7.1 and 7.2 are equivalent to requiring:

$$\gamma\ell = \gamma'\ell'$$

(7.9)

$$\text{where } \gamma = ((\sigma + j\omega\epsilon)(j\omega\mu))^{1/2}$$

γ is the propagation characteristic of a uniform plane wave and ℓ is a distance term. An interpretation is that for uniform plane waves propagating in both model and field, the amount of attenuation and phase shift experienced by the waves should be the same when they have both travelled the same "distance" in proportion to the overall system size.

For a dielectric material ($\sigma=0$) equation 7.9 becomes:

$$\omega(\mu\epsilon)^{1/2}l = \omega'(\mu'\epsilon')^{1/2}l'$$

or

$$p = l/l' = (\omega'/\omega)(\mu'\epsilon'/\mu\epsilon)^{1/2} \quad (7.10)$$

For a conductive material ($\sigma \gg \omega\epsilon$) equation 7.9 becomes:

$$(j\omega\mu\sigma)^{1/2}l = (j\omega'\mu'\sigma')^{1/2}l'$$

or

$$p = l/l' = (\omega'\mu'\sigma'/\omega\mu\sigma)^{1/2} \quad (7.11)$$

In the case of a dielectric coated transmission line there is both a dielectric region and a conduction region surrounding the electrodes. The scaling criteria for both regions must be met simultaneously. This requires:

$$p = (\omega'\mu'\sigma'/\omega\mu\sigma)^{1/2} = (\omega'/\omega)(\mu'\epsilon'/\mu\epsilon)^{1/2} \quad (7.12)$$

If one further restricts consideration to cases with non-magnetic media ($\mu'=\mu=\mu_0$) and assumes the same dielectric coating material is used in both model and field ($\epsilon'=\epsilon$), then the relation reduces to:

$$p = (\omega'\sigma'/\omega\sigma)^{1/2} = \omega'/\omega$$

or

$$p = \omega'/\omega = \sigma'/\sigma \quad (7.13)$$

Note that this result is consistent with the requirement established for uncoated lines (7.8). The addition of the coating material has, however, reduced the degree of freedom present in selecting the modelling scales. Equation 7.13 may now be used in conjunction with equation 7.3 to establish suitable scaling relations for coated lines penetrating a conduction dominated medium.

7.3 Sample of Scaling Calculations

By way of demonstration let us consider the scaling of the uniformly coated line described in section 3.4.1. The model medium used has a conductivity of 0.289 S/m. The postulated corresponding field situation is for a rich, low moisture, oil sand with a conductivity of 2×10^{-3} S/m. In both model and field the conduction current is dominant ($\sigma \gg \omega \epsilon$) in the lossy medium. The mechanical scale factor (field to model) is thus obtained from equation 7.13 as 145. Similarly, from the same equation the model frequency of 12 MHz corresponds to a field operating frequency of 82.8 kHz. These two selections result in the attenuation and wavelength of the coated lines (model and field) being in proportion, with the proportionality factor being the mechanical scale factor. The ratio of field time to model time is determined by equation 7.3. For the thermal properties listed in section 3.4.1 the time ratio is 24587 to 1. Finally, the ratio of applied field power level to applied model power is given by equation 7.4. For the values on hand the equation yields a ratio of 154 to 1. The model power is 715 W to a half element or correspondingly 1430 W to a full element. The equivalent field power to a full element would therefore be 220 kW.

Conclusion

High frequency electromagnetic heating shows the promise of being a viable method of raising blocks of oil sand material to production temperature, in-situ. The attainable heating rate and energy placement efficiency are greater than for methods that depend on conductive heat transfer. The temperature uniformity obtained can be superior to that which is possible for low frequency electrical conduction heating schemes. The formation electrical contact problems encountered in low frequency heating can not only be circumvented by high frequency heating but can actually be put to effective use as a desirable decoupling mechanism.

Six different heating concepts involving the use of high frequency electromagnetic energy were put forward in chapter 2. In order to establish the basic feasibility and relative merits of the various concepts a series of physical experiments and numerical simulations have been undertaken as described in chapters 3 to 6. A brief summary of the conclusions reached is presented here.

The first five concepts to be discussed are all based on the premise of performing a pre-heat cycle to condition the formation for subsequent bitumen production through the injection of a displacing agent such as steam or hot water. Before commenting on the specific temperature profiles obtained with these heating schemes a brief description of what type of temperature profile is desirable is given.

If electromagnetic heating is being used as a pre-heat stage in a bitumen recovery process the form of the temperature profile established in the formation by the pre-heat can greatly affect the efficiency of the subsequent production sweep of the formation. Ideally a channel of hot oil sand containing low viscosity bitumen should be formed which is surrounded by a cold zone containing immobile bitumen (or some other similarly impermeable formation zone). The temperature within the channel should be uniform so that the flow characteristics of the heated channel are as uniform as possible. Such uniformity makes possible the recovery of a high percentage of the bitumen in the channel by a subsequent production sweep of the formation before breakthrough of the displacing agent occurs.

Outside of the pre-heated block to be swept the temperature rise should be minimal as the heating of non-producing volumes represents an inefficiency in the pre-heat cycle. A desirable temperature profile is thus one which is uniform within the block to be heated and which shows a high temperature gradient at the physical limits of the desired pre-heat zone.

The first of the concepts directed toward pre-heating the formation was termed *total evaporation boring*. In this concept the hot channel is created by an advancing heat front which sweeps the length of the channel. The concept of total evaporation boring was examined by heating unscaled physical models containing Athabasca oil sand. The

experimental results suggest that total evaporation boring is a viable means of obtaining the desired heating but is inferior, in terms of heating efficiency, to the partial evaporation and coated electrode heating concepts due to the great amount of moisture that must be driven off.

The second of the concepts directed toward pre-heating the formation was termed *partial evaporation boring*. The heated channel in this case is also generated by a heat front which sweeps the length of the channel. In this case, however, much less of the formation water is evaporated and as such the energy requirements of the pre-heat cycle are much lower than in the total evaporation boring case. The concept of partial evaporation boring was examined by heating both unscaled and scaled physical models. The experimental results indicated that the desired boring action occurred with little evaporation energy loss. Very favourable temperature profiles were obtained between the electrodes. Specifically the heated zone was quite uniform in temperature and high temperature gradients were established at the boundary between the heated and unheated zones.

The third of the concepts directed toward pre-heating the formation involves *coating the electrodes with a suitable layer of dielectric material*. In this concept the entire channel is brought up to the desired temperature simultaneously. Minimal evaporation losses are experienced with this heating method. The concept of coated electrodes

was examined by heating scaled physical models. The results of these experiments indicated that uniform temperature profiles were established across the channel if a relatively short stabilization period was allowed following the heating cycle. The temperature gradient at the edge of the heated zone was again reasonably high. These experiments also helped to identify two naturally occurring mechanisms which assist in the attainment of a uniform temperature distribution. These mechanisms are the *self leveling thermal effect* discussed in section 2.3 and the *self coating effect* discussed in section 3.4.2.

The fourth of the concepts directed toward pre-heating the formation was based on adding *series capacitors to the formation electrodes* to alter the energy deposition profile. The concept of series resonated electrodes was examined through a series of unscaled physical experiments. The results of these experiments demonstrated the wavelength and skin depth expanding properties sought. The previously described work with coated electrodes showed, however, that an adequately uniform temperature distribution could be obtained without using series capacitors. No further work on this concept was undertaken for this reason.

The fifth and final concept directed toward pre-heating the formation was one in which the *energy coupling from the electrode to the formation was field variable* during the actual heating process. The concept of variable coupling electrodes was examined by heating scaled physical models.

The experimental results suggest that the concept does not hold great promise as the selective coupling aspect tends to be overshadowed by an electrode self coating effect.

In terms of creating a uniformly heated zone of oil sand as a pre-heat stage to eventual production, the partial evaporation boring, dielectric coated line and self generated uniform coating schemes show the most promise, since with these schemes acceptable heating profiles are obtained with the simplest electrode structures.

In addition to simply pre-heating the oil sand formation by using one of the five concepts discussed above, a sixth concept was put forward which involves both heating and producing the bitumen in a single process. The concept of *production controlled heating* was examined along two avenues. Firstly, physical experiments were undertaken to demonstrate the basic mechanism of electromagnetic heating leading to production, and production subsequently resulting in the decoupling of the formation from the electrodes. The physical experiments displayed these basic phenomena. Secondly, a first order numerical simulation of the production controlled heating was generated. The simulation results were encouraging in that they suggest an oil sand of the Athabasca type is well suited to production by this method. The production controlled heating concept is particularly attractive since no second stage bitumen production process is required. The results of the first

order numerical simulator are encouraging enough to suggest that an effort to upgrade the numerical simulator to give more detailed production estimates may be worthwhile.

The objectives of the current line of research were outlined in section 1.4. The main objective was to establish the basic feasibility of a number of heating configurations and the relative merits of each compared to the others. Having completed this phase, the results obtained may be reviewed to ascertain what additional work could be undertaken to further delineate the feasibility of high frequency heating of Athabasca oil sand bodies. Two specific items can be identified as candidates for examination in any subsequent study.

The first candidate for further work is the numerical simulator used to examine production controlled heating. More detailed production data could be obtained from this model if the flow modeling code were upgraded to a full two dimensional reservoir simulator that includes partial saturation effects and that contains suitable constriction factors to allow for the finite number of collector wells. In conjunction with this work the electrical modeling could be upgraded to more accurately predict the electrical heating profile.

The other area which would bear closer examination deals with the evolution and removal of moisture from the immediate vicinity of the electrodes during electrical heating. Two of the more promising heating concepts, partial

evaporation boring and self coated electrodes, are dependent on the removal of this moisture. To examine this effect in more detail a cylindrical container could be packed with Athabasca oil sand with a perforated tube in the centre to simulate an electrode. Current could be injected into this electrode and gathered at the outer wall of the cylinder. Impedance measurements between the central tube and the outer wall of the cylinder could be taken during an electric heating process to establish how the insular coating layer grows. Post heating moisture analysis of the oil sand would allow determination of the moisture profile around the electrode.

Assuming the proposed two developments yield results which are as encouraging as the work to date, the next logical extension would be a small scale field test. The probable form of such a field test would be to bore a series of horizontal electrode wells into an exposed outcrop containing an Athabasca oil sand seam. The extent and uniformity of an electric pre-heat cycle could be determined by drilling a number of suitably positioned small bore holes to allow the placement of temperature sensors. A production controlled heating sequence could also be examined but due to the longer time spans involved, compared to a simple pre-heat, this would, to begin with, be limited to an examination of the initial production stages.

Bibliography

1. C.P. Outrim, R.G. Evans, *Alberta Oil Sands Reserves and Their Evaluation*, The Oil Sands of Canada-Venezuela 1977, The Canadian Institute of Mining and Metallurgy Spec. Vol. 17, pp 36-66
2. J.D. Scott (Session Reporter), *AOSTRA Seminar on Underground Excavation in Oil Sands*, University of Alberta, May 19, 1978, Alberta Oil Sands Technology and Research Authority, Edmonton, Alberta
3. F.E. Vermeulen, F.S. Chute, M.R. Cervenán, J. Fearn, *Physical Modelling of Electrical Heating of Oil Sand Deposits*, AOSTRA Research Agreement #58, Case Study #1, Alberta Oil Sands Technology and Research Authority, Edmonton, Alberta, June, 1982
4. J. Bridges et. al., *R.F. Heating of Utah Tar Sands*, U.S. Department of Energy, DOE/GH/90035-4, January 1980
5. J. Bridges, A. Taflove, *Apparatus and Method for In Situ Heat Processing of Hydrocarbonaceous Formations*, U.S. Patent #4,144,935
6. F.E. Vermeulen, F.S. Chute, M.R. Cervenán, *Physical Modelling of the Electromagnetic Heating of Oil Sand and*

other Earth-Type and Biological Materials, Canadian Electrical Engineering Journal, Volume 4, Number 4, 1979, p 19-28

7. F.S. Chute, F.E. Vermeulen, M.R. Cervenak, J.F. McVea, *Electrical Properties of the Athabasca Oil Sands*, Canadian Journal of Earth Sciences, Volume 16, 1979, pp 2009-2021

8. K. Takamura, *Microscopic Structure of Athabasca Oil Sand*, Canadian Journal of Chemical Engineering, Volume 60, August 1982, p 538-546

9. E.R. Abernethy, *Production Increase of Heavy Oils by Electromagnetic Heating*, The Journal of Canadian Petroleum Technology, July-Sept. 1976

10. S.T. Fisher, *Processing of Solid Fossil-Fuel Deposits by Electrical Induction Heating*, IEEE Trans. Ind. Electronic Contr. Instrum., Vol IECI-28, No 1, pp 65-67, 1981

11. J.C. Todd, E.P. Howell, *Numerical Simulation of In Situ Electrical Heating to Increase Oil Mobility*, Canada-Venezuela Oil Sands Symposium Proceedings, Canadian Institute of Mining and Metallurgy, Edmonton 30 May-3 June 1977, Canadian Institute of Mining and Metallurgy Special Volume 17, pp 477-486

12. F.S. Chute, F.E. Vermeulen, R.G. McPherson, *Radio Frequency Evaporative Boring for In-Situ Heating of Oilsands*, progress report for AOSTRA Research Agreement #347, Alberta Oil Sands Technology and Research Authority, Edmonton, Alberta, June 1983

13. R.E. Collin, *Foundations for Microwave Engineering* McGraw-Hill Book Company, 1966, chapters 3 and 5.

14. E.C. Jordan and K.G. Balmain, *Electromagnetic Waves and Radiating Systems 2nd Ed.*, Prentice Hall Ltd. 1968, chapter 7.

15. W.T. Cardwell and R.L. Parsons, *Gravity Drainage Theory*, Transactions of AIME (1949), 179, pp 199-215

16. H. Dykstra, *The Prediction of Oil Recovery by Gravity Drainage*, Journal of Petroleum Technology, May 1978, p 818-830

17. J.M. Dealy, *Viscosity of Oil Sands Fluids*, The Oil Sands of Canada-Venezuela 1977, The Canadian Institute of Mining and Metallurgy, Spec. Vol. 17, pp303-306

18. M.R. Cervenán, F.E. Vermeulen, F.S. Chute, *Thermal Conductivity and Specific Heat of Oilsand Samples*, Canadian

Journal of Earth Sciences, volume 18, number 5, pp926-931

19. R.F. Harrington, *Time-Harmonic Electromagnetic Fields*, McGraw-Hill Book Company, 1961, chapters 3 and 4

20. F.S. Chute, M.R. Cervenak, P.E. Vermeulen, *Simple Cell for the Measurement of the Radio Frequency Electrical Properties of Earth Materials*, American Institute of Physics, Review of Scientific Instruments, 49(12), December 1978, pp 1675-1679.

21. B.C. Craft and M.F. Hawkins, *Applied Petroleum Reservoir Engineering*, Prentice-Hall 1959, Figure 7-1, p357, water-oil relative permeability curves.

22. W.H. Hayt Jr., *Engineering Electromagnetics*: 2nd edition, McGraw-Hill Book Company, 1967, chapter 12.

23. N.R. Morrow, *Irreducible Wetting-Phase Saturations in Porous Media*, Chemical Engineering Science, 1970, volume 25, pp1799-1815.

Appendix A: Transmission Line Theory

Transmission line theory is extensively covered in most electromagnetic theory textbooks (see for example references 22 or 14). The subject matter in this thesis overlaps into a number of scientific disciplines and as such may be of interest to readers unfamiliar with the analysis techniques of transmission line theory. It is planned in this section to present a brief outline of the distributed impedance representation for a transmission line and the analytical techniques used to describe the voltages and currents present on a transmission line. The intended purpose of this section is to provide the reader, unfamiliar with the terminology and concepts of transmission line theory, with some background in these areas. A familiarity with basic AC circuit analysis will be assumed.

A transmission line may be defined as two conductors existing in a medium otherwise occupied by some material of known electrical properties (see, for example, figure 5.1 a). When a sinusoidal voltage source is attached to these two conductors, charge movement will occur in the conductors and electric and magnetic fields will be established in the medium outside the conductors. While the exact form of the electric and magnetic fields can nominally be ascertained using the boundary conditions and Maxwell's equations, somewhat easier analytical techniques may be employed if a certain criteria can be met. Specifically, if all physical dimensions of the system under consideration

are much less than a wavelength in extent, then circuit theory analysis may be employed rather than general electromagnetic field theory. The variables of the problem become the scalar quantities of the phasor voltage established between the two conductors and the phasor current carried on the conductors rather than the electric and magnetic vector fields. Lumped element (resistance, capacitance, inductance) components can be assembled to represent the physical configuration and establish the relationship between the voltage and the current.

Transmission line theory deals with the case where the length of the two conductor transmission line (total distance in the z direction of figure 5.1 a)) is not much less than a wavelength. This situation may still be addressed using circuit theory concepts if the transmission line is considered to be made up of a series cascade of short lengths (Δz long), each of which is much less than a wavelength in extent. The circuit theory lumped element representation for each short length is shown in figure 5.1 b). Note that the R, L, C and G values shown are distributed impedance values. The inter-electrode capacitance, for example, of the short length of line is C (Farads/metre) times Δz (metres).

The phasor voltage between the conductors and the phasor current along the conductors will be a function of what physical point along the length of the line they are to be measured at. The functional relation linking phasor

voltage to position may be obtained as follows. A single section of the line representation is examined. The voltage and current at the input and output of the section are designated and then related using circuit theory and the transmission line impedance values. When these relations are considered for the limiting case of Δz approaching zero, the relations resolve into two linked first order differential equations for the phasor voltage and current. The equations are referred to as the transmission line equations.

$$\begin{aligned} dV/dz &= -(R+j\omega L)I \\ dI/dz &= -(G+j\omega C)V \end{aligned} \quad (A.1)$$

The two equations may be combined into a single second order differential equation for the phasor voltage.

$$d^2V/dz^2 = \gamma^2 V \quad (A.2)$$

where γ is as defined in equation 5.7.

This equation is referred to as the one-dimensional wave equation. A general solution to this equation is:

$$V(z) = Ae^{-\gamma z} + Be^{\gamma z} \quad (A.3)$$

A and B are constants which must be evaluated from knowledge of the particular voltage source attached to the line and the impedance terminating the line.

A physical interpretation for the result quoted in equation A.1 is to consider the two terms to represent two separate voltage waves traversing the length of the transmission line. The first term describes a voltage wave traveling in the $+z$ direction and the second a voltage wave traveling in the $-z$ direction. The actual voltage that would be measured between the electrodes at any given point would be the phasor sum of the two waves.

The propagation characteristic (γ) associated with each wave is a complex number made up of a real (α) and imaginary (β) part. The real part is referred to as the attenuation constant and describes the rate of exponential decay a wave will experience when traveling along a lossy line. The imaginary part is referred to as the phase constant and describes the phase shift established between different points on the line due to the finite velocity of the wave propagating along the line.

It is hoped that this very brief description of transmission line concepts will aid the reader in following the earlier presentations in this thesis.

Appendix B: Microscopic Structure of Oil Sand

A number of structural models have been proposed to describe Athabasca oil sand. The reader is directed to Takamura¹ for a good description of the various models and their refinements as well as a more detailed description of oil sand components. The following is a brief summary of Takamura's model.

The sand grains of the Athabasca deposit are moderately well sorted and include some clay fines. The in-situ packing is such that porosity is about 35% by volume. The pore volume is filled with bitumen and water in various distributions depending on the grade of oil sand. Rich oil sand deposits will have oil saturations up to 18% by weight (90% of pore volume), with water saturations of about 2% by weight (10% of pore volume).

The water in the oil sand appears in three forms; as pendular rings at the grain to grain contact points, as a very thin film covering the sand surfaces, and as water retained in the fines clusters. The remaining void space is occupied by bitumen. A schematic diagram of this arrangement is shown in figure B.1.

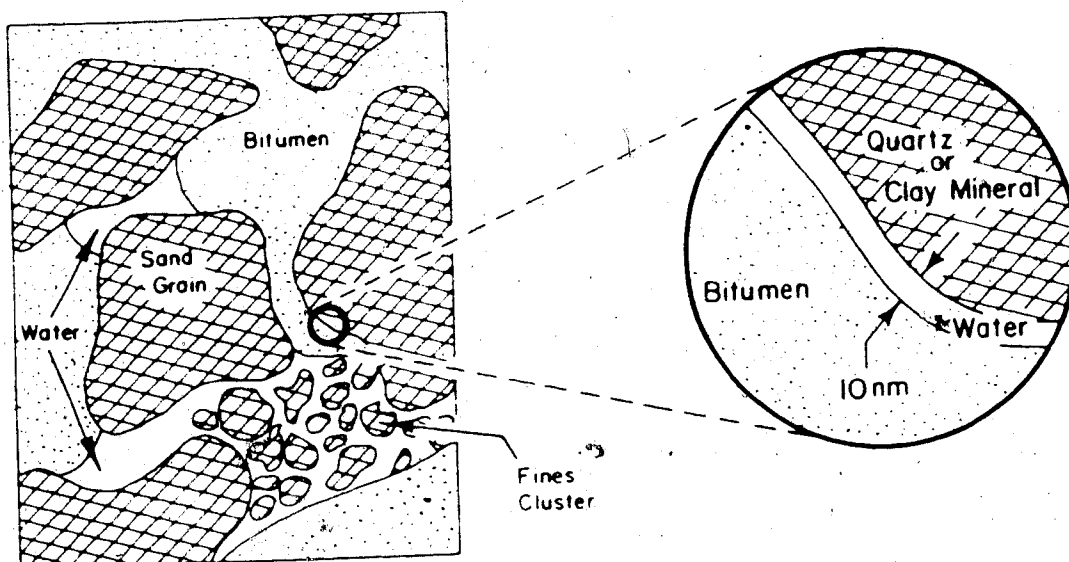


Figure B.1: Schematic diagram showing a structural model of Athabasca oil sand.

Appendix C: Economic Considerations

The present body of work is oriented toward examining the feasibility and desirability of using high frequency electromagnetic energy to heat an oil sand formation as a preliminary step to actual production. It is far beyond the present scope to undertake detailed engineering estimates of the overall costs of any particular production scheme. What can be estimated is the incremental cost an electric pre-heat will add to an insitu recovery scheme. The following is thus applicable to the partial evaporation boring and coated electrode schemes. An estimate for the electrical costs of the production controlled heating scheme is given in chapter 6.

Electrical power may be purchased in bulk, on an interruptable basis, at about \$0.04 per kW·h. Substantial savings on this figure could likely be negotiated if energy use was co-ordinated with the electrical system load demands.

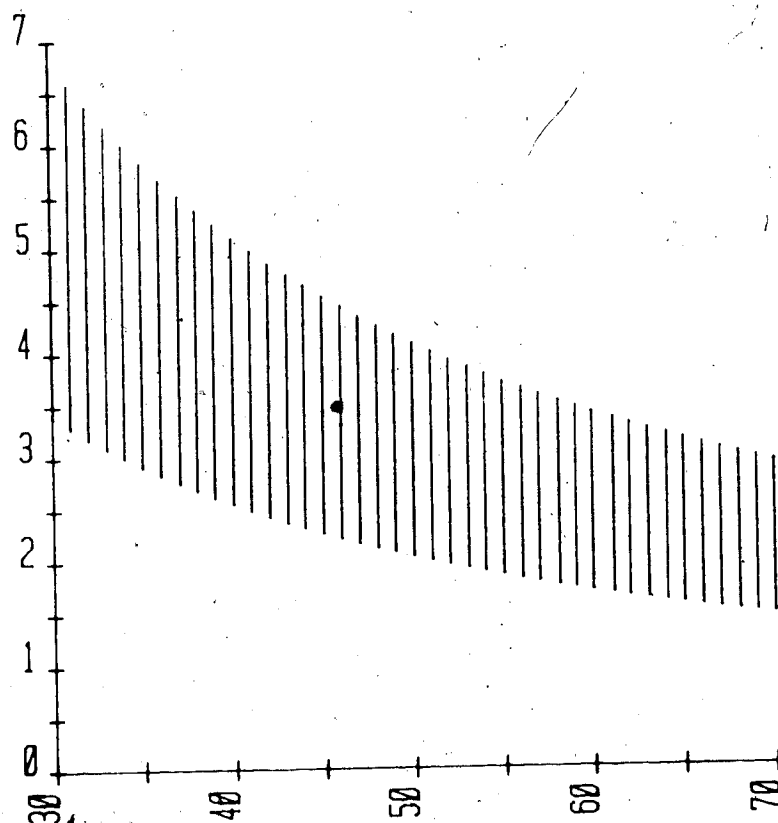
The 60 cycle supply could be rectified at the surface and then transmitted down the main shaft to an amplifier/oscillator operating in a class C mode. A fairly high harmonic content in the amplifier output is acceptable for heating purposes and very little output filtering is expected to be necessary. The losses in this circumstance for frequency conversions and transmission are estimated at between 10 and 20 percent.

It will be assumed that the oil sand is to be heated from an initial temperature of 10°C to a final temperature close to 100°C . No allowance was made for evaporation energy loss as the experiments indicated only a very small portion of the formation moisture had to be removed. A density of 2.1 g/ml and a specific heat of $1 \text{ J/g}^{\circ}\text{C}$ is assumed for the oil sand. Heat losses to the surrounding formations are estimated at 10 to 30% based on the temperature profiles obtained in chapter 3.

The bitumen content of oil sand varies considerably in the various formation layers. In surface mining lean oil sand (less than 6% by weight bitumen) is discarded and only the richer sands processed. Assuming an in-situ scheme would concentrate on the rich bottom third of the deposit, the payzone will be assumed to contain 9 to 14% bitumen by weight. The largest unknown is what portion of the heated bitumen can be swept from the formation. A minimum of 30% does not seem unreasonable and recoveries as high as 70% should be possible.

The previous data may be used to establish a price range for the incremental costs of an electric pre-heat. The information is presented in figure C.1. As the price of oil is commonly quoted in US dollars per barrel, the price presented is also in these terms ($1.35 \text{ Can\$} = 1 \text{ US\$}$). It should be noted that this is the price per barrel of bitumen, a heavy oil product worth less than the quoted world oil price.

Electrical Cost In
US\$/Barrel



Percent Bitumen Recovered

Figure C.1: Estimated cost range for the electrical pre-heat portion of an in-situ recovery scheme.

Plate 1: The crust of dried sand formed around the
 electrode during the heating run of a scale
 model operating in the partial evaporation
 boring mode.

